The University Of Sheffield.

Chemical & Biological Engineering

Low temperature studies for the sulphuric acid decomposition step in the HyS and SI thermochemical cycles

Thesis submitted to the Department of Chemical and Biological Engineering, University of Sheffield, for the Degree of Doctor of Philosophy (PhD)

by

Moisés Alfonso Romero González, B.Eng(Hons)

Department of Chemical and Biological Engineering

University of Sheffield

July 2013

Abstract

Hydrogen is a promising element for the transition from fossil fuels, even though the majority of industrial hydrogen production methods are not carbon-neutral. There are, however, alternatives which could produce this CO_2 free fuel on a massive scale. In particular, thermochemical cycles, including the Hybrid Sulfur (HyS) and Sulfur-Iodine (SI) cycles, which share a common sulphuric acid decomposition step. This project continues the work done by Shaw (2008), which involved the acquisition of experimental data relevant to the production of Hydrogen in the sulphur family of thermochemical cycles. This also lays the framework needed to continue the thermodynamic calculations needed for the design of equipment relevant to the $SO_2/O_2/H_2O$ separation. The model was developed simultaneously with the design of the next generation equilibrium still that was able to incorporate in-situ analysis. Several technical design milestones were achieved in the process, including the development of a sapphire liquid gas cell, a glass reinforced single pass 10 cm Zinc Selenide gaseous cell, several iterations of Raman Spectroscopy probes with ranging capabilities for different purposes, mostly high pressures and temperatures. It was also confirmed that with the low temperature separation approach, materials become an important factor for the success or failure of the process.

Based on the results comparison between the calculations of the Mathematica® model, the GFE model, the available experimental data and general tendencies in the literature, it is concluded that the calculations, as well as the experimental techniques used throughout this project, are successful for their purpose, which is the aiding of equipment design for the HyS and SI cycle, Further efforts can be done to implement this model into process modelling software.

Acknowledgements

I would like to thank Prof. Ray Allen for his continuous guidance, motivation and encouragement; to Dr. Rachael Elder for her everlasting patience and to Dr. Dmitriy Kuvshinov, Dr. Geof Priestman, Prof. Will Zimmerman, Dr. Rile Ristic and Dr. Jordan MacInnes, for the stimulating discussions that helped shape this project.

I would like to acknowledge the support and training received from the brilliant technical staff in the Chemical Engineering Department, Adrian Lumby, Andy Patrick, Stuart Richards, Mike O'Meara, Dave Palmer, Oz McFarlane, Mark McIntosh, Usman Younis and to the very fond memory of the late Clifton Wray.

Finally, I'd like to thank everyone that was involved in this project for all the support they have given me throughout almost 4 years of continuous problem solving, in and out of the lab: my friends in Tampico, Veracruz and other parts of Mexico, my friends in the Chemical Engineering Department, in Sheffield, in London, my 3 brothers and their families (Nico, Bola and Samail) and most importantly, my parents (Nicolas and Carmela).

Without them, this amazing journey would have been impossible.

Indivisa Manent!

(Remain Undivided)

Vince in Bono Malum

(Overcome Evil with Good)

Rerum Cognoscere Causas

(To Discover and Understand)

Table of Contents

Chapter 3 VLE Theoretical Background

Appendixes

Consolidated Reference List

Nomenclature

Symbols

a	Activity	
a	Parameter signifying the hard core size of molecules for the Nakamura equation of state	l mole^{-1}
A	Helmholtz energy	J
A_I	Interfacial area	m^2
b	Parameter signifying the attractive force strength for the Nakamura equation of state	l atm mole^{-1}
B	Second virial coefficient	cm^3 mole^{-1}
c	Constant for the Nakamura equation of state	l mole^{-1}
C_p	Heat capacity	J mol^{-1} K^{-1}
d_0	Density	g cm^{-3}
D_w	Dielectric constant of water	
E	Electrode potential	Volts
E_t	Threshold energy for water splitting	eV
f	Fugacity	atm, bar
G	Gibbs free energy	J
$\bar{G}_i$	Partial molar Gibbs free energy	J mol^{-1}
G^E	Gibbs excess free energy	J
$\bar{G}_i^E$	Partial molar Gibbs excess free energy	J mol^{-1}
G^R	Residual Gibbs energy	J
ΔG^o	Standard Gibbs free energy	J mol^{-1}
h_i^o	Molar enthalpy of pure i	J mol^{-1}
h_G	Gas specific constant	m^3 kmol^{-1}
h_T	Gas parameter for salting out equation	m^3 kmol^{-1} K^{-1}
H	Enthalpy	kJ mol^{-1}
H_{ij}	Henry's constant	atm kg mole^{-1}
ΔH_f^o	Standard enthalpy of formation	kJ mol^{-1}
ΔH^o_{rxn}	Standard enthalpy of reaction	kJ mol^{-1}
I	Ionic strength	mol (kg H_2O)$^{-1}$
I	Current	Amps
k	Boltzmann's constant (see table of constants)	J K^{-1}
k	Reaction rate constant	Specified in text
k_H	Reciprocal of Henry's constant	mole kg^{-1} atm^{-1}
k_{sc}	Salting out coefficient	m^3 kmol^{-1}
K	Equilibrium constant	
K_p	Equilibrium constant in terms of partial pressure of gases	
K_T	Thermodynamic equilibrium constant	
L_v^o	Ostwald coefficient	
m	Molal concentration	mol (kg H_2O)$^{-1}$
m_{SO_2}	Molal concentration of SO_2	moles S_{IV} (kg H_2O)$^{-1}$

m_{O_2}	Molal concentration of O_2	moles O_2 (kg H_2O)$^{-1}$
m_{H2O}	Mass of water	kg
M	Extensive thermodynamic property	
$\bar{M}_i$	Partial molar M of component i	
Me	Metal ion	
M_W	Molecular weight of water (see Appendix C)	g mole^{-1}
n	Moles of species	moles
N_A	Avogadro's number (see table of constants)	mol^{-1}
p	Partial pressure	bar, atm
P	Pressure	bar, atm
P_i	Partial pressure of species i	bar, atm
R	Universal gas constant (see table of constants)	
R	Electrical Resistance	Ohms
s^o	Gas solubility in pure water	Molality
s	Gas solubility in salt solution	Molality
S	Entropy	J K^{-1}
S_{IV}	Total dissolved sulphur dioxide	
S_{IV}^0	Initial concentration of S_{IV}	
t	Time	seconds
T	Absolute temperature	K
T_n	Normal boiling point	K
U	Internal energy	J
v_i	Molar volume of species i	l mole^{-1}
$\bar{v}_i$	Partial molar volume of species i	l mole^{-1}
$v^{-\infty}$	Partial molar volume at infinite dilution	l mole^{-1}
v	Stoichiometric coefficient	
V	Volume	ml, l
V_l^o	Volume of pure liquid	ml, l
x_i	Mole fraction of species i in the liquid	
y	Mole fraction	
Z	Compressibility factor	

Latin

α	Empirical constant in the Nakamura EOS	
β	Empirical constant in the Nakamura EOS	
γ	Empirical constant in the Nakamura EOS	
γ	Activity coefficient	
δ	Empirical constant in the Nakamura EOS	
η	Efficiency	
φ	Fugacity coefficient	
ρ	Density	g cm^{-3}
ω	Acentric factor	
λ	Kuenen absorption coefficient	
λ_{kl}	Short range interaction effects,	kg^2 mol^{-2}
λ_{Ni}	Interaction parameter for neutral and ionic species,	kg mol^{-1}
μ	Chemical potential	
μ_{klh}	Triple body interaction effects	mol kg^{-1}

Subscripts

c	Critical property
g	Gas
i	Any species
i	Ion
j	Any species
k	Any species
l	Liquid
m	Molecule
lj	Liquid junction
r	Reduced property
T	Total
w	Water
±	Molecular species

Superscripts

o	Standard state property
E	Excess property
g	Gas
ig	Ideal gas
l	Liquid
s	Saturated
T	Total

Chapter 1
Introduction

Chapter 1

Table of Contents

1.1 Overview and General Remarks

This work involves the characterization of a vapour liquid equilibrium system both experimentally and mathematically. This system is ideally represented by an enclosed vessel that includes conditions relevant to the sulphur family of thermochemical cycles. The studied media consists of a mixture of chemical species (described below) in both liquid and gaseous phases. These, in turn, achieve chemical and phase equilibrium at a certain temperature and pressure. This equilibrium behaviour is best described with the theory of weak aqueous electrolyte thermodynamics.

The multicomponent gas-liquid mixture at hand contains sulphur dioxide, oxygen, water and traces of sulphuric acid, which is a very important solution in the separation step involving the decomposition of H_2SO_4. The sulphur family of thermochemical cycles, namely the Hybrid Sulphur cycle (HyS) and the Sulphur Iodine (SI) cycle, share this common sulphuric acid step, which leads to products that need to be effectively separated for the efficiency of the cycle not to be compromised.

As part of an international effort to research renewables and the gradual substitution for fossil fuels, the University of Sheffield has contributed towards the advancement of thermochemical cycles, especially towards the research of the H_2SO_4 decomposition step. In this group, thermochemical cycles have been investigated within four main approaches:

- High temperature membrane separation via ceramic membranes
- Low temperature poly-sulphonated ionomer membranes
- Experiments using ionic liquids
- Classic, low temperature vapour-liquid equilibria separation

While the former three have been investigated by other authors in this University, efforts presented here are concerned with the latter, low temperature approach. The hypothesis is that a high-temperature stream of products (after the

sulphuric acid decomposition step) would be lowered to the 30 to 50 °C range, and then separated by conventional means (absorption columns or flash units), which agrees with the optimal separator conditions by the work of Jeong & Kazimi in their HyS optimised flowsheet. (Jeong Y.H., 2005).

To date, no rigorous study of the equilibrium between sulphur dioxide, oxygen and water exists, let alone including sulphuric acid. On the other hand, several studies with subsystems (e.g., SO_2-H_2O, SO_3-H_2SO_4-H_2O, etc.) have been detailed. The aim of this work is to obtain thermodynamic data fully characterizing solubility behaviours of this mixture, as well as advancing spectroscopic knowledge towards it. This thesis continues the work of Dr. Andrew Shaw, which laid an experimental basis for this required data, starting with binary SO_2-O_2 mixtures, followed by a rigorous ternary model containing SO_2, O_2 and H_2O).

In this chapter, hydrogen will be presented as a justification for this project. Hydrogen, an alternative to fossil fuels, sustains the motivation behind this work. The research objectives and the thesis outline will be presented, before briefly describing the hydrogen economy concept, some national programs highlighting H_2 production, before going on to Thermochemical Cycles and acid decomposition on the next chapter.

1.2 Aim

To our knowledge, no full representation of the vapour liquid equilibrium of sulphur dioxide, oxygen, water and sulphuric acid has been reported in literature. Even further, rigorous thermodynamic modelling for this system and information required to develop it, is scarce. According to Duigou et al. (2007), both the SI and the HyS cycles can only be viable if they achieve two important criteria: competitive cost and successful large scale demonstration.

If both cycles are to be competitive, they need to get as close as possible to the maximum theoretical efficiency. These numbers, depending on the methodology, oscillate between 40 and 50%, and it has been discussed often,

according to Elder and Allen (2009). As in all engineering processes, it is standard practice to focus on the separation equipment, which amounts to a considerable percentage of the energy of the cycle, as well as its capital costs. If one is to succeed in developing detailed engineering for the cycles, it is imperative to obtain accurate thermodynamic data that will aid in the design of the aforementioned separation equipment. This work focuses on that effort.

1.3 Background

Early in this project, two stages of research project were set. The first stage included experimental activities to obtain data corresponding to the ternary mixture of SO_2, O_2 and H_2O, which allowed for the model created by Shaw (2008) to be tested and validated. This stage involving the first two years of this project, included commissioning and rebuilding of the former oscillating rig (Mark III), required to make sure that additions were working, familiarization to the operation of the equipment needed to perform the measurements and theoretically, a steep learning curve in practical electrolyte thermodynamics, in particular the experimental part that involves high pressures and temperatures.

After more than 50 binary and ternary runs, the former being SO_2 and water and the latter including oxygen, several milestones were reached including to the contribution of EU FP7 Project Deliverables relevant to Hydrogen Production. On the other hand, and complimentary to the achievements that took place at this stage, the limitations that current equipment had were identified, and after careful observation, a second stage including further modelling and experimentation was deemed necessary to fulfil a more accurate thermodynamic representation of the system, as well as easing it's lengthy operation and take advantage of new instrumental capabilities.

This second stage had to deal with the capabilities of the initial rigs (Mark I-III) and its instrumentation. Limitations including the accuracy of the measurements, as well as the nature of how chemical equilibrium works

(discussed in Chapters 3 and 4), made necessary the development of new experimental approaches, dealing with spectroscopic methods and the development of a new rig (Mark-IV - see Chapter 5). This, in turn, brought new research objectives that proved the most challenging, and ultimately the most productive.

All in all, the commissioning of the Mark-IV and the acquisition of data with it culminates the second stage of this project, bringing to conclusion this summary of research objectives:

- To fully characterize both ternary and quaternary mixtures and their thermodynamic data, both with experiments and calculations;
- To design an apparatus capable of providing solubility data for a broader range of conditions, in order to enhance current separation knowledge within the sulphur thermochemical cycles;
- To be able to cope with more dangerous and corrosive media (such as the addition of dilute sulphuric acid at high temperatures and pressures in this multicomponent mixture of sulphur dioxide, oxygen and water)
- The capability to subject equilibrium mixtures to test in a quicker, better and safer way.
- To pave the way to rigorous modelling in thermochemical flow sheets, relevant to H_2 production.

For its better understanding, the development of this work must then be described methodically. An outline is presented in the next section.

1.4 Outline

The introductory part starts with Chapter One, where the research background is explained, along with general remarks about the hydrogen research field as well as an outline of the thesis structure and its research objectives.

Chapter Two tackles thermochemical cycles, mainly the sulphuric acid decomposition, and a thorough analysis for different hydrogen plant alternatives, including a discussion on the sulphuric acid decomposition step and its recent developments.

Chapter Three lays the theoretical foundation needed to deal with vapour liquid equilibrium, equations of state and aqueous electrolyte solutions.

Chapter Four covers the development of a rigorous vapour-liquid equilibrium model containing equations describing a system containing SO_2, O_2 in an aqueous sulphuric acid solution. This model largely takes from the methodology laid down by Zemaitis et al. (1986).

Chapter Five describes the design and engineering of the new experimental apparatus, as well as a brief description of the analytic techniques intended for it.

Chapter Six presents the tests performed and the results obtained from the apparatuses used in this project, with a focus on solubility diagrams, as well as the compilation of ternary data gathered from the first apparatus. It contains a discussion of the results gathered, contrasting the experimental and the calculations, along with the concluding remarks gathered from the comparison between the model and the experiments,

Chapter 7 contains the conclusions drawn from this project, a summary of findings and finally the recommended future work available for this particular research project.

Finally, included at the end of this dissertation are appendixes that contain calculations relevant to the design of the reactor, as well as parameters useful for the study of this work and experimental procedures that were essential, but not directly related to the results obtained. In the next section, some important aspects of the hydrogen economy are addressed.

1.5 Energy and The Hydrogen Economy

It is unarguable that the fuel for technology advancement in a modern society is energy and its consumption; at least on a large scale (Jorgenson, 1984). Energy not only is related to technological growth, but also to quality the of life, the economy, productivity; even obesity (Drewnowski and Specter, 2004). This is an example of how energy is intimately close to human life. There's no question about the finite nature of fossil fuels, one of the examples being the peak in oil production in the UK, shown in Figure 1.

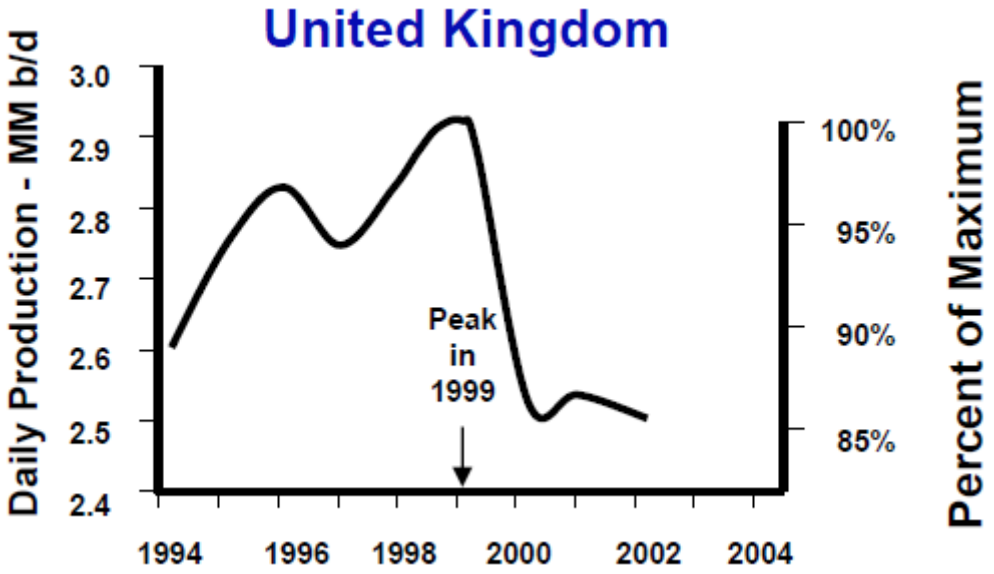

Figure 1. Oil peak in the United Kingdom (Hirsch et al., 2005).

Since the oil crisis in the '70's, and the price spike in 2008, a renewed interest in energy sustainability emerged. It is clear that the problem that arises from energy demand and production must be addressed in the future. Although it is important to state that as we deplete hydrocarbons in general (oil, natural gas, shales and tar sands) new reserves are found, it is clear that the nature of these resources is finite, and it is clear that their extraction and processing is detrimental to the environment (Dudley, 2012).

After the oil price shocks of the 1970's, oil as a share of primary energy has been reduced from 48% in 1973 to 39% in 1985, and BP predicts that it will

continue to be reduced to a further 28% by 2030. However, by 2030, renewables will account for 6% of the global primary energy by 2030. Hydrogen would be included in the ideal diversified energy portfolio of the future (BP, 2012). Current forecasts predict that increasing costs of energy production will deem today's technologies insufficient (Moriarty and Honnery, 2009). Not only do the economic costs of fossil fuels rise, but also the environmental impact, especially in developing countries. A future energy portfolio including hydrogen could alleviate some of the demand problems in the future. This is all but a new idea, dating to the XIXth century.

The concept of the hydrogen economy is a term coined by John O'Mara Bockris in his speech at the General Motors Technical Centre in 1970, and reported in the section 2.20 of the conference proceedings, "On Methods For the Large Scale Production of Hydrogen From Water". It is fundamentally a developed energy system based only on hydrogen. It arose as a response to the environmental concerns that fossil fuel combustion and depletion posed to the scientific community and the energy crisis in the mid-seventies, but as Weston puts it, from the seventies to how we presently got here four decades later is a study worthy of many volumes (Weston, 1992).

Hydrogen is clean in terms of pollutants created by its combustion (only H_2O); and it can also be produced from water, a very abundant resource in the planet. This is one of the reasons why this system could solve the greenhouse effect and regional environmental problems.

For the sole purpose of creating consciousness about this proposed economy, the International Association for Hydrogen Energy (IAHE)[1] was established in Florida, U.S., starting the International Journal of Hydrogen Energy (IJHE) and holding biennial World Hydrogen Energy Conferences (WHEC), helping

the developing concept to be thoroughly studied. By 1980, the hydrogen economy was fully theorized and explained as the transition of non-renewable fuels into a hydrogen-based economy; with its transportation and storage schemes, industrial and domestic usage and appropriate materials to deliver. The hydrogen economy has been fed by research in over 40 countries, with some of them including the scheme in their energy policies (e.g., U.S., Iceland, Japan, Germany) (Goltsov and Veziroglu, 2001). Selected programs are briefly discussed in next section.

1.5.1 Hydrogen National Programs

Many nations have pursued the know-how to make the transition to a hydrogen economy more approachable. Some examples are provided below. This list is not exhaustive, but it is a recap of some of the national hydrogen programs that amounted to a relevant budget figure.

In Japan, the government-funded *WE-NET* Program has already researched hydrogen-combustion technologies, and they presented a prototype hydrogen fuelled burner operating at 1700 °C, with efficiencies of 60%. Hydrogen was produced by a 90% efficient SPEM electrolysis (Hijikata, 2002). Prospective R&D will comprise a short, mid and long-term result analysis, for them to be practically applied throughout 1993-2030. These objectives are proposed: 200,000 m^3 of hydrogen storage; 50,000 m^3 of cryogenic material storage, 30 to 50 kW fuel cells, 100 kW H_2 Diesel engines, 30 Nm^3/h H_2 refuelling, and finally H_2 large-scale utilization (Mitsugi et al., 1998). Public demonstrations are yet to be developed.

In Germany, a H_2 mobility Initiative plans to bring infrastructure for the HE implementation. Germany holds 70% of all fuel cell demonstrations in Europe. The Ministry of Foreign Trade and Investment has a clear intention of propelling the fuel-cell industry, where more than 350 companies and institutes are operating in this matter, particularly in the North-Rhine Westphalia region (Pastowski and

Grube, 2010). The annual growth for fuel cells is expected to be of more than 200 MW from 2015. Partners include among others, Daimler, Linde, Shell, Total and EnBW. Germany also collaborated with Saudi Arabia in HySolar (Abaoud and Steeb, 1998), a program ended in 1995 where they built a Solar H_2 plant near Riyadh, funded with $4.7M split 50-50 between mainly the King Abdulaziz City for Science and Technology, and the German Aerospace Research establishment (DLR).

Canada entered a joint research program with Europe, the Euro-Quebec project (Drolet et al., 1996), where research has been applied to *importing schemes* between them, proving that importing $H_{2(l)}$ from Canada can be successful, especially in the iron and transportation industry; as well in developing a prospective massive transportation infrastructure between the two. More recently, the WHEC 2012 was held in Toronto, where companies from different parts of the world showcased their achievements, including profitability for the first quarter. This is significant, as it shows that hydrogen technologies can overcome negative economic climate if the market is there, even a niche one.

Iceland, on the other hand, is an example of a complete commitment towards a Hydrogen Economy. Several institutions, including the transportation industry, commodity companies, multi-national companies, universities and the government have formed a commitment to a full hydrogen implementation. Currently, there are various programs including the *SMART-H_2*, *H-SHIP* and *PREPAR-H_2*; which are studying experimentally the hydrogen introduction in Iceland at a social, technical and economical level. The transition is planned to be fully completed in 2050, facilitated by partners such as DaimlerChrysler, Norsk Hydro and Shell Hydrogen. Some of the technologies could be integrated with hydroelectric power. In 2007, Hydropower powered almost 73.4% of electricity generation in the country, with a prospective addition of >700 MW to the grid (Orkustofnun, 2007).

In Australia, ACIL Tasman and Parsons Brinckeroff prepared a National Hydrogen Study, in 2007, appointed by the Department of Industry, Tourism and

Resources. It contains an assessment of the role of hydrogen in Australia, plus recommendations that would lay the foundation for their inclusion in the HE.

Veziroglu and several other researchers have compiled the status of Hydrogen Energy in a thorough manner, rendering optimistic results; mentioning enterprises that have already started to commercialize hydrogen production technology, expertise and energy systems; including automotive systems, electrolysis units, battery technologies and hazard studies concerning H_2 transportation (Veziroğlu and Takahashi, 1990) (Momirlan and Veziroglu, 2002) (EHA, 2012). There is a stable scientific community developing new ideas for the H_2 transition, including prospects that go beyond 2100 (Goltsov and Veziroglu, 2001). A comprehensive economic evaluation of Hydrogen national programs has been presented by Khamis, et.al. (2011), whereas Dunn (2002) showed an interesting political narrative for Hydrogen in his publication. In the recent WHEC 2012, held in Toronto, several hydrogen fuel cell companies achieved profitability for the first time since their inception. This further thrusts hydrogen from niche-market towards mass market positioning.

1.5.2 Hydrogen: Energy Carrier

Hydrogen is the most abundant element in the galaxy, and only forms water when lit. Hydrogen is not found naturally, and it is a light, colourless gas with a density of 0.0899 kg/Nm^3, and a boiling point of only 20.39 °K (Haynes and Lide, 2010). The energy stored in 1 kg of H_2 is approximately equivalent to 2.75 kg of gasoline, and it has the most dense energy / mass ratio, compared to other common fuels, although storage remains to be efficiently addressed. However, technological obstacles that were thought to be limiting for the development of the hydrogen economy are quickly fading away as technologies achieve their original benchmark goals.

These factors, along with clean burning and availability; make H_2 a promising *energy carrier,* which, contrary to *energy source,* it is only a means of

transporting and distributing energy for its consumption, according to the ISO 13600:1997 definition 2 (ISO, 1997). This is an important distinction. Petrol, or solar energy, are examples of *energy sources*; whereas hydrogen and electricity are examples of *energy carriers*.

1.6 H_2 Production routes

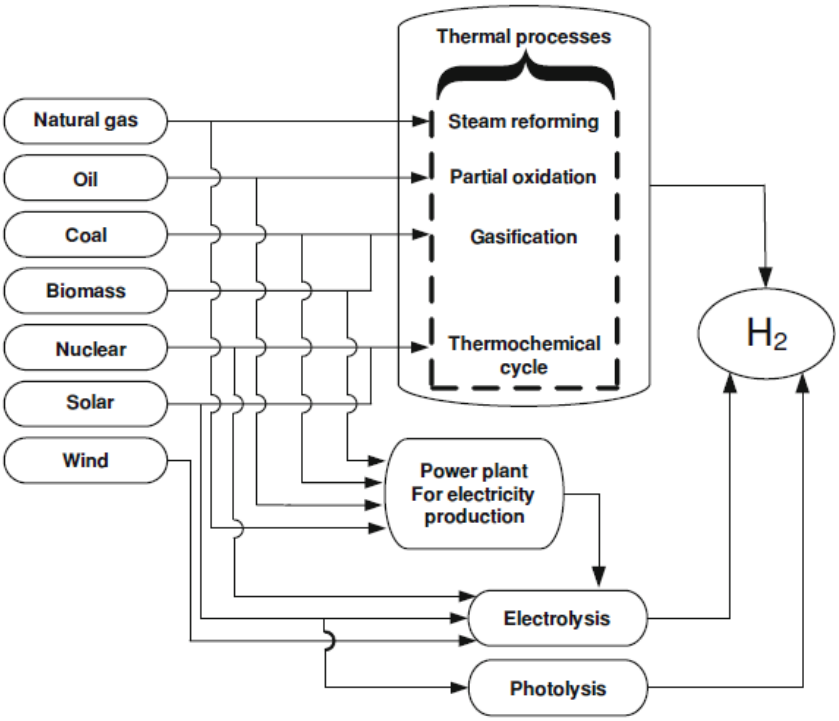

Figure 2. Diagram of the main H_2 production routes (Stolten, 2010).

A number of technologies are available for hydrogen production which can be categorized as renewable and non-renewables (Taylor, 2006), some of them are represented in Figure 2. The main difficulty of hydrogen production is that it continues to be coupled with some non-renewable fuels or processes, like natural gas or gasoline reforming. As of this moment, the most popular industrial method to produce hydrogen comes from reforming hydrocarbons with steam, especially natural gas which contains methane. The EIA gave a rough estimate of hydrogen production costs using different prospective technologies, these are shown below in Table 1.

Table 1. Estimate Hydrogen Production Costs. (J.Joosten, 2008).

Technology and Fuel	Capacity MGPD	Overnight Capital Cost		Capacity Factor (Percent)	Hydrogen Production Cost (Dollars per Kilogram)			
		Million Dollars	Dollars per MGPD		Capital[a]	Feed-stock	O&M	Total
Central SMR of Natural Gas[b]	379,387	$181	$477	90	$0.18	$1.15	$0.14	**$1.47**
Distributed SMR of Natural Gas[c]	1,500	$1.14	$760	70	$0.40	$1.72	$0.51	**$2.63**
Central Coal Gasification w/ CCS[d]	307,673	$691	$2,246	90	$0.83	$0.56	$0.43	**$1.82**
Central Coal Gasification w/o CCS[d]	283,830	$436	$1,536	90	$0.57	$0.56	$0.09	**$1.21**
Biomass Gasification[e]	155,236	$155	$998	90	$0.37	$0.52	$0.55	**$1.44**
Distributed Electrolysis[f]	1,500	$2.74	$1,827	70	$0.96	$5.06	$0.73	**$6.75**
Central Wind (Electrolysis)[g]	124,474	$500	$4,017	90	$1.48	$1.69	$0.65	**$3.82**
Distributed Wind (Electrolysis)[h]	480	$2.75	$5,729	70	$3.00	$3.51	$0.74	**$7.26**
Central Nuclear Thermochemical[i]	1,200,000	$2,468	$2,057	90	$0.76	$0.20	$0.43	**$1.39**

In this EIA publication dated August 2008, it was clearly shown that the most capacity could be achieved by thermochemical cycles. These are not limited to nuclear energy; concentrated solar could also be used as an alternative source.

1.7 Summary

If the Hydrogen Economy is to be achieved, vast quantities of hydrogen are required to be competitive with conventional fuels, and some of the current production technologies are difficult to scale industrially. In this work, thermochemical cycles have been selected for its potential to produce massive amounts of hydrogen if coupled with nuclear or solar sources, using waste heat from the fission processes or in solar tower concentrators. These are addressed in the next chapter.

Chapter 1 References

ABAOUD, H. & STEEB, H. 1998. The German-Saudi HYSOLAR program. International Journal of Hydrogen Energy, 23, 445-449.

DREWNOWSKI, A. & SPECTER, S. 2004. Poverty and obesity: the role of energy density and energy costs. The American Journal of Clinical Nutrition, 79, 6-16.

DROLET, B., GRETZ, J., KLUYSKENS, D., SANDMANN, F. & WURSTER, R. 1996. The euro-québec hydro-hydrogen pilot project [EQHHPP]: demonstration phase. International Journal of Hydrogen Energy, 21, 305-316.

DUDLEY, B. 2012. BP statistical review of world energy.

DUIGOU, A. L., BORGARD, J.-M., LAROUSSE, B., DOIZI, D., ALLEN, R., EWAN, B. C., H. PRIESTMAN, G., ELDER, R., DEVONSHIRE, R., RAMOS, V., CERRI, G., SALVINI, C., GIOVANNELLI, A., DE MARIA, G., CORGNALE, C., BRUTTI, S., ROEB, M., NOGLIK, A., RIETBROCK, P.-M., MOHR, S., DE OLIVEIRA, L., MONNERIE, N., SCHMITZ, M., SATTLER, C., MARTINEZ, A. O., DE LORENZO MANZANO, D., CEDILLO ROJAS, J., DECHELOTTE, S. & BAUDOUIN, O. 2007. HYTHEC: An EC funded search for a long term massive hydrogen production route using solar and nuclear technologies. International Journal of Hydrogen Energy, 32, 1516-1529.

DUNN, S. 2002. Hydrogen futures: toward a sustainable energy system. International Journal of Hydrogen Energy, 27, 235-264.

EHA. 2012. EHA March Newsletter [Online]. Available: http://www.h2euro.org/category/publications/newsletters/newsletters-2012/eha-newsletter-march-2012.

ELDER, R. & ALLEN, R. 2009. Nuclear heat for hydrogen production: Coupling a very high/high temperature reactor to a hydrogen production plant. Progress in Nuclear Energy, 51, 500-525.

GOLTSOV, V. A. & VEZIROGLU, T. N. 2001. From hydrogen economy to hydrogen civilization. International Journal of Hydrogen Energy, 26, 909-915.

HAYNES, W. M. & LIDE, D. R. 2010. CRC Handbook of Chemistry and Physics: A Ready-Reference Book of Chemical and Physical Data, Taylor & Francis Group.

HIJIKATA, T. 2002. Research and development of international clean energy network using hydrogen energy (WE-NET). International Journal of Hydrogen Energy, 27, 115-129.

HIRSCH, R., BEZDEK, R. & WENDLING, R. Peaking of world oil production. Proceedings of the IV International Workshop on Oil and Gas Depletion, 2005. 19-20.

ISO 1997. ISO 13600:1997. 2- Definitions.

J.JOOSTEN, P. G., A. KYDES, J.D.MAPLES 2008. The Impact of Increased Use of Hydrogen on Petroleum Consumption and Carbon Dioxide Emissions. 1 ed. Washington, D.C. U.S. 20585: Energy Information Administration, U.S.DOE.

JEONG Y.H., M. S. K., K.J. HOHNHOLT, AND B. YILDIZ, 2005. Optimization of the Hybrid Sulfur Cycle for Hydrogen Generation. MIT–Nuclear Clear Energy and Sustainability (NES) PROGRAM, 004.

JORGENSON, D. W. 1984. The Role of Energy in Productivity Growth. The American Economic Review, 74, 26-30.

KHAMIS, I. 2011. An overview of the IAEA HEEP software and international programmes on hydrogen production using nuclear energy. International Journal of Hydrogen Energy, 36, 4125-4129.

MITSUGI, C., HARUMI, A. & KENZO, F. 1998. WE-NET: Japanese hydrogen program. International Journal of Hydrogen Energy, 23, 159-165.

MOMIRLAN, M. & VEZIROGLU, T. N. 2002. Current status of hydrogen energy. Renewable and Sustainable Energy Reviews, 6, 141-179.

MORIARTY, P. & HONNERY, D. 2009. Hydrogen's role in an uncertain energy future. International Journal of Hydrogen Energy, 34, 31-39.

PASTOWSKI, A. & GRUBE, T. 2010. Scope and perspectives of industrial hydrogen production and infrastructure for fuel cell vehicles in North Rhine-Westphalia. Energy Policy, 38, 5382-5387.

SHAW, A. C. 2008. The simultaneous solubility of sulphur dioxide and oxygen in water for the hybrid sulphur thermochemical cycle. Ph.D. Doctoral Thesis, University of Sheffield.

STOLTEN, D. 2010. Hydrogen and Fuel Cells: Fundamentals, Technologies and Applications, John Wiley & Sons.

TAYLOR, M. 2006. Improvement of the Sulphur-Iodine cycle through the addition of ionic liquids. M.Phil, University of Sheffield.

VEZIROĞLU, T. N. & TAKAHASHI, P. K. Hydrogen energy progress VIII : proceedings of the 8th World Hydrogen Energy Conference, Honolulu and Waikoloa, Hawaii, U.S.A., 22-27 July 1990. In: VEZIROĞLU, T. N. & TAKAHASHI, P. K., eds., 1990 New York :. Pergamon Press.

WESTON, K. C. 1992. Energy Conversion, West Publishing Company.

ZEMAITIS, J. F., CLARK, D. M., RAFAL, M. & SCRIVINER, N. C. 1986. Handbook of Aqueous Electrolyte Thermodynamics, New York, AIChE.

Chapter 2

Literature Review on the H_2SO_4 decomposition

Chapter 2.

Table of Contents

2.1 Background to Thermochemical Cycles

In thermochemical cycles, water is split to H_2 and O_2 via a series of reactions, while intermediate species are kept inside the cycle. As heat can be directly used and the electrode potential lowered, the efficiency could be potentially enhanced to commercial levels. This group has been involved with the SI and the HyS cycles, which are presented in this chapter, along with important aspects that lead to the literature relevant to the separation.

2.2 SI Cycle

The sulphur family of cycles was jointly developed by General Atomics, Westinghouse and JRC (Funk, 1976). The SI cycle is a promising combination if coupled with nuclear heat (Elder and Allen, 2009). It consists of three steps: the Bunsen reaction, the Sulphuric Acid Decomposition, and the Hydroiodic Acid Decomposition. The overall reactions occur as follows:

$$9I_2 + SO_{2(g)} + 16H_2O_{(l)} \rightleftharpoons (2HI + 10H_2O + 8I_2)_{(l)} + (H_2SO_4 + 4H_2O)_{(l)} \quad \text{Reaction 1}$$

$$(2HI)_{(g)} \rightleftharpoons H_2 + (I_2)_{(l)} \quad \text{Reaction 2}$$

$$L_1 = (H_2SO_4 + 4H_2O) \rightleftharpoons (H_2SO_4)_{(l)} + (4H_2O)_{(l)} \quad \text{Reaction 3}$$

$$(H_2SO_4)_{(l)} \rightleftharpoons (H_2SO_4)_{(g)} \quad \text{Reaction 4}$$

$$(H_2SO_4)_{(g)} \rightleftharpoons (SO_3)_{(g)} + (H_2O)_{(g)} \quad \text{Reaction 5}$$

$$(SO_3)_{(g)} \rightleftharpoons (SO_2)_{(g)} + \tfrac{1}{2}O_2 \quad \text{Reaction 6}$$

General Atomics developed the classification used in this work, consisting of three sections. The first reaction is called the Bunsen reaction, an exothermic and

spontaneous reaction (if ranging from 20 – 100 °C); where water reacts with molecular iodine and sulphur dioxide, that in certain concentrations, happen to produce two liquid sulphuric and hydroiodic acid-rich phases, that are immiscible. The phase containing the hydroiodic acid is called the HI_x phase, due to the average of polyiodide formation that occur inside it. The entire cycle is shown on Figure 1.

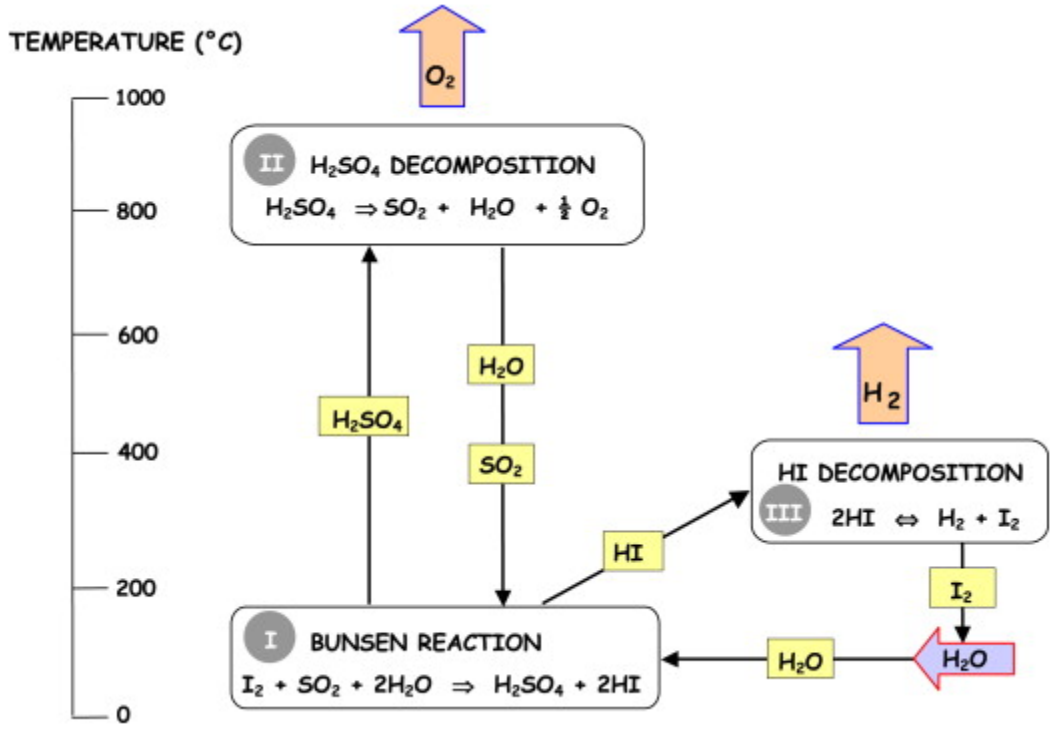

Figure 1. Schematic representation of the SI Cycle, with temperature profiling of the reactions. (E. Funk, 2001)

The second section, the so-called HI_x step, is the most critical step in the cycle. It occurs when the hydrogen iodide decomposes and concentrates to produce H_2. Further, H_2O, I_2 and SO_2 are recycled in the system (O'Keefe et al., 1982). This is shown above. The third section is the sulphuric acid decomposition, after which the system of interest in this project is generated.

Efficiencies of this cycle, calculated by several publications (O'Keefe et al., 1982, Ewan and Allen, 2005, Elder and Allen, 2009, Atkin, 2009), are in the ranges of 51%, without considering estimates from flow sheets; that is, taking into consideration Equation 1,

$$\eta = \frac{\Delta H°_{H_2O@25°C)}}{Q + \frac{W}{\eta *}}$$ Equation 1

where $\Delta H°$ is the enthalpy of formation of liquid water at ambient temperature, Q and W are the heat and work requirements of the cycle and $\eta *$ is the efficiency of the heat to work conversion system, taken as 0.5 (Vitart et al., 2006).

From the set of reactions shown above, the upper bound of this efficiency, calculated from the reversible heat and work requirements of the reactions, can be estimated to be 51%. However, a refinement of the estimation, taking into account a more detailed flow sheet along with plausible values of components efficiencies such as pumps or compressors, leads to a value between 34% and 37%, depending on the optimization assumed for heat recovery in the HI_x Section.

Work at this department has been done to optimize flow sheets with the software ProSimPlus®, estimating improvements up to 40%, using different dewatering parameters, according to Elder (2005). Other work including flow sheet optimization, from the original GA design, include research from Özturk (1995) and Huang and T.Raissi (2005), using ideal and Peng-Robinson models respectively.

2.3 HyS Cycle

The HyS Cycle, known also as the Westinghouse Cycle, is a hybrid thermochemical cycle, as electrolysis is used for the purpose of generating hydrogen, this was originally developed by Brecher and Wu (1977) while working at Westinghouse. The main reactions are shown below:

$$SO_2 + 2H_2O \xrightarrow{0.23V} H_2SO_4 + H_2$$
$$H_2SO_4 \xrightarrow{700°C} SO_2 + H_2O + \tfrac{1}{2}O_2$$ Reaction 7

The main advantage of this cycle is that, compared to normal water electrolysis requiring a potential barrier of 1.23 V; the potential barrier for this first reaction is one

fifth only, with an exact voltage of 0.17 V needed. This theoretically lowers the power required for operation of industrial electrolysers (Atkin, 2009, Ewan and Allen, 2005).

Originally, the energy sources aimed to satisfy the heat requirements of this cycle were nuclear in nature; but recent research has shown that solar heliostats or parabolic troughs can be used to produce the large amounts of heat required for the process.

The focus in this cycle is mainly targeted at electrolyser development, since it is the first step in the cycle and it is a particularly useful point of research in industrial applications. It is also important to mention that according to Jeong & Kazimi (2005) the acid electrolysis is the limiting step in this cycle.

Studies have shown that an electrolyser unit operating in the 500-600 mV per cell can lead to a predicted efficiency of more than 50%, superior to all other cycles. Research by Ewan and Allen (2005) even showed theoretical increases of up to 60%. Analysis of the economic aspects of the cycle give an approximate $1.60 USD per H_2 kilogram for a mature technology coupled with a nuclear plant, but since then prices have changed according to recent data, e.g. Miller et al. (2012) considers a milestone to achieve USD $2/gge ($2-4 dispensed). Summers and co-workers (2005) point out that there are still some obstacles, e.g. current density, operating lifetime and moderate capital cost.

2.3.1 Example Flow sheets in the HyS Cycle

The most up-to-date work in flow sheet optimization was done at MIT, with contributions and comments from partners involved in the project. Other modifications have focused on equipment design, rather than rearranging the whole process. The work is shown in the next page, for clarity purposes.

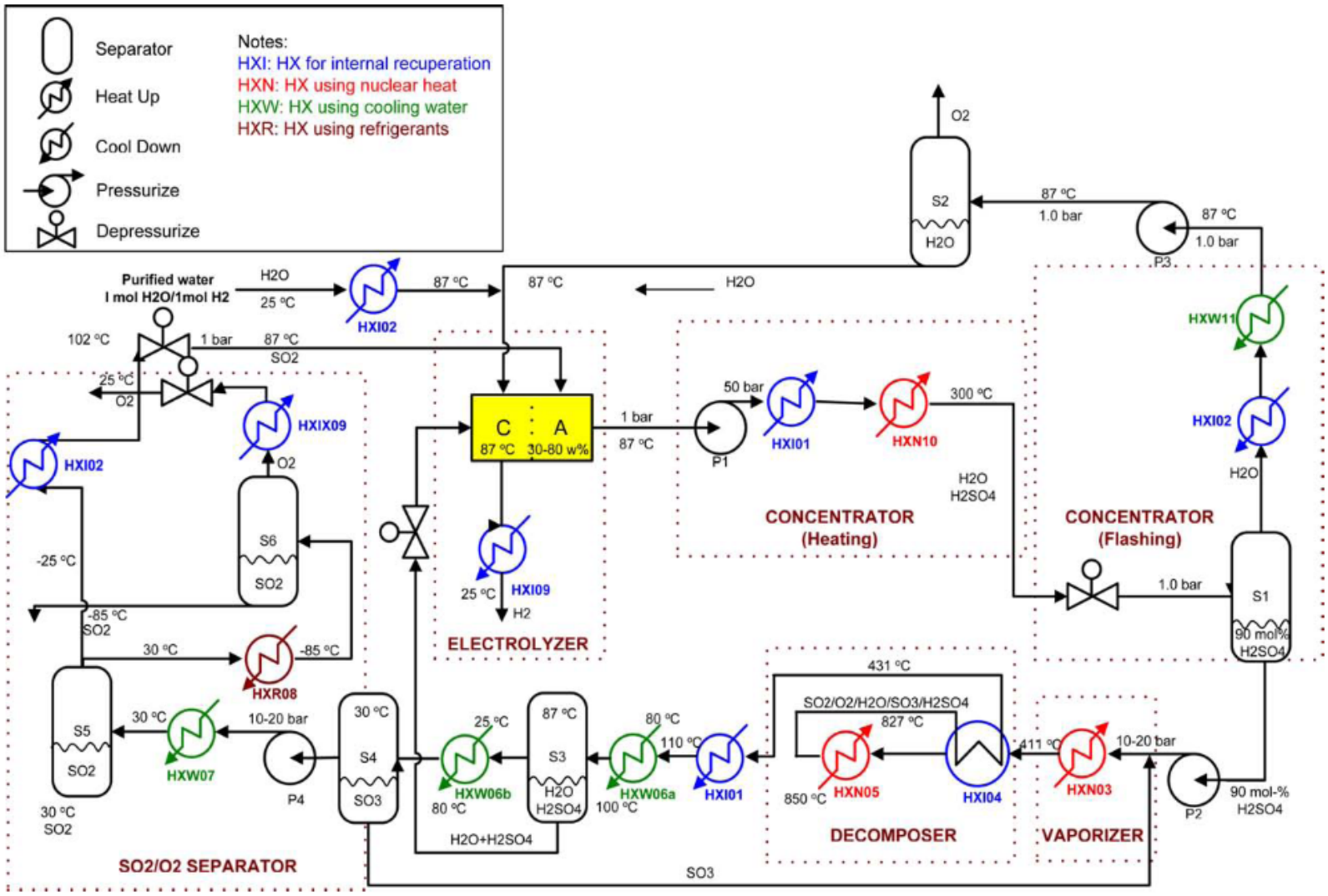

Figure 2. Flow sheet developed by Jeong & Kazimi, et.al. (2005)

Current work at the Massachusetts Institute of Technology diverted focus on the HyS cycle and started working on electrolyser technologies, and their coupling with nuclear power (High Temperature Steam Electrolysers, HTSE); while the Westinghouse Corporation already bet the future of Hydrogen on the HyS Cycle (Lahoda, 2010). Although funding has decreased in the last couple of years, research is still being done on a smaller scale and hopes of funding remain for thermochemical H_2. In the following sections, some related research is discussed.

2.3.2 SO_2 Electrolysers

In the Westinghouse original design, the electrolyser unit has two chambers separated by the electrolysing membrane, where hydrogen occurs at the cathode, while SO_2 is converted to sulphuric acid at the anode, following a scheme represented in Figure 3:

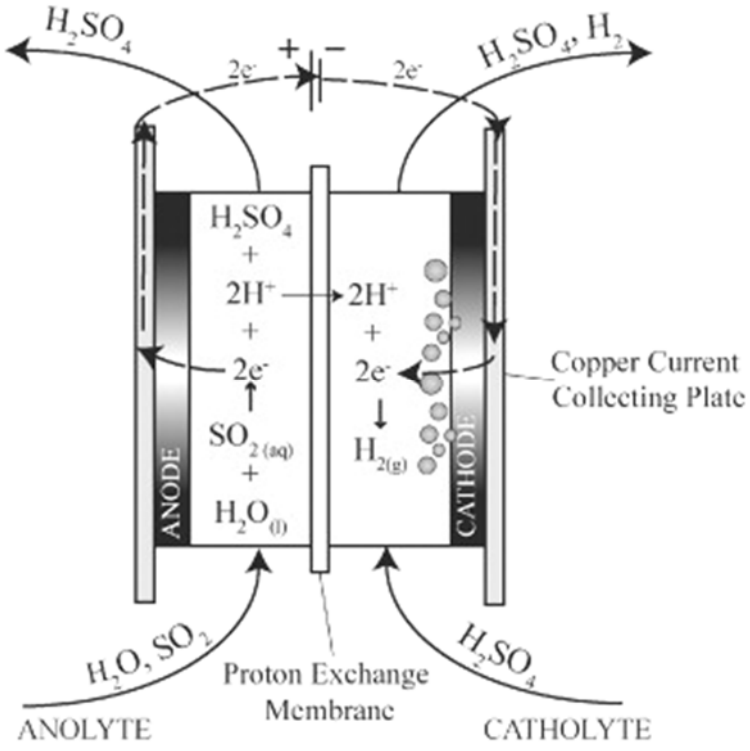

Figure 3. The original electrolyser set-up, designed at Westinghouse. (Lu and Ammon, 1982)

More modern developments include a membrane electrode assembly, MEA; obtaining lower cell resistance in return. The current density at a specific voltage in a cell depends on the operating PT conditions; the composition and the concentration of both the anolyte and catholyte.

The Westinghouse original benchmark of obtaining 500 mA/cm^2 was achieved by Staser, Gorensek and Summers (2009) with a 0.6V current; however, this was done with concentrated sulphur dioxide. The optimal performance with dilute sulphur dioxide concentrations has not been satisfactory yet. This milestone, if reached, would reduce the electrolyser area by 60%, largely decreasing capital costs.

Particular attention has been brought to the research being presently done by Yildiz et.al (2007), where high temperature electrocatalytic materials have been of interest; viz, conducting oxide surfaces for enhanced activity and durability. These materials will prove to be useful for the decomposition stages of the cycles, a materials section is discussed in sections 2.7, 5.7 and 5.12.

2.4 Acid decomposition background

As mentioned previously, sulphuric acid decomposition is common to the two most researched thermochemical cycles for hydrogen production: the SI and the HyS cycles, although it is iterated slightly differently in each technology. In this group, a brief review of the decomposition section developments was conducted by Atkin in his doctoral dissertation (2009), however, since then a number of publications related to the sulphuric acid step have been presented both in refereed papers, as well as conferences where thermochemical cycles play a role as part of the hydrogen production track, e.g. the ICH$_2$P or WHEC conferences. It is worth mentioning again a summary of the many advantages associated with the sulphur cycles, namely:

- Non-volatile price of the end product, regardless of relatively high capital costs associated
- A massive reduction of greenhouse gas emissions throughout the lifespan of a large scale H_2 thermochemical plant.

- Industrial capacities, high output for mass market demand, complimentary to renewable hydrogen generation.
- Lower capital costs compared to conventional electrolyser technologies.
- Compatible with both nuclear and solar energy sources
- Sulphur is cheap and abundant

Further benefits and cost reduction could be reached in the long term. According to a report presented by TIAX LLC, the average HyS production costs will be USD $5.68 in 2015 and USD $3.85 in 2025 (Kromer et al., 2011). Nonetheless, it is necessary to indicate the technical challenges that remain in current research. These aspects of this H_2SO_4 decomposition section will be presented below.

2.4.1 SI and HyS flowsheets

It is important to mention that although the development between the SI and the HyS had stemmed in parallel, it is not to say that the interest is equal for both. Disadvantages regarding the capital cost for iodine feedstock and process solid difficulties somewhat hindered the SI cycle flow sheet development. This is why, throughout this H_2SO_4 chapter, a preference to present selected conditions relevant to the Hybrid Sulphur Cycle are discussed more than SI flowsheets, even if the decomposition section chemistry remains with key similarities between both processes.

2.5 Decomposition Section Development

A great deal of research has been directed at this step in the SI and HyS cycles. The sulphuric acid industry has helped in acquiring the know-how to tackle some of the technical challenges present. The proposed steps, according to the original cycle proposed by Westinghouse and included in flowsheets in the seminal work of Öztürk and colleagues (Öztürk et al., 1995); consist of concentrating sulphuric acid through a series of flashing equipment, starting from low operating pressures. Then, it is dehydrated, before SO_3 is decomposed into SO_2. This decomposition is only partial, for undecomposed sulphur trioxide is recombined with water, which allows

recovering of its heat content (Vitart et al., 2006). As stated by Vitart, for this particular section, several tasks had to be met. Catalyst endurance needed to be analysed, as well as a conceptual decomposer that could tackle the challenges posed by these harsh conditions. Since the mid-2000's, several additions and optimizations have been included in the original flowsheet by Bilgen (1995), and these other technical challenges have been met.

10 years later, Huang and co-workers (2005) analysed and optimized the work carried out by Öztürk (1995) and added some changes to the original flow sheets, achieving energy efficiencies of 76%. Some calculations were based on chemical equilibrium for the sulphuric acid decomposition, where these assumptions were made:

- Simple phase gases were considered ideal,
- Liquid phases were considered to be real solutions
- Henry's Law to predict behaviour of sulphur dioxide and water;

These assumptions were used to optimize the Bilgen's flowsheet, arguably, "without compromising efficiency or process" feasibility, lowering acid decomposition temperatures down to 500 °C. This has important implications for this work: this is a simplification that accounts for a strong argument against the accuracy of the flow sheets, as there is no indication of electrolyte behaviour or non-idealities in the gas phases.

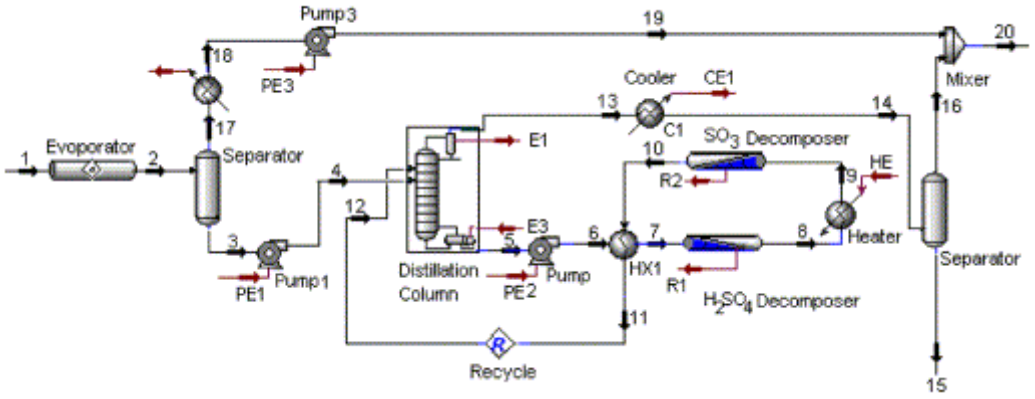

Figure 4. Huang's improved sulphuric acid decomposition step, originally conceived by Bilgen (2005). HySYS was used to enhance the original flow sheet. Three flow sheets were studied in that particular research, simplifications used are stated above.

On behalf of the sulphur-iodine side, in Japan, a week long demonstration of the cycle was conducted, but not in a closed-loop configuration, leaving questions about effects on recycling and reaction completion. In the SI cycle, sulphuric acid is reduced and then the remaining oxygen and SO_2 are reacted in the Bunsen section, leaving hydroiodic and sulphuric acid, whose densities are sufficiently different for them to be separated easily. As stated in an feasibility analysis about the sulphuric acid decomposition from the Sandia National Laboratories (Perret, 2011), in the SI cycle, extractive distillation using phosphoric acid and iodine recovery remain an issue.

On the side of the Hybrid Sulphur side, the acid from the electrolyser side is passed onto the decomposition section to be separated as SO_2, O_2 and H_2O after being concentrated in vacuum columns. An important note is that sulphuric acid and sulphur trioxide will be present as traces in the mixture. Since the decomposer per-pass conversion is ~50%, a large amount of acid is recycled. A temperature of 950 °C is contemplated for a nuclear source in the flowsheets by NGNP reports (Nel et al., 2009), Jeong (2005) uses 850 °C, and according to Summers (2005), a solar source is also available with heat transfer media in the form of sands and helium loops.

2.6 Decomposer Design

The decomposer represents a critical equipment that is also in a relatively early development stage, especially regarding materials and construction. An advanced design was reached in the form of an advanced heat-exchange reactor design made from Silicon Carbide, the Bayonet H_2SO_4 decomposition reactor (Gorensek and Summers, 2009). The material is resistant to corrosive media and high temperatures and pressures, but the real challenge is the integration of the system itself. Metal/ceramic brazing and joining require further development. Machining of silicon carbide remains a problem in big industrial sized vessels of this sort. The reactor is designed to operate in a laminar flow regime for the gas risers, contained in a 3.64 m inside diameter vessel. The reactor operates at 87 bar and a flowrate of 0.073 kg/s gas velocity for the decomposition species. The setup is shown below in Figure 5.

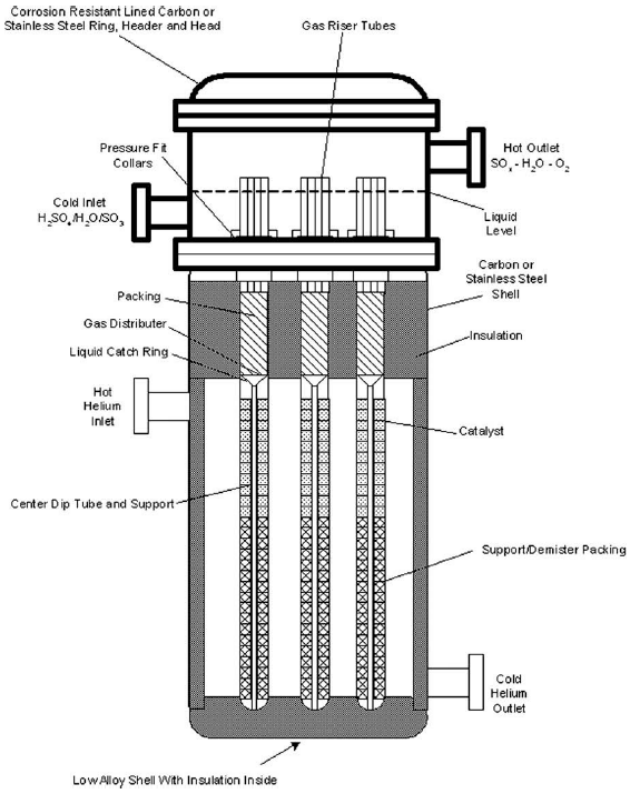

Figure 5. The SiC composite design for the reactor, concentrator and preheater (Connolly et al., 2009).

2.7 Material Development

R&D efforts are continuously required for the harsh conditions and materials in the process. For its complexity, this is completely another area of research that was addressed promptly by Savitzky (1982), although recently a more analytical approach was used to evaluate the feasibility of materials in the high temperature decomposer, catalysts and electrolysers.

Research in the U.S., funded by the National Hydrogen Initiative, developed a silicon carbide design (Nagarajan et al., 2009), whereas Kim, et.al (Kim et al., 2008) designed two shell-and-tube decomposers, for sulphuric acid and sulphur trioxide respectively, where a nominal 66% decomposition yield was reached, at 850 °C and 7 bar(a).

Research has also addressed the catalysts that would withstand the process conditions. Platinum, palladium and palladium oxide have been tested, with good

results. Platinum catalysts were used experimentally by Ginosar (Ginosar et al., 2007), where the activation energy was found to be $8.8034x10^4$ kJ/kmol, and the Arrhenius constant was 0.6218 s^{-1}.

Work conducted by this department, specifically mentioning the experimental set-up designed by this group, show that PTFE-lined stainless steel and PEEK are good materials that can withstand the low temperature separations of sulphuric acid, sulphur dioxide, oxygen and water; showing good resistance to corrosion and ability to withstand moderate temperatures and high pressures. These are results reported in Chapter 5.

A thorough and comprehensive literature review is available in Atkin's thesis (Atkin, 2009) for the high-temperature membrane selection and experiments, including a process description of both SI and HyS cycles; work carried out by Elder showed more interest in the SI Cycle, and the behaviour of porous membranes; whereas work carried out by Shaw (2008) produced an extensive theoretical description of the methodology that is used for the sulphuric acid decomposition modelling that is to follow, in Chapter 4.

2.8 Catalyst Development

In recent years, different catalysts for the high temperature SO_3 decomposition have been researched by different groups. Supported Pt/X catalysts remain the most investigated.

Recently, a series of publications by Ginosar (2007) filled a research gap within SO_3 decomposition catalysts from work in the 70's and 80's, as previous work used very diluted concentrations and very ideal conditions, not representative in thermochemical cycles. One of his main objectives was to explore long-term stability between two different candidates, a Pt/TiO_2 and a $Pt/a\text{-}Al_2O_3$ supported catalysts, with 0.1 and 1% wt loadings of platinum, which were the most promising according to his first study. In his work, these catalysts were tested at 800 to 850 ºC for 24 hours, deeming them reliable for that typical reaction period, in contact with 96% wt H_2SO_4,

not previously used. While the typical loss of activity for the titanium oxide remained acceptable at 24 hours, a 240 h exposure registered a loss of 30% of its initial amount of catalytic metal, but was significantly more surface area retention than zirconia or alumina based catalysts.

In a more integrated study on the catalytic decomposition of sulphur trioxide, a system was modelled with rigorous catalytic packed bed reactor differential equations by Kubo and co-workers (2004), along with experimental characterization. This study contained conditions that included the parametric variables related to a VHTR source, including heat transfer coefficients inside an advanced helium heat exchanger. Reaction rates were formulated, taken from experimental kinetic data with a 1% wt a-Al_2O_3 supported Pt catalyst, with a bulk density of 1.12 g/cm^3. An Arrhenius plot was fitted after catalytic reaction modelling was numerically regressed, ranging from 953 to 1153 K. This data was included in a heat exchanger reactor model that predicted 20-25 m^2 of area needed to achieve nearly chemical equilibrium for the production of 1 mol/s of SO_2.

These high temperature conditions have been investigated by Atkin (2009), in the form of equilibrium calculations along with experimental data from Barbarossa (2006) and Brutti et al. (2006), relevant to the decomposer conditions. These will be discussed in the equilibrium section, Chapter 4.

2.9 Previous work with sulphur species solutions

Earlier in this chapter, it was stated that one of the motivations for this work was to obtain the relevant thermodynamic data that was going to be used for industrial equipment design in the HyS and SI cycles, focusing on post-decomposer separations. While the exact mixture of SO_2, O_2, H_2O has not been pursued in literature, let alone mixtures with sulphuric acid, this group has gathered a large amount of ternary solubility diagrams that, compared with Shaw's model, offers a good starting point for design-specific tasks.

However, several authors have permutated subgroups of the system of interest. The main three sources of data are the work by Que (2011), containing sulphur trioxide solubility in sulphuric acid solutions using the symmetric electrolyte non-random two liquid model; the modelling of Aspen Plus along with the OLI MSE models carried out by Gorensek (2009), with a thermodynamic analysis of SO_2-depolarized electrolysis with focus on the electrochemistry of the process, and finally the work of Leiva (1986), which contains SO_2 and O_2 in a Gibbs-Free energy program in Fortran. In the latter, although the conditions are not broad, they have a fair try at regressing parameters not available in literature, and heavily relying on other authors work for interaction contribution estimation. A brief description of each is presented below.

2.9.1 Binary Mixtures

The seminal work of sulphur dioxide and water by Shaw (2008), taken from the book of Zemaitis (1985), contains the thermodynamics of dissociation into sulphite and bisulphite in water. This was performed by the Henry's law to predict solubility, and liquid phase reactions based on the liquid activity and molar compositions. In this project, experimental data was acquired and published elsewhere (Shaw et al., 2011) as part of the HyCycleS project, along with deliverables relevant to the European FP7 on Hydrogen . These results are presented in Chapter 6.

2.10 Work on O_2 solutions

As stated in the Literature Review by Shaw (2008), a number of papers where the properties of oxygen in aqueous solutions are available. Most of these relate to the atmospheric sciences, as oxygen plays a vital role for different meteorological processes that contain complex yet interesting reactions, taking place in the troposphere.

As stated by Pawlikowski and Prausnitz (1983), although there are several papers containing the thermodynamics of volatile electrolyte in the literature, there is a

difficulty to process them in a simple manner, indicative of the engineering approach. They concluded that a salting out constant calculation was enough and simple to implement, as long as care was taken for complexing electrolytes. Two cases are possible: use the Setschenow salting out contribution equation, or using a rigorous VLE equation set that accounts for non-idealities and reaction dissociations. Both of them are presented in the results chapter, along with their comparison with data from the Mark-1 to III and Mark-IV reactor, in the ranges from 25 to 80 °C, and pressures up to 16 bar containing up to 0.4 mol O_2 and 0.5 mol SO_2. This is also compared with a Gibbs-Free Energy model in further sections.

2.10.1 Tromans Solubility

In 1998's paper, Tromans (2000) stated that when oxygen is dissolved in water, the coefficients of fugacity and liquid activity are close to unity at up to a few tens of atmospheres. This is relevant, as the Henry's Law constant holds up strongly.

$$k_H = \frac{m_{O_2}}{p_{O_2}}$$

According to this simplification, an equation was derived that contains solubility calculations that approximate oxygen in water up to 60 atmospheres.

$$m_{O_2} = P_{O_2}\left\{\frac{0.046T^2 + 203.357T\ln(\frac{T}{298}) - (299.378 + 0.092T)(T - 298) - 20.591\times10^3}{8.3144T}\right\}$$

While this format is not compatible with the rigorous model described in Chapter 4, it is of great help to check internal consistency, for it facilitates an initial guess. This data is compared with the VLE model containing the other species.

2.10.2 Germanium Oxidation

Although the catalytic nature of Germanium does not come very intuitively, it is a concern for ATR measurements in the spectroscopic setup designed for this system.

It has been stated by Chiodo and co-workers (2007) that in certain conditions, that germanium may catalyse the reduction of species in aqueous solutions. In their work, 26 atomic cations were experimentally checked, among them germanium, relevant to the nitrous oxide reduction. Although the aqueous acid system at hand is more susceptible to oxidation rather than reduction, it is worth noting that reduction may disturb chemical equilibrium depending on the pH of the system. It is also of concern that the study was on crushed germanium powder, and according to Baddour and Selvidge (1967), a polished Germanium surface may not have the same effects on species catalysis. However, this is an interesting additional part of this research, and can be quantified as the metal-induced oxidation in the Mark-I rig by Shaw.

2.11 Previous work with sulphuric Acid

Although many authors have worked with sulphuric acid and the CPI has advanced knowledge on its chemical reactions, unit operations and so forth, the only actual work related to sulphuric acid and hydrogen production (in a thermochemical context) has been performed by Gorensek (2009), focusing on the SO_2/H_2SO_4(aq) system, in order to fully understand the depolarised electrolysis power requirements, using OLI MSE, a proprietary electrolyte modelling plug-in for Aspen Plus.

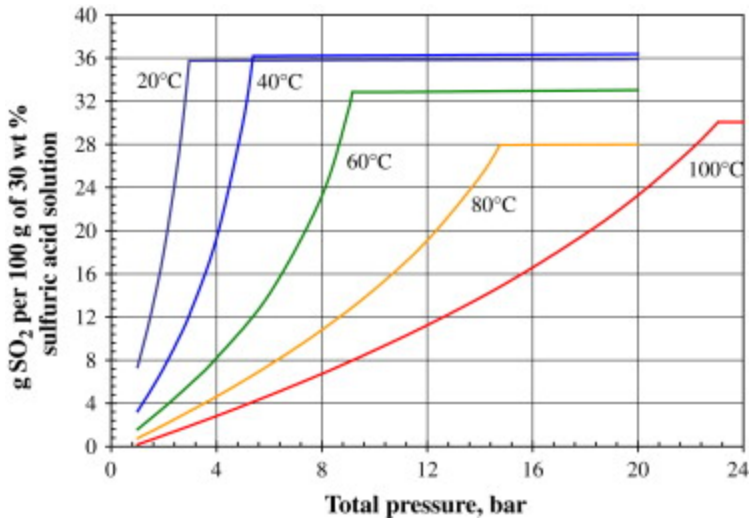

Figure 6. SO_2 solubility in $H_2SO_{4(aq)}$ as a function of system pressure (Gorensek et al., 2009).

Although the concentrations for this work and that of Gorensek were different, the same tendency of increased solubility of SO_2 as the pressure increased is shown. However, there is a saturation limit for SO_2 dissolved, reaching 28 g per 100 g of sulphuric acid solution at 14.76 bar, 80 °C and 30-wt% H_2SO_4 solution. Although this is related to the electrolyser, it is useful to see the effect of concentrated sulphuric acid directly to sulphur dioxide solubility, but one has to take into account the scale of the comparison between concentrations (30%-60% Gorensek's work, 1% for this work).

2.12 Summary

The HyS and the SI cycles pose visible advantages compared to other thermochemical cycles that are currently being developed. Both cycles show promising alternatives for the creation of pure, clean energy without harmful pollutants in the process outputs, as long as the separations carried out are safe and efficient. The efficiency of the separations will be related to the accuracy of the design data for them.

These cycles have been researched since the mid-seventies, but recently the spotlight has been focused on the sulphuric acid decomposition, which is one of the critical steps towards sustainability and efficiency gains. Even though the species at hand (sulphuric acid, sulphur dioxide, oxygen and water) are common and a vast amount of expertise has been brought by industry since the late XIX century, it is clear that better data is needed to characterize the thermodynamic system.

In this Chapter, a review on the work done on this system has been presented, along with related research for sulphur dioxide subsystems, oxygen subsystems and analysis including sulphuric acid. These all incorporate into the thermochemical cycle body of knowledge, as well as the considerations related to the process flowsheets that are necessary to understand the system at hand.

Chapter 2 References

ATKIN, I. 2009. Improvement of conversion in sulphuric acid thermal decomposition process by use of membrane separation. Ph.D., University of Sheffield.

B. YILDIZ, K.-C. C., D. MYERS, J.D. CARTER, AND H. YOU. In situ X-ray and Electrochemical Studies of the Solid Oxide Fuel and Electrolysis Cell Electrodes. Advances in Solid Oxide Fuel Cells III: Ceramic Engineering and Science Proceedings, 28(4), 153., 2007.

BADDOUR, R. F. & SELVIDGE, C. W. 1967. Catalytic and chemical properties of clean germanium surfaces. The Journal of Physical Chemistry, 71, 2536-2544.

BARBAROSSA, V., BRUTTI, S., DIAMANTI, M., SAU, S. & DE MARIA, G. 2006. Catalytic thermal decomposition of sulphuric acid in sulphur-iodine cycle for hydrogen production. International Journal of Hydrogen Energy, 31, 883-890.

BRECHER, L. E., SPEWOCK, S. & WARDE, C. J. 1977. The Westinghouse Sulfur Cycle for the thermochemical decomposition of water. International Journal of Hydrogen Energy, 2, 7-15.

BRUTTI, S., BENCIVENNI, L., BARBAROSSA, V., SAU, S. & MARIA, G. D. 2006. Gas phase dissociation of H2SO4: A computational study. The Journal of Chemical Thermodynamics, 38, 1292-1300.

CHIODO, S., RONDINELLI, F., RUSSO, N. & TOSCANO, M. 2007. On the Catalytic Role of Ge+ and Se+ in the Oxygen Transport Activation of N2O by CO. Journal of Chemical Theory and Computation, 4, 316-321.

CONNOLLY, S. M., ZABOLOTNY, E., MCLAUGHLIN, D. F. & LAHODA, E. J. 2009. Design of a composite sulfuric acid decomposition reactor, concentrator, and preheater for hydrogen generation processes. International Journal of Hydrogen Energy, 34, 4074-4087.

E. FUNK, J. 2001. Thermochemical hydrogen production: past and present. International Journal of Hydrogen Energy, 26, 185-190.

ELDER, R. & ALLEN, R. 2009. Nuclear heat for hydrogen production: Coupling a very high/high temperature reactor to a hydrogen production plant. Progress in Nuclear Energy, 51, 500-525.

ELDER, R. H., PRIESTMAN, G. H., EWAN, B. C. & ALLEN, R. W. K. 2005. The Separation of Hix in the Sulphur–Iodine Thermochemical Cycle for Sustainable Hydrogen Production. Process Safety and Environmental Protection, 83, 343-350.

EWAN, B. C. & ALLEN, R. W. K. 2005. A Figure of Merit Assessment of the Routes to Hydrogen. International Journal of Hydrogen Energy, 30, 809-819.

FUNK, J. E. 1976. Thermochemical production of hydrogen via multistage water splitting processes. Journal Name: Int. J. Hydrogen Energy; (United States); Journal Volume: 1:1, Medium: X; Size: Pages: 33-43.

GINOSAR, D. M., PETKOVIC, L. M., GLENN, A. W. & BURCH, K. C. 2007. Stability of supported platinum sulfuric acid decomposition catalysts for use in thermochemical water splitting cycles. International Journal of Hydrogen Energy, 32, 482-488.

GORENSEK, M. B., STASER, J. A., STANFORD, T. G. & WEIDNER, J. W. 2009. A thermodynamic analysis of the SO2/H2SO4 system in SO2-depolarized electrolysis. International Journal of Hydrogen Energy, 34, 6089-6095.

GORENSEK, M. B. & SUMMERS, W. A. 2009. Hybrid sulfur flowsheets using PEM electrolysis and a bayonet decomposition reactor. International Journal of Hydrogen Energy, 34, 4097-4114.

HUANG, C. & T-RAISSI, A. 2005. Analysis of sulfur-iodine thermochemical cycle for solar hydrogen production. Part I: decomposition of sulfuric acid. Solar Energy, 78, 632-646.

JEONG, Y. H., K. HOHNHOLT, M. S. KAZIMI AND B. YILDIZ. 2005. Optimization of the hybrid sulfur cycle for hydrogen generation. Nuclear Energy and Sustainability Program (NES) Technical Report: MIT-NES-TR-004. Massachusetts, NE: Center for Advanced Nuclear Energy Systems, MIT.

KIM, J., CHANG, J., PARK, B. H., SHIN, Y., LEE, K., LEE, W. & CHANG, J. 2008. A study on the dynamic behavior of a sulfur trioxide decomposer for a nuclear hydrogen production. International Journal of Hydrogen Energy, 33, 7361-7370.

KROMER, M., ROTH, K., ROSALIND, T. & CHIN, P. 2011. Support for Cost Analyses on Solar-Driven High Temperature Thermochemical Water-Splitting Cycles. In: LLC, T. (ed.). TIAX LLC.

KUBO, S., NAKAJIMA, H., KASAHARA, S., HIGASHI, S., MASAKI, T., ABE, H. & ONUKI, K. 2004. A demonstration study on a closed-cycle hydrogen production by the thermochemical water-splitting iodine-sulfur process. Nuclear Engineering and Design

Japan's HTTR, 233, 347-354.

LAHODA, E. 2010. RE: Hydrogen Plant Alternatives Study: Report on Design Readiness Levels and Design Technology Readiness Levels. September, 2007. p.321-340. Type to M.ROMERO.

LEIVA, M. A. & VIVANCO, V. 1986. Vapour-liquid equilibria of aqueous solutions containing volatile weak electrolytes by using the free energy minimization method. Fluid Phase Equilibria, 27, 483-490.

LU, P. W. T. & AMMON, R. L. 1982. Sulfur dioxide depolarized electrolysis for hydrogen production: Development status. International Journal of Hydrogen Energy, 7, 563-575.

MILLER, E., DILLICH, S., WEIL, S., BABICK, K. & STUDER, S. Hydrogen Production: R&D Challenges, Targets and Pathways. In: DOE, U. S., ed. WHEC 2012, 2012 Toronto, Ontario, Canada. WHEC 2012.

NAGARAJAN, V., PONYAVIN, V., CHEN, Y., VERNON, M. E., PICKARD, P. & HECHANOVA, A. E. 2009. CFD modeling and experimental validation of sulfur trioxide decomposition in bayonet type heat exchanger and chemical decomposer for different packed bed designs. International Journal of Hydrogen Energy, 34, 2543-2557.

NEL, B., ANTWERPEN, H. V., VENTER, L., VILJOEN, D., BRUYN, R. D., KAISER, W., PITSO, L. & WELLS, P. 2009. NGNP and Hydrogen Production Conceptual Design Study Section 10: System Integration. NGNP CTF Test Loop Preconceptual Design Report. Pittsburgh, PA: Westinghouse Electric Company LLC.

O'KEEFE, D., ALLEN, C., BESENBRUCH, G., BROWN, L., NORMAN, J., SHARP, R. & MCCORKLE, K. 1982. Preliminary results from bench-scale testing of a sulfur-iodine thermochemical water-splitting cycle. International Journal of Hydrogen Energy, 7, 381-392.

ÖZTÜRK, I. T., HAMMACHE, A. & BILGEN, E. 1995. An improved process for H2SO4 decomposition step of the sulfur-iodine cycle. Energy Conversion and Management, 36, 11-21.

PAWLIKOWSKI, E. M. & PRAUSNITZ, J. M. 1983. Estimation of Setchenow constants for nonpolar gases in aqueous solutions of common salts at moderate temperatures. Industrial & Engineering Chemistry Fundamentals, 22, 86-90.

PERRET, R. 2011. Solar Thermochemical Hydrogen Production Research (STCH). Thermochemical Cycle Selection and Investment Priority. Livermore, CA. U.S.: Sandia National Laboratories.

QUE, H., SONG, Y. & CHEN, C.-C. 2011. Thermodynamic Modeling of the Sulfuric Acid–Water–Sulfur Trioxide System with the Symmetric Electrolyte NRTL Model. Journal of Chemical & Engineering Data, 56, 963-977.

SAVITSKY, E. M., ARSKAYA, E. P., LAZAREV, E. M., KOROTKOV, N. A., VERESHAGIN, I. I. & SHAROV, I. A. 1982. Investigation of corrosion resistance of materials in the presence of sulphuric acid and its decomposition products applied in the thermochemical cycle of hydrogen production. International Journal of Hydrogen Energy, 7, 393-396.

SHAW, A., ROMERO, MOISES, ELDER, R. H., EWAN, B. C. R. & ALLEN, R. W. K. 2011. Measurements of the solubility of sulphur dioxide in water for the sulphur family of thermochemical cycles. International Journal of Hydrogen Energy, 36, 4749-4756.

SUMMERS, W. A., GORENSEK, M. B. & BUCKNER, M. R. 2005. The Hybrid Sulfur Cycle for Nuclear Hydrogen Production.

TROMANS, D. 2000. Modeling Oxygen Solubility in Water and Electrolyte Solutions. Industrial & Engineering Chemistry Research, 39, 805-812.

VITART, X., LE DUIGOU, A. & CARLES, P. 2006. Hydrogen production using the sulfur-iodine cycle coupled to a VHTR: An overview. Energy Conversion and Management, 47, 2740-2747.

Chapter 3
VLE Theoretical Background

Chapter 3.

Table of Contents

3.1 Overview

The study of equilibrium is far from theoretical-driven. A practical approach should always be sought after, as this is the force that accelerates new calculations which facilitate the separation of species. A separation is always possible, if the composition of a vapour mixture is different from the vapour coming from that pure liquid (Daubert, 1985). The greater the difference in this composition, the easier the separation; although separation may be achieved with small differences. It is therefore important to know the composition behaviours in a particular component system.

This relation is usually obtained from information related to the composition of the vapour when it is in equilibrium with the liquid. On this account, the knowledge of VLE is essential for a qualitative approach to design separation equipment. Fundamentally, any method that could produce a vapour of different composition from that of the liquid, is suitable for separation, but usually these types of equipment that include vaporization are subject to equilibrium conditions, which is a good criterion to explore separation possibilities (Clark, 2007). As mentioned in Chapters 1 and 2, in order to keep a healthy compromise between power consumption and efficiency, there must be thermodynamic data for the sulphur cycles, in order for the design equipment to operate at desired standards. There is not enough data at the moment.

There are two ways to obtain equilibrium compositions for a system, namely the experimental approach, as well as theory-based calculations. This work is concerned with both, as the two have been utilized. Although the molecular theory of equilibrium and its thermodynamics is out of the scope of this work, nevertheless it is necessary to outline the basic principles that surround these phenomena. These key concepts are concisely described below, and are mostly taken from the fluid phase equilibria chapter in the seminal work by Reid, Prausnitz and Sherwood (Prausnitz et al., 1986a), and parameters relevant to the SO_2, O_2 and water species from Shaw (2008a), along with the methodology adapted from Zemaitis (1986).

3.2 The equilibrium condition

When one takes a first look at the criteria of modelling, the first guess would have to be the approximate gaseous solubility in a liquid. In certain conditions, this is well predicted by Henry's Law. One simple definition of the Henry's Law is that the solubility of a gas in a liquid solution is directly proportional to its partial pressure. This is not widely applicable, however, successful at predicting a first guess for simple mixtures. Some corrections can be made to the equations, in order to account for non idealities, and then enhance accuracy.

It is important to mention that as the pressure increases, the non-ideal behaviour in the gas phase also increases. In order to correct for these deviations, some special considerations need to be taken into account, and it is the same case for an increasing concentration in relation to activity coefficients in the liquid. Up to higher pressures, and the Krichevsky-Kasarnovsky term, also known as the "Poynting Term", must be added to the calculations to correct deviations on the liquid phase reference fugacities (Krichevsky and Kasarnovsky, 1935).

The result is the 'ensemble' Henry's law. It is applicable for non-reacting binary systems over the entire range of composition. Further, if the phase equilibrium equations are coupled with a reaction equilibrium model, then even systems involving chemical reactions can be handled. It is reported that the ensemble form includes no simplifying assumptions and is even valid near the critical point of the solvent (Carroll, 1991).

$$\gamma_i x_i H_{ij} \exp\left[\int_{p_j^0}^{p}\left(\frac{v_j^{-\infty}}{RT}\right)dP\right] = y_i \hat{\varphi}_i P \qquad \text{Equation 1}$$

Where:

x_i Liquid phase mole fraction

y_i Gas phase mole fraction

γ Liquid phase activity coefficient, non-dimensional

$\widehat{\varphi}_i$ Gas phase fugacity coefficient of component in solution, non-dimensional

H_{ij} Henry's Constant for solute *i* in solvent *j*, atm· kg/mol

P Pressure, atm

R Gas Constant, cm^3·atm/mole K

T Temperature, Kelvin

$v_j^{-\infty}$ Partial molar volume at infinite dilution, dm^3/mole

In equation 1, the liquid phase potential is represented on the left hand side and is equated with the gas phase potential represented on the right. The equation is a realisation of the thermodynamic concept which states that the vapour-liquid equilibrium means the chemical potential of any species *i* in phase '*a*' is equal to the chemical potential of that same species in phase '*b*', denoted below.

$$\mu_{i,a} = \mu_{i,b} \qquad \text{Equation 2}$$

Now that an equation describing vapour liquid equilibrium has been outlined it is necessary to explore some thermodynamics of fluid phase equilibria to bring meaning to the terms in the equation. In doing so the other modelling topics highlighted in the introduction to this chapter will be covered and a set of equations developed for full description of weak electrolyte vapour liquid equilibria.

3.2.1 Gibbs fundamental Equation

According to Malanowski and Anderko (1992), *equilibrium* will be defined as:

"the state in which the thermodynamic variables of the system are independent of time".

A system tends spontaneously to this state, although some systems take considerably longer to achieve equilibrium than others. It is important to remember that the variables required to describe equilibrium are always less than the representing variables of that of a non-equilibrium state: as an example, a pure gas in equilibrium would be described by any two of these: pressure, temperature and volume. This same gas experiencing non-equilibrium conditions would require two gradients (e.g., temperature or pressure).

In this case, to clarify how important measurable conditions are to equilibrium, the phenomenological definition of entropy of phase α in its differential form must be introduced:

$$TdS^{(\alpha)} = dU^{(\alpha)} + PdV^{(\alpha)} - \sum_{j=2}^{l} Y_j^{(\alpha)} dy_j^{(\alpha)} + \sum_{i=1}^{n} \mu_i dN_i^{(\alpha)} \qquad \text{Equation 3}$$

Which is derived from the explicit equation for internal energy

$$U^{(\alpha)} = U^{(\alpha)}(S^{(\alpha)}, V^{(\alpha)}, y_2^{(\alpha)}, \ldots, y_i^{(\alpha)}, N_1, \ldots, N_n) \qquad \text{Equation 4}$$

in its *energetic representation*; where $S^{(\alpha)}$ is a function of the variables of state $U^{(\alpha)}$, the internal energy of phase *i*, its volume $V^{(\alpha)}$, additional work coordinates ($y_i^{(\alpha)}$ for *I* generalized forces $Y_j^{(\alpha)}$, and the number of moles ($N_i^{(\alpha)}$) of each of n different components. This is called the Gibbs fundamental equation, and it is applicable for reversible and irreversible processes. This equation can also be used for open (non isolated) systems, but this property will not be used in this work, as the

experimental conditions mentioned in Chapter 5 are carefully approximated to adiabatic parameters.

This Gibbs equation is called a *characteristic function* as it contains all the thermodynamic information about the system, such as heat capacities, temperature, pressure and chemical potential of each component, in a form that can be measured directly. Interestingly, the fundamental equation represents a surface in a *(n+/+1)-dimensional* space (Malanowski and Anderko, 1992), where a point represents an equilibrium of the system, and this form is almost exclusively used in phase equilibrium thermodynamics. The intensive parameters of interest are the following:

Temperature (T)

$$\left(\frac{\partial U}{\partial S}\right)_{V,N} = T \qquad \text{Equation 5}$$

Pressure (P)

$$\left(\frac{\partial U}{\partial V}\right)_{S,N} = -P \qquad \text{Equation 6}$$

Chemical Potential of species μ_i

$$\left(\frac{\partial U}{\partial N_i}\right)_{V,S,N_{j\neq i}} = \mu_i \qquad \text{Equation 7}$$

Further delving into the different mathematical relationships between thermodynamic functions and variables are out of the scope of this work, but it is strongly recommended to look at the work by Smith & Van Ness, an introductory textbook on thermodynamics (Smith and Van Ness, 1996), as well as the useful Appendix A of thermodynamic relationships by Maxwell relevant to closed systems by Prausnitz (1986b), included in Shaw's doctoral dissertation (Shaw, 2008a).

Although chemical potential is not directly measured (as a consequence of the definition considered above), it is important to state that it is involved in the condition of

equilibrium. Chemical potential is a fundamental property relationship for single systems, fixed or variable mass or composition respectively. According to Daubert (1985), the change in any property can be calculated using partial molar properties. It is important to mention that the chemical potential and the partial molal Gibbs free energy (a partial molar property) are equal. This has consequences that will be explained in the following section.

3.3 Non idealities: Activity and Fugacity

3.3.1 Gas Fugacity and the Fugacity coefficient

G.N.Lewis introduced the concept of fugacity to include a real behaviour of free-energy changes in an isothermal gas, and it relates three key variables: the Gibbs free energy, the chemical potential, and the fugacity, for any component of a mixture.

$$[dG_i = d\mu_i = RTd(\ln \overline{f}_i)]_T \qquad \text{Equation 8}$$

Where *P* was replaced by *f* to correct for real behaviour in the gas. It is generally agreed that the fugacity of a pure component in the ideal state must be equal to the system's pressure, in other words,

$$\text{as } P \to 0\text{, the ratio is } f / P = 1 \therefore$$

If equation 8 is integrated between any state *f* and the ideal-gas state *f**, and then combined with the definition of Gibbs free energy, we obtain equations for non-idealities in a solution for *i* components (Prausnitz et al., 1986b). It is important to introduce the fugacity coefficient, (valid for both gas and liquid phases), which is the ratio of the fugacity of a pure component against its pressure;

$$\varphi_i = \frac{f_i}{P_i}\text{, equally showing that as } P \to 0\text{, } \varphi \to 1$$

Fugacity has units of pressure, therefore the fugacity coefficient is dimensionless. P_i is equal to the total pressure for a one component system, and for

mixtures, it is equal to the sum of partial pressures of the components in the gas phase. Since this coefficient is dimensionless, it is easier to predict than fugacity for generalized methods. Two methods are available to predict fugacity coefficients; corresponding states techniques and analytical equation of states.

Analytical equations of state include equations such as the van der Waals equation, Benedict Webb Rubin type of equations, Redlich-Kwong, Soave's modifications and so on. A review of these equations was performed by Lin and Daubert (1978). On the other hand, the corresponding states EOS are the domain of Lydersen and Prausnitz (Reid et al., 1987), where computers are generally used for subroutines and graphical acquisition of coefficients. Finally, Smith & Van Ness (1996) include worked examples in their work, whereas Daubert (1985) gives further example calculations for fugacity coefficient calculation.

3.3.2 Molality

Literature suggests using the molal scale, which is the amount of component *i* in moles, dissolved in kilograms of solvent (not solution!). In the case of aqueous solutions, *n* moles divided by 1000 grams of water. This is the relevant scale in this work, as we're dealing with aqueous electrolyte solutions. If polymer solutions or normal non-electrolyte solutions are addressed, volumetric forms or simple molar fraction would be suitable. Data acquired in literature usually needs to be converted from one scale to another.

3.3.3 Gibbs Free Energy Change at Equilibrium

The free-energy change of the entire system at equilibrium must remain cero, but not only that, it also aids in the approximation of liquid or solid fugacities from vapour fugacities:

$$\Delta G_{T,P,eq.} = RT \ln \frac{f_{vap}}{f_{liq}} = 0 \qquad \text{Equation 9}$$

, therefore

$$f_i^V = f_i^L \qquad \text{Equation 10}$$

which is derived for multicomponent systems. The fundamental problem is to relate these properties to mixture compositions, since compositions are necessary to provide information about the thermodynamic state of the system. For purposes of simplification, negligible effects brought upon by surface forces, electromagnetic fields, nuclear or gravitational forces or semi-permeable membranes, are ignored.

At low pressures, as stated, one would suspect to find the fugacity coefficient conveniently approximated as 1; but how low? "Low" will depend on the nature of the mixture, its composition and temperature. Typical mixtures of non-polar (or slightly polar) components could be set as "ideal" below a couple of atmospheres. However, molecular repulsion or strongly associating compounds make fugacity coefficients differ appreciably from unity even at pressures less than one atmosphere.

Since high pressures are involved in the separation of species inside the sulphur family of thermochemical cycles, non-idealities need to be taken into account if accurate representation of the system is to be achieved.

3.3.4 Activity Coefficient

The fugacity of a component *i* in the liquid is related to the composition of that phase via the activity coefficient γ_i. The activity coefficient γ_i is related to the mole fraction in the liquid x_i, and the standard state fugacity f°, which is arbitrarily selected but associated with a unique combination of pressure and composition, at the system's temperature:

$$\gamma_i \equiv \frac{a_i}{x_i} = \frac{f_i^L}{x_i f_i^\circ} \qquad \text{Equation 11}$$

It is vital to remember that both the activity and the activity coefficient are meaningless, unless the standard state fugacity is clearly specified. It is also important to mention that the activity coefficient is inextricably linked with the Gibbs free energy.

3.3.5 Approaches for Activity Coefficient Calculation

A table presenting a basic compilation of the models relating activity coefficients and Gibbs free-energy is shown below, containing the different equations used for this purpose. The compilation is taken from the work by Reid, Prausnitz and Sherwood, and it is relevant for binary systems. Multi-component equations can be

derived from these sets of models. This only represents an overview, further reading is strongly recommended [see work by Warn (1996) and Prausnitz (1986a)]. Note these are for binary, non-dissociating systems.

Table 1. Models for Excess Gibbs Energy and subsequent activity coefficients (Binary systems)

Name	Gibbs Free Energy	Binary Parameters	$\ln \gamma_1$ and $\ln \gamma_2$
Two-suffix Margules	$g^E = Ax_1x_2$	A	$RT \ln \gamma_1 = Ax_2^2$ $RT \ln \gamma_2 = Ax_1^2$
Three-suffix Margules	$g^E = x_1x_2[A + B(x_1 - x_2)]$	A B	$RT \ln \gamma_1 = (A + 3B)x_2^2 - 4Bx_2^3$ $RT \ln \gamma_2 = (A - 3B)x_1^2 + 4Bx_1^3$
Van Laar	$g^E = \frac{Ax_1x_2}{x_1(A/B) + x_2}$	A B	$RT \ln \gamma_1 = A\left(1 + \frac{Ax_1}{Bx_2}\right)^{-2}$ $RT \ln \gamma_2 = B\left(1 + \frac{Bx_2}{Ax_1}\right)^{-2}$
Wilson	$\frac{g^E}{RT} = -x_1 \ln(x_1 + \Lambda_{12}x_2) - x_2 \ln(x_2 + \Lambda_{21}x_1)$	Λ_{12} Λ_{21}	$\ln \gamma_1 = -\ln(x_1 + \Lambda_{12}x_2) + x_2\left(\frac{\Lambda_{12}}{x_2 + \Lambda_{12}x_2} - \frac{\Lambda_{21}}{\Lambda_{21}x_1 + x_2}\right)$ $\ln \gamma_2 = -\ln(x_2 + \Lambda_{21}x_1) - x_1\left(\frac{\Lambda_{12}}{x_1 + \Lambda_{12}x_2} - \frac{\Lambda_{21}}{\Lambda_{21}x_1 + x_2}\right)$

Four-suffix Margules	$g^E = x_1 x_2 [A + B(x_1 - x_2) + C(x_1 - x_2)_2]$	A B C	$RT \ln \gamma_1 = (A + 3B + 5C)x_2^2 - 4(B + 4C)x_2^3 + 12Cx_2^4$ $RT \ln \gamma_2 = (A - 3B + 5C)x_1^2 - 4(B - 4C)x_1^3 + 12Cx_1^4$
NRTL[1]	$\frac{g^E}{RT} = x_1 x_2 \left(\frac{\tau_{21} G_{21}}{x_1 + x_2 G_{21}} + \frac{\tau_{12} G_{12}}{x_2 + x_1 G_{12}} \right)$ where $\tau_{12} = \frac{\Delta g_{12}}{RT}$ and $\tau_{21} = \frac{\Delta g_{21}}{RT}$ $\ln G_{12} = -\alpha_{12} \tau_{12}$ and $\ln G_{21} = -\alpha_{12} \tau_{21}$	Δg_{12} Δg_{21} α_{12}	$\ln \gamma_1 = x_2^2 \left[\tau_{21} \left(\frac{G_{21}}{x_1 + x_2 G_{21}} \right)^2 + \frac{\tau_{12} G_{12}}{(x_2 + x_1 G_{12})^2} \right]$ $\ln \gamma_2 = x_1^2 \left[\tau_{12} \left(\frac{G_{12}}{x_2 + x_1 G_{12}} \right)^2 + \frac{\tau_{21} G_{21}}{(x_1 + x_2 G_{21})^2} \right]$
UNIQUAC[2]	$\frac{g^E{}_{(combinatorial)}}{RT} = x_1 \ln \frac{\varphi_1}{x_1} + x_2 \ln \frac{\varphi_2}{x_2} + \frac{z}{2} \left(q_1 x_1 \ln \frac{\theta_1}{\varphi_1} + q_2 x_2 \ln \frac{\theta_2}{\varphi_2} \right)$ $g^E = g^E{}_{(combinatorial)} + g^E{}_{(residual)}$ $z = 10$ $\frac{g^E{}_{(residual)}}{RT} = -q_1 x_1 \ln[\theta_1 + \theta_2 \tau_{21}] - q_2 x_2 \ln[\theta_2 + \theta_1 \tau_{12}]$ $7\ \varphi_1 = \frac{x_1 r_1}{x_1 r_1 + x_2 r_2}$ $\theta_1 = \frac{x_1 q_1}{x_1 q_1 + x_2 q_2}$	Δu_{12} Δu_{21}	$\ln \gamma_i = \ln \frac{\varphi_i}{x_1} + \frac{z}{2} q_i \ln \frac{\theta_i}{\varphi_i} + \varphi_j (\ell_i - \frac{r_i}{r_j} \ell_j)$ $-q_i \ln(\theta_i + \theta_j \tau_{ji}) + \theta_j q_i \left(\frac{\tau_{ji}}{\theta_i + \theta_j \tau_{ji}} - \frac{\tau_{ij}}{\theta_j + \theta_i \tau_{ij}} \right)$ Where $i = 1$, $j = 2$ $\ell_i = \frac{z}{2}(r_i - q_i) - (r_i - 1)$ or $i = 2$ $j = 1$ $\ell_i = \frac{z}{2}(r_j - q_j) - (r_j - 1)$

[1] Non-Random Two Liquid (see the chapter on Free Energy Calculations by Prausnitz for most of the equations above).
[2] Universal Quasi Chemical. See work by Abrams & Prausnitz. Note that these are non-electrolyte models, with no phase dissociation.

Once these definitions have been described, one final practical aspect of phase equilibria must be introduced before crossing to electrolyte modelling choices, which is gas solubility.

3.4 Solubility of Gases

As Battino and Clever explain (1966), gas solubilities can be expressed in many ways, but the most popular will be presented, as they have been the standard for almost half a century.

3.4.1 The Bunsen coefficient α

This coefficient α

$$\alpha = \left[\left(V_g \frac{273.15}{T}\frac{P_g}{760}\right)\left(\frac{1}{V_s}\right)\right]\left(\frac{760}{P_g}\right) \qquad \text{Equation 12}$$

where α V_g is the volume of gas absorbed, T is in K, P_g is the partial pressure of the gas, and V_s is the solvent's volume. The equation above could be simplified further when the liquid pressure is non-negligible (Battino and Clever, 1966).

3.4.2 The Ostwald Coefficient L

The Ostwald coefficient is defined as the relationship between the volume of gas absorbed and the volume of solvent absorbing, g and s standing for its corresponding gaseous or solvent phase. Note absorption and adsorption are not to be confused.

$$L = V_g / V_s$$ Equation 13

3.4.3 The weight solubility

This number, recommended by Cook and mentioned by Battino's review (Battino and Clever, 1966) is defined as the moles of gas that, at a partial pressure of 760 mm Hg per gram of solvent. Since this is a ratio of weights, makes some calculations easier, and should be explored to obtain "trench" calculations.

3.4.4 Henry's Law Constant

Although the approach to use the Henry's Law Constant is tempting for its simplicity, it has no real theoretical deduction and therefore, it is only a macroscopic approximation of the system at hand. Although this clearly lacks a molecular theory foundation, one of the main advantages of this rule is its simplicity, very practical for first guesses. In the simplest version, stating that the partial pressure of the gas is the product of concentration of solute and a proportionality constant, viz, the Henry's constant, particular for a unique system.

$$p_i = k_H c$$ Equation 14

It is significant to mention that the Henry's constant is strongly dependent on temperature.

3.5 Reacting Equilibrium: Electrolytes

3.5.1 Phase and Chemical Equilibrium

With volatile species equilibria that dissociate, we have two types of equilibrium: phase equilibrium and chemical equilibrium. Phase equilibrium is usually achieved by the already mentioned condition, the equivalence of chemical potential. For

chemical equilibrium, it is the reaction rate constants that act as the key element to account for dissociations and concentrations of ions in the liquid, and it's even applicable for gases in theory. With these axioms outlined, the approach to account for phase and chemical equilibrium needs to be met. Work by Shaw included the ensemble Henry equation (Shaw, 2008a), which uses the aqueous electrolyte thermodynamic methodology developed by the seminal work of Zemaitis and coworkers (1986) to calculate reaction constants, activity and fugacity coefficients. However, as the reactions get more complicated, other approaches need to be explored. In current literature, there are three ways to tackle chemical and phase equilibria.

3.6 Approach to Equilibrium Calculations

3.6.1 Reaction Constant Calculation

In this section, consideration will be given to some fundamental thermodynamics and the dissociation of gas molecules dissolved in the liquid phase. The derivation of equations is taken from the work by Leiva (1986). The dissociation of a portion of molecules into ions is a characteristic of weak electrolytes, for a strong electrolyte most if not all molecules are ionised. For a chemical or ionic equilibrium occurring in aqueous solution the reaction can be represented thus

$$aA + bB \rightarrow cC + dD \qquad \text{Equation 15}$$

The condition of chemical or ionic equilibrium in a particular phase would be denoted by

$$a\mu_a + b\mu_b = c\mu_c + d\mu_d \qquad \text{Equation 16}$$

The chemical potential, μ_i, does not have an immediate equivalent in the physical world and it is therefore desirable to express it in terms of some auxiliary function which might be easily identified with physical reality. The basic relationship between activity and chemical potential was developed by G.N. Lewis who first

established a relationship for the chemical potential of a pure ideal gas, and then generalised his result for all systems to define the chemical potential of species *i* in terms of its activity a_i. The following paragraphs show the derivation of this function.

The chemical potential, μ_i, can be expressed as a derivative of an extensive property with respect to the amount of component under consideration, one such derivative involves the fundamental grouping Gibbs free energy; G, Temperature; T and Pressure; P, Equation 17.

$$\mu_i = \left(\frac{\partial G}{\partial n_i} \right)_{T,P,n_j} = \bar{G}_i \qquad \text{Equation 17}$$

μ_i is defined as the partial molar Gibbs free energy because the independent variables T and P, which are arbitrarily chosen in defining partial molar quantities, are also the independent variables for Gibbs free energy (Prausnitz, 1969). Equation 18 is the fundamental thermodynamic relationship of Gibbs energy for a homogeneous closed system. To begin with this simple case is sufficient in which S denotes entropy and V volume.

$$dG = -SdT + VdP \qquad \text{Equation 18}$$

Absolute chemical potential cannot be computed, only changes accompanying an arbitrary change in the independent variables; temperature, pressure and composition. It arises because relations between chemical potential and physically measurable quantities are often in the form of differential equations which, upon integration, give only differences. One such differential equation is given by differentiation of Equation 19 with respect the number of moles of *i*, n_i, which yields,

$$d\mu_i = -s_i dT + v_i dP \qquad \text{Equation 19}$$

Where s_i is the molar entropy and v_i is the molar volume. From Equation 19 it can be shown that the following relation is true

$$\left(\frac{\partial \mu_i}{\partial P}\right)_T = v_i \qquad \text{Equation 20}$$

and in Equation 19 v_i can be substituted for; using the ideal gas equation.

$$v_i = \frac{RT}{P} \qquad \text{Equation 21}$$

After substitution, integration at constant temperature results in

$$\mu_i - \mu_i^0 = RT \ln\frac{P}{P^0} \qquad \text{Equation 22}$$

Equation 22 shows that at constant temperature the change in abstract thermodynamic quantity μ is a simple logarithmic function of the physically real quantity, pressure. However is only valid for pure ideal gases, in order to generalise it Lewis defined a function *f* called the fugacity. For a pure ideal gas the fugacity is equal to the pressure at that temperature. For a component *i* in a mixture of ideal gases it is equal to the partial pressure, y_iP, where y_i is the mole fraction of *i*. An isothermal change for any component in any system was now described by

$$\mu_i - \mu_i^0 = RT \ln\frac{f}{f^0} \qquad \text{Equation 23}$$

In an important step to generalise this result to all phases Lewis called the ratio f/f^0 the activity, which is given the symbol a_i.

$$\mu_i(T) = \mu_i^o(T) + RT\ln(a_i) \qquad \text{Equation 24}$$

Here μ_i^o is a reference chemical potential or the standard chemical potential at an arbitrarily chosen standard state. The activity is a measure of the difference between the components chemical potential at the state of interest and at its standard state. In terms of the fugacity this can be denoted by the equation

$$a_i\left(T,\ P,\ m\right) \ = \ \frac{f_i\left(T,\ P,\ m\right)}{f_i\left(T,\ P^0,\ m^0\right)} \qquad \text{Equation 25}$$

Where P^0 is the standard state pressure and m^0 is the standard state composition. Now we will introduce the activity coefficient γ_i as the ratio of the activity of *i* to some convenient measure of concentration of *i*. Equation 26 gives this relationship where the measure of concentration is taken to be the molality. Thus as the chemical potential of component *i* approaches the chemical potential of itself at its arbitrarily chosen standard state, the activity approaches unity.

$$\gamma_i \ = \ a_i \big/ m_i \qquad \text{Equation 26}$$

There are two types of ideality for liquid phases, Raoult's law and Henry's law, which means that there are two methods for normalising the activity coefficient. For aqueous solutions in which the composition of the solution is expressed in terms of molality, the activity coefficients are defined with reference to an ideal dilute solution which leads to the familiar relation known as Henry's law. This means that as the molality of the solute *i* approaches zero, the ratio of $a_i \big/ m_i$ tends to unity.

$$\gamma_1 \to 1 \ \ as \ \ m_1 \to 1 \ \ \ (solvent)$$
$$\gamma_2 \to 1 \ \ as \ \ m_2 \to 0 \ \ (solute)$$

Equation 24 can now be expressed in terms of the activity coefficient and the molality as follows.

$$\mu_i \ = \ \mu_i^o \ + \ RT \ln\left(\gamma_i m_i\right) \qquad \text{Equation 27}$$

Now the general expression for the equilibrium, Equation 16, can be expanded in terms of the relationship for activity and chemical potential to yield

$$a\left(\mu_A^o + RT\ln\left(\gamma_A m_A\right)\right) + b\left(\mu_B^o + RT\ln\left(\gamma_B m_B\right)\right) = c\left(\mu_C^o + RT\ln\left(\gamma_C m_C\right)\right) + d\left(\mu_D^o + RT\ln\left(\gamma_D m_D\right)\right)$$ Equation 28

By combining terms and simplifying.

$$a\mu_A^o + b\mu_B^o - c\mu_C^o - d\mu_D^o = RT\left(c\ln\left(\gamma_C m_C\right) + d\ln\left(\gamma_D m_D\right) - a\ln\left(\gamma_A m_A\right) - b\ln\left(\gamma_B m_B\right)\right)$$

or

$$a\mu_A^o + b\mu_B^o - c\mu_C^o - d\mu_D^o = RT\ln\frac{\left(\gamma_C m_C\right)^c\left(\gamma_D m_D\right)^d}{\left(\gamma_A m_A\right)^a\left(\gamma_B m_B\right)^b}$$ Equation 29

Recalling that μ_i^o is the standard chemical potential at an arbitrary chosen standard state and that the partial molar Gibbs free energy is also defined as chemical potential, $\bar{G}_i^o(T)$ can be substituted for $\mu_i^o(T)$. Tabulations of partial molar Gibbs free energy are available. These are given in the form of tabulations of ΔG_f^o for a substance. $\Delta G_{f_i}^o$ represents the free energy when one gram-formula weight of the substance *i* is formed isothermally from the constituent elements each in their appropriate reference state. It can be shown that $\Delta G_{f_i}^o$ is a valid form of $\bar{G}_i^o$ and since the left hand side of Equation 16 can be represented by

$$a\bar{G}_A^o + b\bar{G}_B^o - c\bar{G}_C^o - d\bar{G}_D^o$$ Equation 30

Substitution can be made to give

$$a\Delta G_{f_A}^o + b\Delta G_{f_B}^o - c\Delta G_{f_C}^o - d\Delta G_{f_D}^o$$ Equation 31

From Equations 30 & 31 the thermodynamic equilibrium constant, K_T, for this reaction can be defined as

$$K_T = \exp\left\{\left[a\Delta\bar{G}_{f_A}^o + b\Delta\bar{G}_{f_B}^o - \left(c\Delta\bar{G}_{f_C}^o + d\Delta\bar{G}_{f_D}^o\right)\right]/RT\right\}$$ Equation 32

And thus the complete expression for the equilibrium is given by

$$K_T = \frac{\left(\gamma_C m_C\right)^c \left(\gamma_D m_D\right)^d}{\left(\gamma_A m_A\right)^a \left(\gamma_B m_B\right)^b} \qquad \text{Equation 33}$$

This is an important derivation since it means that from Equation 31 a value for K_T can be determined for a particular reaction. Therefore, a unique expression in terms of molalities and activities for each component taking part in the reaction has been found. This can then be used as part of a set of equations, solved simultaneously, to help find the equilibrium conditions of a system.

Since the equilibrium constants in the equations described above have temperature dependence complete description of this topic warrants further discussion. The standard free energy change for reaction is defined as

$$\Delta G^o_{RXN}\left(T\right) = c\Delta G^o_{f_C}\left(T\right) + d\,\Delta G^o_{f_D}\left(T\right) - \left(a\Delta G^o_{f_A}\left(T\right) + b\Delta G^o_{f_B}\left(T\right)\right) \qquad \text{Eq. 34}$$

This can be written in a simplified form for the general case

$$\Delta G^o_{RXN}\left(T\right) = \sum_i v_i \Delta G^o_{f_i}\left(T\right) - \sum_j v_j \Delta G^o_{f_j}\left(T\right) \qquad \text{Equation 35}$$

Where *i* represent products and *j* represents reactants and *v* is the stoichiometric coefficient. Combining Equation 33 and Equation 35 the equilibrium constant K_T is now given by

$$K_T = \exp\left(-\Delta G^o_{RXN}\left(T\right)/RT\right) \qquad \text{Equation 36}$$

Differentiation of Equation d gives

$$R\frac{d\ \ln K_T}{dT} = \frac{d\left(\Delta G^o\left(T\right)/T\right)}{dT} \qquad \text{Equation 37}$$

In a closed system the fundamental thermodynamic relationship of Equation 37 applies where G is a function $G = G(T, P)$; however in an open system there are additional independent variables. The mole numbers of the various species present can be used to represent these independent variables and the Gibbs Free Energy must now be considered as a function of the form, $G = G(T, P, n_1, n_2 \ldots\ldots n_m)$ where m is the number of species. The total differential becomes

$$dG = \left(\frac{\partial G}{\partial T}\right)_{P,\, n_i} dT + \left(\frac{\partial G}{\partial P}\right)_{T,\, n_i} dP + \left(\frac{\partial G}{\partial n_i}\right)_{P,\, T,\, n_j} dn_i \qquad \text{Equation 38}$$

Since the first two derivatives of Equation 38 refer to a closed system the identities resulting from the fundamental thermodynamic equations, given in equation 18 can be substituted for.

$$dG = -SdT + VdP + \sum_i \mu_i dn_i \qquad \text{Equation 39}$$

At constant pressure and composition the following is true

$$\frac{\partial}{\partial T}\left(\frac{\Delta G^o}{T}\right) = \frac{d}{dT}\left(\frac{\Delta G^o}{T}\right) \qquad \text{Equation 40}$$

Equation 40 can be restated using the thermodynamic equation 41 to give Equation 42.

$$\left(\frac{\partial G/T}{\partial T}\right)_P = -\frac{H}{T^2} \qquad \text{Equation 41}$$

$$R\frac{d \ln K}{dT} = \frac{\Delta H}{T^2} \qquad \text{Equation 42}$$

ΔH can be expressed as a function of temperature in terms of heat capacity, C_p

$$\Delta H = \Delta H^o + \int \Delta Cp^o dT$$

Assuming constant ΔCp

$$\Delta H = \Delta H^o + \Delta Cp^o \left(T - T^o \right)$$ Equation 43

Combining 42 and 43

$$R \frac{d \ln K}{dT} = \frac{\Delta H^o}{T^2} \Delta Cp^o \left(\frac{1}{T} - \frac{T^o}{T^2} \right)$$ Equation 44

Finally integrating between the limits of reference temperature, T^o and T the solution is

$$\ln K = \ln K^o - \frac{\Delta H^o}{R} \left(\frac{1}{T} - \frac{1}{T^o} \right) - \frac{\Delta Cp^o}{R} \left(\ln \frac{T}{T^o} - \frac{T^o}{T} + 1 \right)$$ Equation 45

or

$$\ln K - \ln K^o = -\Delta H^o \left(\frac{1}{RT} - \frac{1}{RT^o} \right) - \frac{\Delta Cp^o}{R} \left(\ln T - \frac{T^o}{T} - \ln T^o + 1 \right)$$ (46)

Restating Equation 46, $\ln K = -\frac{\Delta G^o}{RT}$, the solution becomes

$$\ln K = \left(-\frac{\Delta G^o}{RT^o} \right) - \frac{\Delta H^o}{R} \left(\frac{1}{T} - \frac{1}{T^o} \right) - \frac{\Delta Cp^o}{R} \left(\ln \frac{T}{T^o} - \frac{T^o}{T} + 1 \right)$$ Eq. 47

This is the desired definition of a temperature dependent equilibrium constant, K. The assumption of constant heat capacity can be modified by substituting a heat capacity as a function of temperature, Cp(T), into 46.

The usefulness of Equation 47 in predicting the temperature dependence of K is that ΔG^o, ΔH^o and ΔCp^o are tabulated for a great many species. The result of this means that equilibrium constants can be defined for any temperature for each reaction. The constants can be used with Equation 36, restated below, to form an equation in terms of activity coefficients and molalities of each species

$$K_T = \frac{(\gamma_C m_C)^c (\gamma_D m_D)^d}{(\gamma_A m_A)^a (\gamma_B m_B)^b}$$ Equation 48

3.7 Gibbs Free Energy Minimization Technique

A gas-liquid system tending towards thermodynamic equilibrium, at a set of fixed state variables such as pressure and temperature, the Gibbs free energy is represented as

$$G = \sum_i \mu_i N_i$$ Equation 49

Where the chemical potential for the gas phase is

$$\frac{\mu}{p} = V_m$$ Equation 50

Because ions are not in the volatile gas phase, the sole species present in the vapour phase are H_2O and the electrolytes in molecular form. The fugacity of these electrolytes is described with the equation

$$\bar{G}i - \bar{G}_i^0 = \mu_i - \mu_i^0 = RT \ln\left[\frac{\hat{f}_i}{\hat{f}_i^0}\right]$$ Equation 51

And the coefficient of fugacity is calculated by the Nakamura routine (1976). The liquid phase can be represented by three components: the ions, the molecules and water itself. For each of these species, the chemical potential can be formulated as

$$\mu_i - \mu_i^0 = \int_{P_{low}}^{P} \bar{V}_i dP = RT \ln\left[\frac{\hat{f}_i}{y_i P_{tot}}\right]$$ Equation 52

In these equations, 51 and 52 are the reference free energy formation of the i^{th} component, at reference conditions (systems temperature, but atmospheric pressure) compon G° are contained in the HSC Chemistry package.

In the case of the liquid phase fugacity, for each of the components, the equation relevant is

$$\mu_i - \mu_i^0 = RT \ln\left[\frac{\widehat{f}_i}{f_i^0}\right] \qquad \text{Equation 53}$$

Where the water fugacity in its reference state, f(i) is given by

$$\widehat{f}_w = \gamma_w f_w^0 (1-x)\delta_w \qquad \text{Equation 54}$$

And is the fugacity coefficient at saturation of water at the system's temperature. Similarly, the parameter is calculated using the model of Nakamura (1976), and the partial molar volume of water $v_{(w)}$ is calculated using the HSC database data interpolation, and the saturation pressure of water at the system's temperature from Edwards (1974). As for the Henry's constant, from the Antoine equation (Reid et al. 1976), whose dependence with pressure is

$$\log_{10} p = A - \frac{B}{C+T} \qquad \text{Equation 55}$$

Where A is related to the partial molar volume of the solute in molecular form at infinite Solution, taken from the Brelvi and O'Connell relation (1972); this rather simple calculation is obtained from Edwards et al. (1978) and done automatically in the HSC program.

The water activity (a,) and the activity coefficient (α) are calculated from the thermodynamical model constructed by Edwards et al. (1978), with the interaction parameters regressed from the HSC program, and with the Debye-Huckel parameters reported in Chen et al. (1979). When not available, they are considered to be zero. Further, a set of revised parameters was published by Maurer (1980), and the extension for this work's SO_2-O_2 system was presented by Shaw (2008b), where this methodology is taken from.

3.7.1 Gibbs Procedural calculation

The approximation of the aqueous solution vapour liquid equilibrium, with reaction rates of electrolytes included from a set of operating conditions: temperature, pressure and initial compositions is performed using the Gibbs Free Energy algorithm bound in HSC chemistry, as proposed by Thomsen and Rasmussen (1996).

The convergence to minimization using Lagrangian multipliers, once initial guesses of composition in each phases are made, is achieved and equilibrium is approximately represented using thermodynamic relations. The sequence that is followed is this:

1. Assuming that there is no chemical reaction in the aqueous solution, a VLE calculation is performed. This calculation allows us to guess the molar composition of the molecular species approximately in each of the phases.

2. Once an initial approximation is set, containing the number of moles of the molecular solutes in the aqueous solution, the molality can be determined. Further, the ionic species formation is proposed by the partial dissociation of molecular electrolytes. Using the reaction rate equilibrium constants, calculated from the free energy of formation and using the equations of mass balance and electroneutrality, the molar composition of the ions and the molecular species in the mixture are calculated. The algorithm is carried out separating the reaction between each phase, and then doing the material balances to normalize numbers and achieve convergence.

3. The number of moles of each species in the vapour phase, undissociated, and the known mole numbers of the ions and undissociated molecules in the solution are then solved as simultaneous iterations. The sequence is performed for the electrolyte system, depending on the number of desired steps and temperature or pressure ranges. This is set in the options panel in HSC Chemistry. Calculations were performed from 25 to 80 °C, and these are all presented in next chapter.

3.8 Summary

In this chapter, the theoretical foundations needed for the interpretation of vapour liquid equilibria have been briefly explained, with particular focus on the Gibbs Free Energy minimization technique, along with activity coefficient models that are worth knowing due to their importance in industry, and finally the thermodynamic relations that are fundamental for the comprehension of vapour-liquid equilibrium in multicomponent systems.

It is strongly recommended to take this only as an initial reference, due to the nature of Thermodynamics. This section is only a very small review on the very large field of chemical thermodynamics, and one recommends to further deepen the knowledge for volatile weak electrolyte systems that contain mixed strength dissociations. To describe these dissociations, there are three key aspects of the theory covered briefly here:

- Henry's Ensemble Law, to describe solubility of molecular species
- Dissociation of Ionic Species
- Gibbs Free Energy Minimisation Technique

These are part of a generally standard method to get started on thermodynamic modelling, and are enough to give an introductory view on the equations that are implemented in this work's modelling. In the next chapter, the particular equations for this system are discussed, along with results obtained from the Gibbs Free Energy Model as well as the Mathematica Calculations.

References for Chapter 3

BATTINO, R. & CLEVER, H. L. 1966. The Solubility of Gases in Liquids. Chemical Reviews, 66, 395-463.

CARROLL, J. J. 1991. What is Henry's Law? Chemical Engineering Progress, 87, 48-52.

CLARK, S. R. 2007. Elements of Fractional Distillation, Read Books.

DAUBERT, T. E. 1985. Chemical engineering thermodynamics, McGraw-Hill.

KRICHEVSKY, I. R. & KASARNOVSKY, J. S. 1935. Thermodynamical Calculations of Solubilities of Nitrogen and Hydrogen in Water at High Pressures. Journal of the American Chemical Society, 57, 2168-2171.

LEIVA, M. A. & VIVANCO, V. 1986. Vapour-liquid equilibria of aqueous solutions containing volatile weak electrolytes by using the free energy minimization method. Fluid Phase Equilibria, 27, 483-490.

LIN, C.-T. & DAUBERT, T. E. 1978. Prediction of the Fugacity Coefficients of Nonpolar Hydrocarbon Systems from Equations of State. Industrial & Engineering Chemistry Process Design and Development, 17, 544-549.

MALANOWSKI, S. & ANDERKO, A. 1992. Modelling phase equilibria: thermodynamic background and practical tools, Wiley.

MAURER, G. 1980. On the solubility of volatile weak electrolytes in aqueous solutions. Thermodynamics of aqueous systems with industrial applications; ACS Symposium Series, 133, 139-172.

NAKAMURA, R., BREEDVELD, G. J. F. & PRAUSNITZ, J. M. 1976. Thermodynamic properties of gas mixtures containing common polar and nonpolar components. Industrial & Engineering Chemistry Process Design and Development, 15, 557-64.

PRAUSNITZ, J. M. 1969. Molecular Thermodynamics of Fluid-Phase Equilibria (Prentice-Hall International Series in the Physical and Chemical Engineering Sciences).

PRAUSNITZ, J. M., LICHTENTHALER, R. N. & DE AZEVEDO, E. G. 1986a. Molecular thermodynamics of fluid-phase equilibria, Prentice-Hall.

PRAUSNITZ, J. M., LICHTENTHALER, R. N. & DE AZEVEDO, E. G. 1986b. Molecular thermodynamics of fluid-phase equilibria. Prentice-Hall.

REID, R. C., PRAUSNITZ, J. M. & POLING, B. E. 1987. The properties of gases and liquids, McGraw-Hill.

SHAW, A. C. 2008a. The simultaneous solubility of sulphur dioxide and oxygen in water for the hybrid sulphur thermochemical cycle. Ph.D. Doctoral Thesis, University of Sheffield.

SHAW, A. C. 2008b. The simultaneous solubility of sulphur dioxide and oxygen in water for the hybrid sulphur thermochemical cycle. PhD Thesis, University of Sheffield.

SMITH, J. M. & VAN NESS, H. C. 1996. Introduction to chemical engineering thermodynamics, McGraw-Hill.

THOMSEN, K., RASMUSSEN, P. & GANI, R. 1996. Correlation and prediction of thermal properties and phase behaviour for a class of aqueous electrolyte systems. Chemical Engineering Science, 51, 3675-3683.

WARN, J. R. W. & PETERS, A. P. H. 1996. Concise Chemical Thermodynamics, 2nd Edition, N. Thornes.

ZEMAITIS, J. F. J., CLARK, D. M., RAFAL, M. & SCRIVNER, N. D. 1986. Handbook of aqueous electrolyte thermodynamics.

Chapter 4

Thermodynamic Modelling

Chapter 4

Table of Contents

4.1 Overview

The present chapter contains the general description of the methodology used to model the solubilities of the gaseous species in the system sulphuric acid, sulphur dioxide, oxygen and water. Two techniques were used: an extension of the vapour-liquid equilibria method outlined by Shaw in his doctoral dissertation (2008), and a Gibbs Free Energy model taken from HSC® Chemistry software package. These two will be presented in the following sections.

It is important to mention that the methodology of the vapour-liquid equilibrium model, programmed in Mathematica, is derived from the methodology from Zemaitis (1986). Although all of the equations are described in his handbook, the equations are both coded into Mathematica, the description of the equations is presented in Appendix D. Since the ternary model is well documented, this chapter will focus on the quaternary system only.

4.2 Justification

In the last two chapters, the process for hydrogen production was described to a certain extent with the highlighting of two of the sulphur family of thermochemical cycles: the HyS and the SI cycles. Of critical importance is to acknowledge the difficulty of simulating both processes for R&D, feasibility and cost studies, and this is due to the complexity of the thermodynamics of the electrolyte equilibrium reactions, both for the separation equipment as well as the reactors and electrolysers. One needs to know the nature of the species dissociation, the non-idealities of their solubility and the phases involved.

The main criticism for current flowsheets is that they use semi-empiric thermodynamic models that are somewhat restricted in validity (limited temperatures, pressures or both). On the other hand, interestingly, if no data is available, it is of standard practice to use the Gibbs free energy approach, and then use it to regress parameters in different models, like UNIQUAC or UNIFAC (Thomsen et al., 1996).

The model contained in this chapter, along with the model obtained from HSC Chemistry, are a starting point towards rigorous thermodynamic modelling, that in the future could be implemented for more components and modified to predict a broader range of temperature and pressure conditions. This will then be compared with the Gibbs Free Energy model, which is the standard non-experimental electrolyte modelling technique. In the following section, some equilibrium chemistry considerations are mentioned, in order to introduce the speciation that one has to become familiar with in this work.

4.3 Sulphuric Acid Equilibrium

4.3.1 H_2SO_4 dissociation

According to the review performed by Zemaitis (1986), when pure liquid, the electrical conductivity of sulphuric acid is very high, as well as its viscosity. In this state, self-dissociation occurs, according to the following reaction:

$$2H_2SO_4 \rightleftarrows H_3SO_4^+ + HSO_4^-$$

This has been proposed as the main cause for high conductivity. Simultaneously, a second reaction has been suggested:

$$2H_2SO_4 \rightleftarrows H_3O^+ + H_2S_2O_7^-$$

, where self-dissociation products have been estimated at 0.043 molal in total, which is by no means a negligible amount. This needs to be compared with the total proton and hydroxide ion presence in water, calculated as $2x10^{-7}$.

When in solution with water, the polyprotic acid dissociates into sulphite and bi-sulphite, according to the following overall reaction:

$$H_2SO_4 \rightleftarrows H^+ + HSO_4^- \rightleftarrows 2H^+ + SO_4^{2-}$$

While the first reaction is thought to be complete, or having a large reaction constant; the second dissociation prevails in only low sulphuric acid concentrations. This is critical, as low concentrations are relevant to the conditions involved current flowsheets

(Jeong, 2005, Brown et al., 2003). According to research performed by Young and Blatz (1949), the chemical equilibrium diagram between species and concentration of sulphuric acid in solution is shown in Figure 1. The data was taken from 0.06 to 2.34 moles of water per mole of sulphuric acid, a non-standard method of measuring, but revealing experimentally that concentrated sulphuric acid leads to rare species such as $H_5SO_5^+$. However, the equation

$$H_2SO_4 + H_2O \rightleftarrows H_5SO_5^+ + HSO_4^-$$

is very rare for concentrations lower than 50%, and were not included in the model. A review done in this work confirmed that the salting out effects for higher concentration acid solutions of sulphuric acid are scarce, or not at all to be found in literature. In his experiments, a 1040 cm^{-1} band was seen by Young and Walrafen (1961) that we could confirm experimentally for higher concentrations in our Raman setup, discussed in Chapter 5.

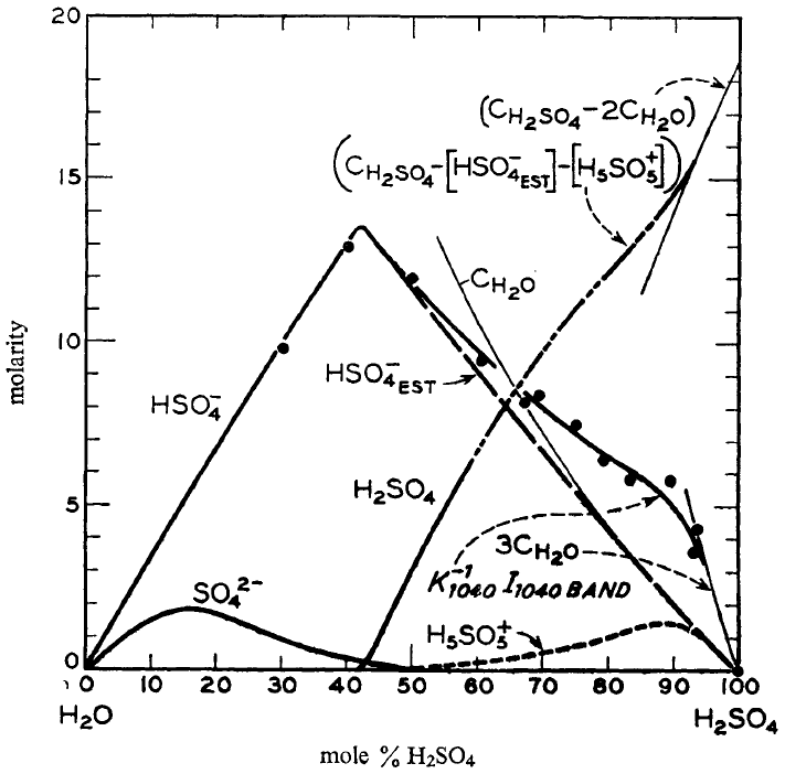

Figure 1. Equilibrium of concentrated aqueous H_2SO_4 at 25 °C.

Interestingly, these measurements were performed using dispersive Raman spectroscopy, an advanced technique at the time.

As pointed out by Zemaitis, the second dissociation constant has been the subject of much study. In this work, the reaction rate was taken as the Gibbs Free energy polynomial function fitted to between 20 to 80 degrees °C. These are shown below, fitted to the simplest equation possible for ease of calculation.

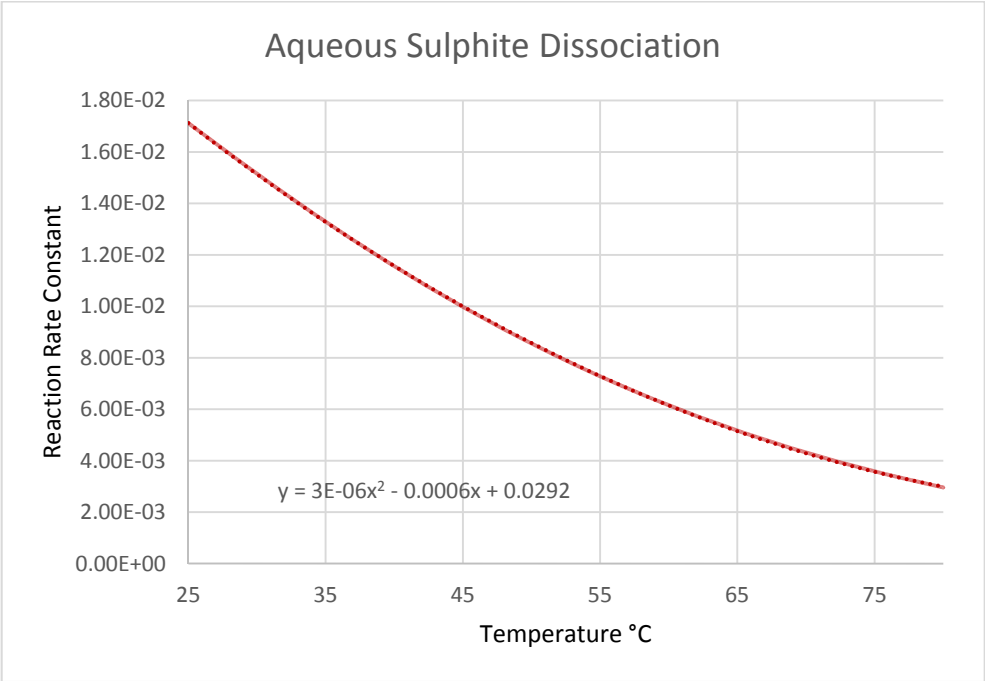

Figure 2. Sulphite formation from SO_2 dissociation equilibrium constant, from 25 to 80 °C.

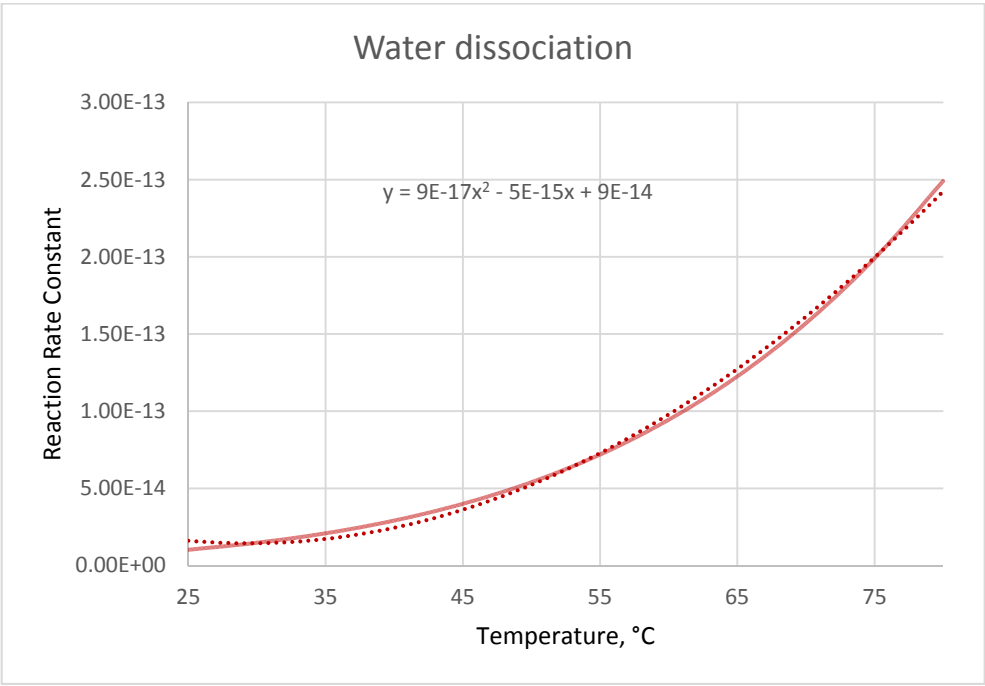

Figure 3. Water dissociation equilibrium constant, from 25 to 80 °C.

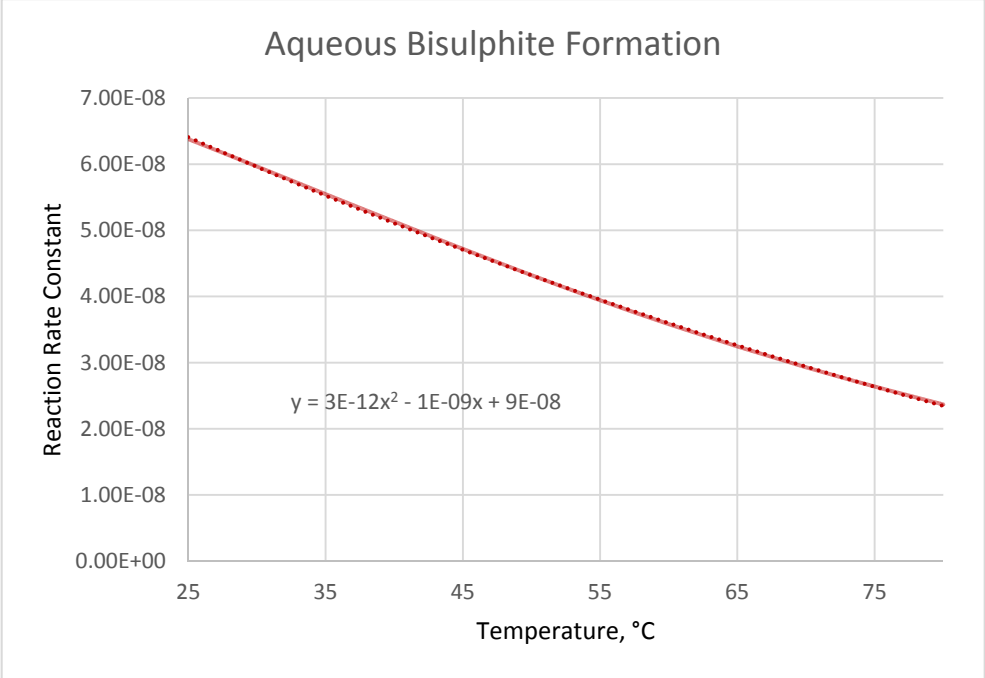

Figure 4. Aqueous Bisulphite formation, from sulphite. 25 to 80 °C.

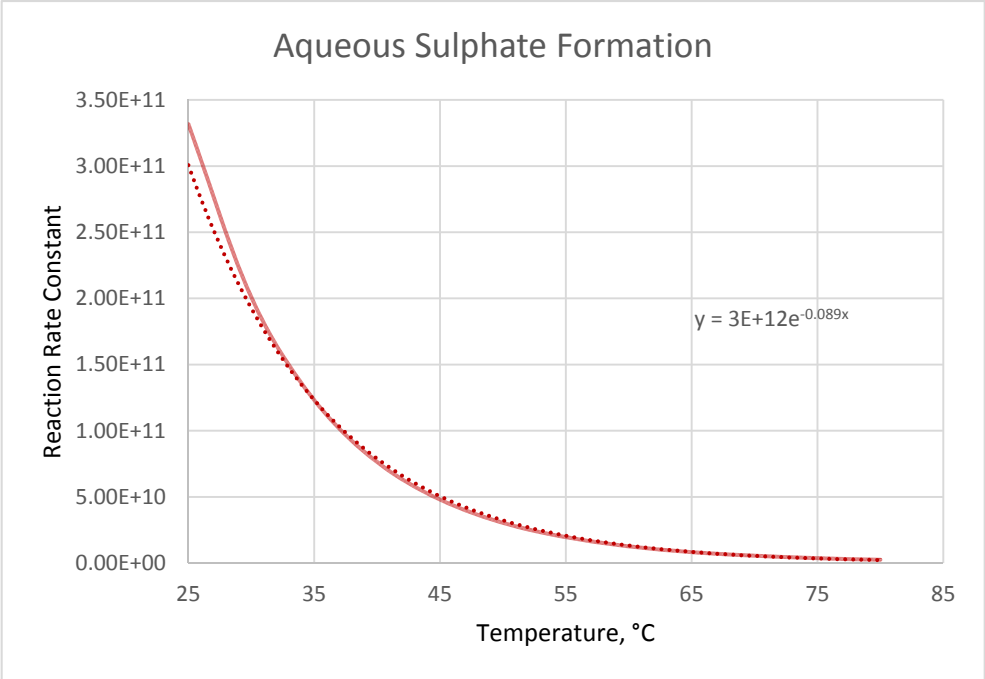

Figure 5. Sulphuric acid ionization, or sulphate formation, 25 to 80 °C.

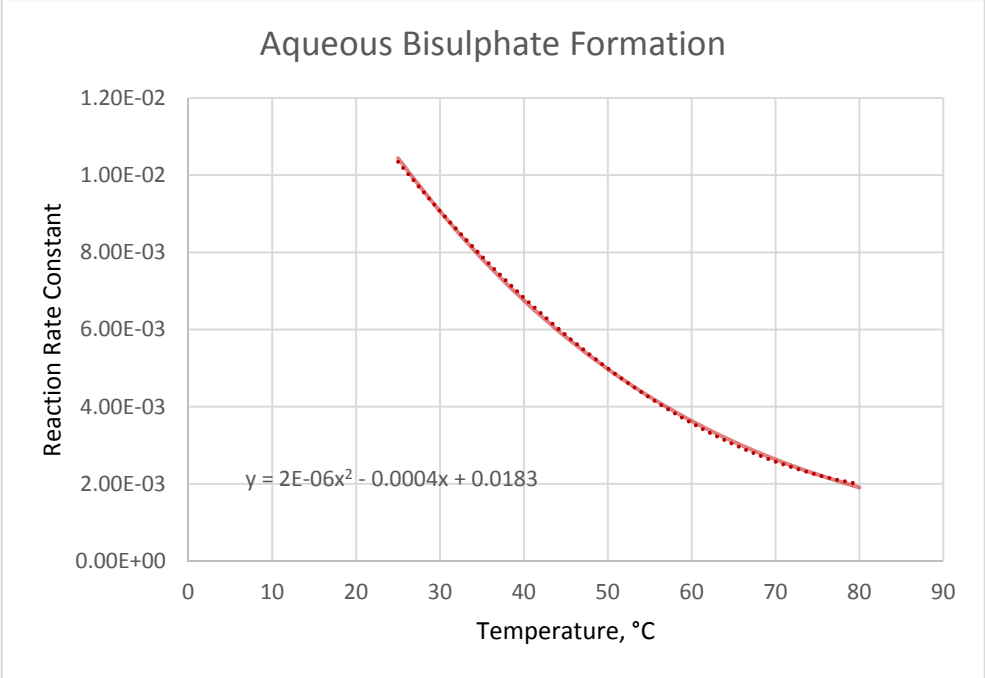

Figure 6. Bisulphate formation, from initial sulphuric acid dissociation. 25 to 80 °C.

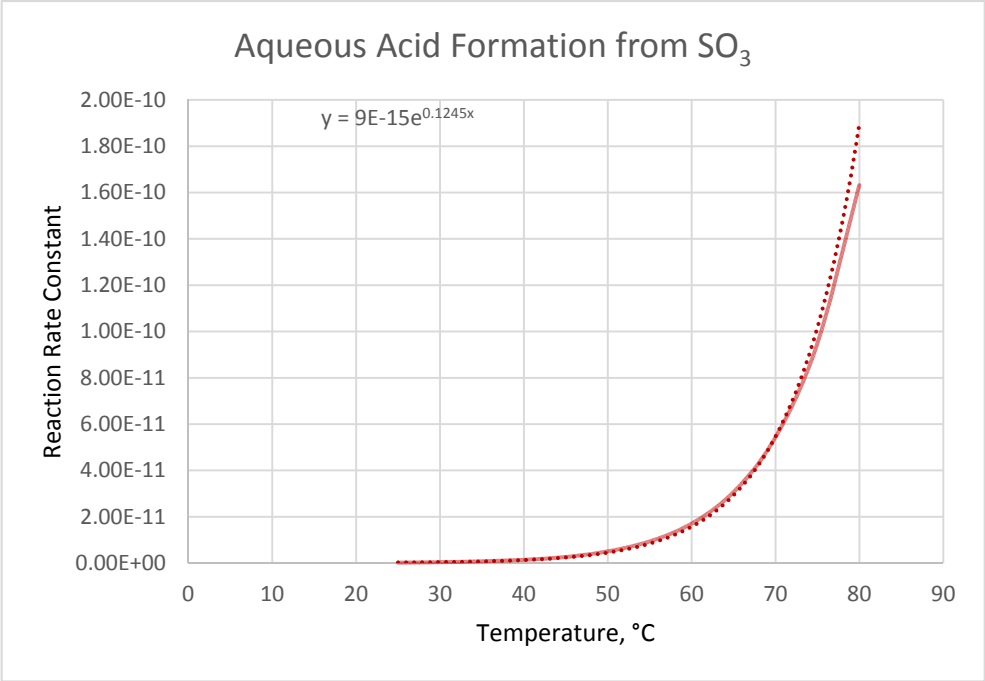

Figure 7. Acid recombination (from sulphur trioxide). 25 to 80 °C.

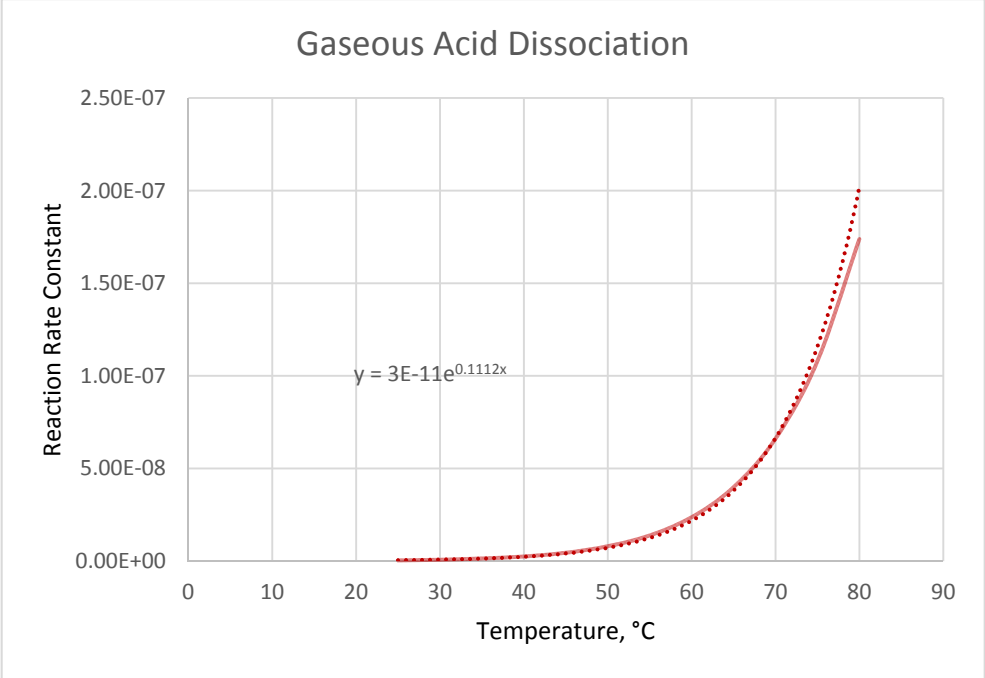

Figure 8. Gaseous acid dissociation to SO_3 in the gas phase, 25 to 80 °C.

Once the reaction rates were developed, and analysed, stating that none of them had negligible effects onto the model, one could then plug in the respective equations into Shaw's model to include H_2SO_4. It is evident that no solid reactions were considered, nor formation of a 2nd liquid phase.

4.4 Problem Set Up

The following is the schematic representation of the problem:

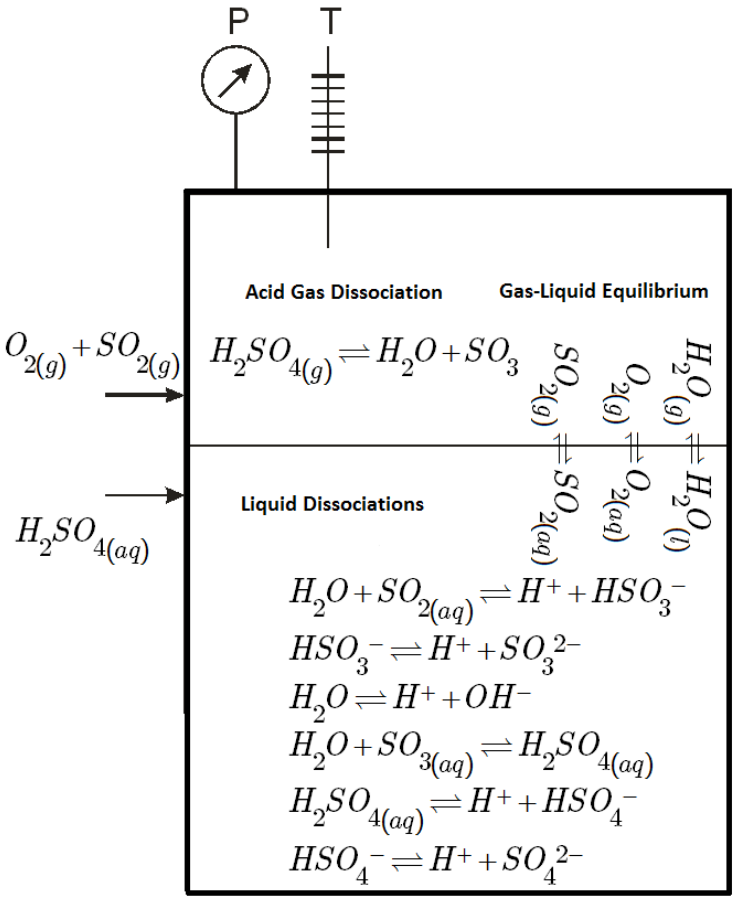

Figure 9. Problem Set up (quaternary).

The aqueous solution containing sulphuric acid consists of the following chemical equilibrium reactions:

- Sulphuric acid first dissociation or sulphate formation
- Bisulphate formation
- Water dissociation
- Sulphur dioxide dissociation or sulphite formation
- Bisulphite formation

4.4.1 Reaction Equations

The following equations are used in the VLE calculations, each equation represents a distinctive reaction, either gaseous or liquid.

Table 1. Reactions involved and corresponding chemical equations.

Reaction	Equation
Sulphur dioxide dissociation (leading to Bisulphite)	$K_{SO_2} = \frac{[HSO_3^-][H^+]}{[SO_2]}$
Water dissociation	$K_{water} = [H^+][OH^-]$
Sulphite dissociation (leading to Sulphite)	$K_{HSO_3^-} = \frac{[SO_3^{2-}][H^+]}{[HSO_3^-]}$
Acid dissociation (leading to Bisulphate)	$K_{H_2SO_4} = \frac{[HSO_4^-][H^+]}{[H_2SO_4]}$
Sulphate dissociation (Leading to Sulphate)	$K_{HSO_4^-} = \frac{[SO_4^{2-}][H^+]}{[HSO_4^-]}$
Liquid Acid formation from Sulphur Trioxide$_{(aq)}$	$K_{SO_{3(aq)}} = \frac{[H_2SO_{4(aq)}]}{[SO_{3(aq)}][H_2O]}$
Gas Acid formation from Gaseous $H_2SO_{4(g)}$	$K_{H_2SO_{4(g)}} = \frac{[SO_{3(g)}][H_2O_{(g)}]}{[H_2SO_{4(g)}]}$

The useful form coded into Mathematica is in the form:

$$K_T = \frac{(\gamma_C m_C)^c (\gamma_D m_D)^d}{(\gamma_A m_A)^a (\gamma_B m_B)^b}$$

Next, the equilibrium equations will be presented.

4.5 Equilibrium equations

In this section, equations from the literature are taken and adapted from the Henry's Ensemble Law, modified via the Zemaitis (1986) methodology, and incorporated to Mathematica, they also represent the dissociation as a function of ionic molarities and activity coefficients for all species. Along with the electroneutrality condition, material balances and fugacity and activity coefficients, the thermodynamic modelling is fully posed.

4.5.1 Vapour-liquid Equilibrium Equations

The following equations are the ensemble equations relevant to the gas-liquid exchange for the species in question.

Vapour-liquid equilibria of oxygen

$$y_{O_2}\varphi_{O_2}P = H_{O_2}m_{O_2}\gamma_{O_2}\exp\left\{\frac{\overline{v}_{O_2,w}(P-P_w^s)}{RT}\right\}$$

Vapour-liquid equilibria of sulphur dioxide

$$y_{SO_2}\varphi_{H_2O}P = H_{SO_2}m_{SO_2}\gamma_{SO_2}\exp\left\{\frac{\overline{v}_{SO_2,w}(P-P_w^s)}{RT}\right\}$$

Vapour-liquid equilibria of sulphuric acid

$$y_{H_2SO_4}\varphi_{H_2SO_4}P = H_{H_2SO_4}m_{H_2SO_4}\gamma_{H_2SO_4}\exp\left\{\frac{\overline{v}_{H_2SO_4,w}(P-P_w^s)}{RT}\right\}$$

Vapour-liquid equilibria of water

$$y_{H_2O}\varphi_{H_2O}P = a_{H_2O}P_w\gamma_w^s\exp\left\{\frac{\overline{v}_w(P-P_w^s)}{RT}\right\}$$

4.5.2 Reaction Equations

These following equations are taken from the identities drawn upon on Chapter 3. They are the equilibrium reaction constants as a function of molar concentration and activities (for the liquid phase).

Water dissociation

$$K_{H_2O} = \frac{\gamma_{H^+} m_{H^+} \gamma_{OH^-} m_{OH^-}}{a_w}$$

Sulphur dioxide dissociation

$$K_{SO_2} = \frac{\gamma_{H^+} m_{H^+} \gamma_{HSO_3^-} m_{HSO_3^-}}{\gamma_{SO_2(aq)} m_{SO_2(aq)} a_w}$$

Bisulphite formation

$$K_{HSO_3^-} = \frac{\gamma_{H^+} m_{H^+} \gamma_{SO_3^{2-}} m_{SO_3^{2-}}}{\gamma_{HSO_3^-(aq)} m_{HSO_3^-}}$$

Sulphuric acid dissociation

$$K_{H_2SO_4} = \frac{\gamma_{H^+} m_{H^+} \gamma_{HSO_4^-} m_{HSO_4^-}}{\gamma_{H_2SO_4(aq)} m_{H_2SO_4(aq)} a_w}$$

Bisulphate formation

$$K_{HSO_4^-} = \frac{\gamma_{H^+} m_{H^+} \gamma_{SO_4^{2-}} m_{SO_4^{2-}}}{\gamma_{HSO_4^-(aq)} m_{HSO_4^-}}$$

The rest of the reactions were implemented as a numerical approximation of the HSC thermochemical database, in order to increase the speed of convergence. It has to

be noted that an accurate first guess is imperative if one is to achieve convergence quickly, or to achieve it at all.

4.5.3 Fugacity Coefficients

For the gaseous phase, the molar volume of the mixture and the fugacity coefficients were required. The equation of Nakamura was used, which is a perturbed harp-sphere model used in Shaw's doctoral thesis (2008) and originally published by Nakamura et al. (1976). This equation makes it possible to determine volumetric properties of gases with different polarities, although approximations on the published parameters were needed as they were not readily available for oxygen, SO_3 and H_2SO_4. The equation of interest is the following:

$$P = \frac{RT}{V}\left\{\frac{1+\xi+\xi^2+\xi^3}{(1-\xi)^3}\right\} - \frac{a}{v(v+c)}$$

Where

$$\xi = \frac{b}{4v}$$

The full method is a semi-empirical way to determine volumetric properties taken from experimental data, and is described elsewhere (Shaw, 2008).

4.5.4 Activity Coefficients

The method of Pitzer (1973), which is a generalized correlation method to calculate activity coefficients depending on the nature of individual electrolytes was used. The method is essentially a sum of the different ion-ion, ion-molecule and molecule-molecule interactions for each species, totalling a repulsive or attractive force that will dictate the solvation behaviour of the mixture.

4.5.5 Selection of Fugacity and Activity Coefficients Methods

Previous to the work of Pitzer and Kim regarding the activity and osmotic coefficients for mixed electrolytes (1974), there was no simple or accurate description of multi-component electrolyte solution behaviour. Their work demonstrates a semi-empirical method to determine solubility behaviour spanning different ionic strengths and chemical compositions over a wide range of single components. These equations were tested for 69 sets of mixtures showing on average a deviation of less than 0.01 in 36 cases and above 0.05 in only seven cases, all involving OH^{1-} and Cs^{+}. Since in this work, the ability to combine solubility properties of such distinct electrolytes (H_2SO_4 and SO_2) was paramount, it was deemed acceptable to continue using the Pitzer model for the prediction of VLE behaviour.

With respect to the fugacity coefficient, and continuing the criteria selected by Shaw in his doctoral dissertation, it was considered prudent to remain using the Nakamura equation of state for gaseous calculations, as this presented reasonable approximations to the experimental data. This was also selected for simplicity and ease of modification, since it's a simple, perturbed hard-sphere equation, originally presented for carbon dioxide, but suitable for SO_2 molecules.

4.6 Summary of Code Changes

This is an overview of the code changes that are included in the ternary vapour-liquid equilibrium model. It is a modified version stemmed from the version submitted in Shaw's doctoral thesis and the results published in the IJHE paper in 2010, and used in the ternary models in this project. These are intended to be merely descriptive, all the code is included in Appendix D. The main modifications had to do with the following aspects:

- Estimation of molecular interaction parameters
- Guessing of initial values
- Mathematical method to solve the system of algebraic equations
- Iterative procedure to improve accuracy of partial pressures
- Fitting of reaction rate constants

These modifications were included in the quaternary system. The reaction rate constant fitted curves are explained in section 4.3.1.

4.6.1 Molecular Interaction Parameters

As stated in the introductory part of this thesis, one of the justifications of this work was to establish the solubility behaviour of sulphur dioxide in aqueous sulphuric acid solutions at moderate temperatures and pressures. The difficulty of pursuing this objective is clearly noticeable by the almost non-existent body of experimental work with this particular set of components.

Apart from the obvious modern approach of molecular simulation, one of the main solutions to this is to approximate values of interaction to similar components, hence acquiring a certain similarity of results in comparison to the original mixture. For example, gathering interaction parameters from a volatile electrolyte vapour liquid equilibrium dataset would be a starting point for a sulphur dioxide mixture in water. This is what it was done in this project, but instead, using the existing parameters of interaction between CO_2 (a mild volatile electrolyte, although less soluble in water than SO_2) and water. If deemed reasonable, molecular weight was used instead for sulphuric acid.

4.6.2 Guessing of initial values

Promotion of convergence in chemical engineering calculations is a daily problem in research. This problem was also noticed in the algorithms used to calculate vapour liquid equilibria in this project. Originally, the ternary code used the Newton's method of solving simultaneous algebraic equations. This was superseded by the Secant method in the quaternary calculations, as it limits the number of a certain variable with the selection of a maximum and a minimum. The other values are then constrained so that the overall calculation takes less computing power, as well as an arithmetically sound result. This was needed as the activity coefficient calculations (and several other variables) acquired a complex number value as the iterations progressed. This optimized the calculations significantly.

4.6.3 Secant Method

A computational procedure described by Wolfe (1959) for the solution of not necessarily linear equations is incorporated in Mathematica software, in which the only hard theoretical assumption is that the solution function has a second derivative, and consists, in short, in the iteration of a step in which there are n trials at hand, where the solutions are replaced between two values (the aforementioned maximum and minimum).

In this work, since the activity coefficient values can only be between 0 and 1 (in a thermodynamically consistent model), it was deemed reasonable to limit these values between -1 and 2, which gave plenty of range to acquire reasonable approximations for other variables. In case a coefficient went slightly below 0, or more than one, which is very common in complex multiphase vapour liquid equilibria calculations, there was enough tolerance for values several iterations previous to the final solution.

4.6.4 Iterative behaviour of VLE model

The methodology outlined by Zemaitis suggested the construction of a equation-based vapour liquid equilibrium model starting from the binary reactions of SO_2-H_2O and increase its complexity by adding subsequently O_2 and then H_2SO_4. As the complexity progressed, the flexibility of the code was reduced, and the initial value “elasticity” was compromised. This affected the accuracy of the vapour pressure guesses of each species, that were directly connected to fugacity calculations. This limitation was solved by looping the entire code in order to achieve an enhanced guess and then proceed with the calculations. This approach reduced the amount of iterations needed for convergence and reduced the amount of complex numbers showing up in the console, by merely doubling the lines of code in the program.

4.6.5 Reaction Rate Constants

Finally, the HSC Chemistry software was used to determine an algebraic expression for reaction rate constants for the different equilibrium reactions taking place, either in the gaseous form or the liquid form. For ease of use, the expressions were then formulated between the temperature ranges of use (20 and 80 degrees) and then were coded into the quaternary model (see section 4.3) These in turn were only used in that particular range, guaranteeing the validity of the values selected in this work.

4.6.6 Electroneutrality

Finally, the condition referred to as “electroneutrality” has to be set, and this just means that the electric forces between ions are so strong that theoretically, they instantly neutralize each other’s fields, so as to have an overall electric charge of ~ 0. This can be expressed as:

$$m_{H^+} = m_{OH^-} + m_{HSO_3^-} + m_{HSO_4^-} + 2[m_{SO_3^{2-}} + m_{SO_4^{2-}}]$$

In essence, the important VLE equilibrium equations have been presented in these sections. These equations, along with their supporting derivations and implementations are entirely presented in code form in Appendix D. This Mathematica model is then compared with the HSC calculations, as well as presented in more detail with a sample calculation, tabulating results as needed.

4.7 Sample Calculations: HSC and Mathematica

Figure 10 shows the calculation of a ternary system at constant temperature, while changing pressures. This data is either tabulated raw in spreadsheet format, or displayed as a diagram with axis and different colors for each species involved in the calculation. This was considered the easiest way to visualise the results, but in order to compare components on an individual basis, tabulated data was converted to multi-curve plots, where each curve represented a single run of one species.

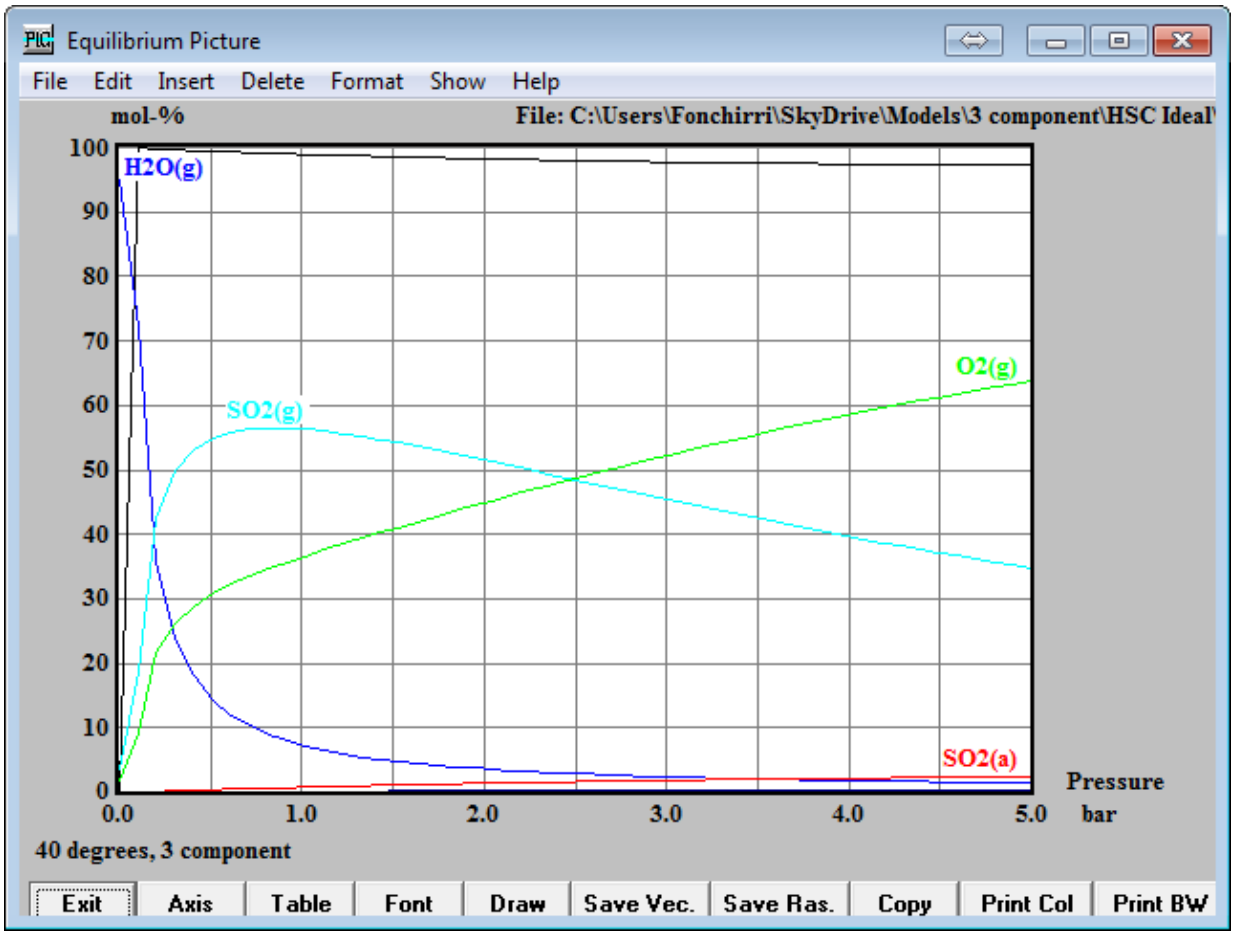

Figure 10. Sample Calculation of ternary system, 40 degrees, 0-5 bar.

In the calculation shown in Figure 10, one can appreciate the decrease of concentration of sulphur dioxide gas as the total pressure of the system increases. One expects then that the solubility of SO_2 increases, and this is confirmed by the rise of the red curve labelled as $SO_{2(a)}$ in the bottom of the graph. It is natural to see that although the concentration of gases in the liquid phase is relatively low in comparison to the gaseous state, it is by no means negligible. This type of visualization is helpful to see the relation held between the gaseous concentrations and the ionic concentrations of the dissociation products.

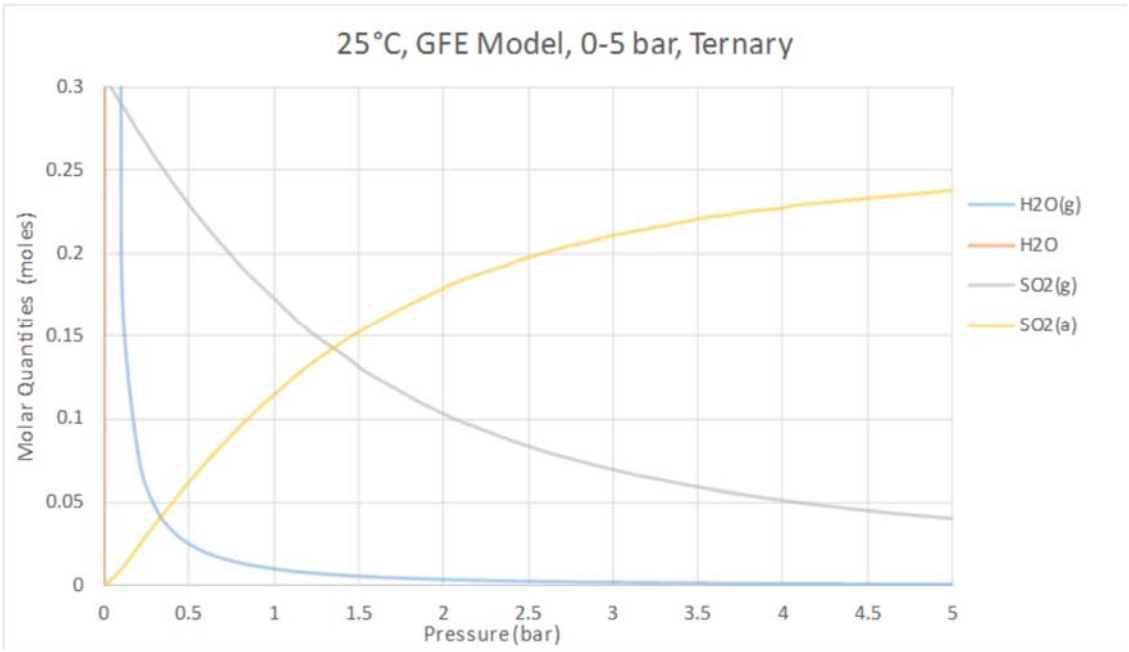

Figure 11. Excel format, from raw tabulated data shown in Appendix C.

In the calculation shown in Figure 11, a more detailed analysis can be performed via either decreasing the scale of the concentration on the y-axis, or one can filter the species involved as to see which ones are the main players in that particular calculation. Evidently, these dissolved amounts will be directly related to the system input in the HSC start spreadsheet. When very little amounts of ions were present, one had to recur to logarithmic scales, or reducing the pressure range in order to visualize and compare between ions.

Table 2. Activity coefficients of quaternary species vs. temperature, from 25 to 80 °C.

80	70	60	50	40	30	25
γ_{H2O} = 0.999959	γ_{H2O} = 0.978452	γ_{H2O} = 0.998127	γ_{H2O} = 0.996734	γ_{H2O} = 0.994803	γ_{H2O} = 0.992053	γ_{H2O} = 0.990238
γ_{SO2} = 1.009	γ_{SO2} = 0.923335	γ_{SO2} = 1.00777	γ_{SO2} = 1.00678	γ_{SO2} = 1.00535	γ_{SO2} = 1.00323	γ_{SO2} = 1.00177
γ_{SO3} = 0.369116	γ_{SO3} = -0.0294417	γ_{SO3} = 0.289892	γ_{SO3} = 0.256717	γ_{SO3} = 0.22587	γ_{SO3} = 0.196839	γ_{SO3} = 0.182945
γ_{HSO3} = 0.792603	γ_{HSO3} = 0.421725	γ_{HSO3} = 0.75642	γ_{HSO3} = 0.740583	γ_{HSO3} = 0.725614	γ_{HSO3} = 0.711453	γ_{HSO3} = 0.704719
γ_{HSO4} = 0.792603	γ_{HSO4} = 0.42174	γ_{HSO4} = 0.75642	γ_{HSO4} = 0.740583	γ_{HSO4} = 0.725614	γ_{HSO4} = 0.711454	γ_{HSO4} = 0.70472
γ_{H2SO4} = 1.00265	γ_{H2SO4} = 0.970414	γ_{H2SO4} = 1.00519	γ_{H2SO4} = 1.00709	γ_{H2SO4} = 1.00969	γ_{H2SO4} = 1.01331	γ_{H2SO4} = 1.01565
γ_{SO4} = 0.369116	γ_{SO4} = -0.0294445	γ_{SO4} = 0.289892	γ_{SO4} = 0.256717	γ_{SO4} = 0.22587	γ_{SO4} = 0.196839	γ_{SO4} = 0.182947
γ_{H} = 0.793218	γ_{H} = 0.423881	γ_{H} = 0.756657	γ_{H} = 0.740558	γ_{H} = 0.725241	γ_{H} = 0.710589	γ_{H} = 0.703527
γ_{OH} = 0.774126	γ_{OH} = 0.410114	γ_{OH} = 0.724476	γ_{OH} = 0.700122	γ_{OH} = 0.674949	γ_{OH} = 0.648504	γ_{OH} = 0.634714

80% of the time of each calculation is spent on the initial guesses. It is extremely important to be familiar with the quantities that are involved in each experiment, since an order or magnitude difference can mean divergence of the calculation and in those situations, restarting of the kernel is unavoidable.

4.8 Discussion

Solubility of SO_2 in water is a subject of many studies in the last century. The publication of Hales (1973) is a fine example of an experimental study of SO_2 solubility for atmospheric purposes, and the author compares it with this work due to the similarities of questions that arose during their experiments and after their work was summarized along with their advantages and disadvantages when making the theoretical considerations included in the publication. A key finding of Hales is the fact that the authors reported an increasing source of error as the concentration of SO_2 decreased in the experiments, acquired via a flow technique, different from the static technique that it's developed in this work and described in Chapters 5 and 6. In this case, the theoretical assumption that the second dissociation did not take place leads them to inconsistencies in their experimental data, which was a source of undesirable discrepancy between experiments.

In this work, and taken from the lessons learned by Hales, there was no single possible reaction that was neglected in the system, including those involving sulphur trioxide. This is a key strength of the Mathematica model, along with the fact that the Mathematica model is the only rigorous equation-based attempt at Vapour Liquid equilibrium, that can be extended for more species and has a strong theoretical foundation with the Pitzer interaction model, the Nakamura equation of state and the ensemble Henry's Law in the form presented by Zemaitis (1986).

Also, the calculations are comparable with the Gibbs free energy model, a well-known industry based method to determine non-ideal behaviour in electrolyte solutions, with a semi-empiric support taken from thermochemical measurements.

Deviations and uncertainties of the calculations developed in this chapter cannot be discussed without the comparison with experimental data (Chapter 6), although it is likely that the lack of a large enough body of data required to regress the interaction parameters needed for the activity coefficient calculations could be a source of instability. Without a sufficient body of experimental data, it is impossible to regress the model adequately enough to be certain that the solubility predictions are within at least 5% of

the true values, considering the uncertainties shown in the experimental section of this work, in Chapter 6.

It is very likely that the prediction at higher pressures is just more than the approximate binary interaction parameters due to the lack of experimental data. One could suggest that there could be other sources of error:

- Neglect of the clathrate hydrate formation in the model, experimentally evidenced when taking small samples from the equilibrium apparatus. This would mark the need for a SVL equilibrium model, with deposited solids that would change entirely the volume calculation equations.
- Wrong prediction of speciation (unknown species are present)
- Formation of complexes, and even elemental sulphur.

Although there are limitations to the not very flexible set of equations in the Mathematica model, it is a very good starting point to aid in the planning of experimental data that is necessary for the conditions relevant to the acid decomposition in both the SI and the HyS cycles.

4.9 Summary

A working set of equations has been devised to represent the vapour-liquid equilibria of multicomponent aqueous solutions, containing sulphuric acid, oxygen and sulphur dioxide; including the formation of sulphur trioxide simultaneously as a dissociated product of the sulphuric acid gaseous dissociation and as a reagent to form acid once dissolved in water.

The thermodynamic treatment together with liquid phase reactions, material balances and the condition of electroneutrality can be used to devise a set of equations so that for known input amounts of species (sulphur dioxide-H_2SO_4-water) and starting conditions the resulting equilibrium is modelled. For a solute and solvent pair there will be x independent equations in x unknowns, which when solved will give the amount of gas that dissolves, associated molalities of all species in the liquid phase, mole fractions in the vapour phase and a vapour production rate.

While there are many ways to calculate the fugacity and the activity of the aforementioned mixture, it was decided to continue the methodology described by Zemaitis, using the parameters determined by Shaw in his doctoral thesis, containing the most applicable calculations for SO_2 and sulphuric acid. Beutier and Renon's (1978) model for the activity coefficient was developed as an extension to the work by Edwards (1975, 1978) and specifically considered sulphur dioxide/water equilibria, amongst other mixtures, for sour water strippers. The Nakamura (1976) method used to predict fugacity coefficients comes from work on prediction of thermodynamic properties of gas mixtures containing polar and non-polar molecules.

This is further supported by the calculation of the same equilibrium using HSC Chemistry, a software package that uses the Gibbs Free Energy minimisation technique to provide a glance at the vapour liquid equilibrium and speciation in the aforementioned system.

It is worth remembering that H_2SO_4, SO_2 and water are polar molecules and this work's rigorous model is intended to be a good approximation for a broad range of conditions, relevant to electrolyte modelling in thermochemical cycles. In the next chapter, the experimental activities of this project will be presented, along with the considerations that were deducted from both models.

References for Chapter 4

BEUTIER, D. & RENON, H. 1978. Representation of ammonia-hydrogen sulfide-water, ammonia-carbon dioxide-water and ammonia-sulfur dioxide-water vapor-liquid equilibriums. Industrial & Engineering Chemistry Process Design and Development, 17, 220-30.

BROWN, L. C., BESENBRUCH, G., LENTSCH, R., SCHULTZ, K. R., FUNK, J. E. & ATOMICS, G. 2003. Alternative flowsheets for the sulfur-iodine thermochemical hydrogen cycle, United States. Department of Energy. Oakland Operations Office.

EDWARDS, T. J., MAURER, G., NEWMAN, J. & PRAUSNITZ, J. M. 1978. Vapor-liquid equilibria in multicomponent aqueous solutions of volatile weak electrolytes. AIChE Journal, 24, 966-976.

EDWARDS, T. J., NEWMAN, J. & PRAUSNITZ, J. M. 1975. Thermodynamics of aqueous solutions containing volatile weak electrolytes. AIChE Journal, 21, 248-59.

HALES, J. M. & SLITTER, S. L. 1973. Solubility of sulfur dioxide in water at low concentrations. Atmospheric Environment (1967), 7, 997-1001.

JEONG, Y. H., K. HOHNHOLT, M. S. KAZIMI AND B. YILDIZ. 2005. Optimization of the hybrid sulfur cycle for hydrogen generation. Nuclear Energy and Sustainability Program (NES) Technical Report: MIT-NES-TR-004. Massachusetts, NE: Center for Advanced Nuclear Energy Systems, MIT.

NAKAMURA, R., BREEDVELD, G. J. F. & PRAUSNITZ, J. M. 1976. Thermodynamic properties of gas mixtures containing common polar and nonpolar components. Industrial & Engineering Chemistry Process Design and Development, 15, 557-64.

PITZER, K. S. 1973. Thermodynamics of electrolytes. I. Theoretical basis and general equations. The Journal of Physical Chemistry, 77, 268-277.

PITZER, K. S. & KIM, J. J. 1974. Thermodynamics of electrolytes. IV. Activity and osmotic coefficients for mixed electrolytes. Journal of the American Chemical Society, 96, 5701-5707.

SHAW, A. C. 2008. The simultaneous solubility of sulphur dioxide and oxygen in water for the hybrid sulphur thermochemical cycle. Ph.D. Doctoral Thesis, University of Sheffield.

THOMSEN, K., RASMUSSEN, P. & GANI, R. 1996. Correlation and prediction of thermal properties and phase behaviour for a class of aqueous electrolyte systems. Chemical Engineering Science, 51, 3675-3683.

WOLFE, P. 1959. The Secant method for simultaneous nonlinear equations. Commun. ACM, 2, 12-13.

YOUNG, T. & WALRAFEN, G. 1961. Raman spectra of concentrated aqueous solutions of sulphuric acid. Transactions of the Faraday Society, 57, 34-39.

YOUNG, T. F. & BLATZ, L. A. 1949. The variation of the properties of electrolytic solutions with degrees of dissociation. Chemical Reviews (Washington, DC, United States), 44, 93-115.

ZEMAITIS, J. F., CLARK, D. M., RAFAL, M. & SCRIVNER, N. C. 1986a. Activity Coefficients of Strongly Complexing Compounds. Handbook of Aqueous Electrolyte Thermodynamics. John Wiley & Sons, Inc.

ZEMAITIS, J. F. J., CLARK, D. M., RAFAL, M. & SCRIVNER, N. D. 1986b. Handbook of aqueous electrolyte thermodynamics.

Chapter 5
Experimental Design

Chapter 5
Table of Contents

List of Figures

List of Tables

Background

5.1 Overview

In this Chapter, the research leading to the design of the final equilibrium apparatus is described. Picking up from Shaw's research and funded by the HyCycleS project, it continued to be funded through the final stage of the EU FP7 final deliverable, as well as being funded partly by the Mexican Government. The author continued the experimental work and pursued the incorporation of sulphuric acid into the project, using novel technologies and one of a kind in-situ setup.

The chapter starts with the aim of the design, as well as the background of the former generation of rigs, discussing shortcomings, possible solutions, making a case for the analysis of the instrumental additions to the apparatus and finally, some findings prior to the operation of the final version of the equilibrium still, the Mark IV.

5.2 Aim

Experimental work in this project consisted on gathering vapour-liquid equilibrium data. This was initially done with Shaw's designed stills, Mark I to III, but some shortcomings were identified, that led to the development of a new rig. The idea behind the new setup was to tackle inconsistencies in the equilibrium measurements, specifically the chemical analysis and the uncertainty of the results, which had to do with two questions:

- How to minimise experimental uncertainties, inherent to the equilibrium still measurements.
- What is the nature of the ionic speciation that could not be determined with analytical techniques featured in previous rigs.

These questions had to be addressed, so a considerable amount of time in this project was allocated to the design of a reactor that could avoid the shortcomings that were identified with the former generation of VLE still.

Analysis of the data acquired with previous rig designs (Mark I to Mark III) led to important findings, including the necessity of refocusing the chemical analysis approach to equilibrium measurements (*in-situ*). A detailed step-by-step description of the engineering that took place to produce the Mark-IV rig is presented in this chapter, along with the associated calculations and technical necessary in the process.

The objective of the experiments is to successfully bring into contact the species of interest (ternary: SO_2, O_2 and H_2O – quaternary: including H_2SO_4). Select quantities of each species would be inserted into the equilibrium apparatus in question, mixed and then analysed, providing a full picture of the thermodynamic status of the system. The rig needs to withstand temperatures of up to the boiling point of the solution, be resistant to acid corrosion and be able to withstand 20 bar of hydraulic static pressure. Ideally, one would sample the species without disturbing the equilibrium.

5.3 Previous Equilibrium Still Designs

Prior to this research project, several VLE stills were designed and are presented in Shaw's doctoral thesis (2008). The principle via which the rigs operated was based on the still developed by Othmer (1952), and was constructed in-house. The original Othmer still is shown in Figure 1. In the figure, several elements are shown: T1-T5 thermocouples, a) cartridge Heater wells, b) liquid sample outlet, c) peep sights, d) cone shape top plate for condensate, e) vapour outlet pipe, f) vent valve for noncondensable gases, g) inlet tube for condensate return. The original equilibrium design in this work was inspired by this first static still. A brief description of the apparatuses leading to the Mark-IV is discussed in the following sections, inspired by the first Othmer still.

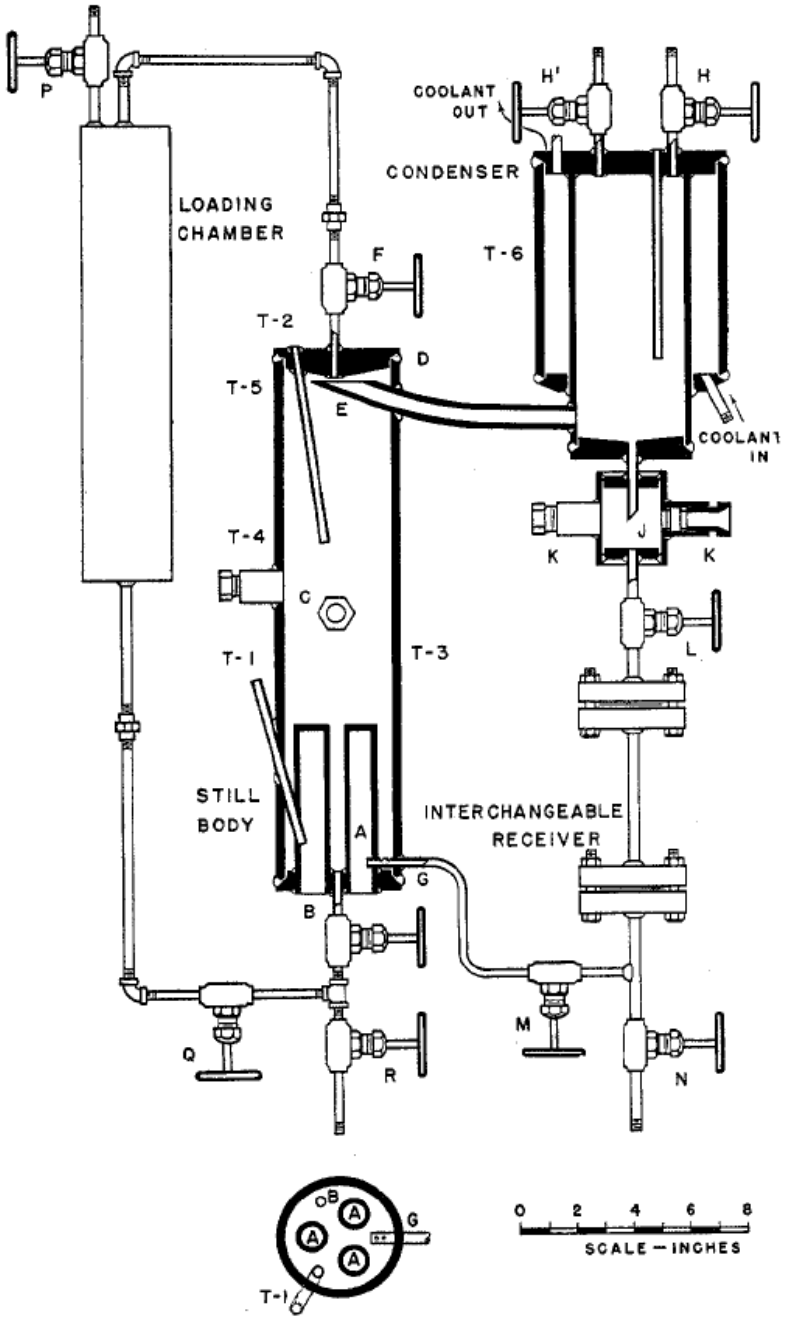

Figure 1. Original still by Othmer (1952), p.1865. Still body, 19” long.

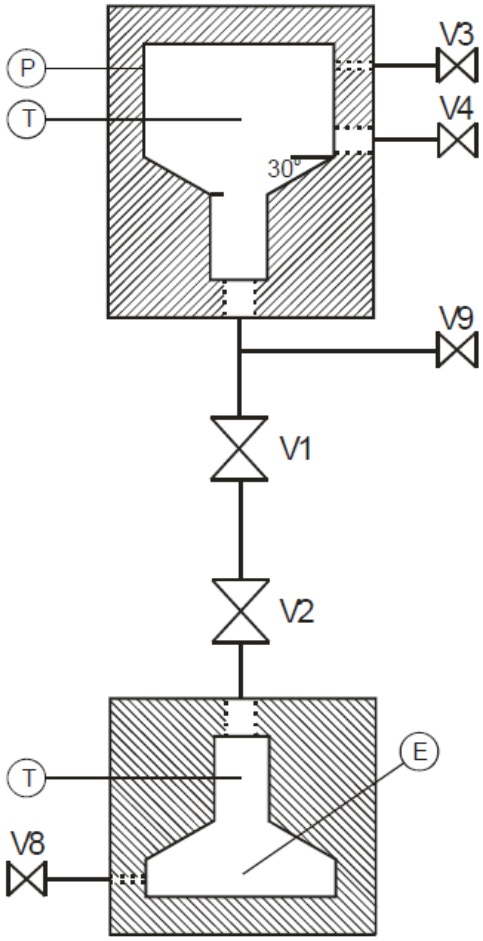

Figure 2. Simplified Schematic diagram of Mark I to III. (Shaw, 2008)

5.3.1 Mark I and Mark II

The first reactor, Mark I, is shown schematically in Figure 2. It had a volume of 1005.8 cm^3 and it was made partly from stainless steel, where sometimes QVF® glass chambers were attached for low pressure experiments. The chambers were united via a pipe and were isolated using Swagelok valves. The outside diameter of the chambers was 140 mm and the inner diameter was 100 mm, which narrowed down to a cone with an angle of 30°, to a minimum through diameter pipe of 30 mm. The length of the apparatus was 800 mm in total, and reached a mass above 10 kg. The pipe connecting the chambers was a ¾" SS pipe that allowed liquids to move freely. The inter-valve section allowed for the expansion of the liquid volume after complete gas dissolution.

Table 1. Volumes of top, bottom and connecting sections of Mark-II

Part	Volume (in cm^3)
Gas chamber (Top)	630.9 cm^3
Liquid Chamber (Bottom)	302.7 cm^3
Connecting Pipe Section	72.2 cm^3

The Mark I design intensified the aqueous sulphur dioxide oxidation as the stainless steel valves provided considerable wetted surface. This was further identified by noting a decrease in operating pressure without apparent leakage. The next iteration of the design included a fluoropolymer (DuPont® B5513-Green) coating to limit the oxidation. Shaw (2008) describes the difference between the Mark I and Mark II designs:

> *"All valves were stainless steel ball valves cleaned to be compatible with pure oxygen. The pressure transducer was a Sensortechnics CTE9035AY7 which had a stainless steel body and diaphragm. The thermocouples were Teflon insulated K type sensors with an outer diameter of 4 mm installed via bored through Swagelok® 4 mm compression fittings. The pH probe was an Omega® PHE-5433-10 electrode housed in a Ryton® body having a Temperature Range of -5 to 135 °C and a pressure rating of 500 psig at 25 °C. The electrode had a triple junction reference cell of KCl/AgCl, 3M KCl and a reference junction of Porous PTFE. The electrode was installed through a 25 mm port gland compression fitting. The apparatus was hydraulically tested to a pressure of 60 bar with a blanking plug in place of the pH electrode. The rig was*

heated by a combination of 5 individually controlled mat, tape and rope heaters attached to the outer surface. The control of the rope heaters and data acquisition was the same for both rigs…" (p.167)

The Mark I had no lining. A fluoropolymer coating was set to the Mark II and is shown in Figure 3. Even though the lining was successful in reducing the metal contact, the valve metal area that was interfacing with the liquid solution nonetheless gave significant catalysis of the oxidation, although significantly less than the original design. The wetted area is clearly shown relative to the coated area in Figure 4. Note that, contrary to the original Othmer still, it is a rotating apparatus and it skips the condenser section (compare with Figure 1).

Figure 3. Fluoropolymer coating used in Mark II, taken from Shaw's thesis (2008).

5.3.1 Mark III

Following the oxidative problems in the Mark I and II, Shaw decided to apply a full inert lining of the metal parts. This also needed to withstand the acidic nature of the SO_2 solutions that were part of the ternary research objective. The logic behind this is explained in a paragraph of Shaw's (2008) doctoral thesis:

"In addition to having low extractable content, fully fluorinated fluoropolymers have very low surface energies, for example Teflon's® lack of polarity causes it to resist polar molecules such as water (Fleming et al., 2001). The non-wetting property had the benefit that, during mixing, water would not remain on the walls of the rig removing the likelihood of a droplet of liquid remaining in the gas phase pot." (p.170)

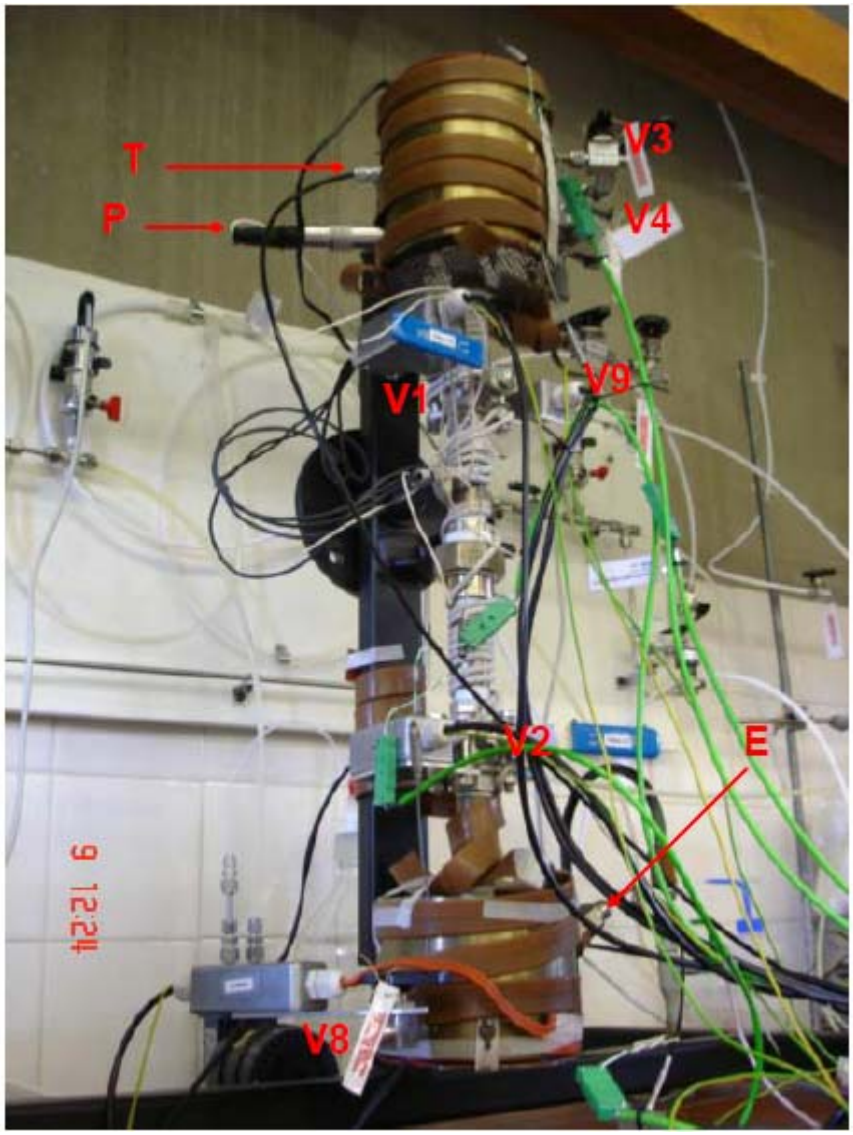

Figure 4. Mark II. T: Thermocouple gland. P: Pressure transducer. V1: Gas Valve. V2: Liquid Valve. E: pH probe. V8: Liquid Sampling valve. V9: Gas sampling valve.

While the metal extractable contents were selected as a critical priority for the new design, the mechanical and thermal properties were omitted during the Mark III design phase. This presented leakage problems throughout the

experimental phase of the Mark III, even though careful machining of the individual components was ensured. This had important consequences in later stages of the project, especially after the thermal switch incident. The mechanical and thermal considerations for the new design will be discussed starting from section 5.9.

A picture of the Mark III in operation is shown in Figure 5, while a more detailed mechanical diagram of the Mark III design is shown in

Figure 6.

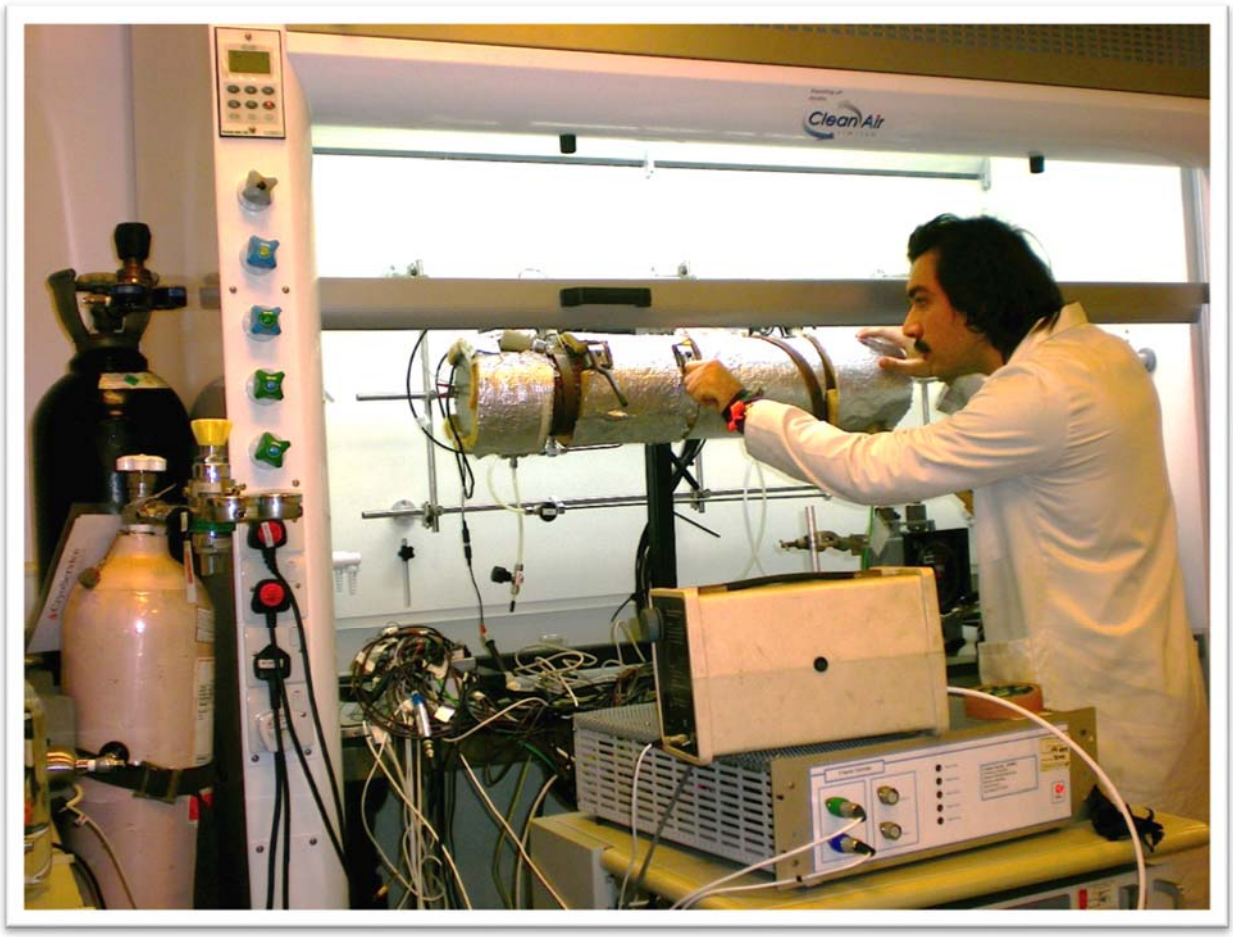

Figure 5. Mark III in operation, with rotating still and insulation in display.

The Mark III design was initially used in the first year of this project to obtain thermodynamic data for binary and ternary mixtures. This data has been published (Shaw et al., 2011), including a comparison with the literature and with models pertaining preliminarily to SO_2, O_2 and water. A detailed discussion of the results obtained with the Mark III rig is given in Chapter 6.

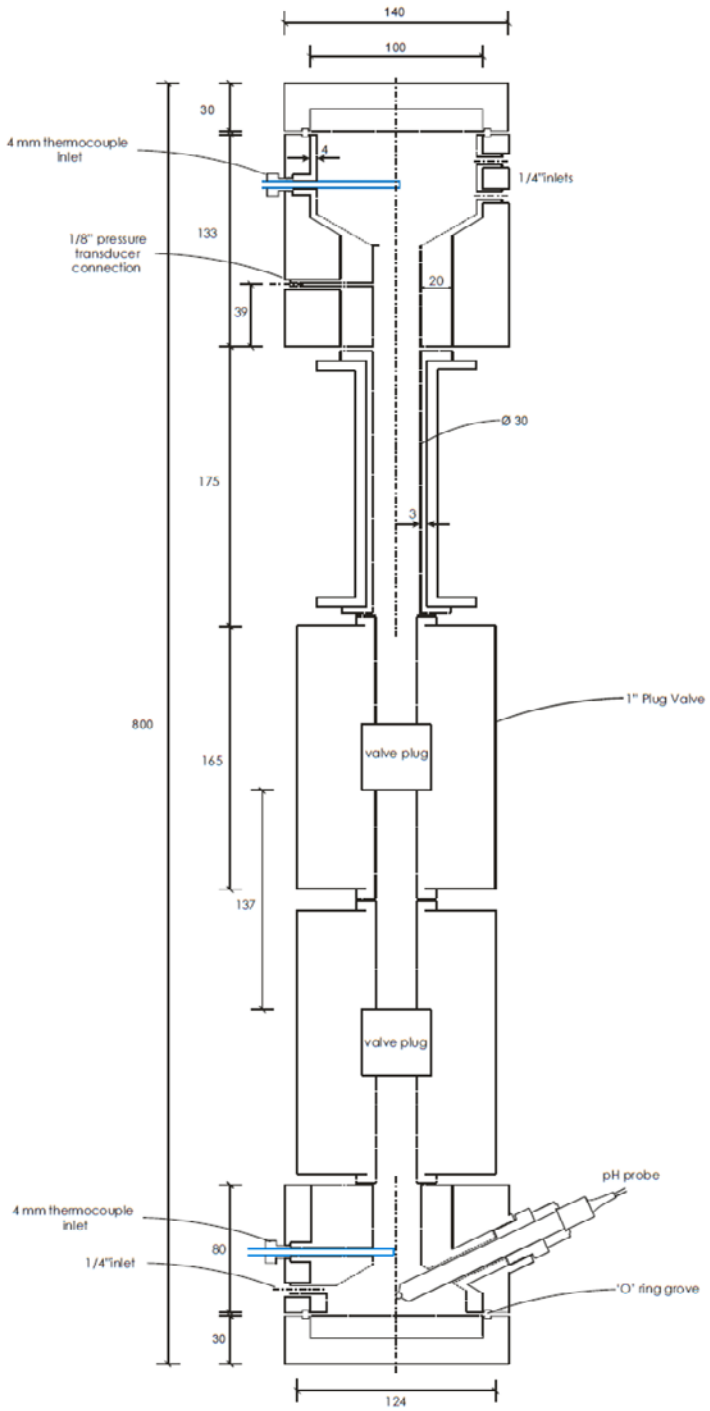

Figure 6. Mark III Mechanical detail. Distances in mm.

Table 2 contains a summary of the different rigs used in this project and their main desired characteristics of the next generation of apparatus.

Table 2. Description of experimental apparatuses used for the acquisition of sulphur dioxide, oxygen, water and sulphuric acid vapour liquid equilibria.

Rig Iteration	Main Characteristics	Length of Operation
Mark I	Metal body, stainless steel liquid and gas valves, QVF® borosilicate glass attachment for liquid phase, <400 cm^3, <1000 cm^3 volume. Wetted metal parts.	See Shaw's doctoral thesis.
Mark II	Stainless steel body with green PTFE coating, SS valves, 800 cm^3 volume.	See Shaw's doctoral thesis.
Mark III	SS body with virgin PTFE lining, PEEK oxygen valves and transducers, PFA gas and liquid valves, 4 mm virgin PTFE lining, PEEK oxygen valves and transducers, 800 cm^3 total volume, 16 bar maximum operating pressure.	In this project, July-2009 to Feb-2011.
Mark IV	15% Glass-reinforced PTFE body with stainless steel modular threaded frame inserts, Raman probe, liquid IR transmission cell, liquid UV-Vis cell and gas IR cell attachments. Maximum hydraulic pressure 16 bar, maximum design temperature 220 °C. Negligible zero-volume.	Aug-2012 to date

The rig had to be operated at relatively dangerous pressures in comparison to other routine experiments and the use of corrosive and very toxic media at high temperatures (SO_2 at 120 °C) has significant health and safety implications. A risk assessment was made. Key safety points were addressed. One of the measures taken to provide a reasonable safety margin for the operating pressure, was to commission the rig made out of steel and PTFE lining. A permissible strength of the stainless steel at the operating pressures of 20 bar was met with a reasonable 10 mm thickness, according to simple pressure vessel calculations. Finally, the decision was made to manufacture the apparatus with at

least a 4mm thick PTFE lining, and a full stainless steel body, machined out of a >180mm diameter rod.

This measure led to the full apparatus to weigh more than 35 kilos, with the rotating stand included. Several rope and mat heaters were purchased, totalling a heating power of almost 2 kW. Even with this heating capacity, the time taken for a mild increase of 20 °C could take hours. And due to the fluctuating behaviour inherent to a PID algorithm, thermal equilibrium between phases was no easy task. This is covered thoroughly in section 5.3.4. Overall, not only was it very tedious to operate, but moving the entire rig and the electrical connections required special logistic arrangements and led to reduced experimental uptime at the end. This has to be improved, and section 5.5 is dedicated to the discussion of these aspects.

5.3.2 Experimental Procedure

A typical operating graph is shown schematically in Figure 7.

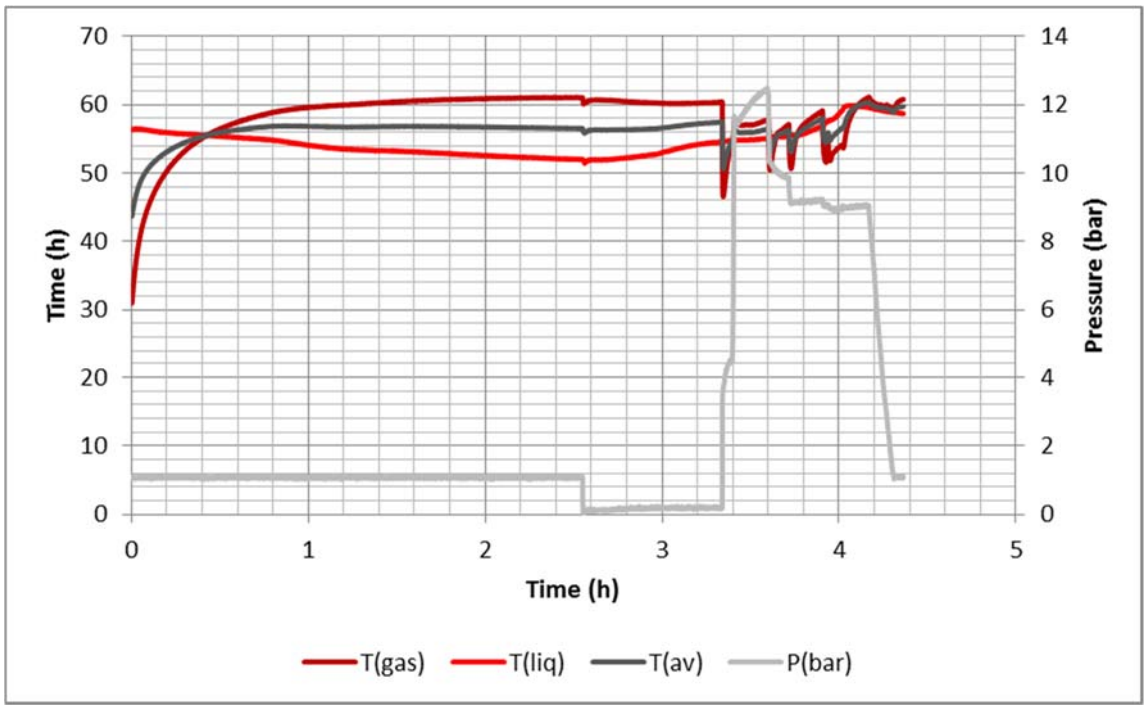

Figure 7. Mark III run at 60 °C.

The experimental procedure is explained in the Appendix A. In summary, the rig is subjected to vacuum, and the valves are closed to isolate the phases. It is important to close the phases and leave an “inter-valve” space to allow for liquid expansion after the volatile electrolytes are fully dissolved in the solution medium. This has an additional advantage discussed in the sampling section of this chapter.

Input of the water is straightforward and is based on calculation of the mass difference between a water bottle before and after its attachment to the rig. The difference is assumed to have transferred to the rig, ignoring little compressed nitrogen bubbles. The mass amount of water compared to the mass of the bubbles that could be seen stagnant in the flow system was at least a thousand times less. However, the volume that the bubbles occupied was not negligible, so an experimental volume calculation was necessary for the individual chambers, as well as the total rig volume.

On the gas side, two approaches could be taken: adding a known composition mixture of O_2 and SO_2, and using a smaller cylinder to measure the mass difference before and after the addition to the rig. On the other hand, one could attach the SO_2 first, add a certain amount (mass would be then dependent on the initial SO_2 cylinder pressure), then attach a higher pressure O_2 cylinder, then take advantage of the higher driving force of the oxygen to diffuse to the rig and calculate the mass added. These data would then be related to the calculations via experimental values of solubility and composition, in each phase. A more detailed procedure for the Mark III and Mark IV is given in the Appendix A.

5.3.3 Spatial Thermal Uniformity

To cope with large amounts of heat transfer, rope heaters were used to increase temperature in incremental discrete steps, following a PID algorithm optimised in LabVIEW. Typical behaviour is shown in Figure 8. Since the feedback thermocouples were in the surface of the chambers, a moving average was taken

into account to modulate the wattage drawn into the heaters. Although the temperature control was achieved easily on the outside, considerable time was required to achieve the gas and liquid bulk temperatures.

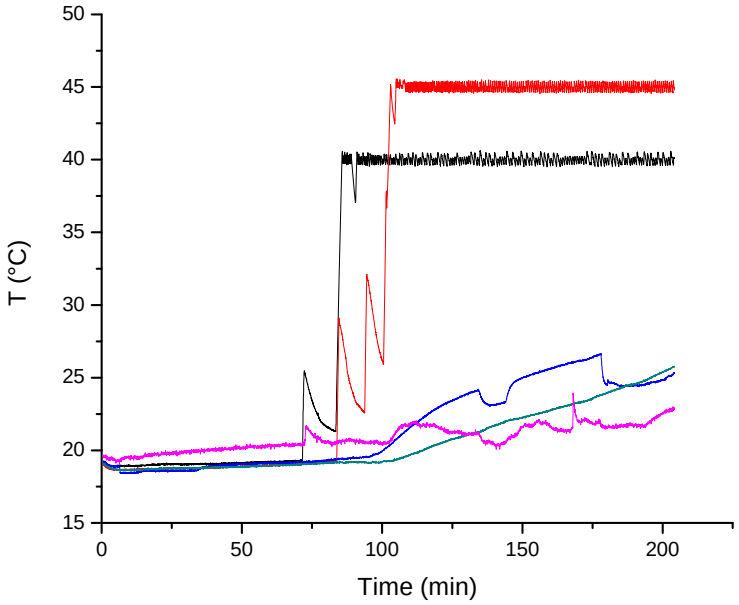

Figure 8. Surface vs. Well thermal measurements, Mark III rig.

The practicality of the experimental procedure was undermined by the amount of time that it took the rig to attain equilibrium, having sometimes to wait 4 hours for near-uniform heating in both chambers, for relatively moderate set temperatures (40 – 80 °C).

5.3.4 PID Damping

An important optimisation was introduced to the heater controller, to avoid excessive heat generation for the rope heaters. This had to do with damping the proportional and integral constants that characterize the behaviour of the PID algorithm, to avoid spiking. An example of the aforementioned “spiking” is shown in Figure 9. In this example, a temperature almost reaching the 120 °C mark was attained when the set temperature was 50 °C. This proved to be hazardous in higher temperatures, ranging from 50 to 80 °C, since the peak was even higher, sometimes reaching the 240 °C maximum from the heaters.

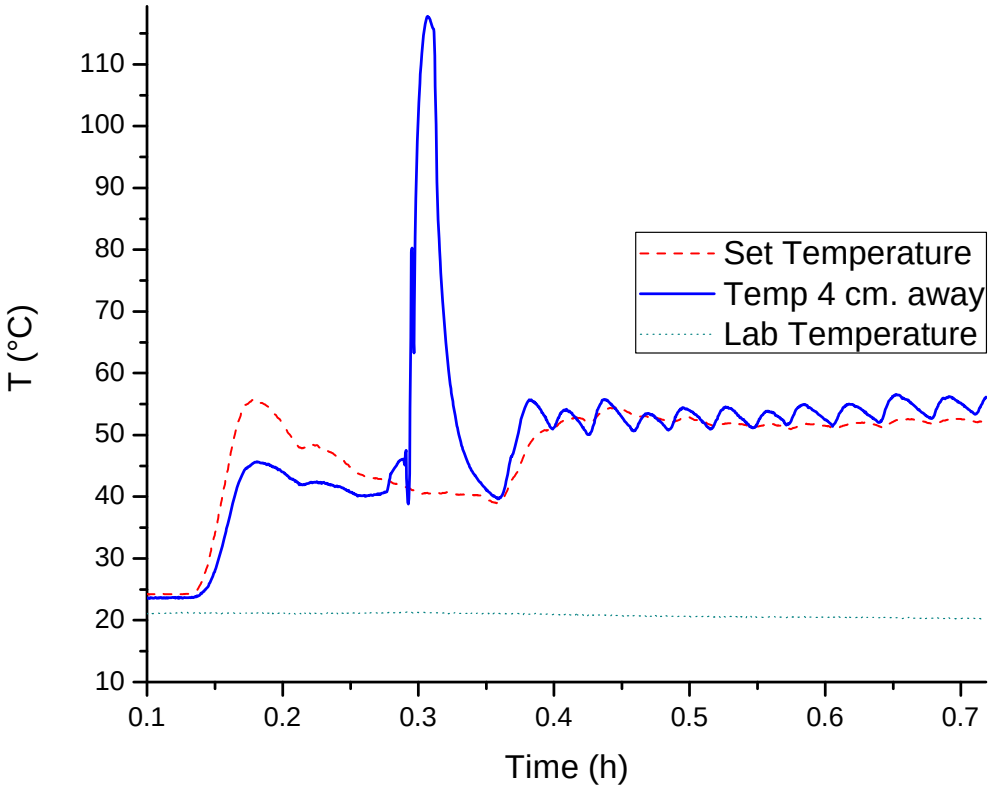

Figure 9. Example of non-dampening of controller signals: “spiking” temperatures.

5.3.5 Sample Flashing

An important aspect of the rig design concerns how representative was the sample taken just after the equilibrium was reached. Although pressurized samples taken from the reactor were relatively much smaller than the overall system volume (~2 cm^3 vs. ~640 cm^3), one could not determine the physical state of the sample (dissolved or mixed immiscible liquid). This problem was highlighted by the observation of a decreasing trend in concentration, as measured by Iodometry of the liquid samples. This is shown in one of the experimental titrimetric analysis in Figure 10.

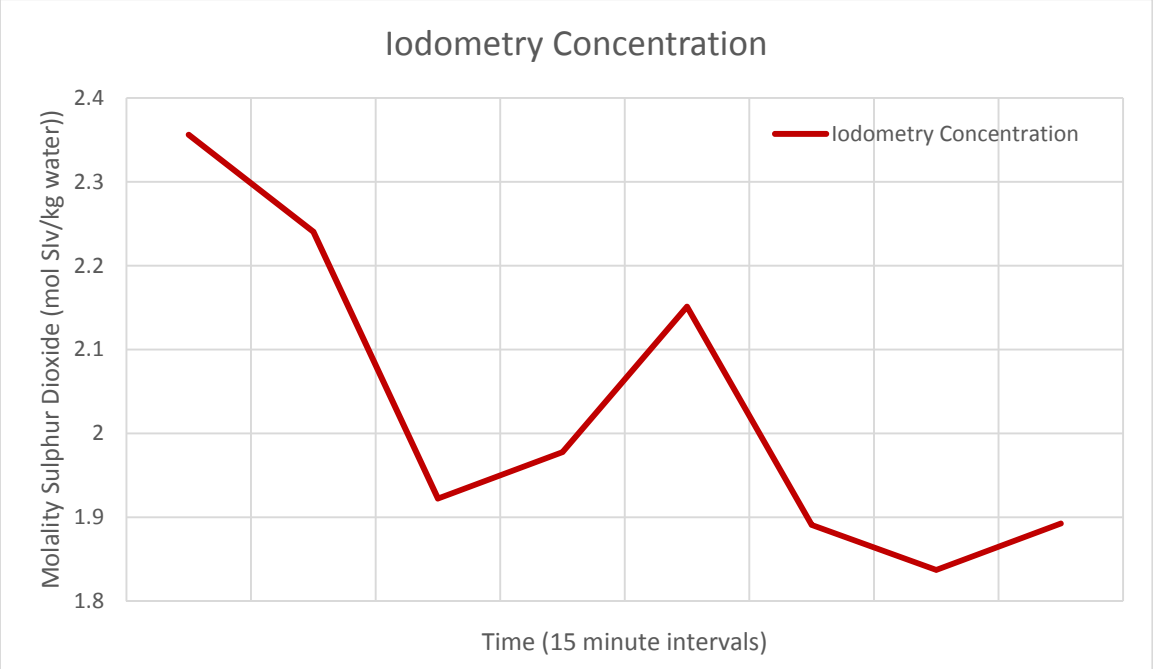

Figure 10. Iodometry analysis in a pressurized aqueous SO_2 solution.

In this example, the std. deviation is σ=0.191 and the 95% confidence interval was 0.132, an average uncertainty of 6.5%. The overall trend for SO_2 to volatilise into the ambient atmosphere while in solution is well defined. This was a constant source of error that crippled efforts to precisely to determine the VLE behaviour of the mixture. This was a vulnerability in comparison with the Othmer still: the lack of a compensating pressure system had a perceivable effect on the results gathered atmospherically.

While it was possible to make modifications to the rig and alleviate certain of these shortcomings, the decision to make a fourth-generation still was hastened by an incident that eventually caused the decommissioning of the Mark III, discussed in section 5.5.

5.4 Requirements: Visualisation, Solids and Phase determination

5.4.1 Flow visualisation

In the literature, particularly the work by Battino (1966) and Maass & Maass (1928), on which Shaw's experiments were based, flow within the system was easily seen as the apparatus that the authors were using was made out of glassware and very simple mercury manometers. Although simple, this greatly eased the pinpointing of important stages within the vapour-liquid equilibrium context of the system, such as the bubble point, dew point and the identification of impurities. In contrast, the Mark III was designed to withstand high pressures while remaining safe to operate, and so there was no opportunity to easily include a sightglass without incurring higher costs and custom machining not possible in the workshop. This was also an approach taken by van Berkum (1979), on which we based the Mark IV sight-glass upgrade, even if only a one-way sight-glass. Although not critical, it was desirable to obtain visual confirmation of the behaviour of the mixture within the system, without the penalty of flashing solutes, as explained in section 5.3.5.

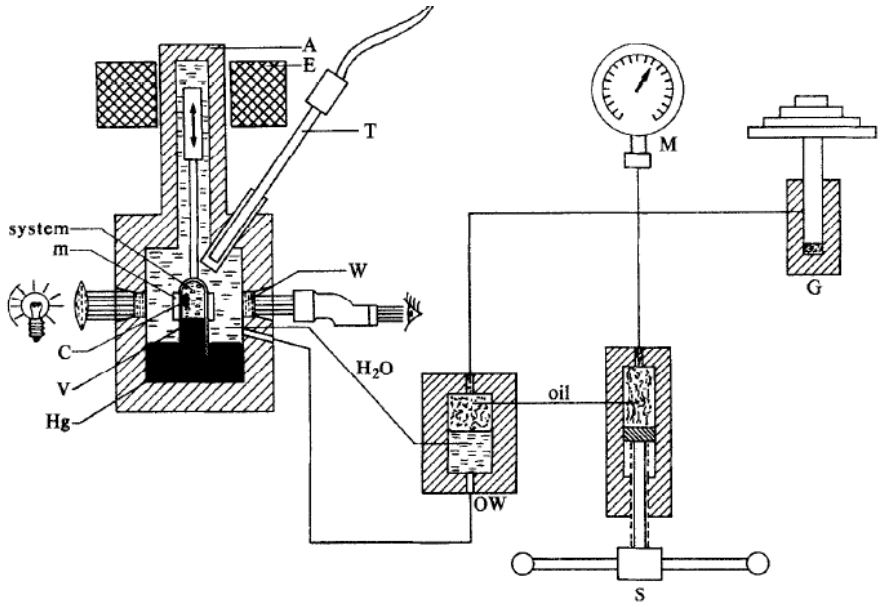

Figure 11. Van Berkum's (1979) optical autoclave, with measurement instruments .

5.4.2 Solid Formation: SO_2 Clathrate Hydrate

According to several authors (Harvey et al., 1964, Mohammadi and Richon, 2010), the conditions necessary for the formation of a crystalline white clathrate hydrate are readily attained with moderate pressures (<10 bar) and temperatures (from 279.9 to 285 K). This was identified as a white watery powder after the sampling of liquids once equilibrium was reached. This was problematic, as the molar quantities that are contained in the SO_2 clathrate crystals are by no means negligible, and were identified to cause further deviation from real molarity values during Iodometry.

It is important to note that the liquid and gas valves providing isolation during sampling is an advantage because each phase does not interfere with the other during sampling. This means that, while the pressure inevitably dropped during liquid sampling (as the liquid sampling valve is opened), the gas in the gaseous chamber remained at equilibrium conditions if the liquid and gaseous chambers were isolated via a valve, as the state variables were not modified (decreased pressure in one chamber, not the two). Once the valves were opened though (and the chambers equalized), equilibrium shifted (towards a higher

flashing and lower pressure) and it wasn't further considered representative of what was inside the rig during the experiment (generally, lower pressure=less solubility, as shown in the Chapter 4 models, for both SO_2 and O_2).

5.4.3 Aqueous and SO_2 phase determination

The validity of the sample taken was not only determined by the possibility of equilibrium shift due to the volume state variable being changed in the system, but also by the physical orientation of the rotating still. In other words, flashing the sample and the rig being vertical or horizontal. This becomes clear if one considers that gravity and density play a key role in the equilibrium distribution of the different hypothetical phases within the liquid chamber. If it is hypothesized that there are two liquid phases within the chamber, depending on the horizontal orientation of the L_1-L_2 interface normal to the sampling point, one could sample either a mixture of different phases, or a representative sample of only one of them, depending on their volume. One could not possibly tell as there was no sight glass as experiments were carried out. In low pressure preliminary spectroscopic experiments (described further in section 5.11.3), peaks pointing to the formation of a second liquid phase increased the suspicion of a second liquid SO_2 phase.

This incident, along with the interest of a fellow researcher involved in thermochemical cycles, Bob Buckingham, from GA, sparked the objective to obtaining visual confirmation of a possible formation of elemental sulphur in these experiments (Buckingham, 2011). The relevance of this hypothetical finding is out of the scope of this project, but it is noteworthy that this possible reaction is relevant to the sulphur-sulphur thermochemical cycle. However, it was impossible to identify the common yellow flakes of elemental sulphur *in-situ*. This was another motivation to go for *in-situ* measurements and a sight glass for the new reactor. In total, prior to the thermal switch incident (see section 5.5), more than 50 binary and ternary data points were acquired.

5.5 Thermal-switch Incident

On the 21st of February 2011, multicomponent experiment #52 concluded. Standard procedure after its conclusion was to prepare the rig for the next day's run. This included drying of the rig for 1 to 2 hours. The method of drying involved a regulated heat supply from the rope heaters and a compressed air current venting out to the fume cupboard. This had two objectives: to delete traces of sulphur dioxide inside the gas chamber and to dry the rig. Heating remained controlled, as it limited excessive temperature drops due to evaporative cooling from droplet remains inside the rig in contact with the compressed air. An operating system crash occurred within the PC and, as there was no implementation of software safe-mode, all five solid state relays in the data acquisition module turned completely on, leading to the rope heaters to reach their maximum temperature, only limited via the thermal switches, set at 240 °C. After three hours, a quick click in the fuse box of the heater controller was noticed and the system was shut down. The PTFE lining melted and was deemed unusable. A root-cause analysis was then performed to determine the causes of the incident.

5.5.1 Root Cause Analysis

A thorough inspection of the rig was performed after the incident. After careful consideration, the conclusion that an electrical failure in the heater/relay subsystem was the main cause of the malfunction was reached. Factors attributed for the system failure were the following:

- Thermal degradation of the continuous use of the rope/mat heaters, including the heaters themselves as well as the cables needed for their electrical connections. This was evidenced by several scorched terminals in the fuse-box.

- Slow response in the event of a malfunction. The fact that the rig is operated under full fume cupboard extraction made difficult to notice appreciably some smoke that came out of the inside of the rig.
- Fluctuation of the PID algorithm. Along with the missing safe-mode implementation that should have been programmed, this was ultimately an accelerating cause of failure. (see section 5.3.4)

After the causes were identified, efforts to fix the Mark III were pursued. These included resurfacing damaged parts of the PTFE lining, plugging blanks where former pieces were deemed unusable, replacing electrical components and updating the LabVIEW software. A noble but unfruitful effort that made evident the necessity of a new reactor.

5.5.2 Mark III Follow-up

Further to the measures taken to update the software used for the data acquisition (see 5.3.4), several conclusions were drawn from this event. These notes account only for technical difficulties encountered during the experiment, and they are not related to theoretical problems that were inherent to the design of the chemical sampling, which are discussed in section 5.3.5. A summary of the formerly mentioned difficulties is presented below.

a) Heating

- Rope and mat non-uniform heating of large areas of the apparatus metal body, leading to higher-than-expected fluctuations between liquid and gas temperatures (see section 5.3.4).
- Temperature gradient extremes, inherent to the PID controller.
- Consistent degradation of the rubber-based heater surface, contributing ultimately to electrical failure of the connections.
- Excessive amount of energy needed to reach desired temperatures, associated with high mass (35 kg), high heat capacity of steel and species contents (~0.6-0.8 kg water).

b) Electrical/Data Acquisition

- Numerous connections and little flexibility of adding new voltage measurements within the DAQ interfaces.

c) Other

- Associated costs with large amounts of chemical reagents to titrate/analyse due to large system volumes.
- Bulky set-up, hard-to reach valve connections once installed. PFA valves accounted for 15% of the reactor weight.
- Non-standard attachments and their associated cost. Modifications to the Mark III had to be done at our Workshop in Buxton, due to specialized large machining tools that were only available there. This was largely a nuisance, rather than a limitation.

After a thorough evaluation, it was decided to continue and develop a new reactor that would improve upon the shortcomings of the Mark III design, and add novel instrumental analysis. In the following section, the detailed design and engineering of the Mark IV rig are presented.

Mark IV Design

5.6 Aim

On account of the shortcomings of the Mark III reactor discussed in previous sections, it was deemed necessary to provide novel alternatives to the thermodynamic determination of equilibrium of the ternary and quaternary mixtures. The aims of the new design are:

- Ease of use
- Smaller, more practical size
- Lightweight
- Cheap to machine
- Simple to operate
- Addition of in-situ measurements

5.7 Material Considerations

There are only few attempts to obtain high-pressure VLE in the literature that include electrolytes, let alone high temperature. Even more so if a limited budget is included in the design constraints. The materials within the Mark III design were very resilient, withstanding harsh SO_2 hot solutions, and capable of sustaining sulphuric acid. Therefore, the idea remained to use high-performance fluoropolymers. As mentioned in section 5.9.1, preliminary calculations indicated that In order to optimize time per run, mass had also to be decreased. With these set of conditions, pure PTFE plastic was not considered, as the costs required for a successful permissive strength would be prohibitive. Additional mechanical strength was required, so the second option was PEEK, but was deemed very expensive (a 200mm rod, 80mm thickness would have been £700.00). Finally, glass-reinforced PTFE was selected over PEEK for price/performance. The

thermal and mechanical properties of GF-PTFE are shown in Table 3. It is worth noting that the dimensional stability of GF-PTFE far succeeds that of virgin PTFE.

Table 3. Thermal and Mechanical Properties of commercial GF-PTFE. (Quadrant, 2011)

Thermal Properties	Units	Result
Melting Temperature (DSC, 10 °C/min)	°C	327
Coefficient of linear thermal expansion, 23-100 °C	m/(m.K)	0.000086
Temperature of deflection under load (1.8 Mpa)	°C	100
Max. Allowable service temperature in air:		
for short periods	°C	280
continuously	°C	260
Minimum service temperarure	°C	-50
Flammability: Oxygen Index	%	>95
Tensile Stress at Yield	Mpa	10
Tensile Strength	MPa	10
Tensile Strain at yield	%	5
Tensile strain at break	%	>50
Tensile modulus of elasticity	MPa	1450
Charpy impact strength - unnotched	kJ/m^2	30
Charpy impact strength - notched	kJ/m^2	7.5
Ball indentation hardness	N/mm^2	40
Rockwell Hardness		R 50

5.8 Pressure Vessel Calculations

As with all other compressed gases, safe engineering practice requires the calculation of the permissible thickness for a given internal diameter D_i,

allowable tress S and internal pressure P_i for a pressure vessel. According to Sinnot's Handbook (2007), p.986,

$$t = \frac{P_i D_i}{2S - P_i} \quad (1$$

the minimum GF-PTFE thickness for a 40mm internal diameter was 20mm, considering a tensile strength of 9 MPa for virgin PTFE and it being a cylindrical vessel where the cone shaped for the gas chamber would be maxed out at 40 mm, giving plenty of safety margin for 60 bar and the 15% overdesign factor.

5.8.1 Operating Pressure

Although the design pressure was 60 bar, the maximum operating pressure was 30 (as it is the maximum pressure reached by 6 grams of oxygen in a 1450 ml container), and including the soft nature of PTFE, even with a mica content, the author dared not to raise the new operating pressures up to 5 bar. Limits on the time available for the operation of the new reactor meant that any failure of the new rig would be catastrophic for the project deadlines. This made sense, as the Kazimi's flowsheet shows a 5-30 bar optimal separation pressure range for a 1 to 70 bar acid decomposer (see Chapter 2).

5.8.2 Allowable Stress

A survey from different plastics providers showed a definite increase in tensile strength on account of the addition of mica to the polytetrafluoroethylene mixture, thus allowing a further safety margin to the operation of the vessel. Depending on the provider (Quadrant, Bay Plastics, Plasteurope), one could reach 15% to 40% mica content, and tensile strengths from the minimum virgin 10 Mpa to 15 Mpa. Although a GF45% (45% glass reinforced PTFE) content was requested, the supplier shipped a 15%GF.

5.9 Thermal Properties

5.9.1 Preliminary thermal calculations

One of the features that was most sought after in the new design was low mass and better operability. This would lessen the time required to run an experiment, and facilitate the acquisition of larger amounts of solubility data. For this, two engineering approaches were taken to explore new design alternatives that would determine how long an experiment would carry on, once the basic engineering of materials and rig geometries was selected. The first is a simple calculation determining the heat required to bring the supposed new design to a certain temperature, compared to the old Mark III. Considering the following equation,

$$Q = mC_p\Delta t \qquad (2$$

and the two materials of interest, steel and PTFE, with their respective specific heats $C_{p(\text{steel})}$ = 0.49 kJ/kg*K, and the $C_{p(\text{PTFEl})}$ = 1.05 kJ/kg*K, one can then calculate that the amount generated by each. Considering the Mark III mass of 20 kg, and a 1 kg mass for the PTFE Mark IV, to 80 °C when an ambient temperature is 20 °C, the energy required is:

$$Q_{steel} = 20 \times 0.49 \times 60 = 588 \text{ kJ} \qquad (3$$

$$Q_{PTFE} = 1 \times 1.05 \times 60 = 63 \text{ kJ} \qquad (4$$

The energy required to heat the Mark IV rig is only 10% of that required for the Mark III rig. Added to this, a size reduction would make it feasible to insert the entire rig into a water bath, eliminating the need for a new PID program in LabVIEW, reducing the risk of burning elements of the plastic rig. This would also remove the necessity to worry about the heating uniformity, since the conductive rope heaters would be substituted by a turbulent convective process within the

water bath. Further calculations were conducted to confirm the selection of glass-reinforced PTFE.

5.9.2 Problem set-up

Some necessary calculations were required in order to determine the approximate time the apparatus would take to reach thermal equilibrium, according to the following constraints:

- The apparatus was certain to be made of a somehow stiffer polytetrafluoroethylene, to sustain the operating pressures and achieve chemical inertness with the species to be investigated. GFPTFE was selected for this process.
- The apparatus was not fully single-component. Stainless steel was certainly going to be used for additional external frame support, but the geometries were not known initially.
- Once the geometry was fully characterized, further analysis of the thermal behaviour of the reactor could take place in a more sophisticated form, or explore structural analysis for instance (see section 5.14.3).

This systematic approach would guarantee maximum experimental productivity with the shortest time per run possible. This was a critical design criterion due to the limited time available for experimental acquisition, once the apparatus was commissioned. Lumped system analysis calculations were performed for preliminary time calculations, using oven-heating scenarios and water-heating scenarios.

5.9.3 Lumped System Analysis for transient heat conduction Rig Design

Consider a cylinder made of PTFE, 8 cm Ø and 20 cm length. Its area and volume would be, respectively

$$V = \frac{\pi D^2}{4} h, \qquad A = \frac{\pi D^2}{4} \tag{5}$$

Its characteristic length, the volume to contact area ratio, would be 1.6 cm. Since a typical natural convective coefficient of water is between 20 and 100, it follows that the Biot number, the ratio of convective to conductive resistance that determines the feasibility of the transient analysis, is

$$Bi = \frac{h \times L_c}{k}, L_c = \frac{V}{A_s} > 1 \tag{6}$$

Since the applicability of the analysis is exploratory when the Bi <0.1, one can assume that the approximations would have a certain error. However, if one considers the transient time equation

$$\frac{T(t) - T_\infty}{T_i - T_\infty} = e^{-bt} \tag{7}$$

the temperature needed for the VLE experiment will be at one degree prior to the set temperature when

$$\frac{T(t) - T_\infty}{T_i - T_\infty} = 0.16\overline{6} \tag{8}$$

Considering an initial temperature T_i, a set temperature of T , and 79 °C in the reactor, one degree less than the set temperature. Since the exponent value b is

$$b = \frac{h}{\rho C_p L_c} \tag{9}$$

Where

- ρ , Density of PTFE, ~2200 kg/m^3
- C_p, Specific heat of PTFE, 1.2 – 1.4 J/kg*C

- L_c, Characteristic length, calculated as 0.016 m
- h, Least convective scenario for water, 20 W/m^2*C

The exponential value b is then 0.004 s^{-1}. Substituting into eq.7,the time it takes for this proposed rig to reach ~80 °C is 10 minutes, a negligible amount and quite an optimistic one, however, this was an approximation that was encouraging, so it was decided that no CFD was required as the heat transfer would not be a problem.

5.10 Equipment & Instrumental Design

One of the key aspects of the new apparatus was to implement the means to look at the physicochemical nature of the media whilst at equilibrium. There were several alternatives that could be practical and were explored via a literature review:

- Interface spectroscopy. These potentially included nanophysics, linear and non-linear optical techniques which were out of the scope of this project, and were of exorbitant cost
- Vibrational spectroscopy. Through the combination of literature review and an informal survey with colleagues at the Chemistry department, it was thought reasonable to include these as quantitative possibilities of analysis within the VLE system.
- Gas Chromatography. Since very little amounts are required for gas chromatography, this was ideal for species calibration, although the discrete nature of sampling would not be considered as the main way to determine composition.
- Titrimetric analysis and Iodometry would still be the staple means to check composition for atmospheric liquid samples, prior or subsequent to the addition of an iodine solution.

The design then would look like the arrangement shown in Figure 12

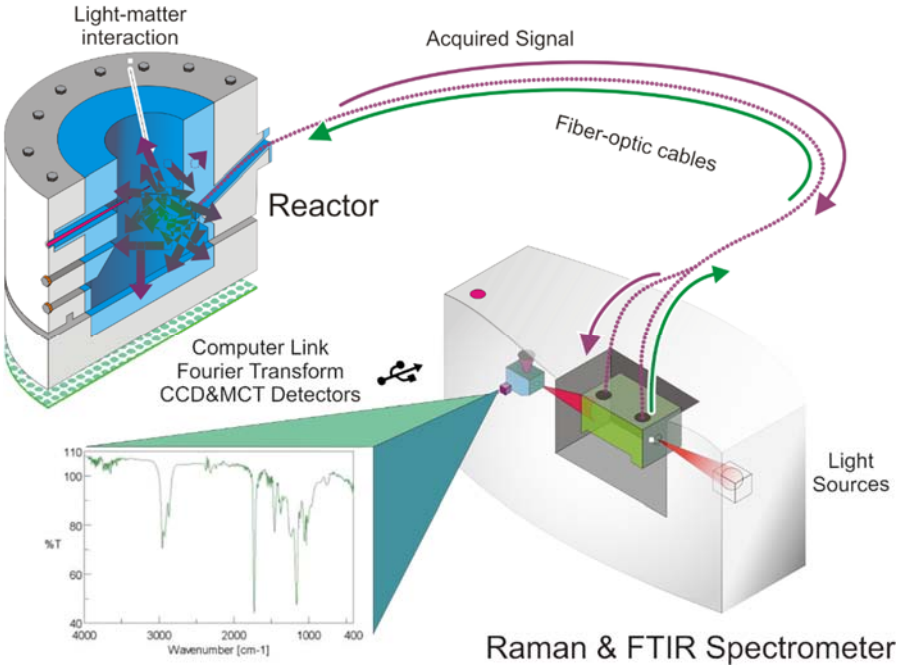

Figure 12. Principle of operation of in-situ vibrational spectrometry.

Once these parameters were decided, the equipment was purchased.

5.11 Spectroscopic theoretical background

Prior to the acquisition of the instruments, a detailed analysis of the theory behind each measurement was performed. In the following sections, a brief yet concise introduction to both spectroscopic measurements will be addressed.

5.11.1 Infrared spectroscopy

Infrared spectroscopy is the most common spectroscopic method, and it was selected as a candidate to obtain a closer look at the vibrations of ions. The method is quick, sensitive, easy to handle and is very versatile. The relative ease of handling and the non-destructive nature are advantageous for an in-situ technique. According to Gauglitz and Vo-Dinh (2006), infrared is “excellently” suited to multi-component, gaseous, liquid and solid quantification of analytes, providing them with an unique fingerprint. The availability of fiber optics has increased the flexibility of the analysis as well. What the spectra shows is the

fundamental vibrations of bound atoms, which is the vibration *j* as a change in molecular dipole moment μ during vibration, according to a normal coordinate *q*:

$$\mu_j = \mu_0 + \left(\frac{\delta\mu}{\delta q_j}\right) q_j + \frac{1}{2}\left(\frac{\delta^2\mu}{\delta q_j^2}\right) q_j^2 + \ldots$$

5.11.2 Raman spectroscopy

The Raman effect is the non elastic scattering of light, in contrast to the Rayleigh light scattering (1000x more common). The Raman effect is very weak, and it occurs when the wavelength of a monochromatic emission changes due to the interaction with the polarity of a molecule, hence causing an induced dipole moment. The condition for Raman to be active in a molecule is a change in polarization of the electrons during the light interaction with the radiation of incidence (Gauglitz and Vo-Dinh, 2006).

In Raman spectroscopy, care has to be taken to avoid fluorescence and light noise, as the effect is very weak and could be overshadowed by several interferences.

5.11.3 Raman Spectrometer

The advantages and characteristics of Raman spectrometry were briefly explained in section 5.11.2. Since the intention was to provide a relatively low-cost, turnkey device that would be sturdy, yet capable of slight modifications, the Raman Systems R-3000 was selected. The Raman R-3000 is a fibre-optic based spectrometer with a short 1m fibre optic and a probe head made out of stainless steel, holding a borosilicate glass lens of approximate 8mm Ø and focal length of 5mm. The Raman spectrometer featured a 785 He-Ne laser capable of 350 mW of excitation. Because it is a Class 3B device, near-IR blocking safety spectacles were obtained and used for all experiments.

The stainless steel tube is approximately 80mm long and 15 mm in diameter, with one side a threaded lid to put against a sample (depending on whether it was liquid or solid) and on the other side a M9x0.75 metric thread that went into the beamsplitter configuration and finally a CCD array of 3648 pixels, capable of a 10 cm^{-1} resolution and a Raman Shift range of between 400 and 3200 wavenumbers. The software provided, RSIQ®, was not capable of adding scans reliably, therefore the author settled with SpectraSuite.

The drivers were modified from an OceanOptics® NIR USB4000. Since it was a charge-coupled device detector and provided only a weak Raman signal (discussed in Chapter 3), noise was a major problem, and it was only possible to obtain delicate signals, not sufficiently reliable for qualitative analysis. A procedure for obtaining Raman spectra is provided in the experimental appendix, and the usual operating parameters are later described in Chapter 6.

Several iterations of probes and Raman configurations were tested:

- *In promptu* alignment of a 100x Carl-Zeiss microscope objective.
- Liquid attachment of the original probe
- Solid attachment of the original probe
- Different laser power configurations and wavelengths.
- Different scans/acquisition time arrangements
- Finally, a PEEK Raman probe, designed and tested in-house.

More than 200 spectra were acquired, testing different settings. Finally, the highest signal-to-noise ratio was found at 5 seconds acquisition time, and 200 scans, for a total acquisition time of ~17 minutes.

In the compilation in Figure 13, one can see the different limitations that were encountered in the Raman Experiments. Acetonitrile, a limited absorbing component is shown to have a convoluted peak in the upper left part of the diagram. These are comparable to the spectra of SO_2, very weak and contaminated with ambient light (see in the light contamination part). Even at one day of exposure, no significant spectrum is shown to have a signal to noise ratio of

more than 5, except a peak between 1100 and 1300 cm^{-1} in the lower left part. These results are discussed in next chapter, in the spectroscopic section.

Preliminary Raman Experiments

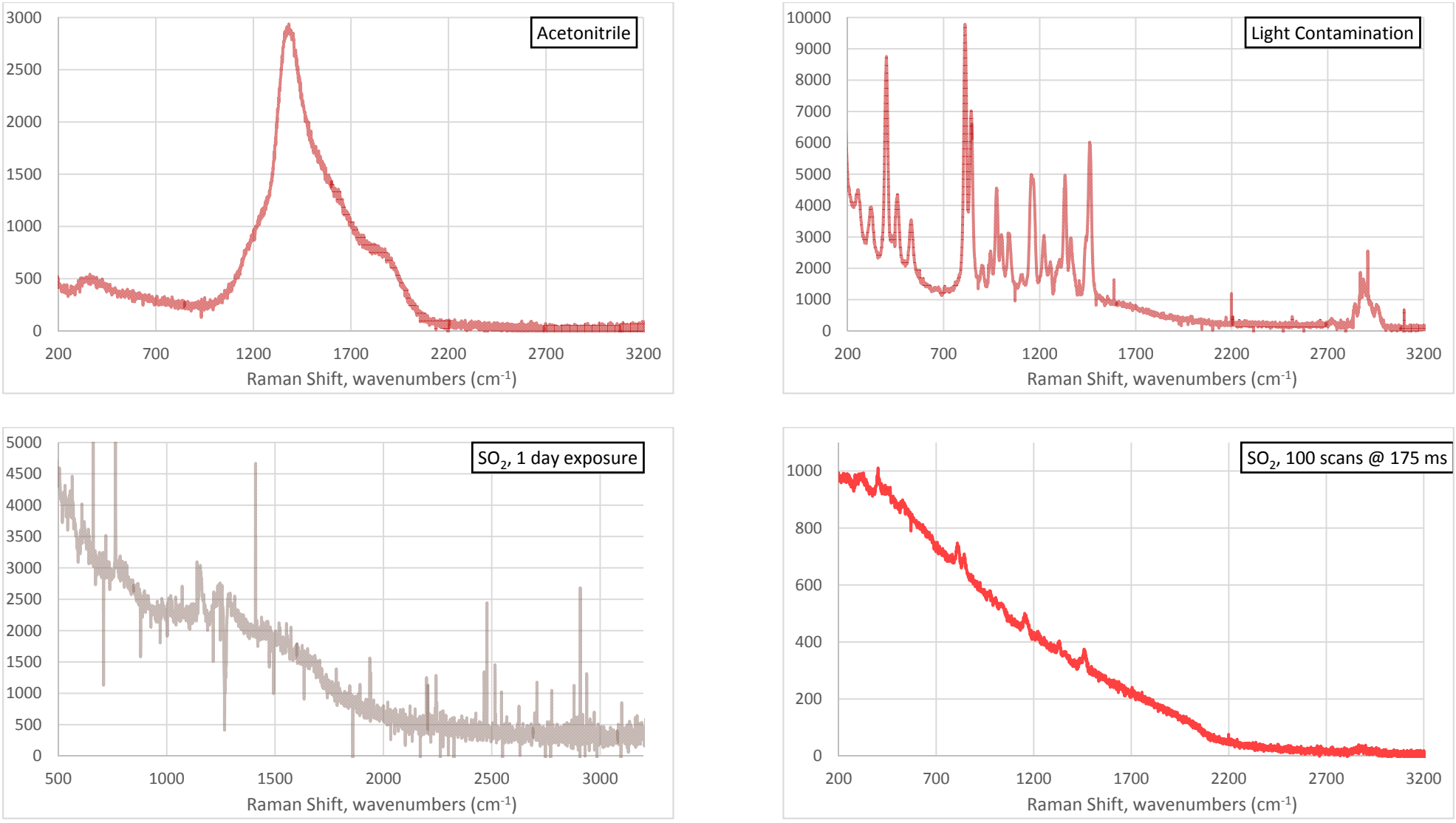

Figure 13. Preliminary Raman Experiments pointing at certain operating aspects of acquisition.
Acetonitrile acquired without caps. Light contamination with Microscope objective. SO_2 exposure, with correlation to light contamination peaks.

Since the normal Raman probe was not able to withstand the harsh corrosive media inside the rig, the idea was to machine a PEEK probe with an O-ring seal that would press against the rig body (to seal against the hydraulic internal pressure of the experiment) and against a lens with similar or better characteristics than the original probe. The final probe design is shown in Figure 14. Detailed drawings are provided in the Appendix.

The probe consisted of a PEEK casing of approximately 40 mm Ø, and a metal, 50mm long internal optical path with a M12 external thread that would fit inside a 3/8” BSP clearance hole in the center of the PEEK casing, that would push against a 6.3mm sapphire lens, with a back focal length of 4.3mm. The wetted surface of the lens was minimal in comparison to the thickness of it. Along with the strong, hard resilience of sapphire, and considering ideal welded efficiency typical for small dimensions; the design pressure for the arrangement was a little above 60 bar. Results of the final Raman configuration are provided in next sections in this chapter.

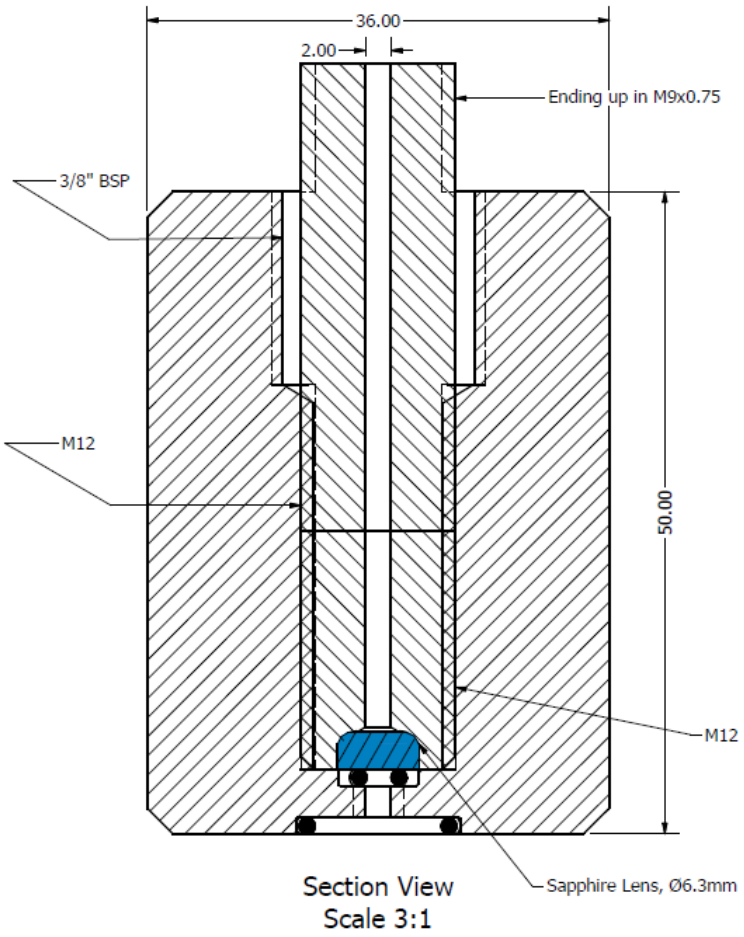

Figure 14. Raman PEEK Probe designed by the author.

5.11.4 FTIR Spectrometer

According to the analysis that was performed during the literature review, it was determined that the SO_2 was going to need a high performance spectrometer if we were to use it quantitatively. The specifications were fulfilled by a research-grade Varian 660 FTIR spectrometer.

The Varian 660 spectrometer features a 10,000:1 signal to noise ratio, as well as a nominal range between 400 cm^{-1} to 15,000 cm^{-1}. The settings used are given in Appendix A. A diagram of the optical path of the FTIR is shown in Figure 15, including the detector arrangement, the optical path, and the internal components.

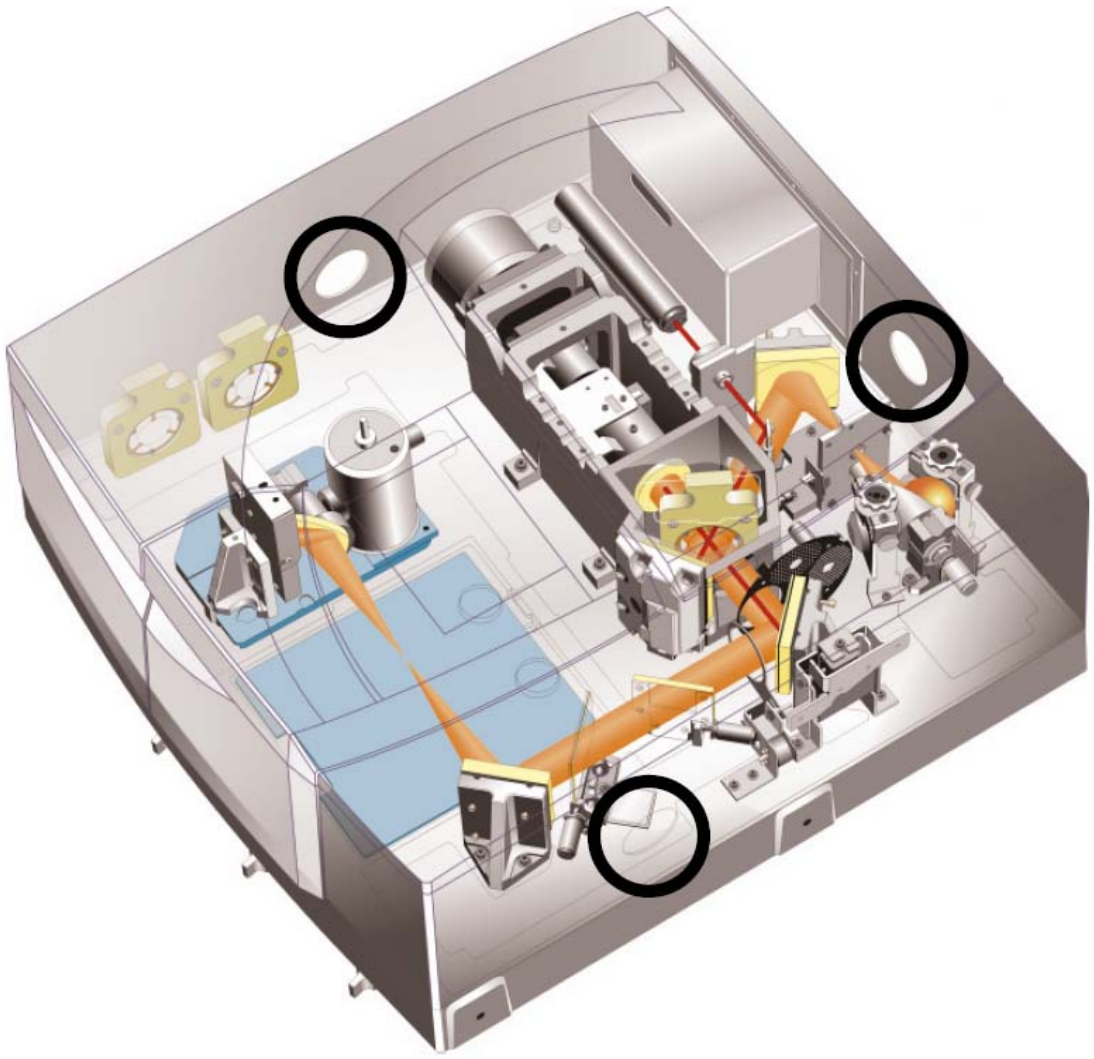

Figure 15. Varian 660 Spectrometer, showing the optical path of the IR source and internal components.

The sensitivity was the main criterion for the selection of the mercury-cadmium-telluride detector, which is in fact an alloy of Cadmium telluride and Mercury Telluride. A linearized broadband MCT detector was selected, nitrogen cooled to avoid noise build-up.

A critical review of the proposed sampling method was undertaken, and it was determined that the required liquid cell and gas cells accessories would be manufactured in the department. These will be covered in Section 5.14.

5.11.5 Auto Titrator

The autotitrator used was a Mettler Toledo® DL 40 with two channels, two detectors (DM-140 for electrode potential measurements, and D90-SC for pH measurements). Once a liquid sample was taken, it was made to react with an excess iodine solution.

Knowing the amount of initial sample, and the mass and concentration of the initial and final Iodine solutions, one could determine the SO_2 reacted with Iodine, and therefore the amount of SO_2 contained in the sample extracted from the Rig at equilibrium. This was done automatically, although the programming of the method in the autotitrator required knowledge of the stoichiometric of the reaction, as well as the results interpretation. The proof of chemistry is taken from the Appendix from Shaw's doctoral thesis (2008).

5.12 Infrared Materials

Along with the selection of accessories and instruments, materials were evaluated for their potential role as IR-transmitting media. Their chemical and mechanical properties were important, as the vibrational excitations of the species to be investigated would not be readily suitable for the transmission spectra of most infrared materials. The properties of the key three analysed materials are described briefly in the next few paragraphs.

5.12.1 Silicon

Silicon is well known for its semiconductor properties; however, it is sometimes not known that elemental silicon has different properties from the more common compound, SiO_2. Silicon, in its elemental form, is a relatively light shiny, dark silvery lustrous element with a cold feel to it. In polycrystalline form, is very sharp and has important optical properties, one of them being the broad capability to transmit a high percentage of IR energy through a relatively thick window

(~10mm would be considered normal). The IR transmission curves for Silicon, Germanium and Zinc Selenide is shown in Figure 16.

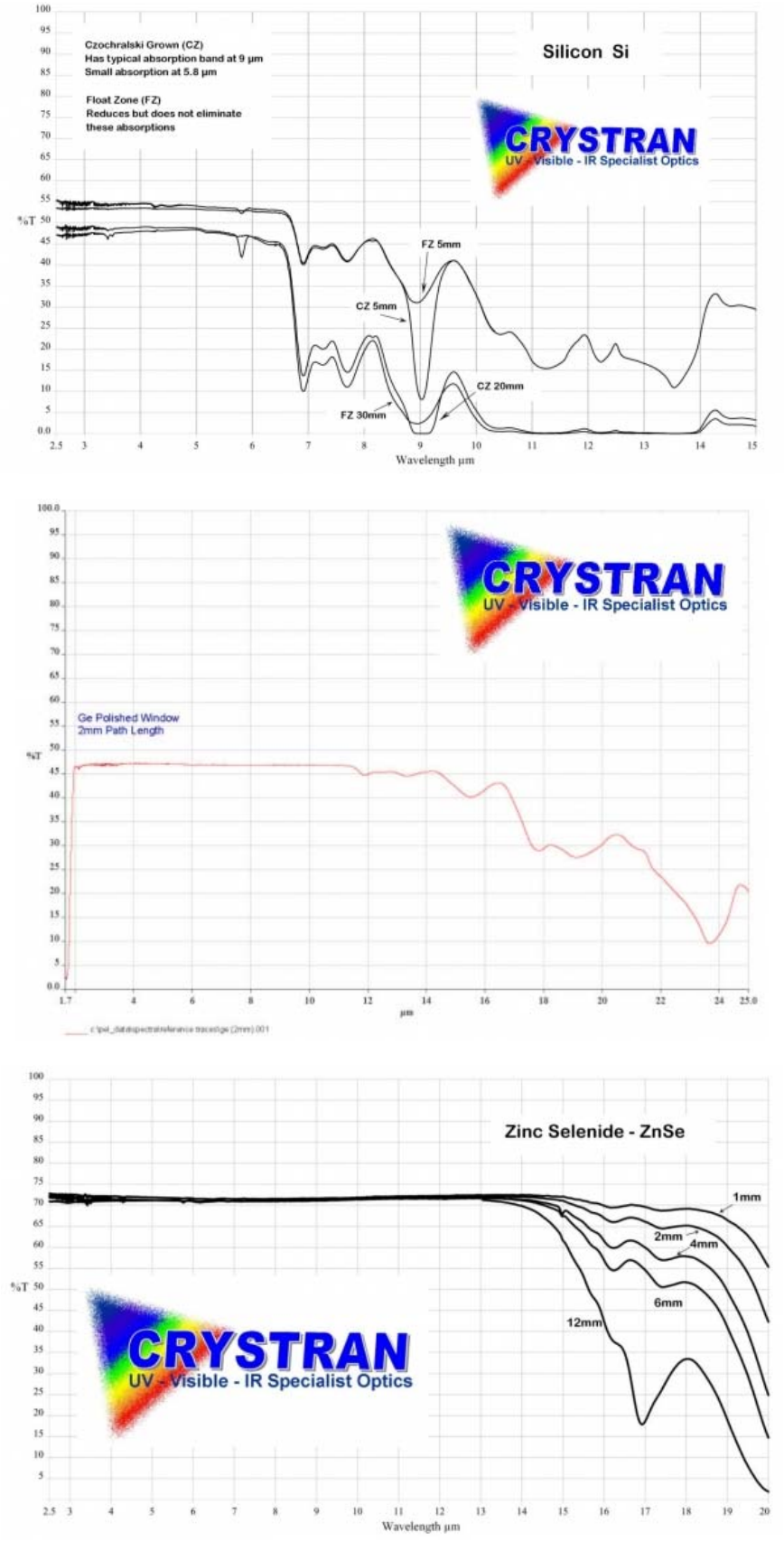

Figure 16. Optical IR Transmission Curves for Silicon, Germanium and ZnSe. (Crystran, 2012)

5.12.2 Germanium

Germanium is a very shiny, dark lustrous material that resembles more a crystal than a metal with an atomic weight of 72.61 g/mol and 5.32 g/cm^3. It is well known for its usage in IR imaging. It is softer than Silicon, yet it presents a higher transmission curve for the same thickness. This material was the baseline used for calculations that would determine the percentage of transmission from a window arrangement of Ge as a function of absorption coefficient, wavelength, thickness and refraction index. The results are shown in Figure 17. The refraction data was taken from the Ge datasheet from Umicore Optical Materials. The code is detailed in the Appendix D.

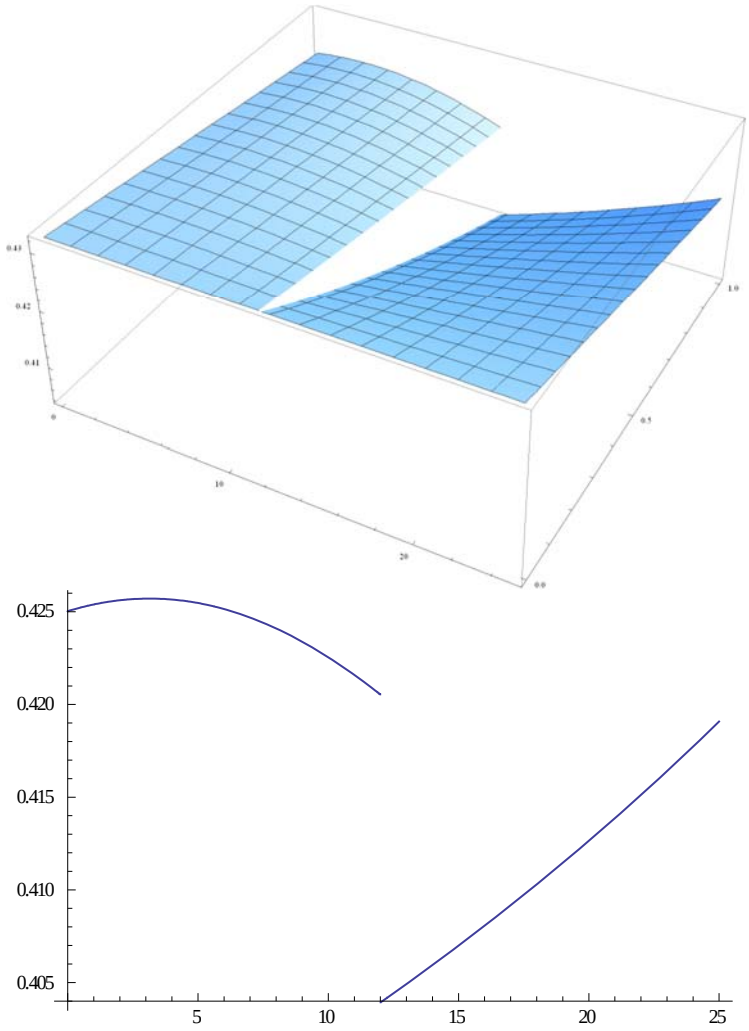

Figure 17. Transmission model $T_{\%}(n,r,t)$ for Germanium, coded in Mathematica.

The data showed a transmission of up to 33% with a maximum permissible thickness of 10 cm, way above the needs of the simple 5 mm window required for a pressure cell. The equation used for the transmission model was taken from the Handbook of Optics by Bass and DeCusatis, on its 3rd edition (Bass et al., 2009),

$$T = \frac{(1-r)^2 e^{-at}}{1-r^2 e^{-2at}} \quad (10$$

where

$$r = \left(\frac{n-1}{n+1}\right)^2 \quad (11$$

with the variables:

- T, the fraction of the energy transmitted, as a function of the absorption coefficient, reflectivity, refractive index and thickness
- r, reflectivity (dimensionless)
- a, absorption coefficient (cm^{-1})
- t, thickness (cm)
- n, refractive index (dimensionless)

5.12.3 Zinc Selenide

Zinc Selenide is another favoured ATR crystal, due to its low solubility in water and high refraction index (n). It's useful range is between the visible to the mid infrared (500 cm^{-1}), and it's insoluble in water, organic solvents, dilute acids and bases (Stuart, 2004). However, its mechanical properties are a different story, making it very unreliable to experiment with it in joints and crevasses, as a small stress can cause it to chip and crack. For this reason, small samples were requested from Crystran® to see the applicability of a possible ATR conical prism. Unfortunately, the mechanical workshop capabilities were not sufficient to

successfully manipulate such small and soft materials. This also would have incurred in a very high cost penalty and further 4-5 months of technicians man-hours.

5.13 Chemical Inertness

Through the literature review, it was suspected that the intention to use a Germanium ATR would interfere with the objective to reduce to the minimum the catalysed oxidation of sulphur species in the liquid, as studies with Iron, Manganese and Cobalt shown this trend. According to Coichev (1992) and Martin & Good (1991), these metals shown evidence of $S_{(IV)}$ to $S_{(VI)}$ transition in aqueous solutions. Since the nature of these metals is varied, it was assumed that germanium would act in approximately the same manner. However, as the design of the ATR prism shows (see figure 26), there are three reasons why the Ge prism was selected as a valid material to obtain the attenuated total reflectance measurements:

- The brittleness of ZnSe proved to be prohibitive for its planned use. The care that it took to place and fix the test pieces, along with the constant chipping due to its soft nature, was the main reason for its dismissal, regardless of the superior transmission properties that provided for the gas cell, which will be discussed in the next section.
- The near-semiconductor nature of Germanium would certainly attenuate its catalyst nature, although to the author's knowledge, no real Ge-catalysed SO_2 oxidation study has taken place;
- The relative wetted Germanium area (~40 mm^2), in comparison to the entire glass-reinforced PTFE area (~500 – 2000 times more) meant that there was little surface contact area to promote oxidative reactions of the sulphur species, without considering reaction rate promoting from the hypothesized catalytic activity of Ge.

5.14 Infrared Developments

Further to the *in-situ* design reported in previous sections (5.10), the need to investigate the gaseous spectra of the mixed species was of interest to the project. It was advantageous that sulphur species in the H_2O-SO_2-O_2-H_2SO_4, along with water, are strong IR absorbants.

Since the densities of gases are much less than liquids, this poses a problem for IR absorption of gaseous species. This is worked around with larger pathlengths, e.g. a liquid cell would be several microns, whereas gas cells could be several centimeters to multiple-path cells of 40 meters. A gas cell is simply a containing media for the gas, with an optical pathlength that will allow the IR energy to absorb it and travel to the detector, on a common configuration.

Since the sampling was to be undertaken at moderate pressures, this design was modified to withstand higher pressures, only constrained by the softness of ZnSe. The windows were provided for free by Crystran®.

5.14.1 Gas Cell

With the constraint of the optical diameter of the windows, it was decided to manufacture a gas cell that would fit inside the sample compartment of the FTIR. The gas cell was manufactured of virgin PTFE, that would hold up to 5 bar, dependent on the effectiveness of the thread. The design is shown in Figure 18 and Figure 19.

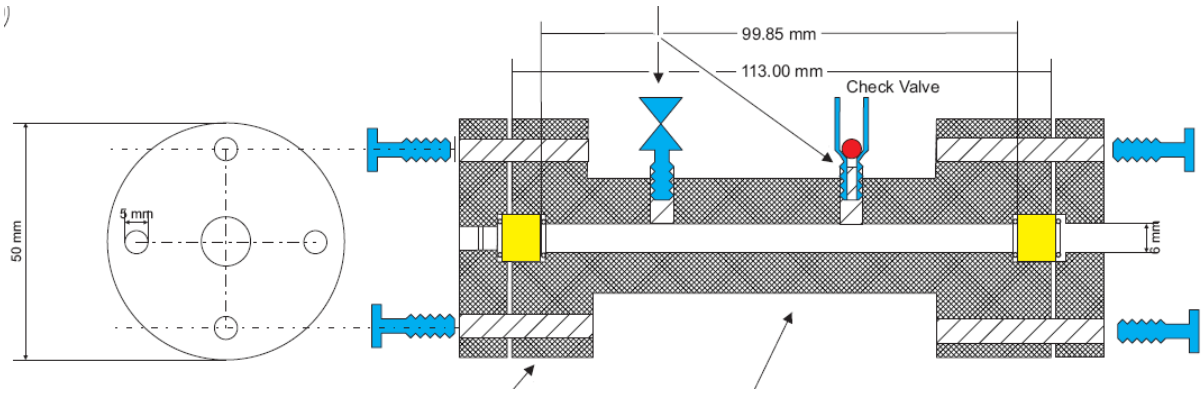

Figure 18. First design attempt at a gaseous cell.

The first potential design had a 50 mm diameter and a 100 mm pathlength, attainable depending on the machining tolerances of the milling machine.

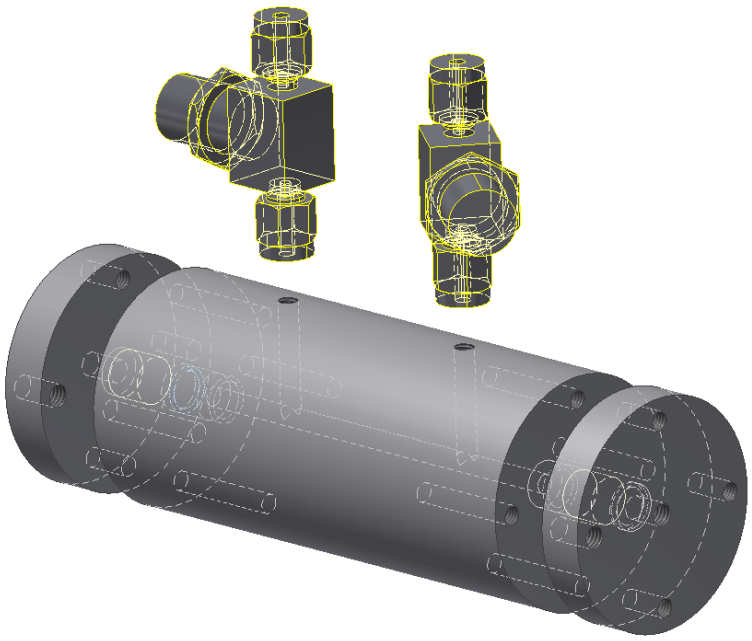

Figure 19. CAD designed cell, using Inventor™.

The optical path was limited. However, optimistic scenarios would put SO_2 absorption noticeable after the Fourier transform. A second iteration of the design was done with aid of stress simulations, shown in Figure 19. The final version is shown in Figure 20. The path length was a little below 100 mm, and it had 6xM3 bolts and nuts to secure 10 mm O-rings with 1mm cross section. The

cell was tested up to 6 bar with compressed air, with no significant leakage. The inlet and outlet was ¼”BSP threaded.

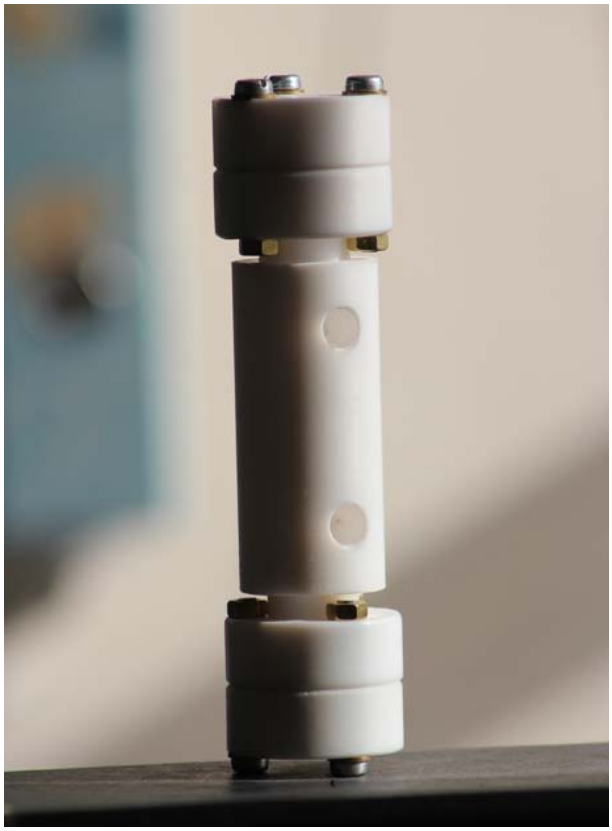

Figure 20. Final Gas Cell Version (Spectroscopic High-Accuracy Gas Cell – SHAG Cell).

The performance of the cell was benchmarked against an attenuated signal using a grated 50% attenuation plate. The results were promising, showing an entire interferogram despite small impurities within the ZnSe crystals (they were not being quality grade, but ex-stock).

The results of the interferogram are shown in Figure 21, where it can be seen that the average voltage achieved, 7.216 V, after the ADC conversion. This is much better than the regular 6.6 V from standard readings.

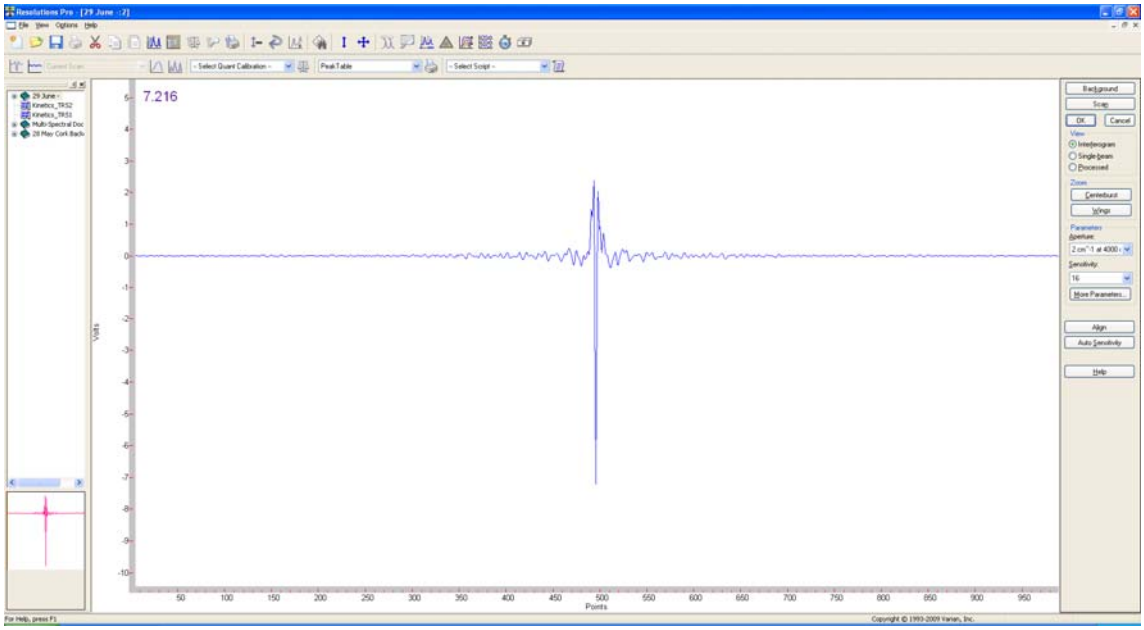

Figure 21. Interferogram of the in-house gas cell, with ZnSe windows.

5.14.2 Full ATR Configuration Results

Further, prior to the failure of the Germanium prism, the complete setup was configured in the sample compartment of the FTIR. This was an experiment to determine

- The accuracy of the Mathematica model to determine the transmission percentage according to a 6-7 V of infrared emission, measured by the MCT detector
- To determine the amount of noise that would have to be offset by the scans in the final experiments.

Only one experiment was conducted with the fiber optic configuration, as well as the germanium prism. The spectrometer used an open aperture, with 16x sensitivity, 25 kHz and only one scan at 4 cm^{-1}. The strength of the background is remarkably strong, considering there is only air in the compartment. This is a huge success considering there was no alignment and the signal to noise ratio could be improved almost a 1000 times, with little time penalty. This was one of the most important findings of this research, which inspired the author to develop further the liquid cell.

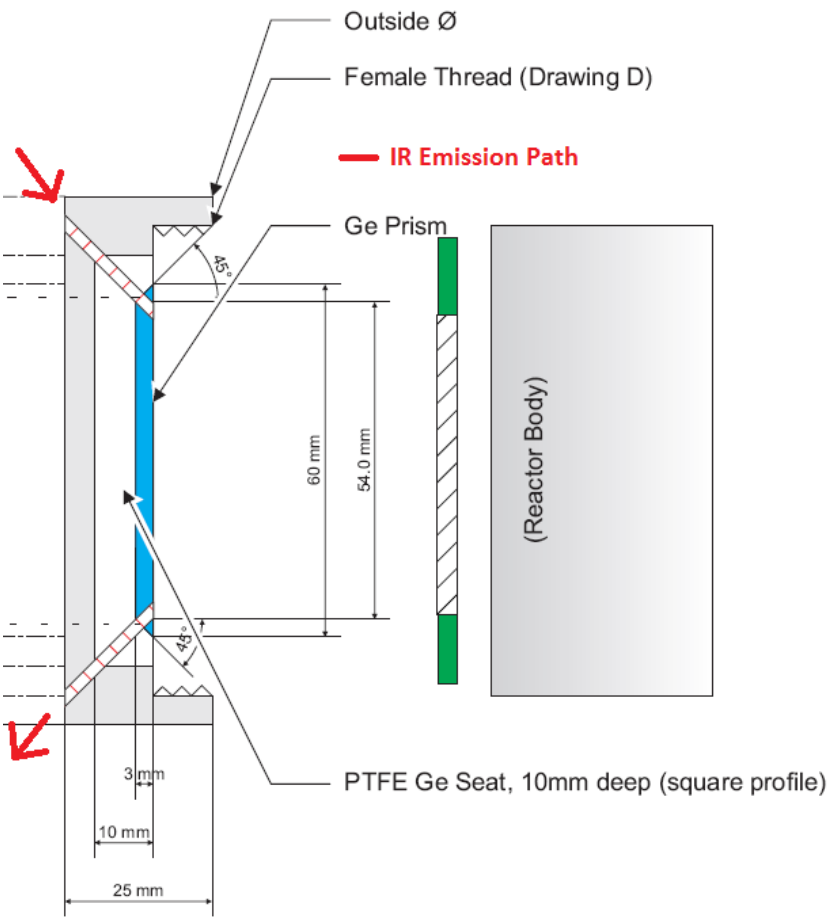

Figure 22. ATR configuration with highlighted IR emission path.

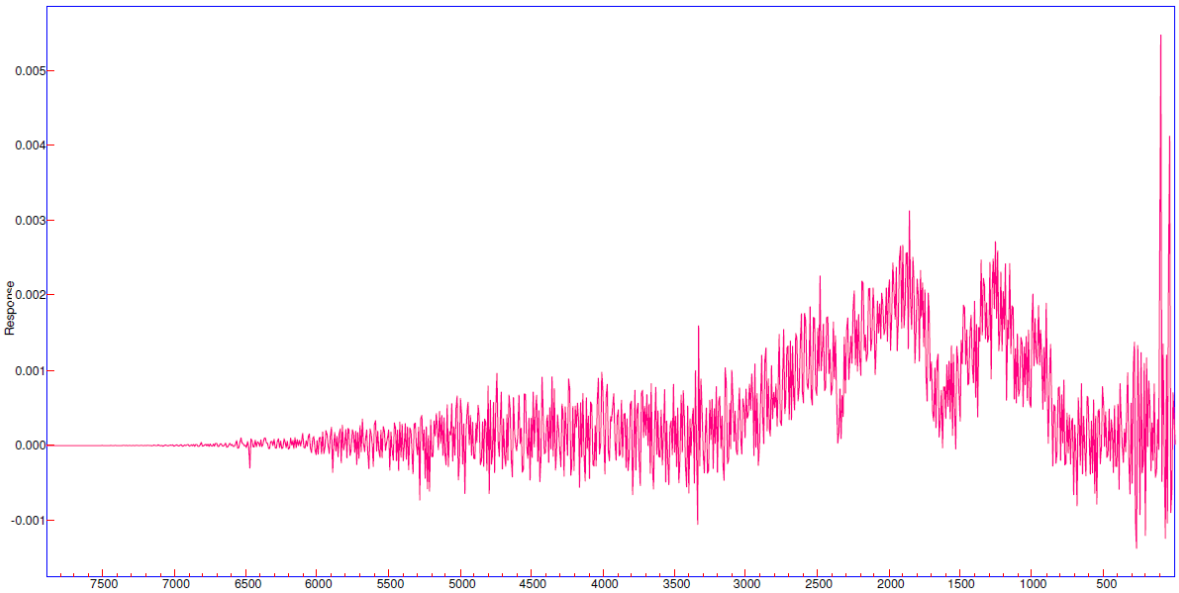

Figure 23. Germanium ATR Configuration with fibre optics and no sample.

5.14.3 Liquid Cell

For the purpose of attempting liquid sampling in the infrared spectra, a liquid cell was designed. The idea would be to obtain a liquid sample in equilibrium, and characterise it without compromising it with a big volume change. One could attach a small size tubing to the liquid chamber and let through the liquid. The driving force of the pressure inside the rig would make the liquid flow towards the lower-pressure of the cell. Although bubbles would be expected, the main factor to investigate would be the feasibility of the concept and the success of the sealing, using sapphire windows.

d) **Sapphire.**

Sapphire is relatively cheap in comparison with other IR materials, and it transmits well into the 1450-1600 cm^{-1} (6-7 μm) range, close to the fingerprint region of interest for SO_2. It also withstands a range of acid media, and it features superior mechanical strength. Since the surface tolerances of the liquid cell would be much smaller than the gas cell, it was decided to select sapphire as the main optical material for this experiment. The spacing between the two 5 mm Ø x 2.5 mm windows was provided by a thin 1mm PTFE liner, later replaced by a deformable NBR sheet, coming down to approximately 700 μm. Preliminary stress calculations performed in AutoCAD Inventor™ showed that the design could withstand further stresses than planned. A cross-section of the aforementioned lining is shown in Figure 24, showing the stresses being well distributed among the liner except where the liquid path takes place.

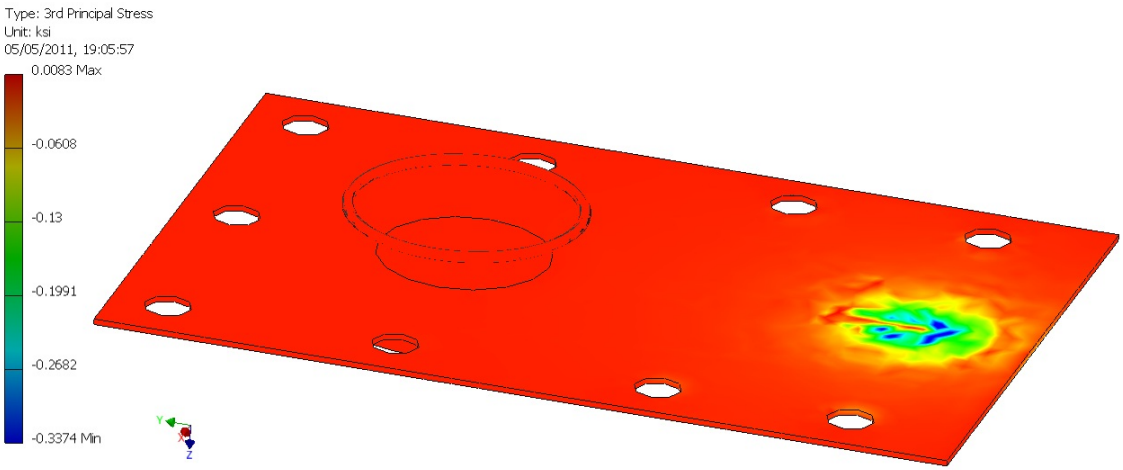

Figure 24. Maximum compressive stress inside the liquid PTFE liner, within the liquid cell.

5.15 Mark IV Additional Considerations

5.15.1 Weight and Dead Volume

To reduce the dead volume, and also to reduce the weight of the final rig to its minimum, valves were constructed within the body of the reactor, in order to decrease its overall length, and to avoid lined metal joints.

The length of the rig body is 250 mm, and it weighs approximately 1.55 kg. The liquid side has a 5 mm perforation that passed through the liquid and gas valve, turning into a 10 mm perforation in the gas side. It then tapers to 50 mm, where the sight glass is added. In the liquid side, a Ge prism is then seated onto a slot, aligned with a steel lid that pushes into the rig body, tightening it.

Further, the valves were designed as plug valves, made of virgin PTFE, with a 5 mm path where the liquid penetrates both ways to the different chambers. A diagram of the rig body is shown in Figure 25.

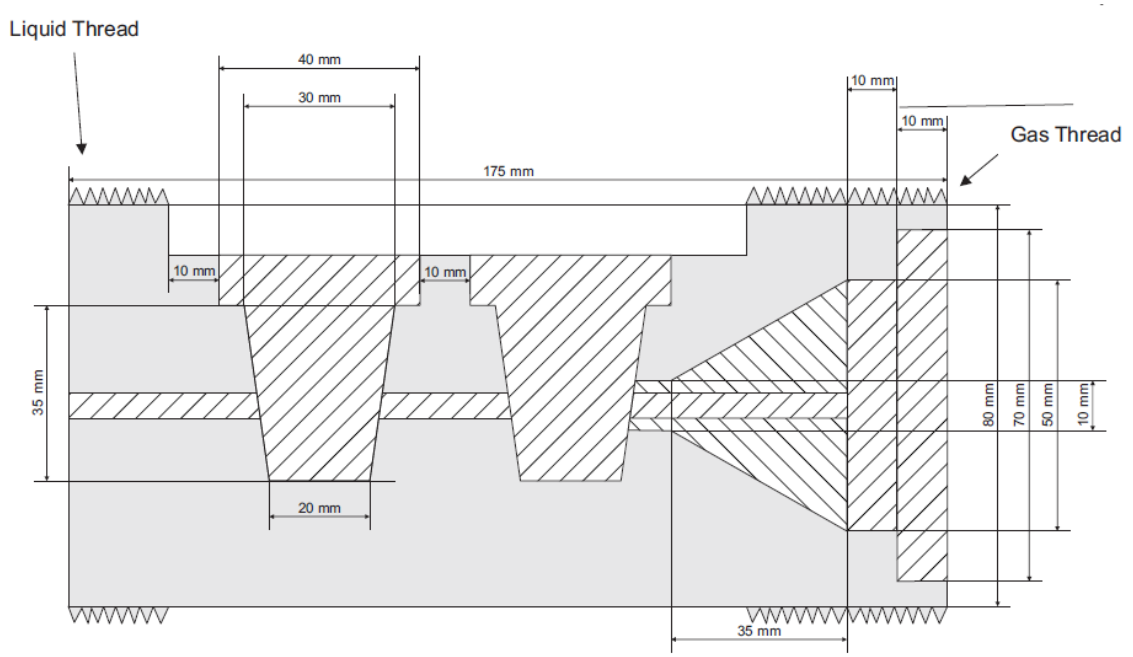

Figure 25. Mark IV rig body, including major sections.

The rig is submerged into a water bath, and rotated and vigorously shaken manually, to guarantee thorough mixing between phases. The valves are pushed against the body using a threaded plate which holds 4 M4 hex-head bolts per valve. On the gaseous side, a sight glass pushes against the body with a threaded metal lid, making it easy to disassemble in case cleaning is needed. On the liquid side, the ATR design was a very delicate process that will be described in the next section.

5.15.2 Germanium ATR Design

Spectroscopic design experience was not readily available in the Department so aid was sought in the Chemistry department. With the help of Dr. M. Hippler and Dr. A. Haynes (2010), specifics of the design were smoothed and a final design came about. The idea was to direct infrared radiation onto the pressurized rig, bounce it in the liquid, and gather the transmission spectra on the other side, where it would then be directed to the detector. Several technical difficulties arose at this stage:

- While the practice of transmitting high powered, visible and UV light through fibre optics without any significant signal loss is fairly standard, a different story holds for infrared. Costly technologies that transmit infrared in the form of waveguides are costly and not very sturdy, rather more suitable to the research subject of photonics, than corrosive thermodynamic electrolyte equilibrium *in situ*.
- The distance between the FTIR spectrometer sample compartment and the cupboard made it difficult to shorten the length of the fibre optics that were to be acquired. Further, a dramatic loss of power is seen with polycrystalline silver chloride per meter of fibre optic.
- Added to that, the internal absorption and consequently the loss of energy from the IR excitation travelling through the Ge prism and absorbing and diffracting over the liquid sample made it clear that a boost of IR energy was needed, as well as the most delicate positioning of the fibre optic cables, to achieve the correct alignment.
- Further, these would have to be hydraulically tested up to 16-20 bar, a 33% safety margin for the maximum operating pressure (15 bar).

These posed significant challenges, all of which were successfully addressed. The final design is shown in Figure 26.

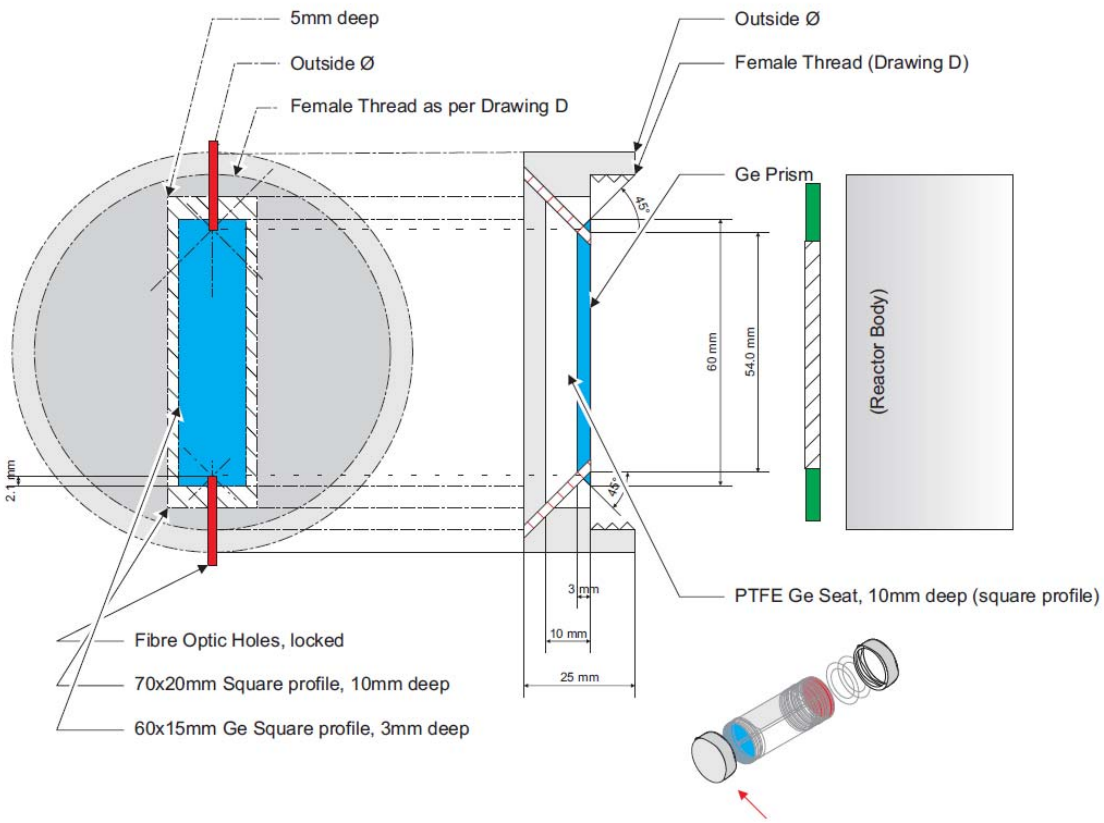

Figure 26. Final ATR configuration, Top and Side view of assembly.

Since the ATR Prism was optimized to maximize the absorption per bounce (5 bounces in fact), there was no possibility to thicken the prism to augment its resistance to failure. A key problem was the amount of shear stress that the prism would withstand before breakage due to two main forces:

- The threaded liquid lid would be subject to a certain torque tension when the maximum displacement towards the reactor body is attained.
- The prism would be subject to compressive stress, due to the action of the lid being pushed against the reactor body.
- The surface roughness of the Ge prism seat would have to be sufficiently small enough to allow for acceptable slip, in order to limit the amount of resistance between the prism and the seat, thus allowing for minimum stress. Quantification of the deformation under load of the Ge prism had to be calculated.

Attempts to model the system at hand, with current time constraints and tools available at the department, were not fruitful and experiments with blank test pieces were conducted.

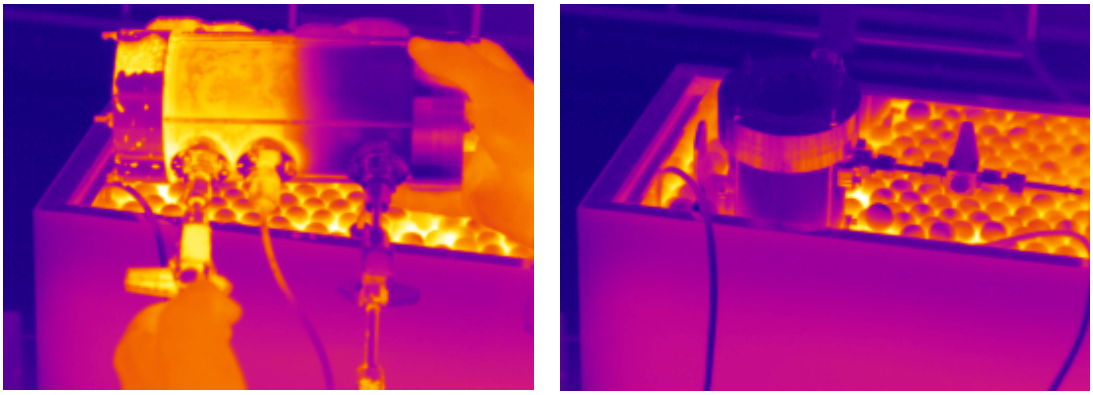

Figure 27. FLIR Imaging of the rig within the water bath a) outside the water bath and b) submerged. Acknowledgments to Dennis Cumming.

5.15.3 Thermal Uniformity

Finally, the fully assembled Mark IV was submitted to a thermal imaging scan. This was to assure that reasonable spatial uniformity of temperature was achieved, important because of the sensitivity of equilibrium temperature, especially in liquid equilibrium kinetics. The results are shown in Figure 27, in different configurations: outside the bath and submerged. The main result shows the uniform distribution of the set temperature (40 °C, bright yellow) throughout the sampling valves. This has huge implications, as the samples will remain at the equilibrium temperature for considerable time. A good feature of the rig, since thermal flashing was a problem in the Mark III.

Lastly, some detailed photos of the manufacturing process of the Mark IV are shown in the next page.

Detailed Manufacturing of the Mark IV

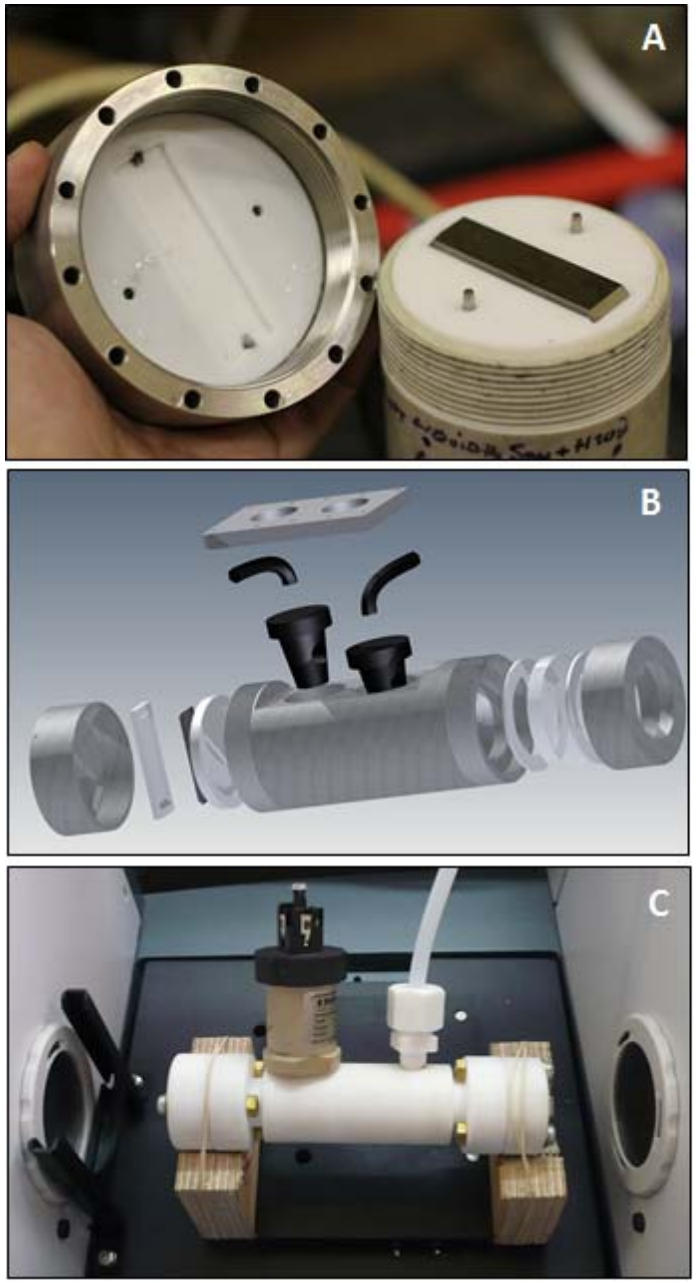

Figure 28.
A) Ge Prism configuration, top lid with recess and locating pins.

B) Full configuration render.

C) Gas Cell inside FTIR Sample Compartment.

D) Upside down orientation, with valves.

E) Full Rig submerged in water bath.

F) FLIR Imaging of the experiment.

5.16 Summary

In this Chapter, the operation of the previous generation of equilibrium apparatus led to important findings and these results aided the development of the next generation of equilibrium apparatus, the Mark IV. The requirements for the design, the desired additions to the reactor and the most relevant calculations have been presented and briefly discussed.

No further modifications were made to the instrumental design. Prior to the acquisition of VLE data with this apparatus, calculations indicated the need for refinement with the mechanical design of the sampling accessories, such as a heated liquid cell with less pressure drop. These desired additions are discussed in Chapter 7. The brittleness of the Ge that led to its demise would also indicate the necessity to design a sturdier ATR element, which would not break or chip easily. Suggestions for the design of this together with detailed drawings are provided in Appendix F. This work was not taken forward in this project due to time constraints.

In Chapter 6, the operation of the Mark III and Mark IV that was executed for the acquisition of the experimental data for each rig is detailed, prior to the presentation of the model calculations and along with a thorough discussion of results and the relationship between gaseous solubilities and acid presence in solutions.

References for Chapter 5

BASS, M., DECUSATIS, C., ENOCH, J., LAKSHMINARAYANAN, V., LI, G., MACDONALD, C., MAHAJAN, V. & VAN STRYLAND, E. 2009. Handbook of Optics, Third Edition Volume I: Geometrical and Physical Optics, Polarized Light, Components and Instruments(set), McGraw-Hill Companies,Incorporated.

BATTINO, R. & CLEVER, H. L. 1966. The Solubility of Gases in Liquids. Chemical Reviews, 66, 395-463.

BUCKINGHAM, B. 2011. RE: Generation of Sulphur in vapour-liquid experiments. Type to M.ROMERO.

COICHEV, N., BAL REDDY, K. & VAN ELDIK, R. 1992. The synergistic effect of manganese (II) in the sulfite-induced autoxidation of metal ions and complexes in aqueous solution. Atmospheric Environment. Part A. General Topics, 26, 2295-2300.

CRYSTRAN. 2012. Optical Properties of Materials [Online]. Available: http://www.crystran.co.uk/materials-data.htm.

GAUGLITZ, G. & VO-DINH, T. 2006. Handbook of Spectroscopy, Wiley.

HARVEY, K. B., MCCOURT, F. R. & SHURVELL, H. F. 1964. INFRARED ABSORPTION OF THE SO_2 CLATHRATE-HYDRATE MOTION OF THE SO_2 MOLECULE. Canadian Journal of Chemistry, 42, 960-963.

HIPPLER, M. & HAYNES, A. 2010. RE: Raman Spectroscopy Laboratory, Introduction. Type to M.ROMERO.

MAASS, C. E. & MAASS, O. 1928. Sulfur Dioxide and its aqueous solutions. I. Analytical Methods, Vapor Density and Vapor Pressure of Sulfur Dioxide. Vapor Pressure and Concentrations of the Solutions. . Journal of the American Chemical Society, 50, 1352-1368.

MARTIN, L. R. & GOOD, T. W. 1991. Catalyzed oxidation of sulfur dioxide in solution: The iron-manganese synergism. Atmospheric Environment. Part A. General Topics, 25, 2395-2399.

MOHAMMADI, A. H. & RICHON, D. 2010. Equilibrium Data of Sulfur Dioxide and Methyl Mercaptan Clathrate Hydrates. Journal of Chemical & Engineering Data, 56, 1666-1668.

OTHMER, D. F., SILVIS, S. J. & SPIEL, A. 1952. Composition of Vapors from Boiling Binary Solutions: Pressure Equilibrium Still for Studying Water–Acetic Acid System. Industrial & Engineering Chemistry, 44, 1864-1872.

QUADRANT. 2011. Fluorosint® 207 Product Data Sheet [Online]. Available: http://www.quadrantplastics.com/fileadmin/quadrant/documents/QEPP/EU/Product_Data_Sheets_PDF/AEP/Fluorosint_207_E_PDS_2011.pdf.

SHAW, A., ROMERO, MOISES, ELDER, R. H., EWAN, B. C. R. & ALLEN, R. W. K. 2011. Measurements of the solubility of sulphur dioxide in water for the sulphur family of thermochemical cycles. International Journal of Hydrogen Energy, 36, 4749-4756.

SHAW, A. C. 2008. The simultaneous solubility of sulphur dioxide and oxygen in water for the hybrid sulphur thermochemical cycle. Ph.D. Doctoral Thesis, University of Sheffield.

STUART, B. H. 2004. Infrared Spectroscopy: Fundamentals and Applications, John Wiley & Sons.

TOWLER, G. & SINNOTT, R. K. 2007. Chemical Engineering Design: Principles, Practice and Economics of Plant and Process Design, Elsevier Science.

VAN BERKUM, J. G. & DIEPEN, G. A. M. 1979. Phase equilibria in SO_2 + H_2O: the sulfur dioxide gas hydrate, two liquid phases, and the gas phase in the temperature range 273 to 400 K and at pressures up to 400 MPa. The Journal of Chemical Thermodynamics, 11, 317-334.

Chapter 6
Results & Discussion

Chapter 6
Table of Contents

List of Figures

List of Tables

6.1 Overview

As mentioned in the previous chapter, two distinct apparatuses were used in this project, the Mark III and the still operational Mark IV. Although the design of each differ, the procedure used to gather data remained consistent throughout the entire experimental part of the project (see Appendix A). In the following sections, the methodology for the acquisition of data is explained, along with additional experiments that built up to the final results compilation, along with a discussion of the results and the main findings of these experiments and modelling efforts.

It is worth noting that the main intention has been to develop an experimental body of knowledge that is key to develop thermodynamically a rigorous vapour-liquid equilibrium model for SO_2/O_2 separation. This, in turn, highlights the differences with a very common commercial package, HSC Chemistry, which is used by many researchers in different fields, and adds a practical focus to this project.

6.2 Aim

The fundamental idea is to mix the species adequately in order to achieve equilibrium. In principle, the species are brought together using chaotic movement leading to thermodynamic equilibrium and then carefully sampled and characterized. This, in turn, provides a snapshot of the behaviour of the individual species within the system, if sampling is performed correctly. A detailed procedure is in Appendix A. Although the operation during the more recent experiments is identical to the Mark III, the sampling of the species is slightly different for the current Mark IV, as it contains additional steps for flushing through the gaseous cell, as well as the liquid cell. The universal experimental setup is shown in Figure 1.

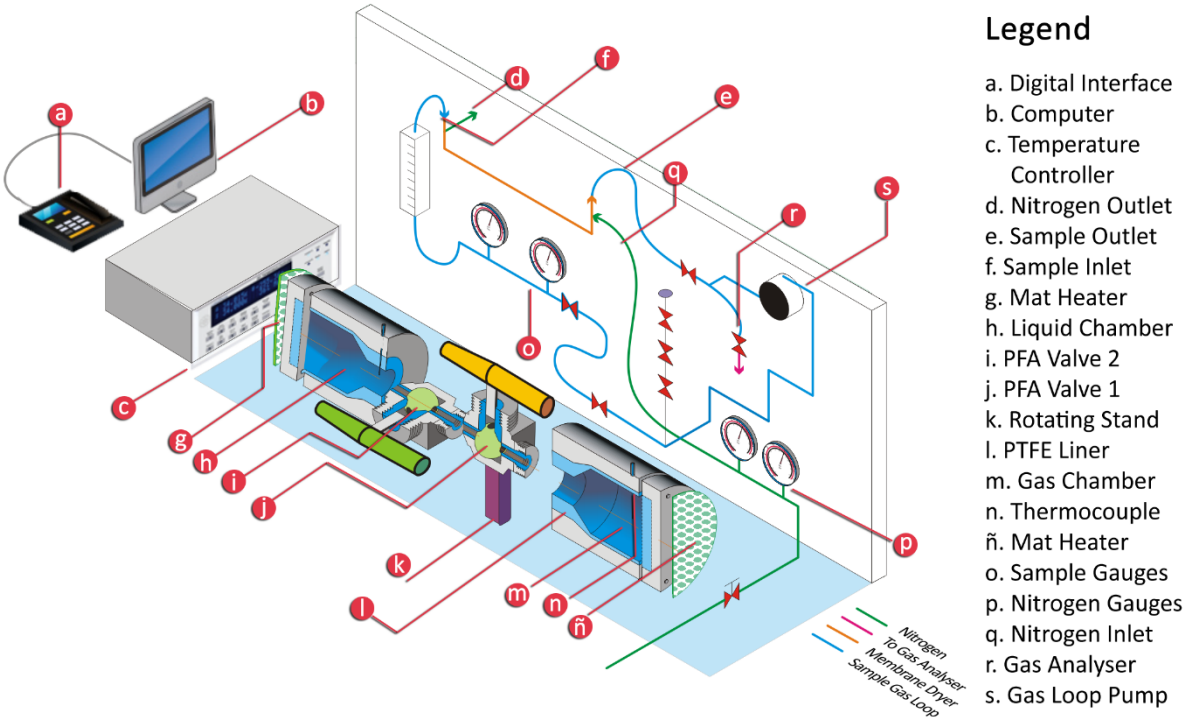

Figure 1. Experimental setup, including membrane dryer. This is valid for the Mark-III. (Romero, 2011)

The Mark III was, as described before, heated by rope heaters. In the case of the Mark IV, the entire apparatus is submerged in the water bath, with only the species valves sticking out, along with the Raman probe and the pressure gauges. This is shown in Figure 2.

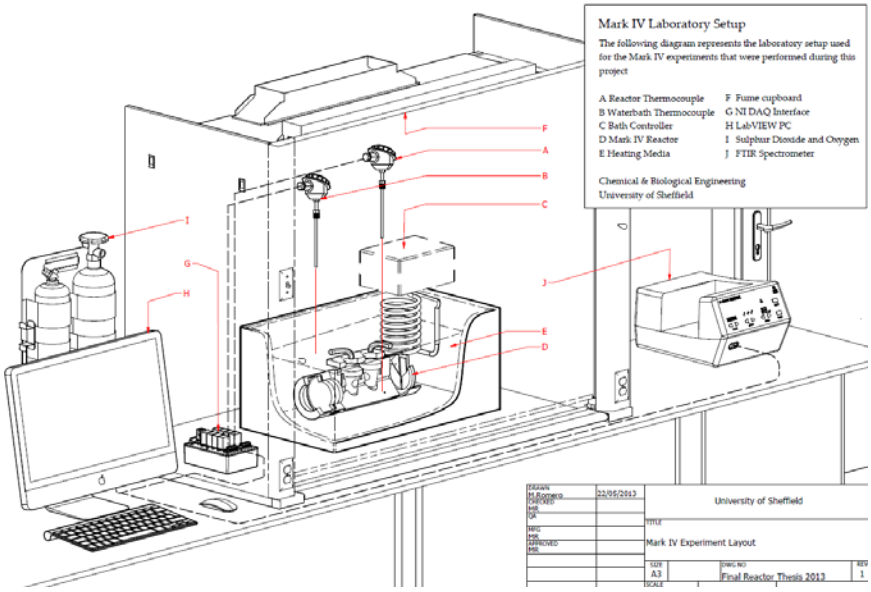

Figure 2. Experimental Setup of the Mark-IV. See Appendix G.

Then it is subjected to vacuum, to a maximum of 5 mbar. Any vacuum gauge pressure over 5 mbar indicates a slight leakage in the rig. The vacuum hose can be connected in the liquid or gaseous side, as long as the rig is dry. Then, the liquid chamber (m) is filled with water for ternary experiments, or for quaternary runs with a 1%wt solution of H_2SO_4, prepared in a clean glass bottle. This is subsequently pressurized with pure nitrogen, using an OmniFit cap and PTFE tubing that goes to the chamber. N_2 is used due to its inertness, safety and economy. Due to the nature of the PTFE tubing, only limited pressure is retained in the solution bottle. Nitrogen is carefully regulated as to not increase the solution bottle above 1.8 bar. The solution, once transferred, is then detached and the weight difference is calculated as the difference of the initial bottle attached, and after the addition of the solution. This is then entered manually into a spreadsheet containing the experimental measurements.

Once the liquid and gas valves are closed (j, I, respectively), one can then add the gaseous species, in the order SO_2, then O_2, according to the maximum pressure on the sample cylinder pressure regulators. As mentioned in the previous chapter, an inter-valve space is left to account for the slight expansion of the liquid once the gaseous species are dissolved and in equilibrium.

The rig is mixed vigorously. In the case of the Mark III, rotated, in the Mark IV, manually agitated and resubmerged. Once the pressure is stabilized, indicated by negligible changes in the pressure gauge, liquid and gas valves are closed on the vertical position, and sampling (described in Chapter 5 and in Appendix A) is performed. In the next section, the data acquisition is briefly described.

6.3 Data Acquisition

In addition to the characteristics of the previous design, the Mark IV needed to be easy to use, and the data acquisition hardware, inherited from the previous project, simplified. However, it was decided to continue using LabVIEW® for its familiarity, ease of use and modularity.

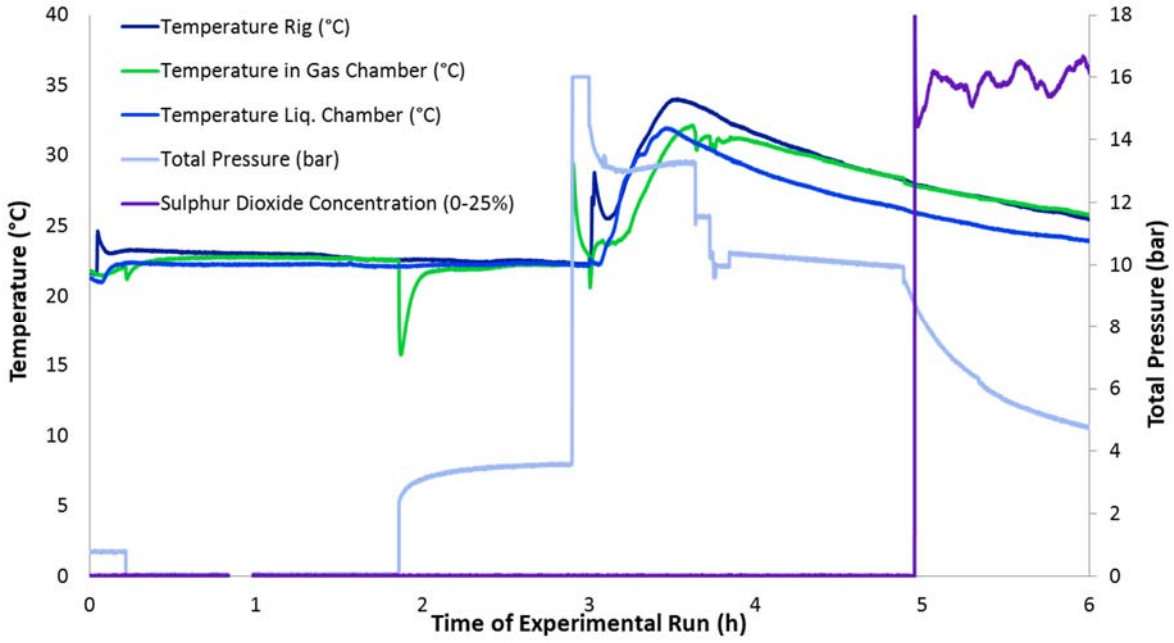

Figure 3. Snapshot of a typical Ternary run, data acquired with LabVIEW®.

A sample of a ternary run and the data acquired with the LabVIEW interface is shown in Figure 3.

K-type thermocouples are placed in strategic places to determine uniformity, and plotted for the purpose of monitoring the equilibrium process, connected to a NI-9211 thermocouple analog to digital module. Pressure transducers (SensorTechnics®, Impress®) were calibrated to a high accuracy, to a

minimum R^2 of 0.999 and connected to a NI 9220 Analog input module. Finally, the individual NI modules are connected to a NI-9178 USB data acquisition chassis, with up to 8 individual module slots.

The data is then acquired every 2 seconds to limit the amount of data gathered, but with 4-10 data channels, in a couple of hours the datasets can become very complex. Automated macros were developed in Visual Basic (in Microsoft Excel), to automate, post-process and arrange the data in a consistent-error-free way. This is also discussed in the uncertainty section, 6.8. These pieces of code are shown in Appendix E. Once the raw pressure and temperature data (along with voltages from other components) are stored in a text file, the species can then be sampled. This is discussed in section 6.4.

6.4 Sample Analysis

Statistical treatment is performed on the different data. In Table 1, the equipment used for sample preparation and analysis is summarized. This is relevant to the vapour liquid equilibrium measurements.

Table 1. Chemical species preparation and equipment required to measure and analyse each.

Species	Preparation & Addition	Equipment
Sulphuric Acid	Gravimetric Preparation	Mass Balance, pH, Raman Spectrometry
Water	Deionized Purification, Preparation	PermaPure Deionizer, Mass Balance, pH
Sulphur Dioxide	Pressure Gauge addition, Condensation with Liquid N_2	N_2 Dewar, Qualitative FTIR, Gas Chromatography, Dispersive IR, Titrimetric Analysis, Raman spectrometry
Oxygen	Pressure Gauge addition	Paramagnetic Analyser

The confidence intervals for all species and their uncertainties are discussed in section 6.8. In the following section, the results gathered for the ternary system, as well as the quaternary system, are presented and discussed.

Results

In this final section, the results obtained with the Mark-III and the Mark-IV will be presented, and compared with the predictions of the four models mentioned in Chapter 4: the Gibbs Free Energy model (ternary and quaternary), the ternary Mathematica model developed by Shaw, as well as the author's quaternary model. Some of the work detailed here has been published elsewhere (Shaw et al., 2011, Romero, 2011, Elder et al., 2010), as part of the HyCycleS FP7 project, and in refereed journal articles.

The results are presented on an individual species basis, with an explanation behind the binary, ternary and quaternary nature of the experiments, and its relevance in comparison with the respective calculations. In that respect, focus on the dissolved molecular sulphur dioxide is presented starting in section 6.5, along with a discussion of the different experimental conditions of binary, ternary and quaternary data.

a) Conditions Selection

The conditions most relevant to the separation of the sulphur dioxide and oxygen in the sulphur family of thermochemical cycles are reviewed by Shaw in his doctoral thesis (2008). Several important points arise from this review:

- In the work by Jeong, Yildiz and Kazimi (2005), part of the optimization of the HyS was to cool down the decomposer stream (containing a sulphuric acid, oxygen and sulphur dioxide and sulphur trioxide water solution) in three stages: at 431, 110 and finally 87 °C in the flashing unit, where most of the sulphuric acid would be condensed, concentrated and sent to the electrolyser, while the ternary mixture would be separated. Most of the separation actually occurs at these low temperatures (between 25 - 80 °C) at pressures ranging from 1 to 20 bar for efficient separation.

- It is important to state that no sulphur trioxide is thought to be present in the SO_2/O_2 separator, due to the conversion to sulphuric acid. These quantities are considered to be "traces", hence the 1% weight in the quaternary experiments.
- Farbman (2005), on his thermochemical status report for the HyS cycle, considered a gas mixture of sulphur dioxide and oxygen (with no unreacted species) that would be cooled to 100 °F, where bulk SO_2 would be removed, further cooled to 68 F and recovered for the electrolyser system. These are temperatures ranging from (20 to 37.7) degrees Fahrenheit.

In sections 6.5 and 6.6, experimental results for dissolved SO_2, dissolved O_2 and the dissolved ionic species (respectively) are subjected to discussion, and compared with the calculations for both models.

6.5 Dissolved Sulphur Dioxide

6.5.1 Binary Data

The initial step for comparison of the binary model and the experimental data is to determine the reliability of the equilibrium still. Not only is it critical to be able to reproduce data from the literature, but also to aim at reproducibility of Shaw's experiments after the 2010 recommissioning of the apparatus. This is shown in Figure 4, where one can the new experimental data at 25 °C, at a range of pressures. This is the most common approach to present experimental data points in the binary system SO_2-H_2O, as other species do not interfere with the graphical representation of solubility.

Several things can observed from the data:

- The experimental data (in red) and the literature show very good correlation. This proves that the new equilibrium still is able to acquire reliable thermodynamic data.

- At approximately 1 atm, the experimental data of this work, and the literature, agree on an inflection in the curve at approximately 1.5 mol S_{IV}/kgH_2O.
- After this inflection, the model then starts slightly to over-predict the solubility of sulphur dioxide species As the pressure increases, the overall tendency is for the calculations to further over-predict dissolved species in the liquid.

While the calculations aren't ideal, it is worth mentioning that as explained in Chapter 4, no rigorous effort to compare experimental data with an analytical equation based vapour-liquid equilibrium model on the same project has been done over the past 30 years, the being most recent worked example by Zemaitis (1986), as part of the DIPPR initiative.

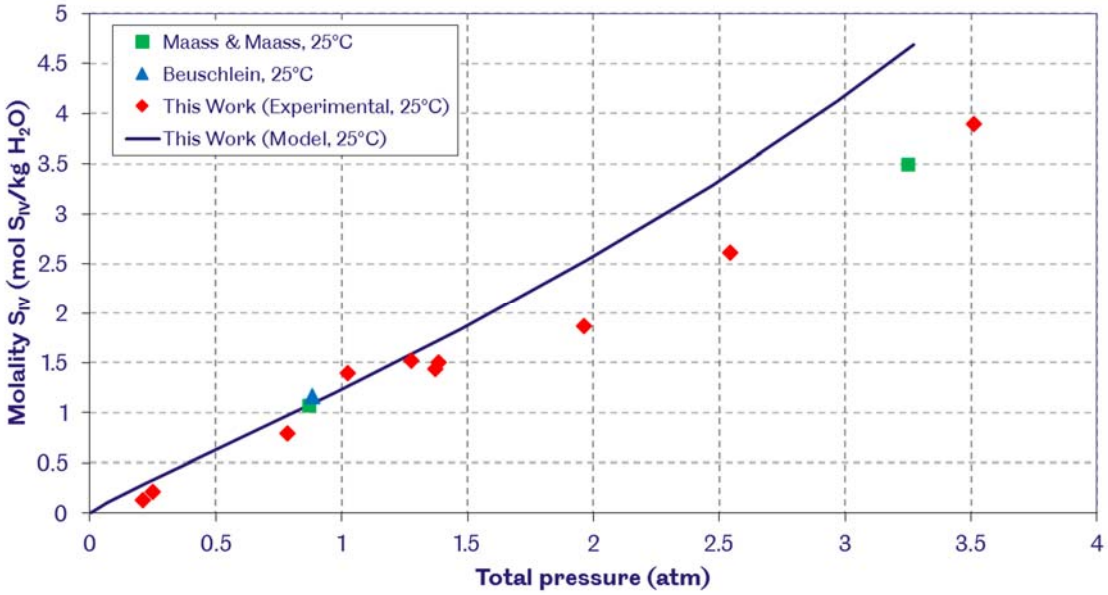

Figure 4. Binary data, 25 °C. Compared with Beuschlein & Maass & Maass (1940, 1928) & Shaw's Model (2008).

As the temperature increases, one needs to take into account that the amount of SO_2 that can be inserted to the reactor is limited by two factors: the SO_2 containing flask, and the volume by which the gas is allowed to expand. In the following plot, Figure 5, one can appreciate a cut off in experimental points, at approximately 3.5 atm. This is related to the maximum amount of SO_2 that could

be inserted into the gas chamber without it liquefying. In the 40 °C series, which is the staple work of our 2011 publication (Shaw et al.), an overall trend of agreement with the literature is clearly seen. One interesting aspect of it is that the model does not seemingly over predict SO_2 molality by as much as for the 25 °C experiments. There is also a point of inflection 1 atm that might not necessarily be supported by the literature data. Once more, an increase of pressure (induced by the expanding mass of the gas) is only limited by the maximum amount of gas that can be introduced to the experiments. Again, this is limited only by the sampling cylinders and the physical dimensions of the rig, in this case, the Mark III.

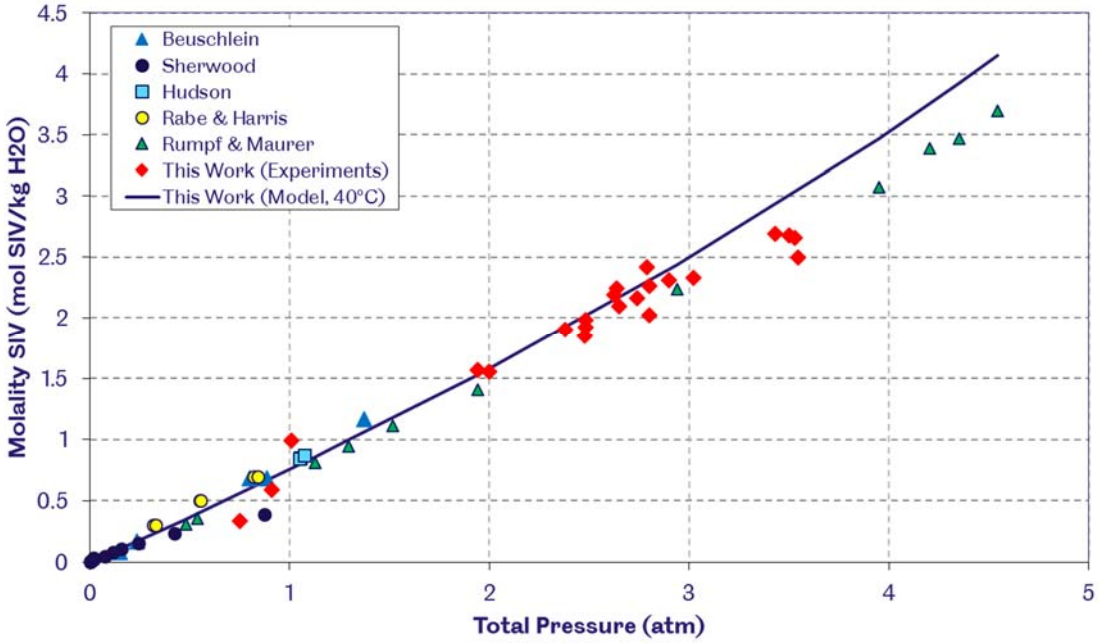

Figure 5. Binary, 40 °C. Compared with Beuschlein and Simenson (1940), Sherwood (1925), Hudson (1925), Rabe and Harris (1963), Rumpf et al. (1993) and Romero, labelled as “This Work” (2011).

As in our previously mentioned publication (Shaw & Romero, 2011), most of the work available in the literature reports SO_2 solubility as a ratio of solubility vs. total pressure, whereas Beuschlein subtracted the partial pressure of H_2O from the total experiment pressure. For those non-standard datasets, the relevant corrections were made in order to compare them with this work.

6.5.2 Ternary Data

The addition of oxygen to the experiments increased significantly the maximum pressure that could be achieved, but there was no experiment done above 16 bar. The nature of ternary data made the orthodox method of presenting solubility in terms of total pressure vs. molality of the species of interest meaningless, so a new method, founded in isomolar curves was developed. This is explained in section 5.5.3.

6.5.3 Isomolar Calculation Method

Equilibrium curves contain three main variables; pressure, temperature and composition and are presented according to the species of interest:. For binary data, one can present an equilibrium curve with only one composition (in most cases, for aqueous solutions, the solute). In this work, SO_2 is the species of interest. The amount of SO_2 dissolved in the solution is a portion of the total amount of SO_2 in the system, and there is a finite amount of molecules that will be solvated in water. Without taking into account excess SO_2 that could form a second liquid phase, one could plot in a single graph the entire range of temperatures and pressures achieved in experimental runs, each curve representing a temperature and each point representing an equilibrium measurement in one phase. This is slightly different for ternary systems, as explained in section 5.5.3b.

a) Experimental implications of the Gibbs Phase Rule

The Gibbs Phase Rule states the degrees of freedom in a system (F) with this simple equation:

$$F = C - P + 2 \qquad \text{Eq.1}$$

which simply states the relationship between every component (C) that is added to the system and the number of phases (P) that correspond to the degrees of freedom. In the case of a binary, two phase system, this equates to F=2. This

amounts to the number of intensive properties of the system that will be needed for the characterization of the system. If no equilibrium knowledge is available, then the composition of one of the species (the solute) is needed.

With three components, SO_2-O_2-H_2O, one does not only need to state pressure and temperature, but also composition of one of the solute species. Since there is no knowledge of equilibrium behaviour, the compositions of O_2 and SO_2 will suffice to characterise the entire system.

b) Isochoric Behaviour of a Ternary Mixture

To successfully represent the system at hand, and to be able to compare it with the different models that were prepared in this work, some assumptions were made, founded by the brief theoretical reminder of part a) of this section:

- In an isomolar process, a compression of volume would pose no change in the pressure, as long as equilibrium remains stable.
- Shift in equilibrium would be noticeable if a physical ternary system is subjected to this piston-like theoretical behaviour, due to differences in vapour pressure and fugacity of two or more species.

With these assumptions, one can construct a curve containing a modelled solubility curve for one component, while the amounts of each species remains constant in the system, but shifts between phases due to differences in fugacity. This is more clearly explained if you imagine a piston containing known amounts of SO_2, O_2 and water, and then expanding the piston. This would certainly make O_2 bubble quicker, due to the fact that its vapour pressure is significantly higher than the sulphur dioxide's, and therefore the phase composition relative to each would change. This principle is used to represent the solubility behaviour of SO_2 in ternary mixtures containing oxygen, by only changing the total pressure of the system (simulating a compression of a piston-like device). The model is compared at the exact pressure of the experiment that was performed. In turn, the pressure is dependent on the amount inserted in our rig.

c) Case Study Compositions

In order to compare both models sensibly, a case study was selected to represent only one set of mole amounts for the ternary (and quaternary system). The compositions are shown in Table 2.

Table 2. Case Study Composition for ternary and quaternary models.

Composition Table	
HSC Ternary	Water=8.292 mol $SO_{2(g)}$=0.135 mol $O_{2(g)}$=0.139 mol
HSC Quaternary	Added 0.01 mol of acid to the composition
Mathematica Ternary	Water=8.292 mol $SO_{2(g)}$=0.135 mol $O_{2(g)}$=0.139 mol
Mathematica Quaternary	Water=8.292 mol $SO_{2(g)}$=0.135 mol $O_{2(g)}$=0.139 mol H_2SO_4=0.01 mol

The entire input in Mathematica consists only of 5 or 6 numbers: 3 or 4 molar inputs (for ternary and quaternary respectively), temperature and pressure. Units are converted accordingly. In HSC, the inputs differ slightly, and are shown in Table 3. For blanks, the program calculates the amount of moles that will be shifted due to Gibbs Free Energy Minimisation.

Table 3. Liquid composition for quaternary comparison.

Liquid Phase		Total Moles: 8.292	Percent (Total) 100
H_2O	40	8.271	99.753
$H_{(+a)}$	40	0.006	0.072
$OH_{(-a)}$	40	0.001	0.012

$HSO_{3(-a)}$	40	0.001	0.012
$SO_{3(-2a)}$	40	0.001	0.006
$SO_{2(a)}$	40		
H_2SO_4	40	0.01	0.121
$O_{2(a)}$	40		
$HSO_{4(-a)}$	40	0.001	0.012
$SO_{4(-2a)}$	40	0.001	0.012
$SO_{3(a)}$	40		

Table 4. Gaseous composition for quaternary comparison.

Gaseous Phase		Total Moles 0.274	Percent (Total) 100
$H_2O_{(g)}$	40		
$O_{2(g)}$	40	0.139	50.823
$SO_{2(g)}$	40	0.135	49.177
$SO_{3(g)}$	40		
$H_2SO_{4(g)}$	40		

It is important to remember that all the quaternary species are not included in the ternary calculations and *vice versa*. Sulphur trioxide and its reactions are specific to the quaternary system and would render erroneous results if inserted onto the ternary calculations. Again, the blanks are calculated by the models.

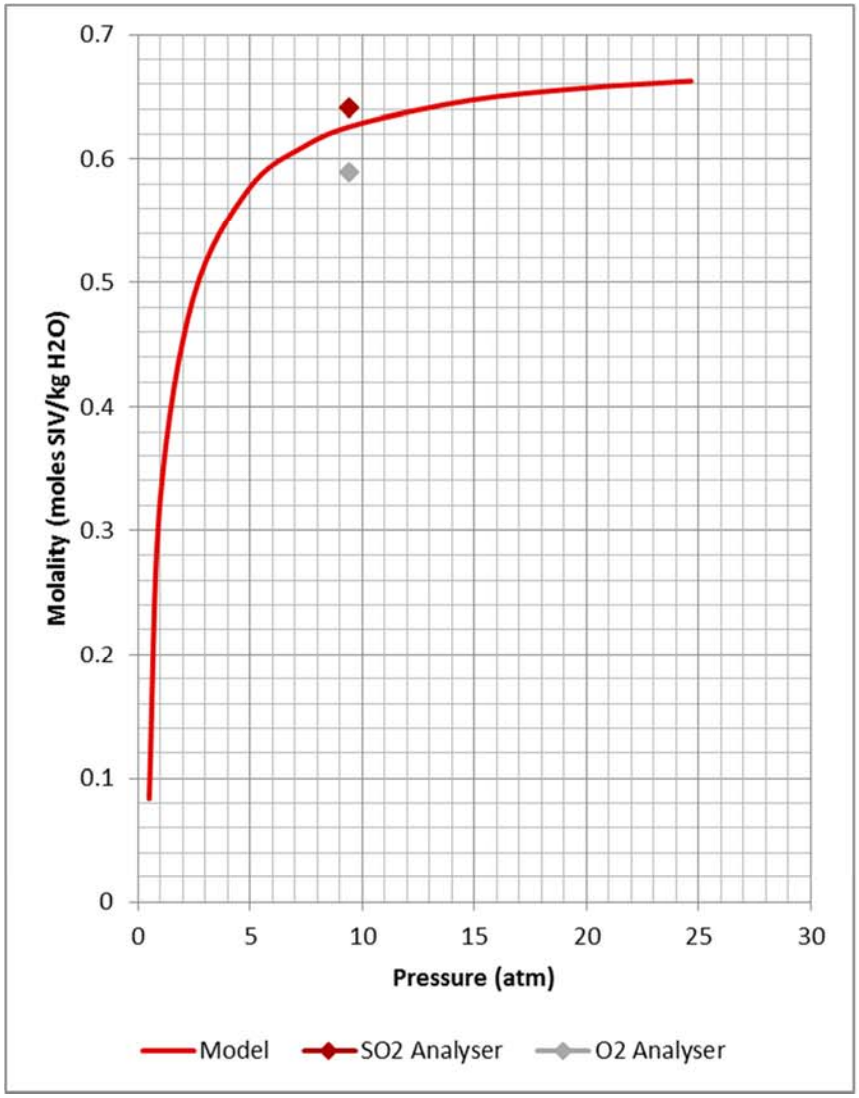

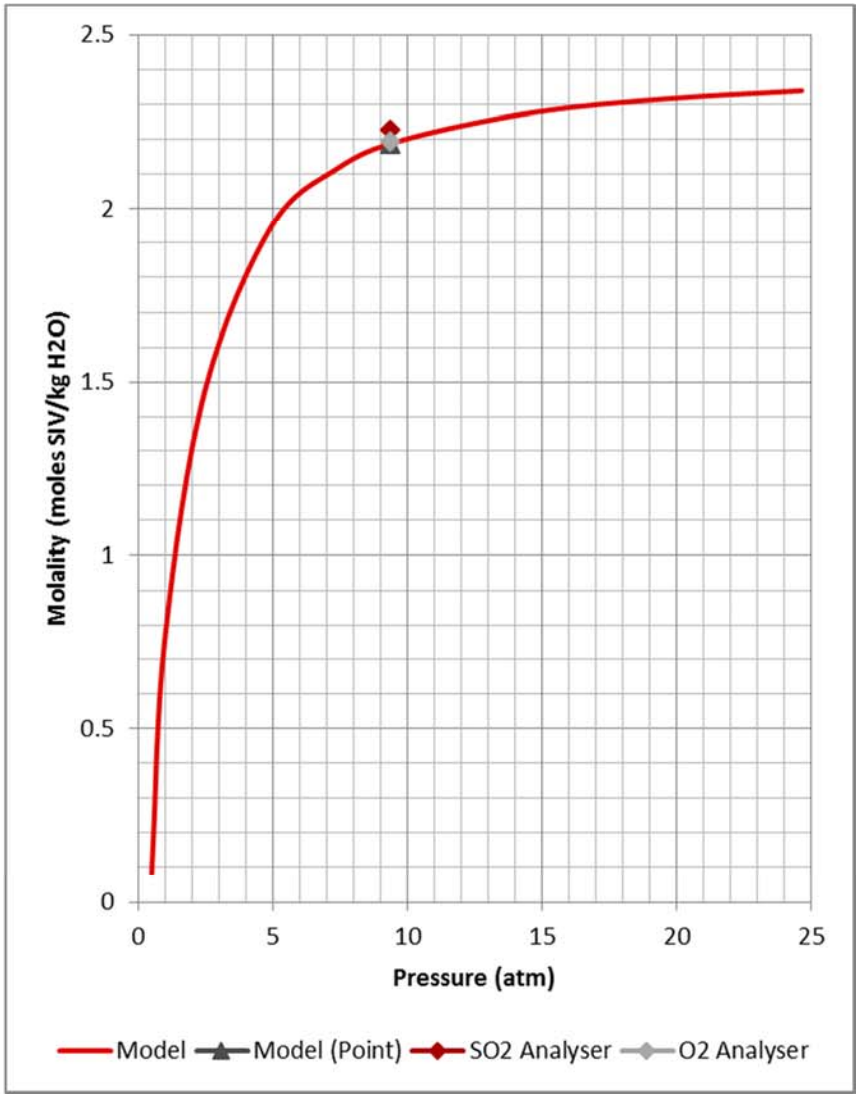

Figure 6. 25 °C, Ternary, Isomolar curves

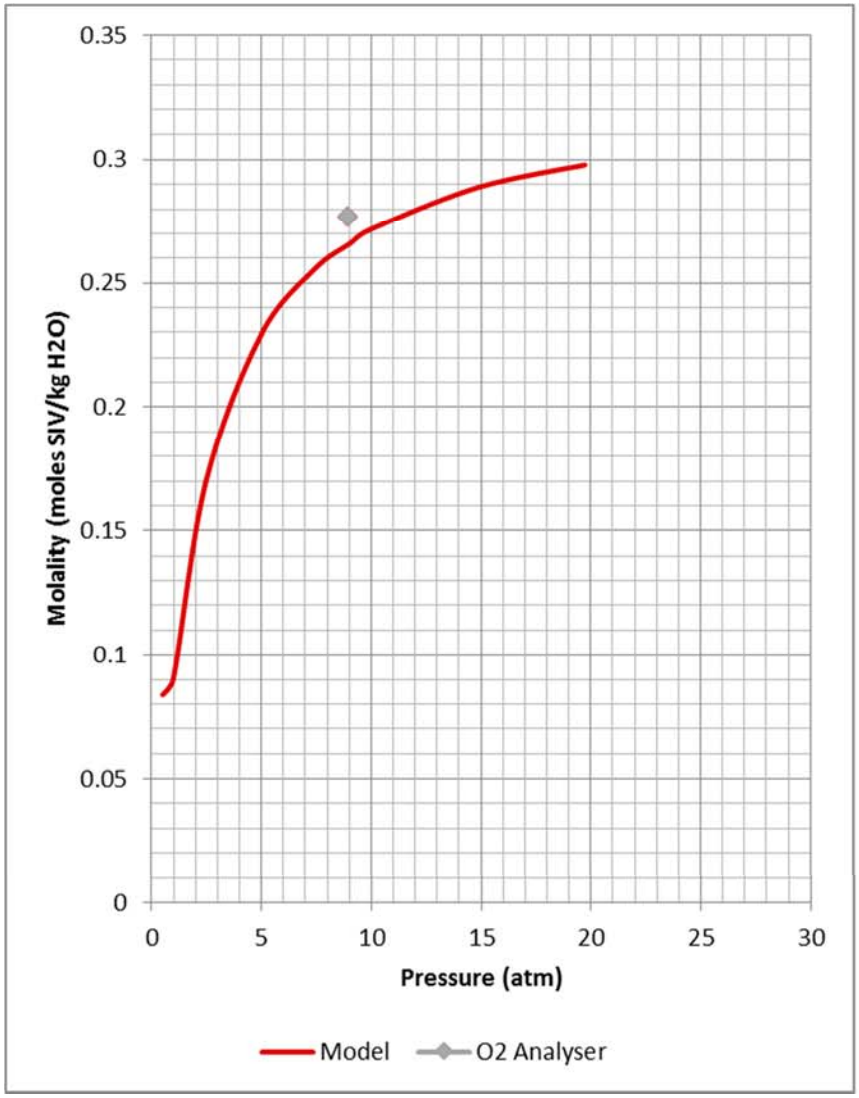

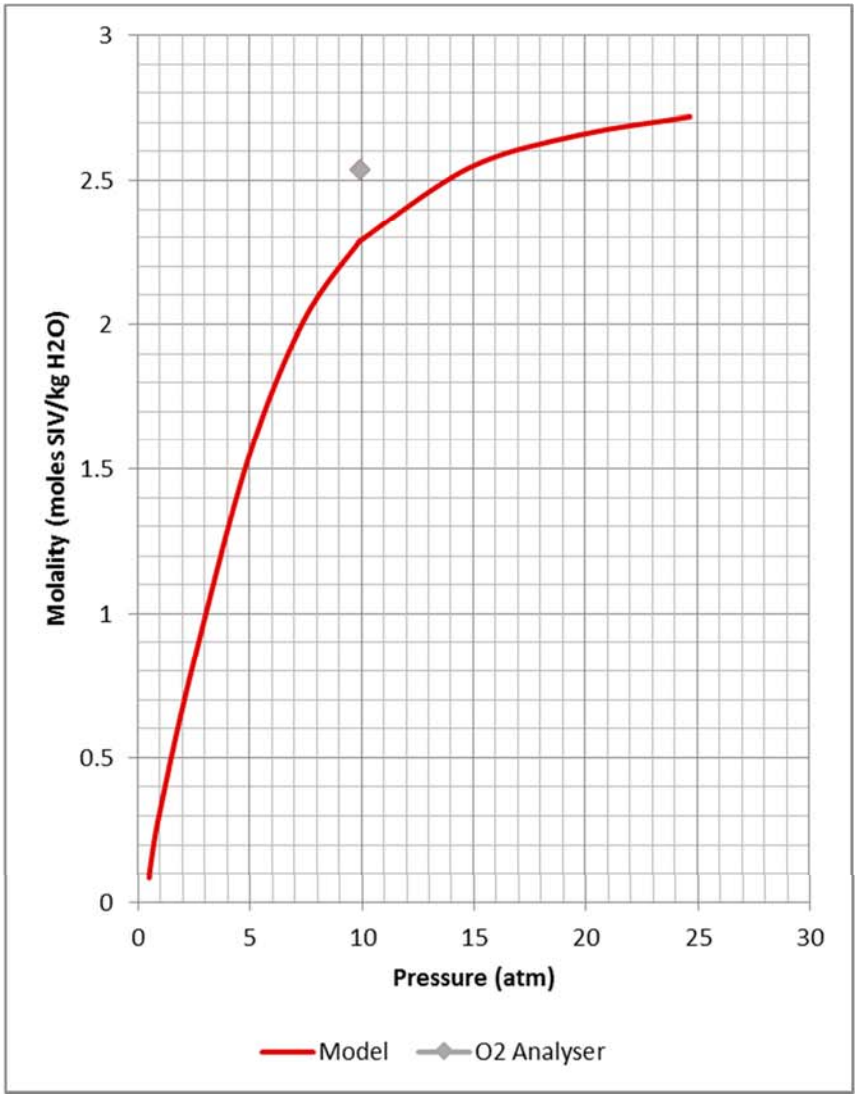

Figure 7. Ternary, 60 °C. Isomolar Curves.

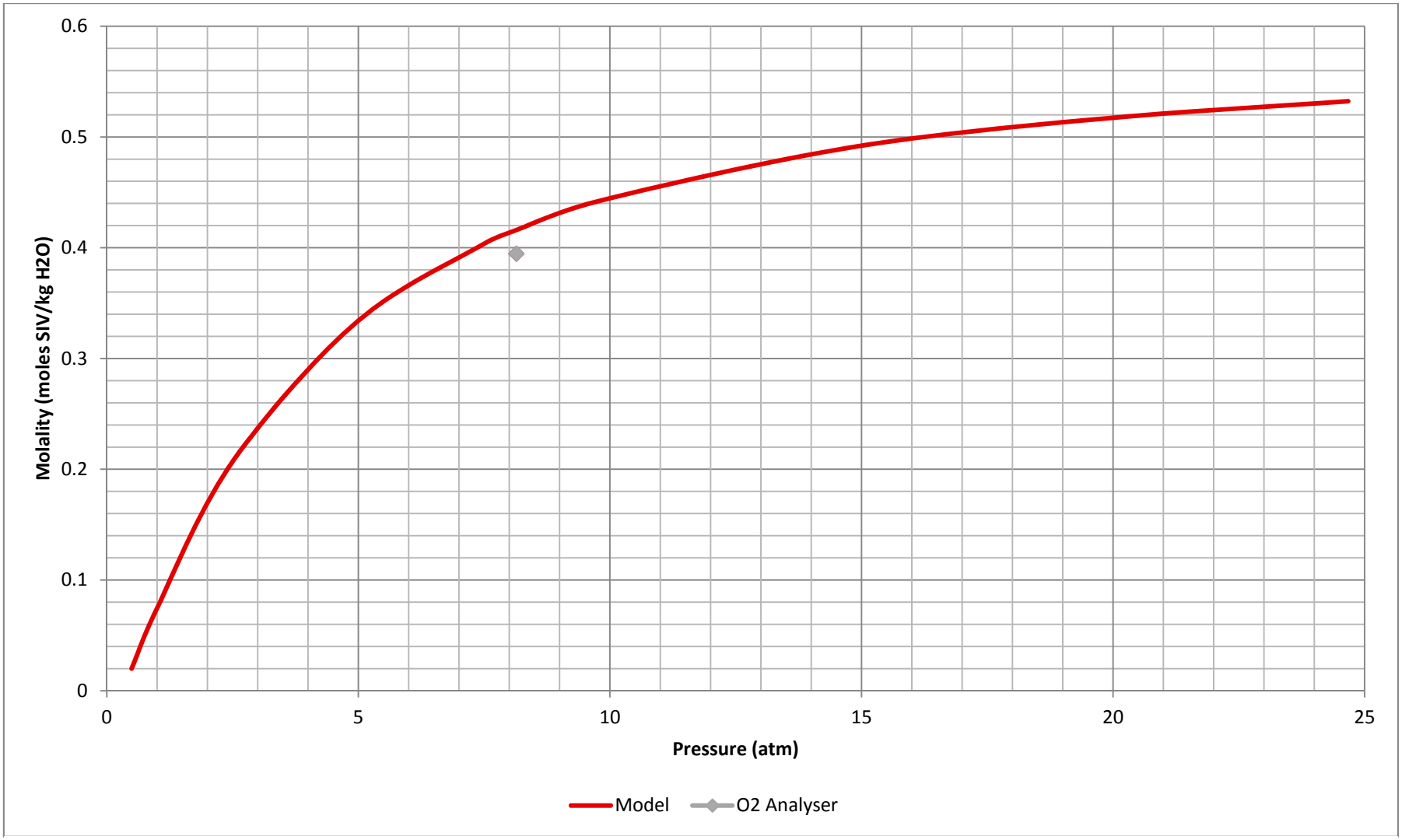

Figure 8. Isomolar curve at 80 °C. Only experiment.

d) Ternary Mathematica Model

Examples of the predictions of the Mathematica® model developed for this work and these isomolar curves are presented in Figure 6 and Figure 7. Contrary to the binary discussion, the tendency towards over predicting the solubility is not as clear as in the ternary system. One can even argue towards the system *under predicting* the solubility, as most of the experimental points lie above the model curve. However, it is clear from the uncertainty analysis (shown in Table 5) that Temperature played a key part in the model predictions. This can be explained if once considers the uncertainty analysis in section 6.8.1. When only one analyser was available, the other gas quantity was determined by mass balance, not considering the water that was taken out with the membrane dryer.

It is worth noting that, while moderately unstable, throughout the entire range, the model predicts accurately to less than 5.20% error the solubility of SO_2 in water, below pressures of up to 13 atm and temperatures up to 80 C. This is a remarkable finding, bearing in mind that a considerable number of parameters in the modelling were missing or approximated.

Table 5. Maximum error between experimental point and

Experiment Temperature	Model vs. Sample Analysis
25°C	2.41%
40°C	2.60%
60°C	4.21%
80°C	5.20%

e) Ternary Gibbs Free Energy Model

The Gibbs Free Energy model is an aggregation of algorithms that minimize the total Gibbs Free Energy of the system, as explained in Chapter 3. This, in turn, is related to the chemical potential, the variable responsible for the

equilibrium of phases. The method is implemented in the program HSC Chemistry, and here it is compared graphically with the Mathematica® model.

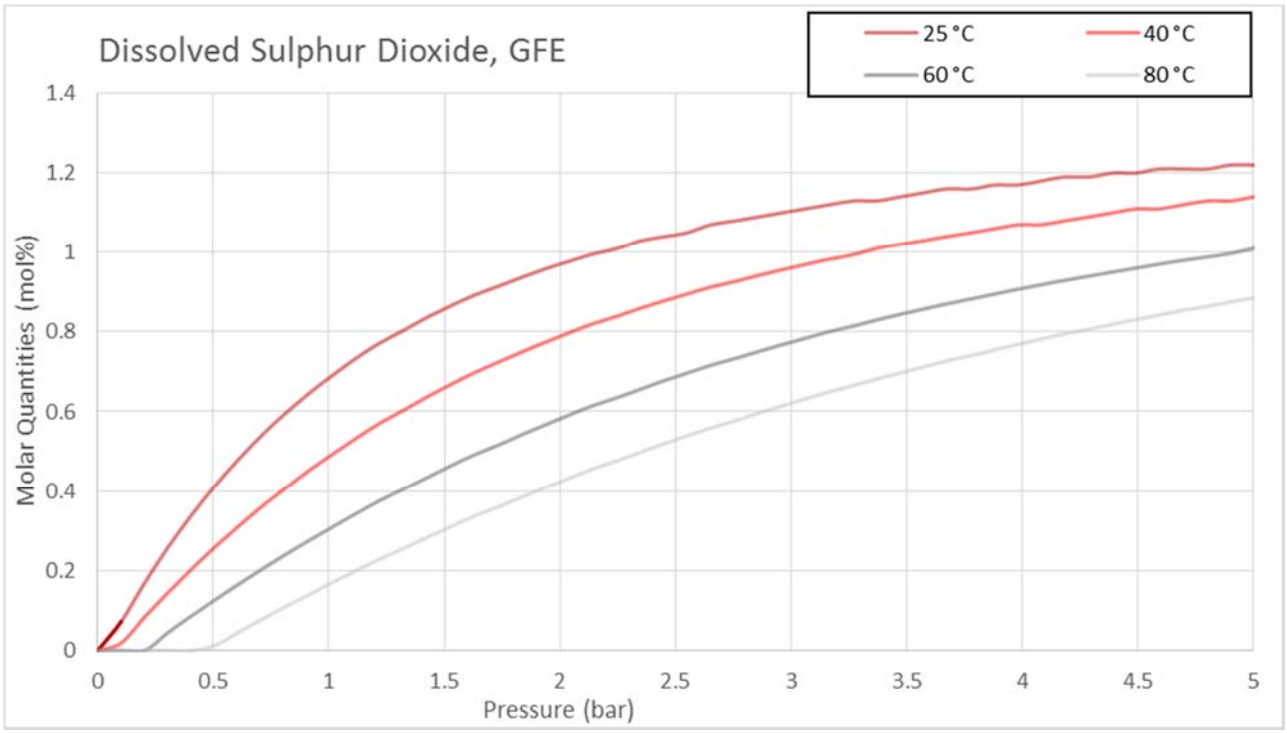

Figure 9. HSC Chemistry Model, $SO_{2(aq)}$, 25 to 80 C.

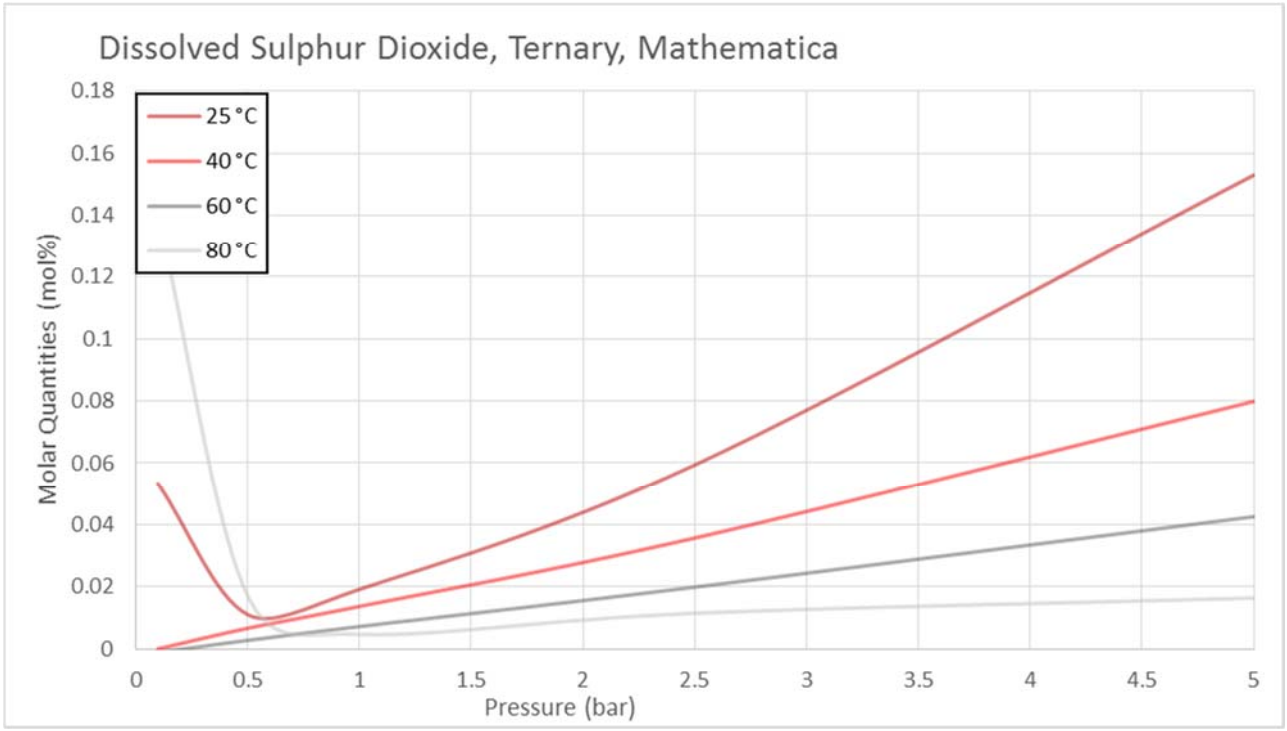

Figure 10. Mathematica Ternary Model, $SO_{2(aq)}$, 25 to 80 C.

The ternary Mathematica model developed for this work contains two key differences, in comparison to the HSC ternary model. These differences are clearly seen if one compares the prediction of dissolved SO_2 in Figure 9 and Figure 10. These differences are similar to the analysis discussed for the quaternary model in section 6.5.5:

- The Mathematica model predicts a solubility of between 0.16 to 0.01 mol% in the liquid phase, whereas the HSC model predicts it at between 1.2 to 0.9 mol %. This is a difference of half an order of magnitude that shows that the HSC model is not as accurate as its Mathematica counterpart.
- The HSC model does not take into account the different volatilities under atmospheric pressures, and the condensation that occurs as atmospheric pressure is reached. This is seen as an inflection point as the curves reach 1 bar in Figure 10.

While the differences between models are appreciable, there are certain similarities that are remarkable, especially considering the entirely different approaches to measure equilibrium. These similarities are discussed in section 6.5.4, and they are principally related to the equilibrium shift as a function of temperature.

6.5.4 Temperature Effects

While these differences are to be highlighted, there are similarities that lead to interesting conclusions for the ternary models:

- Consistent representation on the effect of temperature against SO_2 solubility is seen on both models. This is a similarity that shows the relative thermodynamic consistency of both models, regardless of the quantitative aspects of solute prediction in the liquid phase. This is a familiar aspect of rigorous thermodynamic modelling vs. more semi-empiric calculations, pointed out by Shaw (2008).

- Nevertheless, the difference in solubility due to temperature seems to have an asymptotic effect on SO_2 solubility in the Mathematica model, contrasted to a more linear effect in the HSC model. It seems that even as temperatures reach the boiling point of the aqueous solution (regardless of composition), there is a balance between the number of allowed SO_2 molecules and the vapour pressure of the gas "pushing out" of the solution.

To assume that the temperature has a detrimental effect on the solubility of gaseous species is not entirely correct all the time. One must carefully take into account also the effect on oxygen, which is much more volatile than sulphur dioxide and, when in the gaseous phase, would increase the total pressure of the system and conversely push the SO_2 solvation further. While this was identified, due to the complexity of the ternary data, no further quantification or sensitivity analysis was performed.

6.5.5 Quaternary Data

An important finding with the quaternary data is the remarkable effect of a very small amount of sulphuric acid in the mixture, provokes such a great effect on salting out of the dissolved species, and shifts entirely the stoichiometric relationship between them, specially sulphite and bisulphite species. This effect is more pronounced in the HSC model than the Mathematica model.

6.5.6 Effect of Acid species

As the principal focus of this research was sulphur dioxide solubility, a compilation of different predictions of solubility are shown in Figure 11. This graph compares the acid effect on the results of the Mathematica models, as the temperature is modified. The overall tendency is that the acid addition on the system increases the difference in SO_2 solubility proportionally to temperature and pressure, however, an interesting feature can be noticed at 80 degrees, where the difference is the maximum at pressures lower than one bar. This coincides with

abrupt ion concentration changes shown in the HSC chemistry results stated in part d) of section 6.5.3.

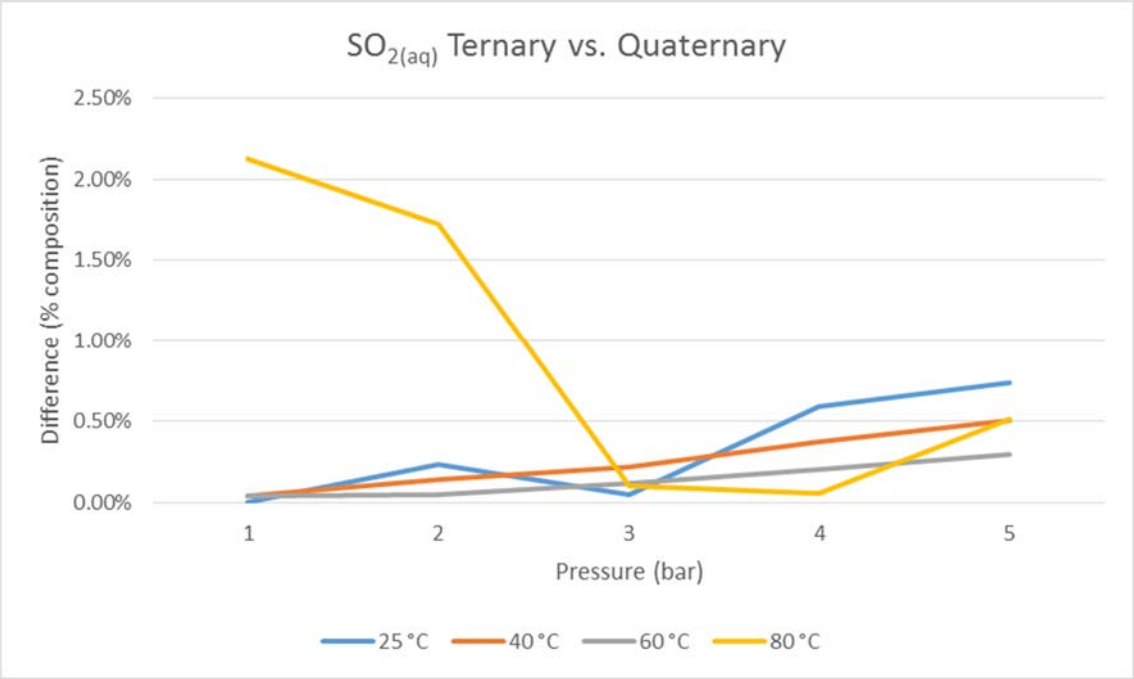

Figure 11. Dissolved $SO_{2(aq)}$ comparison between ternary and quaternary Mathematica models.

This is related to the sensitivity of sulphur dioxide to salt-out in low pressures and high temperatures, that is where the difference is greatest, e.g. high temperature means a SO_2 molecule is less likely to accommodate in an empty space in the liquid, therefore decreasing the chances of solvation.

Then, a tendency towards salting out (seen as an increase in the difference between ternary and quaternary models) is shown as being proportional to the pressure. Apart from the 80 °C curve, one can assume this as a consequence of the increased pressure which equates to a more intimate contact between molecular and ionic species, enhancing the repulsive effects and thus, increasing the differences of solubilities among models. To make this statement clearer, one can imagine an increased difference between models if we added a component that would scavenge for solvation spaces, further salting out the volatile electrolytes.

While the behaviour of dissolved sulphur dioxide is a delicate balance related to temperatures, relative volatilities, and the amount of salting out caused by the sulphuric acid, this is not the case with oxygen, and this is discussed in the next section.

6.6 Dissolved Oxygen

The results for dissolved oxygen are shown in Figure 12. The contrast between the GFE model and the rigorous semi-empirical equation-based model written in Mathematica for this work is remarkable, although slightly ambiguous. Hayduk et al. (1988) measured SO_2 solubilities in concentrated H_2SO_4 solutions, and similar to the work of Gubbins and Walker (1965), found a slight reduction from the original pure water solubility to a mere 2% in acid solutions. This is seen also in the present work, but in this case, it consists of reduced O_2 solubility.

There is more than 2 orders of magnitude difference between the ternary and quaternary $O_{2(aq)}$ quantities, getting to a minimum of $2x10^{-5}$ % at all temperatures at approximately 1.5 bar.

Again, the Mathematica model agrees with statements from the literature, that show that while the general tendency is to slightly over predict solubilities of the volatile electrolytes, a good thermodynamic consistency is shown for the ionic species and the predicted acid effect on solvation of ions.

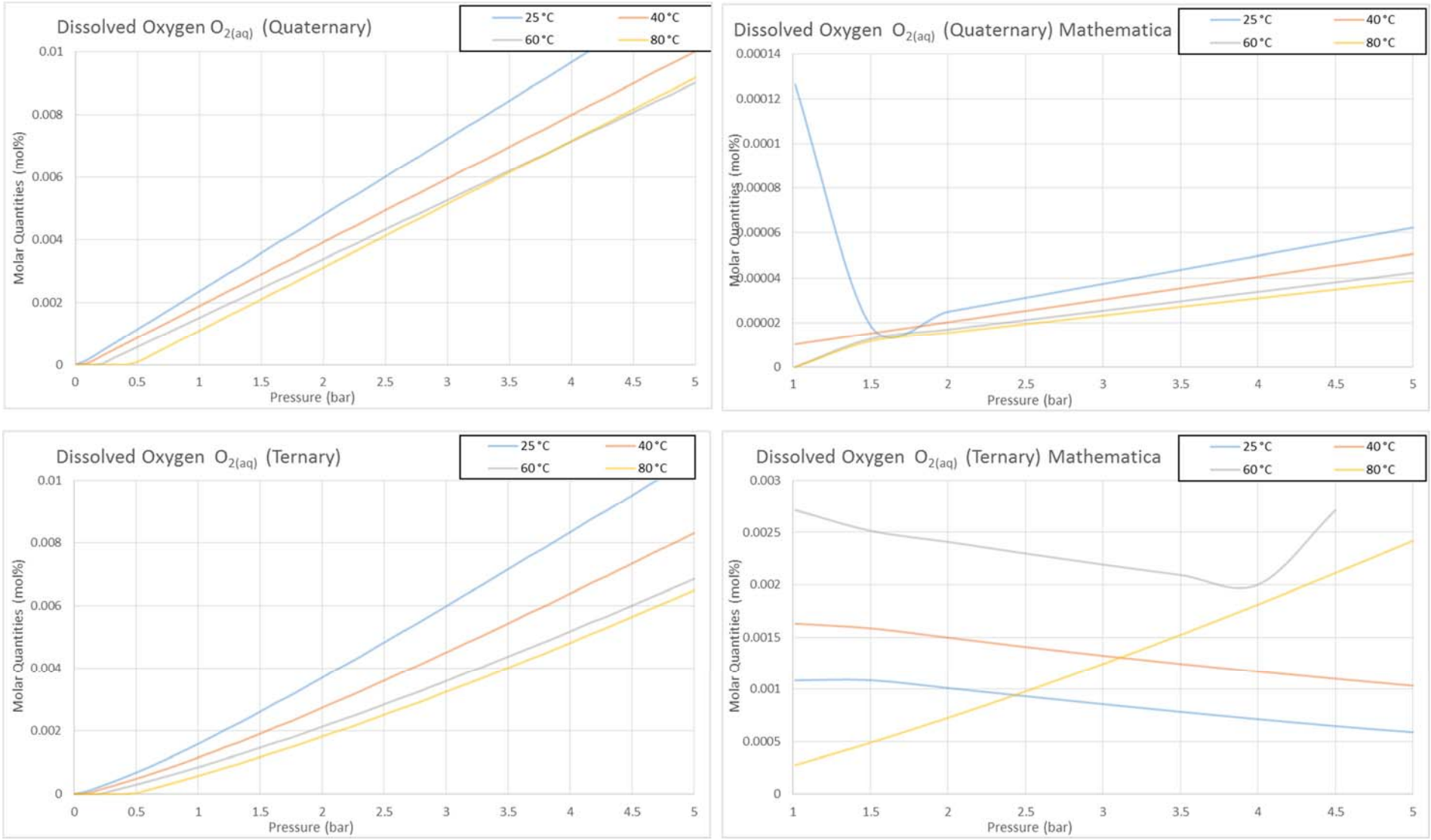

Figure 12. Compilation of dissolved oxygen results between 25 to 80 C, HSC, Mathematica, Ternary vs. Quaternary.

6.6.1 Salting Out Effect

In Figure 12, the addition of sulphuric acid and its salting out effect is calculated arithmetically as the difference in molar percentage between ternary and quaternary models vs. pressure in Mathematica. It would be an arithmetic representation of the differences in Figure 11. This reduction of almost 100% in gaseous form is consistent with Hayduk's observations (1988), marking progress towards a good approximation to the thermodynamic behaviours of this system of electrolytes.

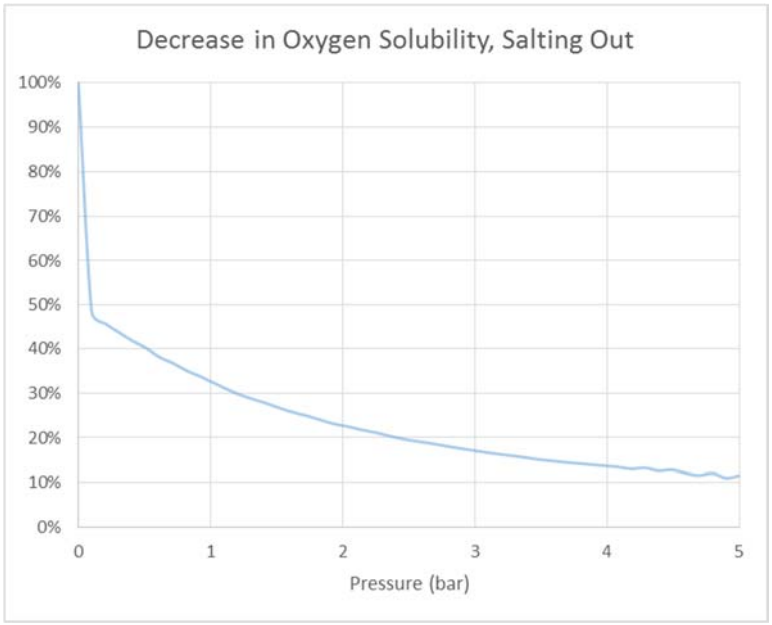

Figure 13. Oxygen solubility, difference in percentage between ternary and quaternary models in Mathematica.

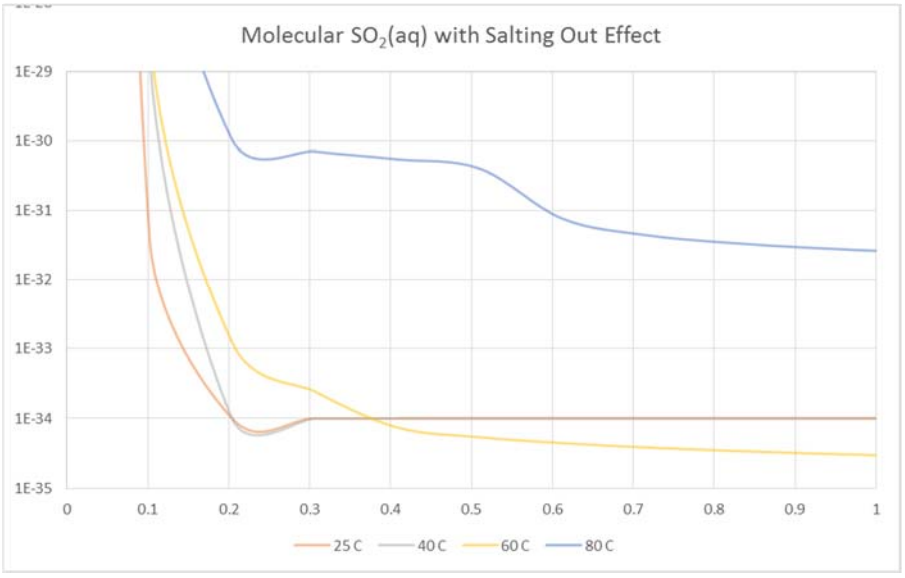

Figure 14. Salting out effect due to 1% addition of sulphuric acid (HSC Model)

In contrast, the effect was remarkably large in the GFE model, where the solubility had to be expressed in logarithmic scale due to its small magnitude. One only needs to simply check the difference of scales in the axis to determine the difference in solubility caused by the addition of a small amount of sulphuric acid. This is marked for both model methodologies: the HSC model and the Mathematica model.

6.7 Sulphites and other species

Finally, a summary of dissolved species (acquired with the GFE model) is presented in figures Figure 15, Figure 16 and Figure 17. Dissolved species, following the analogy of the molecular species, occupy spaces inside the solution, affecting the solubility of the gaseous species (especially SO_2), that could be detrimental to the efficiency of the absorption columns.

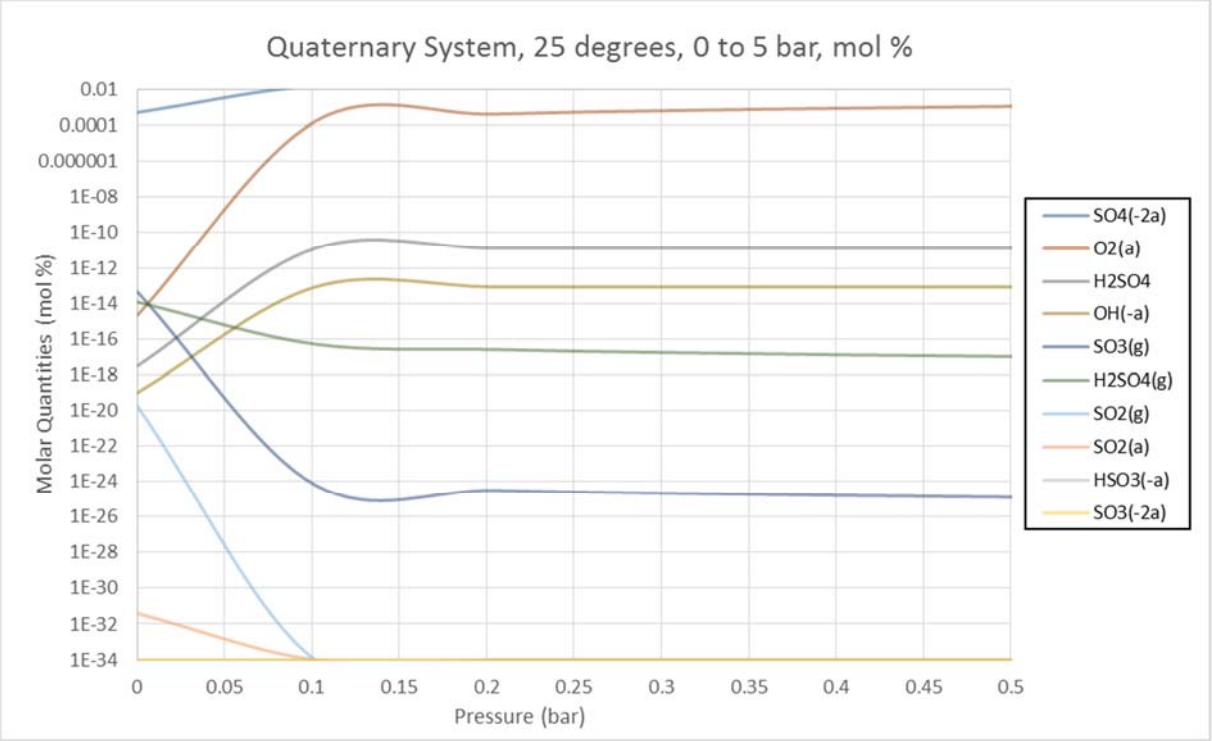

Figure 15. HSC Model, quaternary, 25 C, 0 – 0.5 bar.

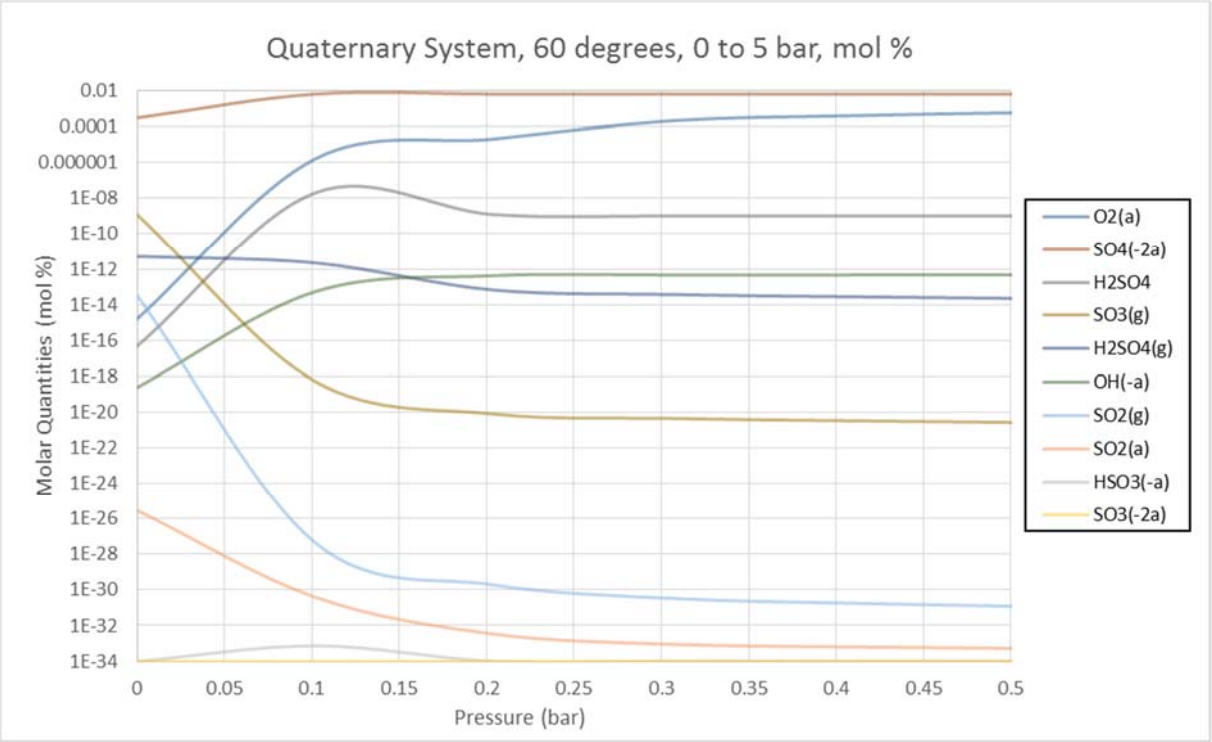

Figure 16. HSC Model, quaternary, 60 C, 0 – 0.5 bar.

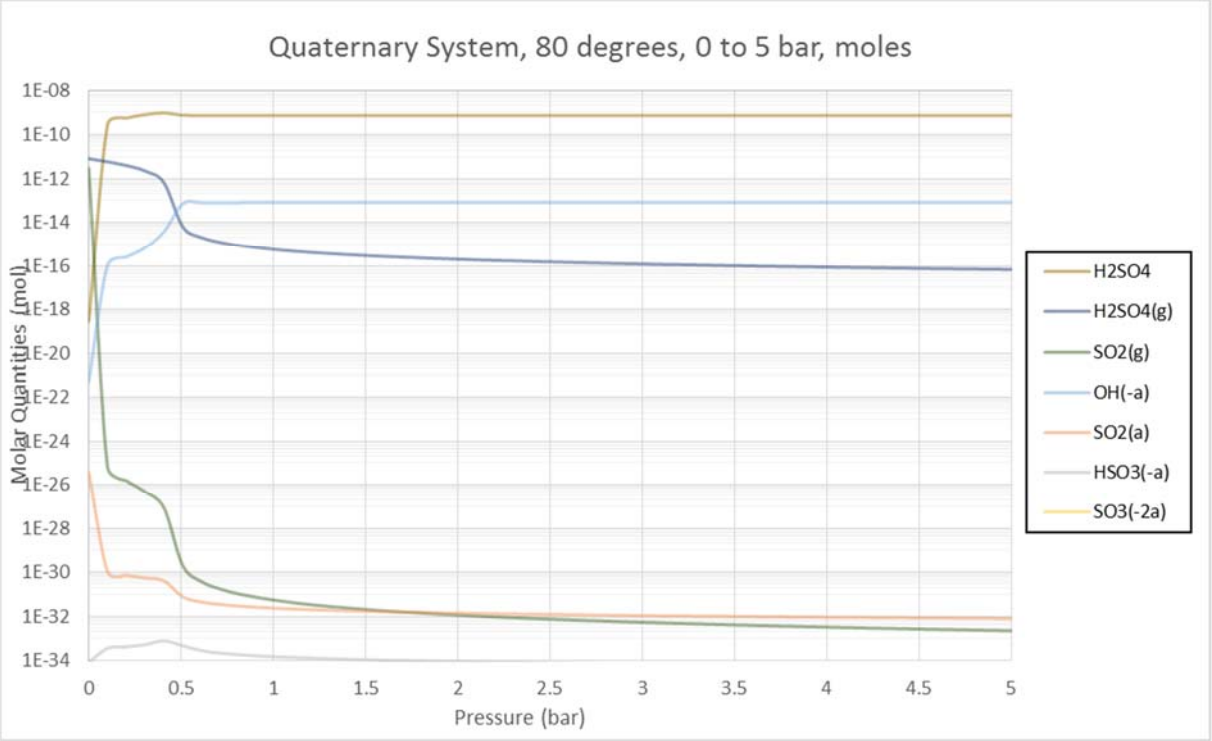

Figure 17. HSC Model, quaternary, 80 C, 0 – 5 bar.

The full extent of dissolved species is shown in the figures but for the most part concentrations are extremely small. However, ion concentrations, even if very diluted, have a massive impact in the design of separation equipment, as the concentrations cannot be regarded as negligible as they affect largely the solubility of the gaseous media. On a modelling perspective, this is advantageous as the mixture of SO_2-O_2-$H_2SO_{4(g)}$ could be treated as a pseudo-ternary mixture when the acid concentrations reach no more than 1% molar concentration. This has implications towards the design of the separation equipment, as it is critical to maintain acid concentrations to a minimum.

This is not new, and flow sheets including H_2SO_4 and $SO_{3(aq)}$ assume only ppm traces after the sulphuric acid flashing. However, it is important to mention that it is the first time (to the author's knowledge) that this weak-electrolyte treatment to mixtures including low concentration H_2SO_4 in the HyS and SI cycle (when doing process optimization) has been justified.

6.8 Uncertainty Analysis

One of the objectives of this project was to accurately measure equilibrium with a corrosive mixture of dilute hot acid media. This proved to be extremely difficult experimentally, but a good approximation was achieved, and the method was reproducible to most extent. However, a large amount of the experimental work was spent analysing the uncertainties of all the variables included in the determination of vapour liquid equilibrium. This section contains the most important aspects that affected the experimental measurements, section 6.8.1, mass measurements, section 6.8.2, gaseous uncertainties and finally section 6.8.3, iodometric analysis.

6.8.1 Species Mass Addition

The evaluation of the scattering resulted from the quaternary experiments indicated a source of uncertainty in the mass, mole and volume calculations that affected the gaseous species. This needs to be explained a bit more carefully within the context of the model, in comparison with the experimental data.

a) Representative Mass Measurement

The accuracy of ternary data consists of primarily three variables: the amount of oxygen, the amount of SO_2 and the amount of water in the system. One of the most critical parameters during the acquisition of the data was the mass that was transferred from the sample cylinders, to the actual rig. It is clear that the easiest quantity to measure is the mass of water transferred to the apparatus, due to the relatively low mass of the container compared to the actual moles of water that are inserted to the rig. This is not the case with the gases, as the minimum resolution of the measurement is 0.01 g, using the Precisa 2200g balance available. This requires a minimum amount of 6.37 g of sulphur dioxide, and a further 8.29 g of oxygen (considering an approximate value of 1.274 kg for the SO_2 cylinder, and 1.658 kg for the O_2 cylinder).

Considering that the average amount of SO_2 and O_2 that were added to the rig were in the region between 0.5 g and 13 g (when at its maximum extent), one can conclude that the accuracy of the measured mass fell short of the desired accuracy of 0.5%. This numbers are shown in Figure 18.

The propagation of error for a resolution drift of 0.01 g is shown in the calculation of volume of vessel, density (relative to room temperature) and finally, averaged between the maximum and the minimum.

The important number, for the gaseous species, is the volume. With it, one can approximate the amount added via the ideal gas law (or the Redlich-Kwong EOS) and compare it with the experimental mass. From an uncertainty of 2% from the mass addition of species (0.01 g from a mass of 0.5 g), and comparing it with the ideal gas law, one could achieve errors of less than 17% for oxygen, and less than 10% for sulphur dioxide. These ranges of uncertainty are in no way negligible, but the limitations resided with the mass of the entire rig, and the maximum sensitivity achievable with the balance available.

The analysis of these uncertainties are covered only for quaternary experiments, and is presented in Table 6. It should be noted that quaternary experiments 4 and 7 were rejected as the amounts of oxygen added to the rig were not significant (<30 mg, <0.001 mol). Uncertainties of mass, volume and density as fluctuations of temperature are derived from these formulas of error propagation:

$$v = \frac{m}{\rho(T)};$$ volume as a function of mass over density as a function of T

$$err = \frac{m_{\max}}{\rho(T)_{\min}} - \frac{m_{\min}}{\rho(T)_{\max}};$$ maximum uncertainty achieved for temperature fluctuations

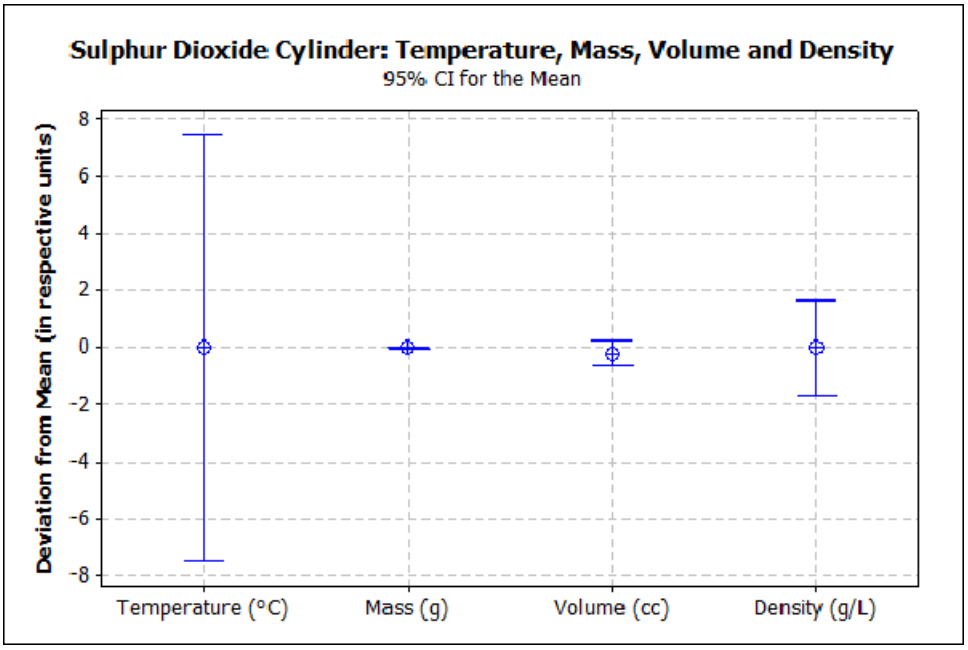

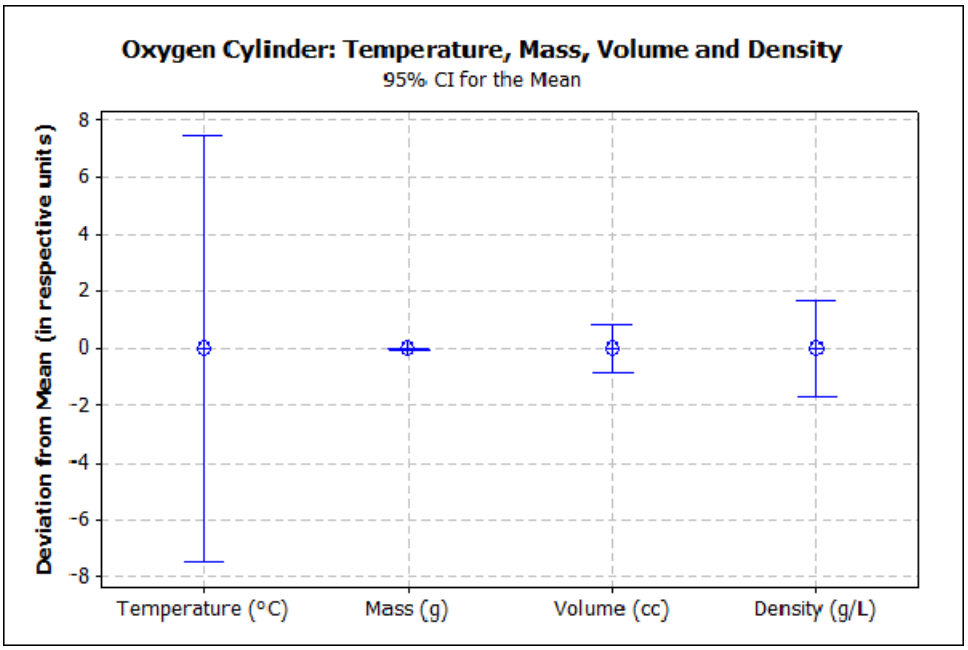

Figure 18. Mass analysis of the species addition stage.

Table 6. Mass uncertainties of gaseous species for quaternary experiments, expressed in percentages.

Temperature (K)	333		313				298		
Experiment (#)	1	6	2	3	5	11	8	9	10
Added O_2 (g)	0.43	2.27	1.99	1.43	2.4	1.43	1.34	0.6	0.53
Added SO_2 (g)	0.75	0.38	0.64	1.49	0.34	2.57	0.89	0.85	1.66
Predicted O_2 (g)	0.488	2.397	2.034	1.463	2.453	1.487	1.323	0.638	0.625
Predicted SO_2 (g)	0.768	0.349	0.631	1.485	0.371	2.599	0.846	0.842	1.497
Error O_2 (%)	13.55%	5.58%	2.19%	2.31%	2.19%	4.01%	1.27%	6.27%	17.90%
Error SO_2 (%)	2.36%	8.17%	1.39%	0.34%	9.19%	1.11%	4.93%	0.92%	9.80%

These findings provide a general explanation to the deviation of experimental data against the two types of models used for comparison: the Gibbs Free Energy model and the equation-based calculations in Mathematica, and it makes sense to assume that deviation shown in the calibration curves (obtained via gas chromatography) attest to this experimental shortcoming.

6.8.2 Gas Uncertainty

The experimental procedure (Appendix A) is that, once equilibrium is established inside the rig, indicated by a non-perceptible change of pressure, then gaseous samples are analysed. The voltage is logged in a text file, then converted to XY scattered data, that can be plotted in spreadsheet software. One needs to keep the flow rates constant, as fluctuations affect the voltage readings in both analysers, O_2 and SO_2. In contrast, the FTIR spectrometer, as long as the pressure does not change suddenly, readings remain constant. If pressure changes abruptly, this would contribute to rapid droplet formation that could affect the analysis.

Using the programming code in Visual Basic shown in appendix E, the "stable zone" is identified and used as N samples that are then analysed with statistical software (Minitab®) for descriptive information about the confidence interval of the measurements.

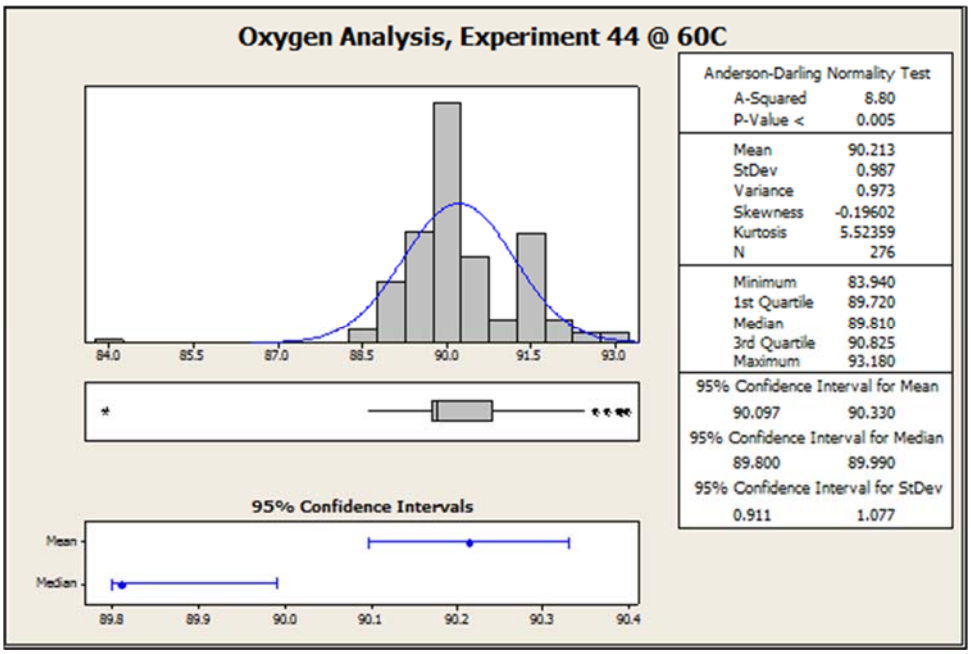

Figure 19. Statistical treatment for paramagnetic gaseous oxygen analysis.

In Figure 19 and Figure 20, one can see the histograms for ternary gaseous analysis of oxygen and sulphur dioxide, respectively. It can be contrasted with the Iodometry measurements (discussed in section 6.8.3), that have considerably more standard deviation than the gaseous measurements.

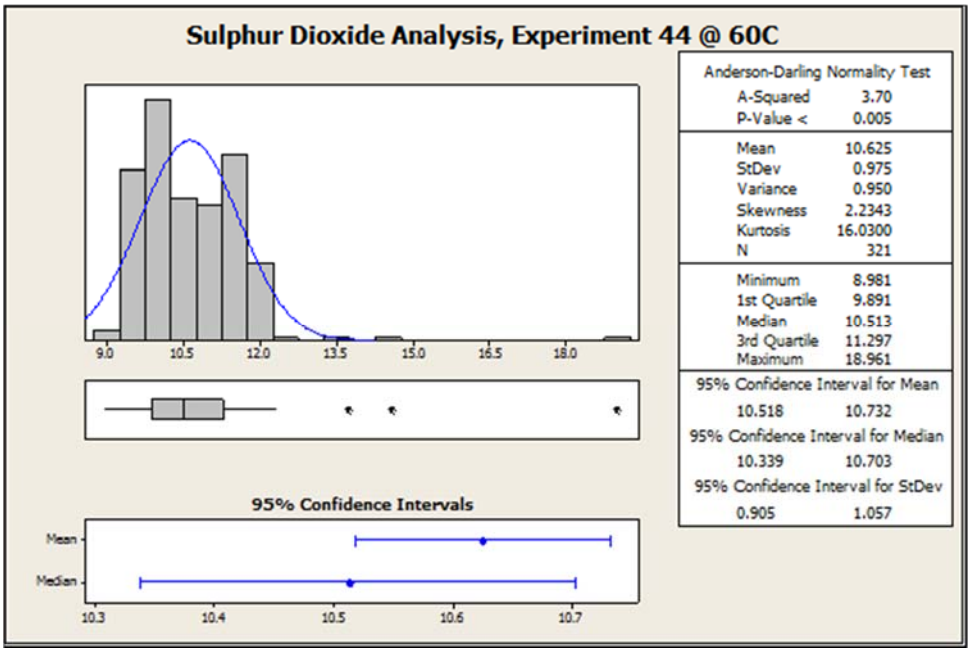

Figure 20. Statistical treatment of Sulfur Dioxide analysis with the IR analyser.

The main comparison for reliability of measurements is related to the composition change of the gases, the standard deviation just below 1% (vol.), in

contrast with the Iodometry that reaches approximately >6%, mentioned earlier as a limitation for the design of the Mark-IV in Chapter 5.

6.8.3 Iodometry Uncertainty

As explained in Chapter 5, a sensitivity analysis on one particular experiment shows that the standard deviation of a typical titration is approximately σ=0.191 and the confidence interval at 95% is 0.132, an uncertainty value of 6.5% at a concentration of slightly over 1.9 mol S_{IV}/kg H_2O. It is stated that sample flashing due to differences in a) temperature and b) pressure at the exit of the system returned erroneous or highly noisy results. This is qualitatively represented in Figure 21, where one can see this trend represented schematically. This iodometric uncertainty leads one to assume that temperature has an important role in the accuracy of the chemistry involved in the titrimetric analysis, or the unreliability of the sampling mechanism.

Experiment	25	40	60	80
34		X		
39		X		
40		X		
41	X			
42	X			
43			X	
44			X	
46			X	
47			X	
48			X	
49			X	
51				X
52				X
53				X

Figure 21. Representation of increasing titrimetric uncertainty vs. operating temperature

6.8.4 Gas Chromatography

In order to reach the maximum amount of technical simplicity with the last quaternary experiments, and due to time constraints, the only available analytical measurements for these runs were chosen to be discrete gaseous samples. This were analysed with a Varian StarChrom system, with a Hayesep-N® 1.5 m column, enough to provide reasonable resolution for gaseous samples, as long as the sulphuric acid concentrations remained low. Further details about the analysis are explained in the sampling section in Chapter 5.

Being a gaseous sample, the amounts injected were chosen to be between 100 to 1000 μL. A method was developed to provide the most accurate reading of SO_2 and O_2 concentrations, with a total running time of less than 5 min. The retention times and the voltage response were clearly related to the amount injected, so it was kept constant to 500 μL, which equates to less than 1% of the total gaseous chamber volume in the Mark-IV, and even less in the previous Mark-III.

However, the minuscule amounts leaked while transferring the equilibrated gaseous media to the sampling chromatography bag may have affected the accuracy of the readings, as it is clearly shown in Table 7, where one can appreciate the large differences in predicted concentration against the experimental GC data. It is important to state that because of time constraints, the concentration peaks in the chromatogram were processed manually, without any electronic baseline correction.

Table 7. Mass addition measurements for SO_2 and O_2, highlighting deviations between prediction and chromatography values.

Experiment	1	2	3	5	6	8	9	10	11
Date	01-Oct	01-Oct	04-Oct	09-Oct	10-Oct	12-Oct	12-Oct	13-Oct	15-Oct
Mass of SO_2 added (g)	0.75	0.64	1.49	0.34	0.38	0.89	0.85	1.66	2.57
Mass of O_2 added (g)	0.43	1.99	1.43	2.40	2.27	1.34	0.60	0.53	1.43
Temperature (C)	60	40	40	40	60	25	25	25	40
Mass of SO_2 predicted (g)	0.77	0.63	1.48	0.37	0.35	0.85	0.84	1.50	2.60
Predicted SO_2 (%)	43.99%	13.42%	33.64%	7.03%	6.78%	24.21%	39.75%	54.48%	46.60%
Chromatograph SO_2 (%)	82.05%	19.58%	61.35%	9.77%	5.40%	33.87%	65.29%	91.01%	87.27%
Prediction Deviation (%)	38.06%	6.16%	27.71%	2.74%	1.38%	9.66%	25.54%	36.53%	40.67%

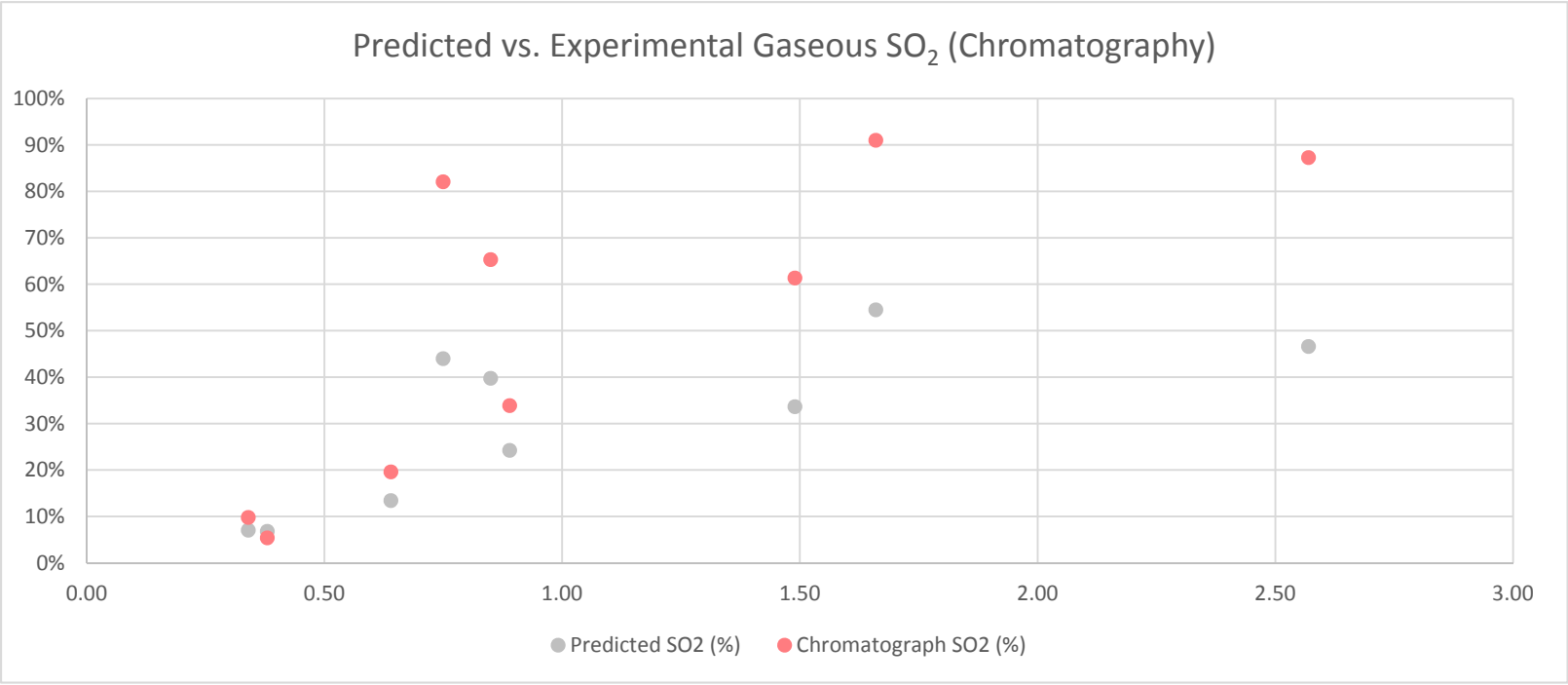

Figure 22. Differences between ideal-gas predicted composition of SO_2 vs. Experimental GC analysis. Quaternary experiments.

6.9 Summary

In this Chapter, results derived from calculations devised to predict the thermodynamic equilibrium of different mixtures were presented. The calculations involved different techniques:

- Using the Gibbs Free Energy minimisation technique, a very commonly implemented technique for complex chemistries and aqueous electrolytes not readily available experimentally, developed by Thomsen and Rasmussen (Outokumpu, 2002), using 3-component calculations and a 4-component calculation, including sulphuric acid. The importance of having a comparison with the HSC Chemistry package, which is used for most flow sheets in the H_2 production research field as well as general industry, is fundamental to this project.
- Using a rigorous thermodynamic model derived from the methodology by Zemaitis et al. (1986), which contains phase-equilibrium equations, equilibrium rate constants and further equations describing activity and fugacity of the species of interest, both ternary (SO_2, O_2 and water) and quaternary, including sulphuric acid and its associated species (sulphates, bisulphates and sulphur trioxide).
- Additional calculations (unit, scale and group conversions) to bridge the two models, in order to be able to compare the two.

The models concur in certain aspects (SO_2 solubility prediction, temperature effects on solubility of gaseous species), but in others they differ considerably (effect on dissolved ionic species concentration and salting out effects due to acid addition).

Several questions arise from these differences. On the Gibbs Free Energy model, it is not clear whether the experimental data that was used to obtain the

HSC predictions is slightly off, or the algorithms used for the minimisation do not weight justly the effects of acid concentration.

On the other hand, it is also not clear if the assumptions utilised by the Mathematica Model (both ternary and quaternary) are *sufficient* to predict ionic species. Until the in-situ solution is available, no possible determination of the relationship between equilibrium and dissociation can be established successfully.

However, great success is reported for the in-situ Fourier-Transform spectroscopic preliminary solutions, which clearly show promise to deliver clear, successful characterization of the dilute ionic species inside a liquid (and possibly a gaseous) chamber. This is a remarkable achievement that to the author's knowledge, has not been achieved for weak-electrolyte thermodynamics research.

In Chapter 7, conclusions drawn from this project are presented, along with the recommended work needed to address the questions left unanswered in this project.

References for Chapter 6

BEUSCHLEIN, W. L. & SIMENSON, L. O. 1940. Solubility of Sulfur Dioxide in Water. Journal of the American Chemical Society, 62, 610-612.

ELDER, R. H., SHAW, A., ROMERO, M., ELBAKHBAKHI, N., PRIESTMAN, G. H. & ALLEN, R. W. K. 2010. Low Temperature Separations in the Sulphuric Acid Decomposition Stage of the Sulphur Iodine and Hybrid Sulphur Thermochemical Water Splitting Cycles. In: DETLEF STOLTEN, T. G. E. F. J. G. (ed.) WHEC 2010. Essen, Germany: Forschungszentrum Jülich GmbH, Zentralbibliothek, Verlag.

GUBBINS, K. & WALKER, R. 1965. The Solubility and Diffusivity of Oxygen in Electrolytic Solutions. Journal of the Electrochemical Society, 112, 469.

HAYDUK, W., ASATANI, H. & LU, B. C. Y. 1988. Solubility of sulfur dioxide in aqueous sulfuric acid solutions. Journal of Chemical and Engineering Data, 33, 506-9.

HUDSON, J. C. 1925. The solubility of sulphur dioxide in water and in aqueous solutions of potassium chloride and sodium sulphate. Journal of the Chemical Society, 127, 1332-1347.

JEONG, Y. H., K. HOHNHOLT, M. S. KAZIMI AND B. YILDIZ. 2005. Optimization of the hybrid sulfur cycle for hydrogen generation. Nuclear Energy and Sustainability Program (NES) Technical Report: MIT-NES-TR-004. Massachusetts, NE: Center for Advanced Nuclear Energy Systems, MIT.

MAASS, C. E. & MAASS, O. 1928. Sulfur Dioxide and its aqueous solutions. I. Analytical Methods, Vapor Density and Vapor Pressure of Sulfur Dioxide. Vapor Pressure and Concentrations of the Solutions. . Journal of the American Chemical Society, 50, 1352-1368.

OUTOKUMPU 2002. Software: HSC chemistry version 5.0. Chemical Engineering Progress, 98, 28.

RABE, A. E. & HARRIS, J. F. 1963. Vapor Liquid Equilibrium Data for the Binary System Sulfur Dioxide and Water. Journal of Chemical & Engineering Data, 8, 333-336.

ROMERO, M. Low temperature SO2-O2-H2O VLE in the sulphur family of thermochemical cycles. In: ALLEN, R. W. K., ed. International Conference on Hydrogen Production, 2011 Thessaloniki, Greece. Hellas Research Centre, Greece.

RUMPF, B., WEYRICH, F. & MAURER, G. 1993. Simultaneous solubility of ammonia and sulfur dioxide in water at temperatures from 313.15 K to 373.15 K and pressures up to 2.2 MPa. Fluid Phase Equilibria, 83, 253-260.

SHAW, A., ROMERO, MOISES, ELDER, R. H., EWAN, B. C. R. & ALLEN, R. W. K. 2011. Measurements of the solubility of sulphur dioxide in water for the sulphur family of thermochemical cycles. International Journal of Hydrogen Energy, 36, 4749-4756.

SHAW, A. C. 2008. The simultaneous solubility of sulphur dioxide and oxygen in water for the hybrid sulphur thermochemical cycle. Ph.D. Doctoral Thesis, University of Sheffield.

SHERWOOD, T. K. 1925. Solubilities of Sulfur Dioxide and Ammonia in Water. Industrial & Engineering Chemistry, 17, 745-747.

ZEMAITIS, J. F. J., CLARK, D. M., RAFAL, M. & SCRIVNER, N. D. 1986. Handbook of aqueous electrolyte thermodynamics.

Chapter 7

Conclusions & Future Work

Chapter 7

Table of Contents

7.1 Overview

In this Chapter, conclusions are drawn from the set of equations that were used to describe weak electrolyte thermodynamic behaviour in the ternary system containing SO_2-O_2-H_2O with the GFE and Shaw's model, the mixed electrolyte vapour-liquid equilibrium behaviour in the quaternary system including sulphuric acid, and lastly the ternary and quaternary data acquired with the equilibrium stills operated and developed for this objective. Each stage of this project is discussed below, and related to a specific chapter in this thesis.

Chapter 1 and 2 are the introduction and the Literature review. These are mainly the background to the project, the justification for it and how relevant this separation stage is for the sulphuric acid decomposition step, largely documented in the literature pertaining to the Hybrid-Sulphur and Sulphur-Iodine cycles. One cannot skip the important point that

Chapter 3 gave the necessary theory behind electrolyte dissolutions and vapour liquid equilibrium, and should be considered an introductory body of work for the further study of vapour liquid equilibria for volatile species, and its intention is to provide the necessary foundations to understand the calculations in Chapter 4. The theory is mainly taken from work from Malanowski and Anderko (1992), as well as Shaw's doctoral thesis (2008) and the work done by Smith and Van Ness (1996).

Chapter 4 is an extension of the calculations performed in Shaw's doctoral thesis (2008), containing sulphuric acid in the equilibrium equations. Most of the binary interaction parameters and quaternary variables were extrapolated to account for the presence of H_2SO_4, in the temperature range between 293 and 353 K. This calculation is a promising prediction tool for gaseous solubilities, key to the design of separation equipment. In comparison with the ternary models, it is shown that the salting out effect of the acid contained in the solution, even at low concentrations, deviates from the ideal behaviour of the mixture, reverts the behaviour of the electrolytes to a lesser soluble species and strengthens the case for the importance of separating sulphuric acid after the decomposer if efficiencies in the absorber are to be maintained at an optimum level.

Chapter 5 present a thorough explanation through the design and operating process of the equilibrium stills necessary to gather experimental solubility data for the ternary and quaternary systems. All of the technical developments in this project are presented in these chapters, along with the design process followed and the respective uncertainty analysis for each of the experimental aspects of the project.

Finally, Chapter 6 presents the results from both the experimental activities in this project as well as the modelling that was performed bot in Mathematica and in HSC chemistry. A comparison between HSC results and the Mathematica model is also included, analysed and discussed.

7.2 Discussion

7.2.1. Gibbs Free Energy Calculations

The Gibbs Free energy calculations showed a very interesting ionic species behaviour. Even more when the species were subject to the salting out effect of the acid media in the calculations. This unfortunately could not be confirmed experimentally, as the possibility of using in-situ analysis was not available, although the instrumental design proved to be successful.

A very important similarity between the Gibbs Free Energy calculations and the Mathematica models is the consistent representation on the effect of pressure and temperature in the solubility of both gases, and marked further in sulphur dioxide. Although thermodynamic consistency proofs have not been performed, this is a good indicator that the accuracy of the macroscopic phenomena that both techniques are trying to achieve, are on the right direction and can be deemed reliable, at least for an approximate level. Without an in-situ analysis, one cannot determine how accurate the models are.

One also needs to highlight a difference in the way solubility is affected in both models. The difference in solubility due to temperature seems to have an asymptotic effect on SO_2 solubility in the Mathematica model, in contrast to a more linear effect in the HSC model. It seems that even as temperatures reach the boiling point of the

aqueous solution (regardless of composition), there is a balance between the number of allowed SO_2 molecules and the vapour pressure of the gas "pushing out" of the solution. A more dramatic effect is shown in the Gibbs model, however, the causes of these are not quantified yet. One could assume discontinuities in the solution algorithms, or even wrong thermochemical database numbers, where the Gibbs Free Energy is derived from.

Another interesting finding is the unorthodox effect of temperature on oxygen solubility. There is a certain compromise between the partial pressure exerted by oxygen and the fugacity that makes it less soluble as the temperature reaches the boiling point of the solution. This effect is highlighted in the upper plot in Figure 1, where the solubility of oxygen is similar between 60 and 80 °C, in contrast with a more orthodox result in the ternary system (less solubility at a higher temperature).

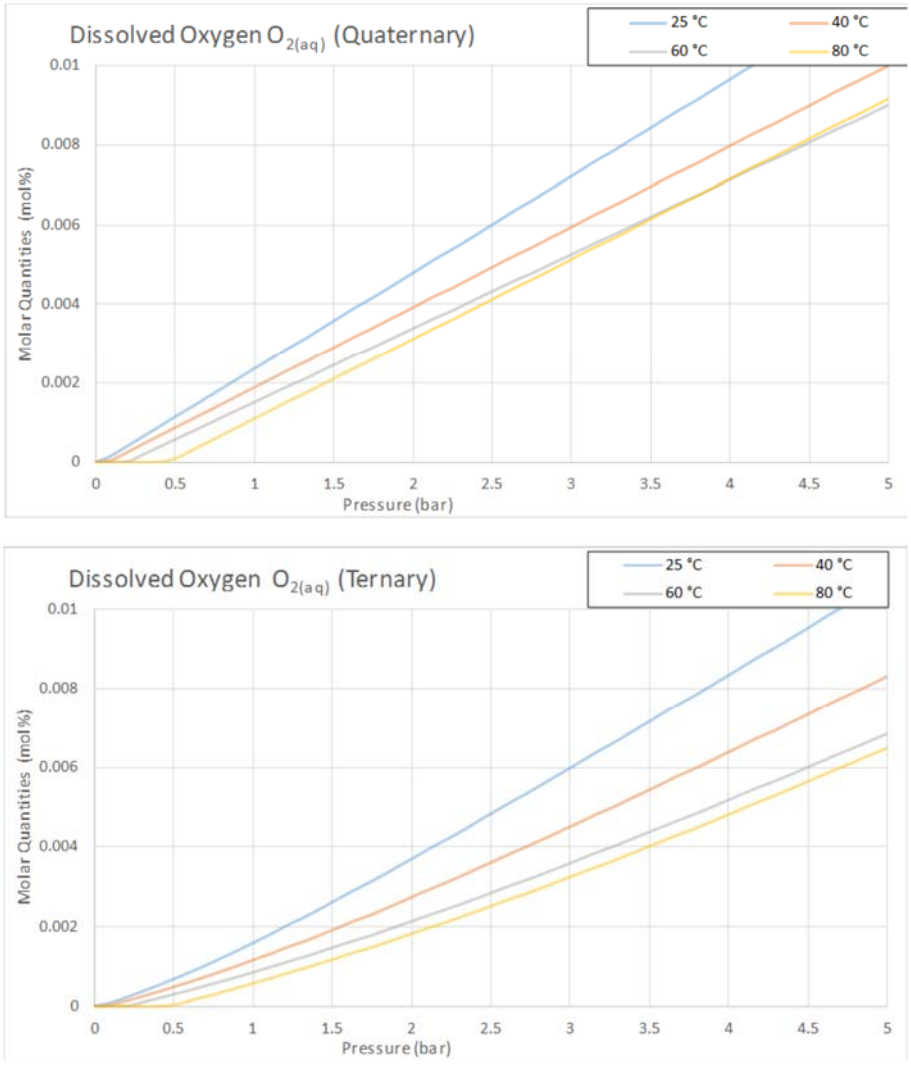

Figure 1. Comparison between Quaternary and Ternary for dissolved oxygen, 0-5 bar, 25 to 80 °C.

7.2.2. Acid threshold in HyS and SI operation

Due to the weak electrolytic behaviour of sulphur dioxide in aqueous solutions, including dilute acid solutions the quaternary model is shown to be accurate in determining the gaseous solubility to an average of 20%. Although this is definitely not ideal, again, it is important to acknowledge the current limitations of the model:

- The majority of interaction parameters were extrapolated to the best of the author's knowledge, or on a molecular weight basis
- Due to time constraints, the regression of data was not feasible as the number of experiments was not enough for that purpose
- As with all rigorous models, the flexibility of the model is not massive, hence modifications to a core set of equations is difficult. This does not help when trying to achieve adaptability for different input conditions.

However these shortcomings, the Mathematica model agrees with statements from the literature (Hayduk et al., 1988), that show that while the general tendency is to slightly over predict solubilities of the volatile electrolytes, a good thermodynamic consistency is shown for the ionic species and the predicted acid effect on solvation of ions.

While some accomplishments have been achieved throughout the entirety of this project, particularly on the experimental side of technology development and the know-how for equilibrium, further work is strongly recommended for the remaining questions in this field of weak aqueous electrolyte thermodynamics.

7.3 Suggested Future Work

In the following sections, the recommended future work is laid out, as well as the technical developments that were not achieved due to time constraints, and that could be implemented easily in a timeframe of no more than 4 months.

7.2.3. Spectroscopy

Shaw (2008) initially recommended Raman for its low sensitivity to water and applicability for symmetrical molecules, such as nitrogen or oxygen, even if the induced dipole moment is very little. Now that equipment is available in the university, several experiments must be conducted to conclude the questions of acid speciation in the near infrared, in situ analysis and the first dual in-situ IR and Raman set-up for vapour liquid equilibrium purposes.

7.2.4. Prismatic In-situ Acquisition

After a failure of the Germanium prism that was featured for the ATR measurement in the Mark IV, the author believes that a substitution of the same prism, but made out of silicon, would prove equally successful. This has to do with the brittleness of Si in comparison to Germanium, and its enhanced mechanical properties, which would make it a good choice for compressive / shear stress tests in the ATR configuration explained in Chapter 5.

7.2.5. Conical In-situ Acquisition

Another choice would be to include a plug-shaped cone prism and a back-scattering fibre optic configuration to achieve the in-situ measurements. The idea would be to emit from the spectrometers infrared source, let the emission travel through the fibre optic cables, be collimated at the end of the fiber where it would be concentrated via mirrors or a focusing IR lens, then incide at a 90° angle from the surface of the outside polished surface of the prism, travel through the prism and bounce at an angle, ideally two times for a 45° angle, and come back from the other side, making it a dual bounce configuration and travel back to another route until gathered by the MCT detector (Gauglitz and Vo-Dinh, 2006). This has the advantage of solving only one problem, rather than various for a horizontal ATR configuration: alignment, brittleness of the prism, shear stress and torque in the twist required to close the ATR lid. The only compromise would be to decrease overall transmission due to the thickness of the conical prism.

One would have to acquire the maximum permissible thickness of Silicon to simulate the strength of the emission, however, an initial and successful attempt was made for Germanium. The optics of the Silicon Cone are shown in Figure 1.

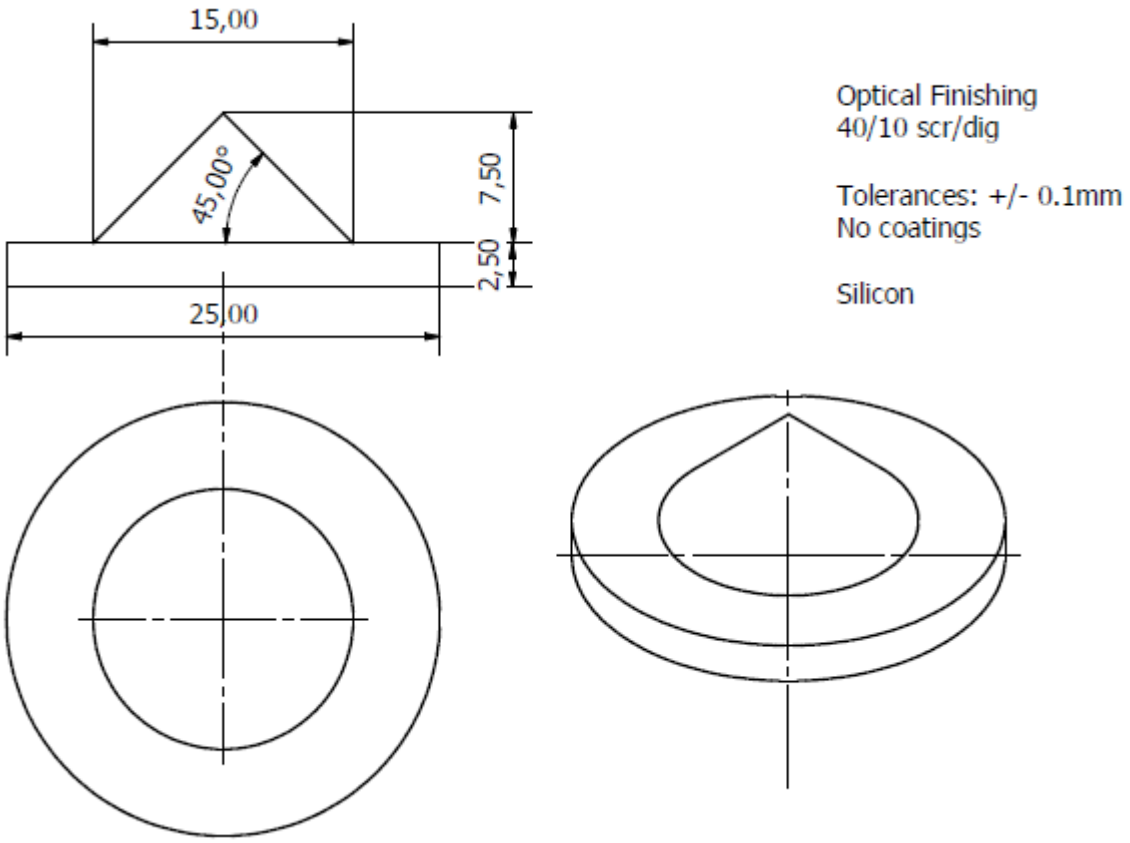

Figure 2. Conical Silicon/Germanium ATR prism for in-situ determinations.

Finally, the intention of the model is to overcome the programming language barriers and be implemented in C or C++. This will make the program compatible with the Aspen scripts, and would be eventually usable for a flowsheeting software, not limited to Aspen, but available also to ProSIM® or even multiphysics models, such as COMSOL® or FLUENT®.

One disadvantage of using the methodology of Zemaitis is the fact that the poor flexibility of the model limits its practical applicability. This perspective has led to the development of different methods that have tried to implement electrolyte thermodynamics, such as the eNRTL model or the UNIFAC or UNIQUAC with

electrolytes. This needs to be explored, as well as different equations available for different species, if one desires to add traces of components to the model.

7.4 Summary

The objective of this thesis was to follow up on the project initiated by Shaw, which involved the acquisition of experimental data that would enable the thermodynamic characterization of a mixture of gases relevant to the production of Hydrogen in the sulphur family of thermochemical cycles. This would also lay the framework needed to continue the thermodynamic calculations needed for the design of equipment relevant to the $SO_2/O_2/H_2O$ separation. This work was a two part project in conjunction with the European Union, and partly funded by the Mexican Government, who provided funding for the author during the 4 years of the duration of his stay in the University of Sheffield.

The model was developed, simultaneously with the design of the next generation equilibrium still that was able to incorporate in-situ analysis, which for a short time it did accomplish. Several technical design milestones were achieved in the process, including the development of a sapphire liquid gas cell, a glass reinforced single pass 10 cm Zinc Selenide gaseous cell, several iterations of Raman Spectroscopy probes with ranging capabilities for different purposes, mostly high pressures and temperatures. It was also confirmed that on low temperature conditions such as this one, materials become an important factor for the success or failure of the process.

Based on the results comparison between the calculations of the Mathematica model, the GFE model, the little available experimental data and general tendencies in the literature, one can conclude that the calculations, as well as the experimental techniques used throughout this project, are successful for their purpose, which is the aiding of equipment design for the HyS and SI cycle, ideally leading to the reduction of carbon emissions and the reduction on foreign oil imports for Europe, and for countries such as Mexico.

References for Chapter 7

GAUGLITZ, G. & VO-DINH, T. 2006. Handbook of Spectroscopy, Wiley.

HAYDUK, W., ASATANI, H. & LU, B. C. Y. 1988. Solubility of sulfur dioxide in aqueous sulfuric acid solutions. Journal of Chemical and Engineering Data, 33, 506-9.

MALANOWSKI, S. & ANDERKO, A. 1992. Modelling phase equilibria: thermodynamic background and practical tools, Wiley.

SHAW, A. C. 2008. The simultaneous solubility of sulphur dioxide and oxygen in water for the hybrid sulphur thermochemical cycle. Ph.D. Doctoral Thesis, University of Sheffield.

SMITH, J. M. & VAN NESS, H. C. 1996. Introduction to chemical engineering thermodynamics, McGraw-Hill.

Appendix A.
Experimental Operating Procedure

Appendix A. Experimental Procedure

Location:	Hydrogen Lab, G61
Operator:	Moises Romero
Additional equipment:	Sulphur dioxide cartridge mask, cryo gloves, nitrile gloves, safety goggles, howie coat, sulphur dioxide detector, faceplate, Liquid Nitrogen dewar, ToolBox,

1. THINK, is it safe to remove an item from the fume hood?

Do not remove any items of equipment which may be contaminated with sulphur dioxide from the fume hood including tissues, gloves, pipe work, glassware etc. Be aware of electric shocks, be aware of laser light, sulphuric acid, and moisturize skin often. Do not wear contact lenses for extended periods. Do not use chemicals out of hours. When using high pressure gases, make sure there is a cylinder sample prior to attaching it to media.

Cartridge mask should be COSHH checked monthly. Cartridges should be changed every 15 user hours or 6 months which ever is sooner. SO2 alarm should be taken care of. DO NOT splash water into the FTIR.

This is intended as an experimental procedure summary. For a detailed version of the valves, use COSHH form.

Before the Experimental Activities

1. Check that all items are in good condition. Check for leaks, bad smells, water, rust, hissing sounds or any other type of unusual condition that was not on previous experiments. This is particularly important for the sample cylinders.
2. The FTIR should be cooled down with liquid nitrogen, use 250 ml. For help, refer to the Varian 660 Manual.
3. The Raman probe should be aligned, dry and with no signs of lens corrosion.
4. The rig should be tightened every week if PTFE, if SS, it is not necessary.

Experimental Procedure (Summary)

1. Weight the Mark IV in a balance, with 4kg capacity and 0.01 gr resolution. Contact K. Penny. Note the number, then subject the rig to vacuum, weight. The difference can be used to determine within certain accuracy the air inside the rig.
2. After reaching less than 10 mbar pressure, close the PTFE valves and the tube fitting used to connect the vacuum pump. Check for leaks.
3. Once the rig is subject to vacuum, one can then submerge the Mark IV in the waterbath. Set temperature, note for any leaks. If necessary, try pressurizing it with nitrogen.
4. Once the rig is subjected to vacuum, the addition of species may occur. The gas species could be premixed and calculated using partial pressures, the solutions using gravimetry. The solutions will be going into the liquid part, and the gases into the gaseous part, while maintaining the contact between the two sections of the rig isolated.
5. Once the species have been added, the rig may be weighted again, and the accuracy of the masses can be calculated. The mixing can be started, by chaotically shaking the rig until no bubbles are seen through the sightglass. Equilibrium then will be reached carefully monitoring LabVIEW, and noting constant pressure and temperatures.
6. Sampling can occur from this point, using syringe sampling for gaseous (FTIR, GC) and carefully iodometric analysis with the liquids.
7. Purging the rig with compressed air and rinsing it with water overnight is advisable for following runs.

Appendix B.
LabVIEW Program

Appendix B.

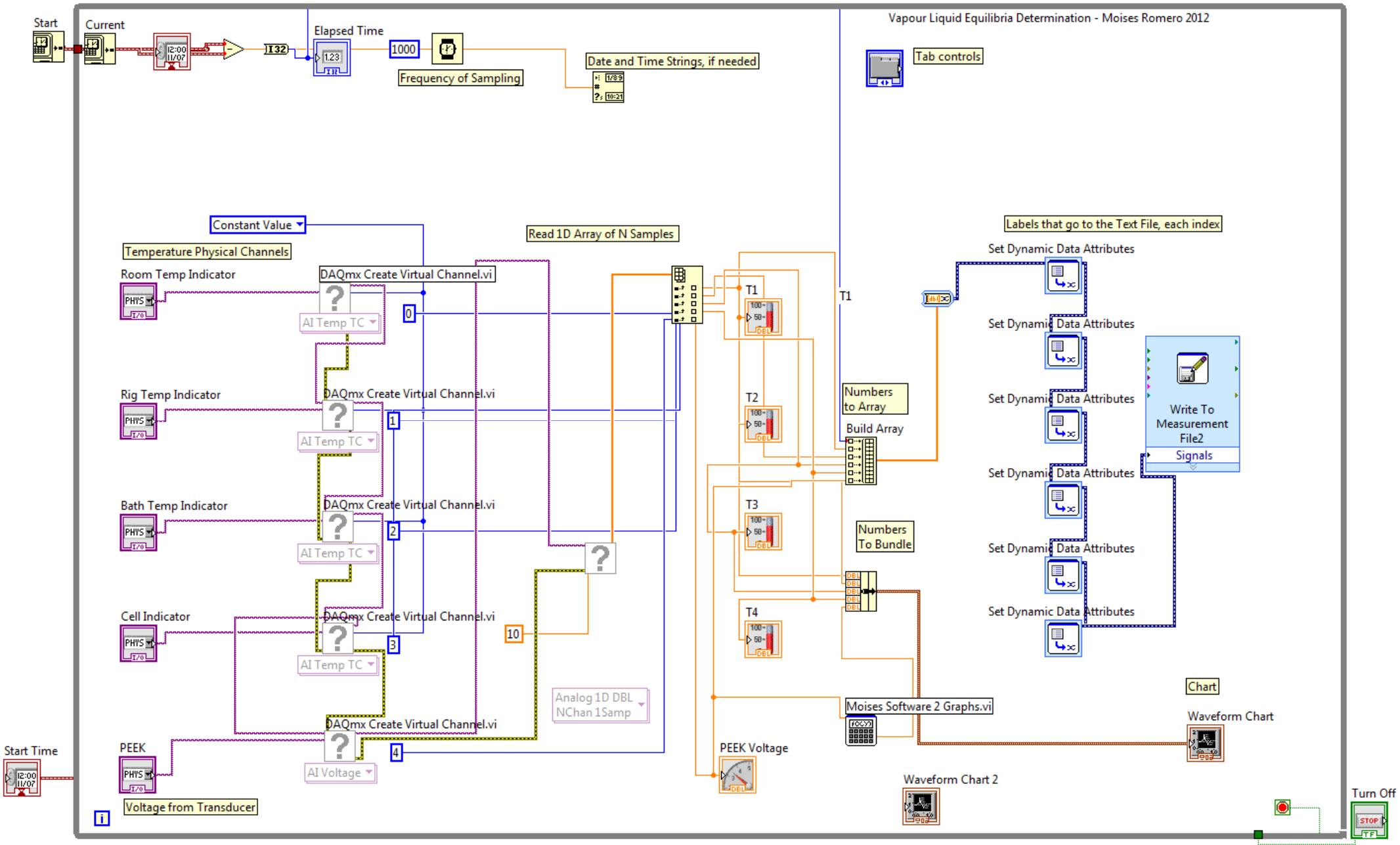
Vapour Liquid Equilibria Determination - Moises Romero 2012
Start
Current
I32
Elapsed Time
1000
Frequency of Sampling
Date and Time Strings, if needed
Tab controls
Constant Value
Temperature Physical Channels
Read 1D Array of N Samples
Labels that go to the Text File, each index
Room Temp Indicator
DAQmx Create Virtual Channel.vi
AI Temp TC
Rig Temp Indicator
Bath Temp Indicator
Cell Indicator
PEEK
AI Voltage
Voltage from Transducer
Start Time
Analog 1D DBL NChan 1Samp
T1
T2
T3
T4
Numbers to Array
Build Array
Numbers To Bundle
Set Dynamic Data Attributes
Write To Measurement File2
Signals
PEEK Voltage
Moises Software 2 Graphs.vi
Chart
Waveform Chart
Waveform Chart 2
Turn Off
STOP

A. Description of the LabVIEW 2011-2012 program.

The code consists of a manual timestamp acquisition right at the top of the Navigation Window. Considerable effort was put to make the code legible and under one page, using the newest datalogging tools from the program. Since the heating control was taken care of by the external water bath, there was no need for additional VI's including PID algorithms and digital in/outs (thermal switches=in, discrete on/off signal=out).

Next block includes the 5 main DAQ physical channels, configurable in different tabs within the graphic user interface. From those configurable physical channels, an error is carried out from the initial temperature channels to the last one, the pressure transducer, via a series of virtual channels, that will eventually hold the variables in place and log the raw data.

Once the indexes for each variable/channel is set, one can then concatenate them in a set of arrays, that will function in two ways: 1) obtain the numerical data on the frequency of the loop stated in the label "Frequency of Sampling", and 2) convert raw data into readable floating-point numbers that can be, in turn, converted to strings.

Finally, each signal gets grouped into a Convert to Dynamic Data, where each signal is added with a different attribute to ease text logging in a *.txt file of the user preference, and then finally ordered to print in two forms: a dynamic sweep waveform chart, as well as the aforementioned text file. In this command the filepath, the filename and the headers are set.

For ease of use and practicality, a custom script determining the maximum filesize of the text file is added in the code, which, if needed, will split the text files and continue to write in another new one, providing protection for buffer overrun. This is seen in the properties of the LabVIEW VI.

For enhanced interoperability, the code was compiled onto the laboratory PC, so that it could be accessed without the need for LabVIEW installation, however, drivers are required to read the signals from the DAQ-module.

Appendix C.

HSC Calculation – Example

Equilibrium Calculation (Isothermic)

```
File Name: C:\USERS\FONCHIRRI\SKYDRIVE\MODELS\3 COMPONENT\HSC IDEAL\60 DEGREES 0 TO

§60 deg, 0 to 5 bar

Temperature             333.15   K
Pressure                0.0000000001         bar
Volume                  0.000E+00 m3 ( NPT )
Reaction enthalpy       3.520E+02 kJ
Reaction entropy        9.460E+02 J/K
Iterations              16        ( Limit =  100  )

                      INPUT AMOUNT EQUIL AMOUNT MOLE FRACT  ACTIVITY  ACTIVITY
PHASE 1:                    mol         mol               COEFFICI
H2O                     8.2713E+00  0.0000E+000  0.000E+00  1.00E+00  0.000E+00
H(+a)                   3.0000E-03  0.0000E+000  0.000E+00  1.00E+00  0.000E+00
OH(-a)                  1.0000E-03  0.0000E+000  0.000E+00  1.00E+00  0.000E+00
HSO3(-a)                1.0000E-03  0.0000E+000  0.000E+00  1.00E+00  0.000E+00
SO3(-2a)                5.0000E-04  0.0000E+000  0.000E+00  1.00E+00  0.000E+00
SO2(a)                  0.0000E+00  0.0000E+000  0.000E+00  1.00E+00  0.000E+00
O2(a)                   0.0000E+00  0.0000E+000  0.000E+00  1.00E+00  0.000E+00
Total :                 8.2768E+00  0.0000E+000

PHASE 2 :                                  MOLE FRACT
H2O(g)                  0.0000E+00  8.2738E+000  9.677E-01  1.00E+00  9.677E-01
O2(g)                   1.3938E-01  1.3938E-001  1.630E-02  1.00E+00  1.630E-02
SO2(g)                  1.3487E-01  1.3637E-001  1.595E-02  1.00E+00  1.595E-02
Total :                 2.7425E-01  8.5495E+000

************************************************************************
Iteration  20  GMIN =      -953.50791750888

§60 deg, 0 to 5 bar

Temperature             333.15   K
Pressure                0.102         bar
Volume                  0.000E+00 m3 ( NPT )
Reaction enthalpy       3.520E+02 kJ
Reaction entropy        9.460E+02 J/K
Iterations              20        ( Limit =  100  )

                      INPUT AMOUNT EQUIL AMOUNT MOLE FRACT  ACTIVITY  ACTIVITY
PHASE 1:                    mol         mol               COEFFICI
H2O                     8.2713E+00  0.0000E+000  0.000E+00  1.00E+00  0.000E+00
H(+a)                   3.0000E-03  0.0000E+000  0.000E+00  1.00E+00  0.000E+00
OH(-a)                  1.0000E-03  0.0000E+000  0.000E+00  1.00E+00  0.000E+00
HSO3(-a)                1.0000E-03  0.0000E+000  0.000E+00  1.00E+00  0.000E+00
SO3(-2a)                5.0000E-04  0.0000E+000  0.000E+00  1.00E+00  0.000E+00
SO2(a)                  0.0000E+00  0.0000E+000  0.000E+00  1.00E+00  0.000E+00
O2(a)                   0.0000E+00  0.0000E+000  0.000E+00  1.00E+00  0.000E+00
Total :                 8.2768E+00  0.0000E+000

PHASE 2 :                                  MOLE FRACT
H2O(g)                  0.0000E+00  8.2738E+000  9.677E-01  1.00E+00  9.677E-01
O2(g)                   1.3938E-01  1.3938E-001  1.630E-02  1.00E+00  1.630E-02
SO2(g)                  1.3487E-01  1.3637E-001  1.595E-02  1.00E+00  1.595E-02
Total :                 2.7425E-01  8.5495E+000
```



```
************************************************************************
Iteration  13  GMIN =      -946.600606196743

§60 deg, 0 to 5 bar

Temperature             333.15   K
Pressure                0.408         bar
Volume                  5.382E-01 m3 ( NPT )
Reaction enthalpy       1.048E+01 kJ
Reaction entropy        2.810E+01 J/K
Iterations              13        ( Limit =  100  )

                      INPUT AMOUNT EQUIL AMOUNT MOLE FRACT  ACTIVITY  ACTIVITY
PHASE 1:                    mol         mol               COEFFICI
H2O                     8.2713E+00  8.0202E+000  9.985E-01  1.00E+00  9.985E-01
H(+a)                   3.0000E-03  2.5024E-003  3.115E-04  1.00E+00  3.115E-04
OH(-a)                  1.0000E-03  7.9175E-013  9.857E-14  1.00E+00  9.857E-14
HSO3(-a)                1.0000E-03  2.5024E-003  3.115E-04  1.00E+00  3.115E-04
SO3(-2a)                5.0000E-04  5.1929E-009  6.465E-10  1.00E+00  6.465E-10
SO2(a)                  0.0000E+00  7.0369E-003  8.761E-04  1.00E+00  8.761E-04
O2(a)                   0.0000E+00  1.6544E-005  2.060E-06  1.00E+00  2.060E-06
Total :                 8.2768E+00  8.0322E+000

PHASE 2 :                                  MOLE FRACT
H2O(g)                  0.0000E+00  2.5111E-001  4.854E-01  1.00E+00  4.854E-01
O2(g)                   1.3938E-01  1.3936E-001  2.694E-01  1.00E+00  2.694E-01
SO2(g)                  1.3487E-01  1.2683E-001  2.452E-01  1.00E+00  2.452E-01
Total :                 2.7425E-01  5.1730E-001


************************************************************************
Iteration  14  GMIN =      -946.495954290727

§60 deg, 0 to 5 bar

Temperature             333.15   K
Pressure                0.51          bar
Volume                  4.353E-01 m3 ( NPT )
Reaction enthalpy       6.796E+00 kJ
Reaction entropy        1.798E+01 J/K
Iterations              14        ( Limit =  100  )

                      INPUT AMOUNT EQUIL AMOUNT MOLE FRACT  ACTIVITY  ACTIVITY
PHASE 1:                    mol         mol               COEFFICI
H2O                     8.2713E+00  8.1044E+000  9.980E-01  1.00E+00  9.980E-01
H(+a)                   3.0000E-03  3.0583E-003  3.766E-04  1.00E+00  3.766E-04
OH(-a)                  1.0000E-03  6.6187E-013  8.150E-14  1.00E+00  8.150E-14
HSO3(-a)                1.0000E-03  3.0583E-003  3.766E-04  1.00E+00  3.766E-04
SO3(-2a)                5.0000E-04  5.2502E-009  6.465E-10  1.00E+00  6.465E-10
SO2(a)                  0.0000E+00  1.0401E-002  1.281E-03  1.00E+00  1.281E-03
O2(a)                   0.0000E+00  2.5232E-005  3.107E-06  1.00E+00  3.107E-06
Total :                 8.2768E+00  8.1209E+000

PHASE 2 :                                  MOLE FRACT
H2O(g)                  0.0000E+00  1.6636E-001  3.881E-01  1.00E+00  3.881E-01
O2(g)                   1.3938E-01  1.3935E-001  3.251E-01  1.00E+00  3.251E-01
SO2(g)                  1.3487E-01  1.2291E-001  2.867E-01  1.00E+00  2.867E-01
Total :                 2.7425E-01  4.2862E-001


************************************************************************
Iteration  12  GMIN =      -946.422296508146

§60 deg, 0 to 5 bar

Temperature             333.15   K
Pressure                0.612         bar
Volume                  3.648E-01 m3 ( NPT )
Reaction enthalpy       4.899E+00 kJ
```



```
O2(g)                   1.3938E-01  1.3938E-001  1.630E-02  1.00E+00  1.630E-02
SO2(g)                  1.3487E-01  1.3637E-001  1.595E-02  1.00E+00  1.595E-02
Total :                 2.7425E-01  8.5495E+000


************************************************************************
Iteration  36  GMIN =      -947.581824497072
```

```
§60 deg, 0 to 5 bar

Temperature             333.15   K
Pressure                0.204         bar
Volume                  0.000E+00 m3 ( NPT )
Reaction enthalpy       3.520E+02 kJ
Reaction entropy        9.460E+02 J/K
Iterations              36        ( Limit =  100  )

                      INPUT AMOUNT EQUIL AMOUNT MOLE FRACT  ACTIVITY  ACTIVITY
PHASE 1:                    mol         mol               COEFFICI
H2O                     8.2713E+00  0.0000E+000  0.000E+00  1.00E+00  0.000E+00
H(+a)                   3.0000E-03  0.0000E+000  0.000E+00  1.00E+00  0.000E+00
OH(-a)                  1.0000E-03  0.0000E+000  0.000E+00  1.00E+00  0.000E+00
HSO3(-a)                1.0000E-03  0.0000E+000  0.000E+00  1.00E+00  0.000E+00
SO3(-2a)                5.0000E-04  0.0000E+000  0.000E+00  1.00E+00  0.000E+00
SO2(a)                  0.0000E+00  0.0000E+000  0.000E+00  1.00E+00  0.000E+00
O2(a)                   0.0000E+00  0.0000E+000  0.000E+00  1.00E+00  0.000E+00
Total :                 8.2768E+00  0.0000E+000

PHASE 2 :                                  MOLE FRACT
H2O(g)                  0.0000E+00  8.2738E+000  9.677E-01  1.00E+00  9.677E-01
O2(g)                   1.3938E-01  1.3938E-001  1.630E-02  1.00E+00  1.630E-02
SO2(g)                  1.3487E-01  1.3637E-001  1.595E-02  1.00E+00  1.595E-02
Total :                 2.7425E-01  8.5495E+000


************************************************************************
Iteration  13  GMIN =      -946.77930713362

§60 deg, 0 to 5 bar

Temperature             333.15   K
Pressure                0.306         bar
Volume                  6.952E-01 m3 ( NPT )
Reaction enthalpy       2.104E+01 kJ
Reaction entropy        5.669E+01 J/K
Iterations              13        ( Limit =  100  )

                      INPUT AMOUNT EQUIL AMOUNT MOLE FRACT  ACTIVITY  ACTIVITY
PHASE 1:                    mol         mol               COEFFICI
H2O                     8.2713E+00  7.7751E+000  9.991E-01  1.00E+00  9.991E-01
H(+a)                   3.0000E-03  1.7529E-003  2.252E-04  1.00E+00  2.252E-04
OH(-a)                  1.0000E-03  1.0616E-012  1.364E-13  1.00E+00  1.364E-13
HSO3(-a)                1.0000E-03  1.7529E-003  2.252E-04  1.00E+00  2.252E-04
SO3(-2a)                5.0000E-04  5.0312E-009  6.465E-10  1.00E+00  6.465E-10
SO2(a)                  0.0000E+00  3.5616E-003  4.577E-04  1.00E+00  4.577E-04
O2(a)                   0.0000E+00  8.1040E-006  1.041E-06  1.00E+00  1.041E-06
Total :                 8.2768E+00  7.7821E+000

PHASE 2 :                                  MOLE FRACT
H2O(g)                  0.0000E+00  4.9700E-001  6.476E-01  1.00E+00  6.476E-01
O2(g)                   1.3938E-01  1.3937E-001  1.816E-01  1.00E+00  1.816E-01
SO2(g)                  1.3487E-01  1.3105E-001  1.708E-01  1.00E+00  1.708E-01
Total :                 2.7425E-01  7.6742E-001


************************************************************************
Iteration  13  GMIN =      -946.600606196743

§60 deg, 0 to 5 bar
```



```
Pressure                0.612         bar
Volume                  3.648E-01 m3 ( NPT )
Reaction enthalpy       4.899E+00 kJ
Reaction entropy        1.268E+01 J/K
Iterations              12        ( Limit =  100  )

                      INPUT AMOUNT EQUIL AMOUNT MOLE FRACT  ACTIVITY  ACTIVITY
PHASE 1:                    mol         mol               COEFFICI
H2O                     8.2713E+00  8.1468E+000  9.975E-01  1.00E+00  9.975E-01
H(+a)                   3.0000E-03  3.5137E-003  4.302E-04  1.00E+00  4.302E-04
OH(-a)                  1.0000E-03  5.8242E-013  7.131E-14  1.00E+00  7.131E-14
HSO3(-a)                1.0000E-03  3.5137E-003  4.302E-04  1.00E+00  4.302E-04
SO3(-2a)                5.0000E-04  5.2803E-009  6.465E-10  1.00E+00  6.465E-10
SO2(a)                  0.0000E+00  1.3658E-002  1.672E-03  1.00E+00  1.672E-03
O2(a)                   0.0000E+00  3.4163E-005  4.183E-06  1.00E+00  4.183E-06
Total :                 8.2768E+00  8.1675E+000

PHASE 2 :                                  MOLE FRACT
H2O(g)                  0.0000E+00  1.2351E-001  3.233E-01  1.00E+00  3.233E-01
O2(g)                   1.3938E-01  1.3935E-001  3.647E-01  1.00E+00  3.647E-01
SO2(g)                  1.3487E-01  1.1919E-001  3.120E-01  1.00E+00  3.120E-01
```

```
Total :                 2.7425E-01  3.8205E-001


************************************************************************
Iteration  12  GMIN =      -946.365759145114

§60 deg, 0 to 5 bar

Temperature             333.15   K
Pressure                0.714         bar
Volume                  3.138E-01 m3 ( NPT )
Reaction enthalpy       3.731E+00 kJ
Reaction entropy        9.346E+00 J/K
Iterations              12        ( Limit =  100  )

                      INPUT AMOUNT EQUIL AMOUNT MOLE FRACT  ACTIVITY  ACTIVITY
PHASE 1:                    mol         mol               COEFFICI
H2O                     8.2713E+00  8.1722E+000  9.970E-01  1.00E+00  9.970E-01
H(+a)                   3.0000E-03  3.9041E-003  4.763E-04  1.00E+00  4.763E-04
OH(-a)                  1.0000E-03  5.2771E-013  6.438E-14  1.00E+00  6.438E-14
HSO3(-a)                1.0000E-03  3.9041E-003  4.763E-04  1.00E+00  4.763E-04
SO3(-2a)                5.0000E-04  5.2993E-009  6.465E-10  1.00E+00  6.465E-10
SO2(a)                  0.0000E+00  1.6810E-002  2.051E-03  1.00E+00  2.051E-03
O2(a)                   0.0000E+00  4.3330E-005  5.286E-06  1.00E+00  5.286E-06
Total :                 8.2768E+00  8.1969E+000

PHASE 2 :                                  MOLE FRACT
H2O(g)                  0.0000E+00  9.7677E-002  2.770E-01  1.00E+00  2.770E-01
O2(g)                   1.3938E-01  1.3934E-001  3.951E-01  1.00E+00  3.951E-01
SO2(g)                  1.3487E-01  1.1565E-001  3.279E-01  1.00E+00  3.279E-01
Total :                 2.7425E-01  3.5267E-001


************************************************************************
Iteration  12  GMIN =      -946.320086842726

§60 deg, 0 to 5 bar

Temperature             333.15   K
Pressure                0.816         bar
Volume                  2.753E-01 m3 ( NPT )
Reaction enthalpy       2.932E+00 kJ
Reaction entropy        7.018E+00 J/K
Iterations              12        ( Limit =  100  )

                      INPUT AMOUNT EQUIL AMOUNT MOLE FRACT  ACTIVITY  ACTIVITY
PHASE 1:                    mol         mol               COEFFICI
H2O                     8.2713E+00  8.1891E+000  9.965E-01  1.00E+00  9.965E-01
```

	INPUT AMOUNT	EQUIL AMOUNT	MOLE FRACT	ACTIVITY	ACTIVITY
PHASE 1:	mol	mol		COEFFICI	
H2O	8.2713E+00	8.1891E+000	9.965E-01	1.00E+00	9.965E-01
H(+a)	3.0000E-03	4.2477E-003	5.169E-04	1.00E+00	5.169E-04
OH(-a)	1.0000E-03	4.8725E-013	5.929E-14	1.00E+00	5.929E-14
HSO3(-a)	1.0000E-03	4.2477E-003	5.169E-04	1.00E+00	5.169E-04
SO3(-2a)	5.0000E-04	5.3127E-009	6.465E-10	1.00E+00	6.465E-10
SO2(a)	0.0000E+00	1.9857E-002	2.416E-03	1.00E+00	2.416E-03
O2(a)	0.0000E+00	5.2729E-005	6.417E-06	1.00E+00	6.417E-06
Total :	8.2768E+00	8.2175E+000			

PHASE 2 :		MOLE FRACT			
H2O(g)	0.0000E+00	8.0426E-002	2.422E-01	1.00E+00	2.422E-01
O2(g)	1.3938E-01	1.3933E-001	4.196E-01	1.00E+00	4.196E-01
SO2(g)	1.3487E-01	1.1226E-001	3.381E-01	1.00E+00	3.381E-01
Total :	2.7425E-01	3.3201E-001			

****

Iteration 12 GMIN = -946.281919706285

§60 deg, 0 to 5 bar

Temperature	333.15 K
Pressure	0.918 bar
Volume	2.452E-01 m3 (NPT)
Reaction enthalpy	2.345E+00 kJ
Reaction entropy	5.272E+00 J/K
Iterations	12 (Limit = 100)

	INPUT AMOUNT	EQUIL AMOUNT	MOLE FRACT	ACTIVITY	ACTIVITY
PHASE 1:	mol	mol		COEFFICI	
H2O	8.2713E+00	8.2011E+000	9.961E-01	1.00E+00	9.961E-01
H(+a)	3.0000E-03	4.5553E-003	5.533E-04	1.00E+00	5.533E-04
OH(-a)	1.0000E-03	4.5588E-013	5.537E-14	1.00E+00	5.537E-14
HSO3(-a)	1.0000E-03	4.5553E-003	5.533E-04	1.00E+00	5.533E-04
SO3(-2a)	5.0000E-04	5.3228E-009	6.465E-10	1.00E+00	6.465E-10
SO2(a)	0.0000E+00	2.2804E-002	2.770E-03	1.00E+00	2.770E-03
O2(a)	0.0000E+00	6.2355E-005	7.574E-06	1.00E+00	7.574E-06
Total :	8.2768E+00	8.2331E+000			

PHASE 2 :		MOLE FRACT			
H2O(g)	0.0000E+00	6.8105E-002	2.152E-01	1.00E+00	2.152E-01
O2(g)	1.3938E-01	1.3932E-001	4.403E-01	1.00E+00	4.403E-01
SO2(g)	1.3487E-01	1.0901E-001	3.445E-01	1.00E+00	3.445E-01
Total :	2.7425E-01	3.1643E-001			

****

Iteration 12 GMIN = -946.249243385007

§60 deg, 0 to 5 bar

Temperature	333.15 K
Pressure	1.02 bar
Volume	2.210E-01 m3 (NPT)
Reaction enthalpy	1.894E+00 kJ
Reaction entropy	3.895E+00 J/K
Iterations	12 (Limit = 100)

	INPUT AMOUNT	EQUIL AMOUNT	MOLE FRACT	ACTIVITY	ACTIVITY
PHASE 1:	mol	mol		COEFFICI	
H2O	8.2713E+00	8.2101E+000	9.957E-01	1.00E+00	9.957E-01
H(+a)	3.0000E-03	4.8339E-003	5.862E-04	1.00E+00	5.862E-04
OH(-a)	1.0000E-03	4.3072E-013	5.224E-14	1.00E+00	5.224E-14
HSO3(-a)	1.0000E-03	4.8339E-003	5.862E-04	1.00E+00	5.862E-04
SO3(-2a)	5.0000E-04	5.3307E-009	6.465E-10	1.00E+00	6.465E-10
SO2(a)	0.0000E+00	2.5650E-002	3.111E-03	1.00E+00	3.111E-03
O2(a)	0.0000E+00	7.2004E-005	8.757E-06	1.00E+00	8.757E-06

HSO3(-a)	1.0000E-03	4.8339E-003	5.862E-04	1.00E+00	5.862E-04
SO3(-2a)	5.0000E-04	5.3307E-009	6.465E-10	1.00E+00	6.465E-10
SO2(a)	0.0000E+00	2.5650E-002	3.111E-03	1.00E+00	3.111E-03
O2(a)	0.0000E+00	7.2204E-005	8.757E-06	1.00E+00	8.757E-06
Total :	8.2768E+00	8.2455E+000			

PHASE 2 :		MOLE FRACT			
H2O(g)	0.0000E+00	5.8875E-002	1.936E-01	1.00E+00	1.936E-01
O2(g)	1.3938E-01	1.3931E-001	4.582E-01	1.00E+00	4.582E-01
SO2(g)	1.3487E-01	1.0588E-001	3.482E-01	1.00E+00	3.482E-01
Total :	2.7425E-01	3.0406E-001			

****

Iteration 12 GMIN = -946.22075476658

§60 deg, 0 to 5 bar

Temperature	333.15 K
Pressure	1.122 bar
Volume	2.011E-01 m3 (NPT)
Reaction enthalpy	1.533E+00 kJ
Reaction entropy	2.769E+00 J/K
Iterations	12 (Limit = 100)

	INPUT AMOUNT	EQUIL AMOUNT	MOLE FRACT	ACTIVITY	ACTIVITY
PHASE 1:	mol	mol		COEFFICI	
H2O	8.2713E+00	8.2170E+000	9.953E-01	1.00E+00	9.953E-01
H(+a)	3.0000E-03	5.0885E-003	6.164E-04	1.00E+00	6.164E-04
OH(-a)	1.0000E-03	4.1002E-013	4.967E-14	1.00E+00	4.967E-14
HSO3(-a)	1.0000E-03	5.0885E-003	6.164E-04	1.00E+00	6.164E-04
SO3(-2a)	5.0000E-04	5.3373E-009	6.465E-10	1.00E+00	6.465E-10
SO2(a)	0.0000E+00	2.8399E-002	3.440E-03	1.00E+00	3.440E-03
O2(a)	0.0000E+00	8.2270E-005	9.965E-06	1.00E+00	9.965E-06
Total :	8.2768E+00	8.2557E+000			

PHASE 2 :		MOLE FRACT			
H2O(g)	0.0000E+00	5.1711E-002	1.760E-01	1.00E+00	1.760E-01
O2(g)	1.3938E-01	1.3930E-001	4.740E-01	1.00E+00	4.740E-01
SO2(g)	1.3487E-01	1.0288E-001	3.501E-01	1.00E+00	3.501E-01
Total :	2.7425E-01	2.9389E-001			

****

Iteration 12 GMIN = -946.195562311129

§60 deg, 0 to 5 bar

Temperature	333.15 K
Pressure	1.224 bar
Volume	1.846E-01 m3 (NPT)
Reaction enthalpy	1.236E+00 kJ
Reaction entropy	1.822E+00 J/K
Iterations	12 (Limit = 100)

	INPUT AMOUNT	EQUIL AMOUNT	MOLE FRACT	ACTIVITY	ACTIVITY
PHASE 1:	mol	mol		COEFFICI	
H2O	8.2713E+00	8.2225E+000	9.949E-01	1.00E+00	9.949E-01
H(+a)	3.0000E-03	5.3227E-003	6.441E-04	1.00E+00	6.441E-04
OH(-a)	1.0000E-03	3.9265E-013	4.751E-14	1.00E+00	4.751E-14
HSO3(-a)	1.0000E-03	5.3227E-003	6.441E-04	1.00E+00	6.441E-04
SO3(-2a)	5.0000E-04	5.3429E-009	6.465E-10	1.00E+00	6.465E-10
SO2(a)	0.0000E+00	3.1053E-002	3.757E-03	1.00E+00	3.757E-03
O2(a)	0.0000E+00	9.2549E-005	1.120E-05	1.00E+00	1.120E-05
Total :	8.2768E+00	8.2643E+000			

PHASE 2 :		MOLE FRACT			
H2O(g)	0.0000E+00	4.5995E-002	1.612E-01	1.00E+00	1.612E-01
O2(g)	1.3938E-01	1.3929E-001	4.883E-01	1.00E+00	4.883E-01

PHASE 2 :		MOLE FRACT			
H2O(g)	0.0000E+00	4.5995E-002	1.612E-01	1.00E+00	1.612E-01
O2(g)	1.3938E-01	1.3929E-001	4.883E-01	1.00E+00	4.883E-01
SO2(g)	1.3487E-01	9.9989E-002	3.505E-01	1.00E+00	3.505E-01
Total :	2.7425E-01	2.8527E-001			

****

Iteration 12 GMIN = -946.172819846493

§60 deg, 0 to 5 bar

Temperature	333.15 K
Pressure	1.327 bar
Volume	1.704E-01 m3 (NPT)
Reaction enthalpy	9.835E-01 kJ
Reaction entropy	1.001E+00 J/K
Iterations	12 (Limit = 100)

	INPUT AMOUNT	EQUIL AMOUNT	MOLE FRACT	ACTIVITY	ACTIVITY
PHASE 1:	mol	mol		COEFFICI	
H2O	8.2713E+00	8.2270E+000	9.946E-01	1.00E+00	9.946E-01
H(+a)	3.0000E-03	5.5413E-003	6.699E-04	1.00E+00	6.699E-04
OH(-a)	1.0000E-03	3.7771E-013	4.566E-14	1.00E+00	4.566E-14
HSO3(-a)	1.0000E-03	5.5413E-003	6.699E-04	1.00E+00	6.699E-04
SO3(-2a)	5.0000E-04	5.3478E-009	6.465E-10	1.00E+00	6.465E-10
SO2(a)	0.0000E+00	3.3638E-002	4.067E-03	1.00E+00	4.067E-03
O2(a)	0.0000E+00	1.0314E-004	1.247E-05	1.00E+00	1.247E-05
Total :	8.2768E+00	8.2718E+000			

PHASE 2 :		MOLE FRACT			
H2O(g)	0.0000E+00	4.1292E-002	1.487E-01	1.00E+00	1.487E-01
O2(g)	1.3938E-01	1.3928E-001	5.014E-01	1.00E+00	5.014E-01
SO2(g)	1.3487E-01	9.7186E-002	3.499E-01	1.00E+00	3.499E-01
Total :	2.7425E-01	2.7775E-001			

****

Iteration 12 GMIN = -946.152495180145

§60 deg, 0 to 5 bar

Temperature	333.15 K
Pressure	1.429 bar
Volume	1.584E-01 m3 (NPT)
Reaction enthalpy	7.698E-01 kJ
Reaction entropy	2.905E-01 J/K
Iterations	12 (Limit = 100)

	INPUT AMOUNT	EQUIL AMOUNT	MOLE FRACT	ACTIVITY	ACTIVITY
PHASE 1:	mol	mol		COEFFICI	
H2O	8.2713E+00	8.2306E+000	9.942E-01	1.00E+00	9.942E-01
H(+a)	3.0000E-03	5.7424E-003	6.937E-04	1.00E+00	6.937E-04
OH(-a)	1.0000E-03	3.6494E-013	4.408E-14	1.00E+00	4.408E-14
HSO3(-a)	1.0000E-03	5.7424E-003	6.937E-04	1.00E+00	6.937E-04
SO3(-2a)	5.0000E-04	5.3520E-009	6.465E-10	1.00E+00	6.465E-10
SO2(a)	0.0000E+00	3.6107E-002	4.362E-03	1.00E+00	4.362E-03
O2(a)	0.0000E+00	1.1383E-004	1.375E-05	1.00E+00	1.375E-05
Total :	8.2768E+00	8.2783E+000			

PHASE 2 :		MOLE FRACT			
H2O(g)	0.0000E+00	3.7428E-002	1.380E-01	1.00E+00	1.380E-01
O2(g)	1.3938E-01	1.3927E-001	5.135E-01	1.00E+00	5.135E-01
SO2(g)	1.3487E-01	9.4516E-002	3.485E-01	1.00E+00	3.485E-01
Total :	2.7425E-01	2.7121E-001			

****

Iteration 12 GMIN = -946.13399878298

****

Iteration 12 GMIN = -946.13399878298

§60 deg, 0 to 5 bar

Temperature	333.15 K
Pressure	1.531 bar
Volume	1.479E-01 m3 (NPT)
Reaction enthalpy	5.841E-01 kJ
Reaction entropy	-3.396E-01 J/K
Iterations	12 (Limit = 100)

	INPUT AMOUNT	EQUIL AMOUNT	MOLE FRACT	ACTIVITY	ACTIVITY
PHASE 1:	mol	mol		COEFFICI	
H2O	8.2713E+00	8.2337E+000	9.939E-01	1.00E+00	9.939E-01
H(+a)	3.0000E-03	5.9298E-003	7.158E-04	1.00E+00	7.158E-04
OH(-a)	1.0000E-03	3.5378E-013	4.271E-14	1.00E+00	4.271E-14
HSO3(-a)	1.0000E-03	5.9298E-003	7.158E-04	1.00E+00	7.158E-04
SO3(-2a)	5.0000E-04	5.3558E-009	6.465E-10	1.00E+00	6.465E-10
SO2(a)	0.0000E+00	3.8488E-002	4.646E-03	1.00E+00	4.646E-03
O2(a)	0.0000E+00	1.2471E-004	1.505E-05	1.00E+00	1.505E-05
Total :	8.2768E+00	8.2842E+000			

PHASE 2 :		MOLE FRACT			
H2O(g)	0.0000E+00	3.4172E-002	1.288E-01	1.00E+00	1.288E-01
O2(g)	1.3938E-01	1.3926E-001	5.248E-01	1.00E+00	5.248E-01
SO2(g)	1.3487E-01	9.1947E-002	3.465E-01	1.00E+00	3.465E-01
Total :	2.7425E-01	2.6537E-001			

****

Iteration 12 GMIN = -946.117053383697

§60 deg, 0 to 5 bar

Temperature	333.15 K
Pressure	1.633 bar
Volume	1.388E-01 m3 (NPT)
Reaction enthalpy	4.206E-01 kJ
Reaction entropy	-9.045E-01 J/K
Iterations	12 (Limit = 100)

	INPUT AMOUNT	EQUIL AMOUNT	MOLE FRACT	ACTIVITY	ACTIVITY
PHASE 1:	mol	mol		COEFFICI	
H2O	8.2713E+00	8.2363E+000	9.936E-01	1.00E+00	9.936E-01
H(+a)	3.0000E-03	6.1050E-003	7.365E-04	1.00E+00	7.365E-04
OH(-a)	1.0000E-03	3.4396E-013	4.149E-14	1.00E+00	4.149E-14
HSO3(-a)	1.0000E-03	6.1050E-003	7.365E-04	1.00E+00	7.365E-04
SO3(-2a)	5.0000E-04	5.3592E-009	6.465E-10	1.00E+00	6.465E-10
SO2(a)	0.0000E+00	4.0783E-002	4.920E-03	1.00E+00	4.920E-03
O2(a)	0.0000E+00	1.3579E-004	1.638E-05	1.00E+00	1.638E-05
Total :	8.2768E+00	8.2894E+000			

PHASE 2 :		MOLE FRACT			
H2O(g)	0.0000E+00	3.1392E-002	1.207E-01	1.00E+00	1.207E-01
O2(g)	1.3938E-01	1.3924E-001	5.353E-01	1.00E+00	5.353E-01
SO2(g)	1.3487E-01	8.9477E-002	3.440E-01	1.00E+00	3.440E-01
Total :	2.7425E-01	2.6011E-001			

****

Iteration 12 GMIN = -946.101439183434

§60 deg, 0 to 5 bar

Temperature	333.15 K
Pressure	1.735 bar

```
Temperature             333.15   K
Pressure                1.735         bar
Volume                  1.307E-01 m3 ( NPT )
Reaction enthalpy      2.752E-01 kJ
Reaction entropy        -1.416E+00 J/K
Iterations              12        ( Limit =  100  )

                      INPUT AMOUNT EQUIL AMOUNT MOLE FRACT  ACTIVITY  ACTIVITY
PHASE 1:                    mol         mol              COEFFICI
H2O                      8.2713E+00  8.2385E+000  9.933E-01  1.00E+00  9.933E-01
H(+a)                    3.0000E-03  6.2692E-003  7.559E-04  1.00E+00  7.559E-04
OH(-a)                   1.0000E-03  3.3523E-013  4.042E-14  1.00E+00  4.042E-14
HSO3(-a)                 1.0000E-03  6.2692E-003  7.559E-04  1.00E+00  7.559E-04
SO3(-2a)                 5.0000E-04  5.3623E-009  6.465E-10  1.00E+00  6.465E-10
SO2(a)                   0.0000E+00  4.2995E-002  5.184E-03  1.00E+00  5.184E-03
O2(a)                    0.0000E+00  1.4705E-004  1.773E-05  1.00E+00  1.773E-05
Total :                  8.2768E+00  8.2942E+000

PHASE 2 :                                MOLE FRACT
H2O(g)                   0.0000E+00  2.8994E-002  1.136E-01  1.00E+00  1.136E-01
O2(g)                    1.3938E-01  1.3923E-001  5.453E-01  1.00E+00  5.453E-01
SO2(g)                   1.3487E-01  8.7101E-002  3.411E-01  1.00E+00  3.411E-01
Total :                  2.7425E-01  2.5533E-001


*****************************************************************************
Iteration  12  GMIN =      -946.086979047128

§60 deg, 0 to 5 bar

Temperature             333.15   K
Pressure                1.837         bar
Volume                  1.235E-01 m3 ( NPT )
Reaction enthalpy      1.448E-01 kJ
Reaction entropy        -1.882E+00 J/K
Iterations              12        ( Limit =  100  )

                      INPUT AMOUNT EQUIL AMOUNT MOLE FRACT  ACTIVITY  ACTIVITY
PHASE 1:                    mol         mol              COEFFICI
H2O                      8.2713E+00  8.2405E+000  9.930E-01  1.00E+00  9.930E-01
H(+a)                    3.0000E-03  6.4235E-003  7.740E-04  1.00E+00  7.740E-04
OH(-a)                   1.0000E-03  3.2743E-013  3.946E-14  1.00E+00  3.946E-14
HSO3(-a)                 1.0000E-03  6.4235E-003  7.740E-04  1.00E+00  7.740E-04
SO3(-2a)                 5.0000E-04  5.3651E-009  6.465E-10  1.00E+00  6.465E-10
SO2(a)                   0.0000E+00  4.5127E-002  5.438E-03  1.00E+00  5.438E-03
O2(a)                    0.0000E+00  1.5848E-004  1.910E-05  1.00E+00  1.910E-05
Total :                  8.2768E+00  8.2986E+000

PHASE 2 :                                MOLE FRACT
H2O(g)                   0.0000E+00  2.6906E-002  1.072E-01  1.00E+00  1.072E-01
O2(g)                    1.3938E-01  1.3922E-001  5.548E-01  1.00E+00  5.548E-01
SO2(g)                   1.3487E-01  8.4815E-002  3.380E-01  1.00E+00  3.380E-01
```



```
Total :                  2.7425E-01  2.5094E-001


*****************************************************************************
Iteration  12  GMIN =      -946.073528176035

§60 deg, 0 to 5 bar

Temperature             333.15   K
Pressure                1.939         bar
Volume                  1.171E-01 m3 ( NPT )
Reaction enthalpy      2.686E-02 kJ
Reaction entropy        -2.310E+00 J/K
Iterations              12        ( Limit =  100  )

                      INPUT AMOUNT EQUIL AMOUNT MOLE FRACT  ACTIVITY  ACTIVITY
```



```
Reaction entropy        -2.310E+00 J/K
Iterations              12        ( Limit =  100  )

                      INPUT AMOUNT EQUIL AMOUNT MOLE FRACT  ACTIVITY  ACTIVITY
PHASE 1:                    mol         mol              COEFFICI
H2O                      8.2713E+00  8.2422E+000  9.927E-01  1.00E+00  9.927E-01
H(+a)                    3.0000E-03  6.5687E-003  7.912E-04  1.00E+00  7.912E-04
OH(-a)                   1.0000E-03  3.2041E-013  3.859E-14  1.00E+00  3.859E-14
HSO3(-a)                 1.0000E-03  6.5687E-003  7.912E-04  1.00E+00  7.912E-04
SO3(-2a)                 5.0000E-04  5.3677E-009  6.465E-10  1.00E+00  6.465E-10
SO2(a)                   0.0000E+00  4.7180E-002  5.683E-03  1.00E+00  5.683E-03
O2(a)                    0.0000E+00  1.7009E-004  2.049E-05  1.00E+00  2.049E-05
Total :                  8.2768E+00  8.3026E+000

PHASE 2 :                                MOLE FRACT
H2O(g)                   0.0000E+00  2.5073E-002  1.016E-01  1.00E+00  1.016E-01
O2(g)                    1.3938E-01  1.3921E-001  5.638E-01  1.00E+00  5.638E-01
SO2(g)                   1.3487E-01  8.2616E-002  3.346E-01  1.00E+00  3.346E-01
Total :                  2.7425E-01  2.4690E-001


*****************************************************************************
Iteration  12  GMIN =      -946.060966726339

§60 deg, 0 to 5 bar

Temperature             333.15   K
Pressure                2.041         bar
Volume                  1.113E-01 m3 ( NPT )
Reaction enthalpy      -8.042E-02 kJ
Reaction entropy        -2.705E+00 J/K
Iterations              12        ( Limit =  100  )

                      INPUT AMOUNT EQUIL AMOUNT MOLE FRACT  ACTIVITY  ACTIVITY
PHASE 1:                    mol         mol              COEFFICI
H2O                      8.2713E+00  8.2436E+000  9.924E-01  1.00E+00  9.924E-01
H(+a)                    3.0000E-03  6.7056E-003  8.073E-04  1.00E+00  8.073E-04
OH(-a)                   1.0000E-03  3.1407E-013  3.781E-14  1.00E+00  3.781E-14
HSO3(-a)                 1.0000E-03  6.7056E-003  8.073E-04  1.00E+00  8.073E-04
SO3(-2a)                 5.0000E-04  5.3701E-009  6.465E-10  1.00E+00  6.465E-10
SO2(a)                   0.0000E+00  4.9159E-002  5.918E-03  1.00E+00  5.918E-03
O2(a)                    0.0000E+00  1.8186E-004  2.189E-05  1.00E+00  2.189E-05
Total :                  8.2768E+00  8.3064E+000

PHASE 2 :                                MOLE FRACT
H2O(g)                   0.0000E+00  2.3452E-002  9.645E-02  1.00E+00  9.645E-02
O2(g)                    1.3938E-01  1.3920E-001  5.725E-01  1.00E+00  5.725E-01
SO2(g)                   1.3487E-01  8.0501E-002  3.311E-01  1.00E+00  3.311E-01
Total :                  2.7425E-01  2.4315E-001


*****************************************************************************
Iteration  12  GMIN =      -946.049194420007

§60 deg, 0 to 5 bar

Temperature             333.15   K
Pressure                2.143         bar
Volume                  1.060E-01 m3 ( NPT )
Reaction enthalpy      -1.786E-01 kJ
```



```
Reaction entropy        -3.071E+00 J/K
Iterations              12        ( Limit =  100  )

                      INPUT AMOUNT EQUIL AMOUNT MOLE FRACT  ACTIVITY  ACTIVITY
PHASE 1:                    mol         mol              COEFFICI
H2O                      8.2713E+00  8.2450E+000  9.922E-01  1.00E+00  9.922E-01
H(+a)                    3.0000E-03  6.8349E-003  8.225E-04  1.00E+00  8.225E-04
OH(-a)                   1.0000E-03  3.0831E-013  3.710E-14  1.00E+00  3.710E-14
HSO3(-a)                 1.0000E-03  6.8349E-003  8.225E-04  1.00E+00  8.225E-04
SO3(-2a)                 5.0000E-04  5.3724E-009  6.465E-10  1.00E+00  6.465E-10
SO2(a)                   0.0000E+00  5.1065E-002  6.145E-03  1.00E+00  6.145E-03
O2(a)                    0.0000E+00  1.9380E-004  2.332E-05  1.00E+00  2.332E-05
Total :                  8.2768E+00  8.3099E+000

PHASE 2 :                                MOLE FRACT
H2O(g)                   0.0000E+00  2.2009E-002  9.183E-02  1.00E+00  9.183E-02
O2(g)                    1.3938E-01  1.3919E-001  5.808E-01  1.00E+00  5.808E-01
SO2(g)                   1.3487E-01  7.8466E-002  3.274E-01  1.00E+00  3.274E-01
Total :                  2.7425E-01  2.3966E-001


*****************************************************************************
Iteration  12  GMIN =      -946.038126534489

§60 deg, 0 to 5 bar

Temperature             333.15   K
Pressure                2.245         bar
Volume                  1.012E-01 m3 ( NPT )
Reaction enthalpy      -2.688E-01 kJ
Reaction entropy        -3.412E+00 J/K
Iterations              12        ( Limit =  100  )

                      INPUT AMOUNT EQUIL AMOUNT MOLE FRACT  ACTIVITY  ACTIVITY
PHASE 1:                    mol         mol              COEFFICI
H2O                      8.2713E+00  8.2461E+000  9.919E-01  1.00E+00  9.919E-01
H(+a)                    3.0000E-03  6.9572E-003  8.369E-04  1.00E+00  8.369E-04
OH(-a)                   1.0000E-03  3.0305E-013  3.645E-14  1.00E+00  3.645E-14
HSO3(-a)                 1.0000E-03  6.9572E-003  8.369E-04  1.00E+00  8.369E-04
SO3(-2a)                 5.0000E-04  5.3745E-009  6.465E-10  1.00E+00  6.465E-10
SO2(a)                   0.0000E+00  5.2900E-002  6.363E-03  1.00E+00  6.363E-03
O2(a)                    0.0000E+00  2.0589E-004  2.477E-05  1.00E+00  2.477E-05
Total :                  8.2768E+00  8.3131E+000

PHASE 2 :                                MOLE FRACT
H2O(g)                   0.0000E+00  2.0718E-002  8.764E-02  1.00E+00  8.764E-02
O2(g)                    1.3938E-01  1.3917E-001  5.887E-01  1.00E+00  5.887E-01
SO2(g)                   1.3487E-01  7.6507E-002  3.236E-01  1.00E+00  3.236E-01
Total :                  2.7425E-01  2.3640E-001


*****************************************************************************
Iteration  12  GMIN =      -946.027690869883

§60 deg, 0 to 5 bar

Temperature             333.15   K
Pressure                2.347         bar
Volume                  9.686E-02 m3 ( NPT )
Reaction enthalpy      -3.522E-01 kJ
Reaction entropy        -3.731E+00 J/K
Iterations              12        ( Limit =  100  )

                      INPUT AMOUNT EQUIL AMOUNT MOLE FRACT  ACTIVITY  ACTIVITY
PHASE 1:                    mol         mol              COEFFICI
H2O                      8.2713E+00  8.2472E+000  9.917E-01  1.00E+00  9.917E-01
H(+a)                    3.0000E-03  7.0730E-003  8.505E-04  1.00E+00  8.505E-04
OH(-a)                   1.0000E-03  2.9824E-013  3.586E-14  1.00E+00  3.586E-14
HSO3(-a)                 1.0000E-03  7.0729E-003  8.505E-04  1.00E+00  8.505E-04
SO3(-2a)                 5.0000E-04  5.3765E-009  6.465E-10  1.00E+00  6.465E-10
SO2(a)                   0.0000E+00  5.4669E-002  6.574E-03  1.00E+00  6.574E-03
O2(a)                    0.0000E+00  2.1812E-004  2.623E-05  1.00E+00  2.623E-05

Total :                  8.2768E+00  8.3162E+000

PHASE 2 :                                MOLE FRACT
```



```
Total :                  8.2768E+00  8.3162E+000

PHASE 2 :                                MOLE FRACT
H2O(g)                   0.0000E+00  1.9557E-002  8.381E-02  1.00E+00  8.381E-02
O2(g)                    1.3938E-01  1.3916E-001  5.964E-01  1.00E+00  5.964E-01
SO2(g)                   1.3487E-01  7.4623E-002  3.198E-01  1.00E+00  3.198E-01
Total :                  2.7425E-01  2.3334E-001


*****************************************************************************
Iteration  12  GMIN =      -946.017825419089

§60 deg, 0 to 5 bar

Temperature             333.15   K
Pressure                2.449         bar
Volume                  9.286E-02 m3 ( NPT )
Reaction enthalpy      -4.295E-01 kJ
Reaction entropy        -4.029E+00 J/K
Iterations              12        ( Limit =  100  )

                      INPUT AMOUNT EQUIL AMOUNT MOLE FRACT  ACTIVITY  ACTIVITY
PHASE 1:                    mol         mol              COEFFICI
H2O                      8.2713E+00  8.2481E+000  9.915E-01  1.00E+00  9.915E-01
H(+a)                    3.0000E-03  7.1827E-003  8.634E-04  1.00E+00  8.634E-04
OH(-a)                   1.0000E-03  2.9381E-013  3.532E-14  1.00E+00  3.532E-14
HSO3(-a)                 1.0000E-03  7.1827E-003  8.634E-04  1.00E+00  8.634E-04
SO3(-2a)                 5.0000E-04  5.3783E-009  6.465E-10  1.00E+00  6.465E-10
SO2(a)                   0.0000E+00  5.6372E-002  6.776E-03  1.00E+00  6.776E-03
O2(a)                    0.0000E+00  2.3050E-004  2.771E-05  1.00E+00  2.771E-05
Total :                  8.2768E+00  8.3191E+000

PHASE 2 :                                MOLE FRACT
H2O(g)                   0.0000E+00  1.8507E-002  8.030E-02  1.00E+00  8.030E-02
O2(g)                    1.3938E-01  1.3915E-001  6.038E-01  1.00E+00  6.038E-01
SO2(g)                   1.3487E-01  7.2810E-002  3.159E-01  1.00E+00  3.159E-01
Total :                  2.7425E-01  2.3047E-001


*****************************************************************************
Iteration  12  GMIN =      -946.00847655558

§60 deg, 0 to 5 bar

Temperature             333.15   K
Pressure                2.551         bar
Volume                  8.918E-02 m3 ( NPT )
Reaction enthalpy      -5.013E-01 kJ
Reaction entropy        -4.310E+00 J/K
Iterations              12        ( Limit =  100  )

                      INPUT AMOUNT EQUIL AMOUNT MOLE FRACT  ACTIVITY  ACTIVITY
PHASE 1:                    mol         mol              COEFFICI
H2O                      8.2713E+00  8.2490E+000  9.912E-01  1.00E+00  9.912E-01
H(+a)                    3.0000E-03  7.2869E-003  8.756E-04  1.00E+00  8.756E-04
OH(-a)                   1.0000E-03  2.8974E-013  3.482E-14  1.00E+00  3.482E-14
HSO3(-a)                 1.0000E-03  7.2869E-003  8.756E-04  1.00E+00  8.756E-04
SO3(-2a)                 5.0000E-04  5.3801E-009  6.465E-10  1.00E+00  6.465E-10
SO2(a)                   0.0000E+00  5.8014E-002  6.971E-03  1.00E+00  6.971E-03
O2(a)                    0.0000E+00  2.4302E-004  2.920E-05  1.00E+00  2.920E-05
Total :                  8.2768E+00  8.3218E+000

PHASE 2 :                                MOLE FRACT
H2O(g)                   0.0000E+00  1.7554E-002  7.707E-02  1.00E+00  7.707E-02
O2(g)                    1.3938E-01  1.3914E-001  6.109E-01  1.00E+00  6.109E-01
SO2(g)                   1.3487E-01  7.1064E-002  3.120E-01  1.00E+00  3.120E-01
Total :                  2.7425E-01  2.2776E-001


*****************************************************************************
Iteration  12  GMIN =      -945.999597605388
```

```
§60 deg, 0 to 5 bar

Temperature            333.15   K
Pressure               2.653          bar
Volume                 8.577E-02 m3 ( NPT )
Reaction enthalpy     -5.684E-01 kJ
Reaction entropy      -4.575E+00 J/K
Iterations             12        ( Limit =  100  )

                      INPUT AMOUNT EQUIL AMOUNT MOLE FRACT  ACTIVITY  ACTIVITY
PHASE 1:                   mol          mol              COEFFICI
H2O                      8.2713E+00  8.2497E+000  9.910E-01  1.00E+00  9.910E-01
H(+a)                    3.0000E-03  7.3859E-003  8.873E-04  1.00E+00  8.873E-04
OH(-a)                   1.0000E-03  2.8597E-013  3.435E-14  1.00E+00  3.435E-14
HSO3(-a)                 1.0000E-03  7.3859E-003  8.873E-04  1.00E+00  8.873E-04
SO3(-2a)                 5.0000E-04  5.3817E-009  6.465E-10  1.00E+00  6.465E-10
SO2(a)                   0.0000E+00  5.9595E-002  7.159E-03  1.00E+00  7.159E-03
O2(a)                    0.0000E+00  2.5566E-004  3.071E-05  1.00E+00  3.071E-05
Total :                8.2768E+00  8.3244E+000

PHASE 2 :                                     MOLE FRACT
H2O(g)                   0.0000E+00  1.6686E-002  7.410E-02  1.00E+00  7.410E-02
O2(g)                    1.3938E-01  1.3912E-001  6.178E-01  1.00E+00  6.178E-01
SO2(g)                   1.3487E-01  6.9384E-002  3.081E-01  1.00E+00  3.081E-01
Total :                2.7425E-01  2.2519E-001


******************************************************************************
Iteration  12  GMIN =      -945.991147710912

§60 deg, 0 to 5 bar

Temperature            333.15   K
Pressure               2.755          bar
Volume                 8.262E-02 m3 ( NPT )
Reaction enthalpy     -6.312E-01 kJ
Reaction entropy      -4.824E+00 J/K
Iterations             12        ( Limit =  100  )

                      INPUT AMOUNT EQUIL AMOUNT MOLE FRACT  ACTIVITY  ACTIVITY
PHASE 1:                   mol          mol              COEFFICI
H2O                      8.2713E+00  8.2504E+000  9.908E-01  1.00E+00  9.908E-01
H(+a)                    3.0000E-03  7.4800E-003  8.983E-04  1.00E+00  8.983E-04
OH(-a)                   1.0000E-03  2.8247E-013  3.392E-14  1.00E+00  3.392E-14
HSO3(-a)                 1.0000E-03  7.4800E-003  8.983E-04  1.00E+00  8.983E-04
SO3(-2a)                 5.0000E-04  5.3833E-009  6.465E-10  1.00E+00  6.465E-10
SO2(a)                   0.0000E+00  6.1119E-002  7.340E-03  1.00E+00  7.340E-03
O2(a)                    0.0000E+00  2.6844E-004  3.224E-05  1.00E+00  3.224E-05
Total :                8.2768E+00  8.3268E+000

PHASE 2 :                                     MOLE FRACT
H2O(g)                   0.0000E+00  1.5892E-002  7.134E-02  1.00E+00  7.134E-02
O2(g)                    1.3938E-01  1.3911E-001  6.245E-01  1.00E+00  6.245E-01
SO2(g)                   1.3487E-01  6.7766E-002  3.042E-01  1.00E+00  3.042E-01
Total :                2.7425E-01  2.2277E-001


******************************************************************************
Iteration  12  GMIN =      -945.983090915618

§60 deg, 0 to 5 bar

Temperature            333.15   K
Pressure               2.857          bar
Volume                 7.969E-02 m3 ( NPT )
Reaction enthalpy     -6.900E-01 kJ
Reaction entropy      -5.061E+00 J/K
Iterations             12        ( Limit =  100  )
```



```
Reaction entropy      -5.061E+00 J/K
Iterations             12        ( Limit =  100  )

                      INPUT AMOUNT EQUIL AMOUNT MOLE FRACT  ACTIVITY  ACTIVITY
PHASE 1:                   mol          mol              COEFFICI
H2O                      8.2713E+00  8.2511E+000  9.906E-01  1.00E+00  9.906E-01

H(+a)                    3.0000E-03  7.5697E-003  9.088E-04  1.00E+00  9.088E-04
OH(-a)                   1.0000E-03  2.7923E-013  3.352E-14  1.00E+00  3.352E-14
HSO3(-a)                 1.0000E-03  7.5697E-003  9.088E-04  1.00E+00  9.088E-04
SO3(-2a)                 5.0000E-04  5.3848E-009  6.465E-10  1.00E+00  6.465E-10
SO2(a)                   0.0000E+00  6.2588E-002  7.514E-03  1.00E+00  7.514E-03
O2(a)                    0.0000E+00  2.8133E-004  3.378E-05  1.00E+00  3.378E-05
Total :                8.2768E+00  8.3291E+000

PHASE 2 :                                     MOLE FRACT
H2O(g)                   0.0000E+00  1.5163E-002  6.878E-02  1.00E+00  6.878E-02
O2(g)                    1.3938E-01  1.3910E-001  6.309E-01  1.00E+00  6.309E-01
SO2(g)                   1.3487E-01  6.6208E-002  3.003E-01  1.00E+00  3.003E-01
Total :                2.7425E-01  2.2047E-001


******************************************************************************
Iteration  12  GMIN =      -945.975395423059

§60 deg, 0 to 5 bar

Temperature            333.15   K
Pressure               2.959          bar
Volume                 7.697E-02 m3 ( NPT )
Reaction enthalpy     -7.454E-01 kJ
Reaction entropy      -5.284E+00 J/K
Iterations             12        ( Limit =  100  )

                      INPUT AMOUNT EQUIL AMOUNT MOLE FRACT  ACTIVITY  ACTIVITY
PHASE 1:                   mol          mol              COEFFICI
H2O                      8.2713E+00  8.2517E+000  9.904E-01  1.00E+00  9.904E-01
H(+a)                    3.0000E-03  7.6551E-003  9.188E-04  1.00E+00  9.188E-04
OH(-a)                   1.0000E-03  2.7621E-013  3.315E-14  1.00E+00  3.315E-14
HSO3(-a)                 1.0000E-03  7.6551E-003  9.188E-04  1.00E+00  9.188E-04
SO3(-2a)                 5.0000E-04  5.3862E-009  6.465E-10  1.00E+00  6.465E-10
SO2(a)                   0.0000E+00  6.4003E-002  7.682E-03  1.00E+00  7.682E-03
O2(a)                    0.0000E+00  2.9434E-004  3.533E-05  1.00E+00  3.533E-05
Total :                8.2768E+00  8.3313E+000

PHASE 2 :                                     MOLE FRACT
H2O(g)                   0.0000E+00  1.4493E-002  6.639E-02  1.00E+00  6.639E-02
O2(g)                    1.3938E-01  1.3909E-001  6.372E-01  1.00E+00  6.372E-01
SO2(g)                   1.3487E-01  6.4707E-002  2.964E-01  1.00E+00  2.964E-01
Total :                2.7425E-01  2.1829E-001


******************************************************************************
Iteration  13  GMIN =      -945.968032988573

§60 deg, 0 to 5 bar

Temperature            333.15   K
Pressure               3.061          bar
Volume                 7.442E-02 m3 ( NPT )
Reaction enthalpy     -7.975E-01 kJ
Reaction entropy      -5.497E+00 J/K
Iterations             13        ( Limit =  100  )

                      INPUT AMOUNT EQUIL AMOUNT MOLE FRACT  ACTIVITY  ACTIVITY
PHASE 1:                   mol          mol              COEFFICI
H2O                      8.2713E+00  8.2522E+000  9.903E-01  1.00E+00  9.903E-01
H(+a)                    3.0000E-03  7.7365E-003  9.284E-04  1.00E+00  9.284E-04
OH(-a)                   1.0000E-03  2.7338E-013  3.281E-14  1.00E+00  3.281E-14
HSO3(-a)                 1.0000E-03  7.7365E-003  9.284E-04  1.00E+00  9.284E-04
```



```
H2O                      8.2713E+00  8.2522E+000  9.903E-01  1.00E+00  9.903E-01
H(+a)                    3.0000E-03  7.7365E-003  9.284E-04  1.00E+00  9.284E-04
OH(-a)                   1.0000E-03  2.7338E-013  3.281E-14  1.00E+00  3.281E-14
HSO3(-a)                 1.0000E-03  7.7365E-003  9.284E-04  1.00E+00  9.284E-04
SO3(-2a)                 5.0000E-04  5.3875E-009  6.465E-10  1.00E+00  6.465E-10
SO2(a)                   0.0000E+00  6.5368E-002  7.844E-03  1.00E+00  7.844E-03
O2(a)                    0.0000E+00  3.0746E-004  3.690E-05  1.00E+00  3.690E-05
Total :                8.2768E+00  8.3333E+000

PHASE 2 :                                     MOLE FRACT
H2O(g)                   0.0000E+00  1.3874E-002  6.417E-02  1.00E+00  6.417E-02
O2(g)                    1.3938E-01  1.3907E-001  6.432E-01  1.00E+00  6.432E-01
SO2(g)                   1.3487E-01  6.3260E-002  2.926E-01  1.00E+00  2.926E-01

Total :                2.7425E-01  2.1621E-001


******************************************************************************
Iteration  14  GMIN =      -945.960978418851

§60 deg, 0 to 5 bar

Temperature            333.15   K
Pressure               3.163          bar
Volume                 7.204E-02 m3 ( NPT )
Reaction enthalpy     -8.467E-01 kJ
Reaction entropy      -5.699E+00 J/K
Iterations             14        ( Limit =  100  )

                      INPUT AMOUNT EQUIL AMOUNT MOLE FRACT  ACTIVITY  ACTIVITY
PHASE 1:                   mol          mol              COEFFICI
H2O                      8.2713E+00  8.2527E+000  9.901E-01  1.00E+00  9.901E-01
H(+a)                    3.0000E-03  7.8143E-003  9.375E-04  1.00E+00  9.375E-04
OH(-a)                   1.0000E-03  2.7075E-013  3.248E-14  1.00E+00  3.248E-14
HSO3(-a)                 1.0000E-03  7.8142E-003  9.375E-04  1.00E+00  9.375E-04
SO3(-2a)                 5.0000E-04  5.3888E-009  6.465E-10  1.00E+00  6.465E-10
SO2(a)                   0.0000E+00  6.6684E-002  8.000E-03  1.00E+00  8.000E-03
O2(a)                    0.0000E+00  3.2069E-004  3.847E-05  1.00E+00  3.847E-05
Total :                8.2768E+00  8.3353E+000

PHASE 2 :                                     MOLE FRACT
H2O(g)                   0.0000E+00  1.3301E-002  6.209E-02  1.00E+00  6.209E-02
O2(g)                    1.3938E-01  1.3906E-001  6.491E-01  1.00E+00  6.491E-01
SO2(g)                   1.3487E-01  6.1867E-002  2.888E-01  1.00E+00  2.888E-01
Total :                2.7425E-01  2.1423E-001


******************************************************************************
Iteration  14  GMIN =      -945.954209155361

§60 deg, 0 to 5 bar

Temperature            333.15   K
Pressure               3.265          bar
Volume                 6.980E-02 m3 ( NPT )
Reaction enthalpy     -8.933E-01 kJ
Reaction entropy      -5.891E+00 J/K
Iterations             14        ( Limit =  100  )

                      INPUT AMOUNT EQUIL AMOUNT MOLE FRACT  ACTIVITY  ACTIVITY
PHASE 1:                   mol          mol              COEFFICI
H2O                      8.2713E+00  8.2531E+000  9.899E-01  1.00E+00  9.899E-01
H(+a)                    3.0000E-03  7.8885E-003  9.462E-04  1.00E+00  9.462E-04
OH(-a)                   1.0000E-03  2.6827E-013  3.218E-14  1.00E+00  3.218E-14
HSO3(-a)                 1.0000E-03  7.8885E-003  9.462E-04  1.00E+00  9.462E-04
SO3(-2a)                 5.0000E-04  5.3901E-009  6.465E-10  1.00E+00  6.465E-10
SO2(a)                   0.0000E+00  6.7954E-002  8.151E-03  1.00E+00  8.151E-03
O2(a)                    0.0000E+00  3.3402E-004  4.006E-05  1.00E+00  4.006E-05
Total :                8.2768E+00  8.3372E+000
```



```
O2(a)                    0.0000E+00  3.3402E-004  4.006E-05  1.00E+00  4.006E-05
Total :                8.2768E+00  8.3372E+000

PHASE 2 :                                     MOLE FRACT
H2O(g)                   0.0000E+00  1.2770E-002  6.014E-02  1.00E+00  6.014E-02
O2(g)                    1.3938E-01  1.3905E-001  6.548E-01  1.00E+00  6.548E-01
SO2(g)                   1.3487E-01  6.0523E-002  2.850E-01  1.00E+00  2.850E-01
Total :                2.7425E-01  2.1234E-001


******************************************************************************
Iteration  14  GMIN =      -945.947704926596

§60 deg, 0 to 5 bar

Temperature            333.15   K
Pressure               3.367          bar
Volume                 6.770E-02 m3 ( NPT )
Reaction enthalpy     -9.373E-01 kJ

Reaction entropy      -6.075E+00 J/K
Iterations             14        ( Limit =  100  )

                      INPUT AMOUNT EQUIL AMOUNT MOLE FRACT  ACTIVITY  ACTIVITY
PHASE 1:                   mol          mol              COEFFICI
H2O                      8.2713E+00  8.2536E+000  9.898E-01  1.00E+00  9.898E-01
H(+a)                    3.0000E-03  7.9595E-003  9.545E-04  1.00E+00  9.545E-04
OH(-a)                   1.0000E-03  2.6595E-013  3.189E-14  1.00E+00  3.189E-14
HSO3(-a)                 1.0000E-03  7.9595E-003  9.545E-04  1.00E+00  9.545E-04
SO3(-2a)                 5.0000E-04  5.3912E-009  6.465E-10  1.00E+00  6.465E-10
SO2(a)                   0.0000E+00  6.9179E-002  8.296E-03  1.00E+00  8.296E-03
O2(a)                    0.0000E+00  3.4744E-004  4.166E-05  1.00E+00  4.166E-05
Total :                8.2768E+00  8.3390E+000

PHASE 2 :                                     MOLE FRACT
H2O(g)                   0.0000E+00  1.2276E-002  5.831E-02  1.00E+00  5.831E-02
O2(g)                    1.3938E-01  1.3903E-001  6.604E-01  1.00E+00  6.604E-01
SO2(g)                   1.3487E-01  5.9227E-002  2.813E-01  1.00E+00  2.813E-01
Total :                2.7425E-01  2.1054E-001


******************************************************************************
Iteration  13  GMIN =      -945.941447455312

§60 deg, 0 to 5 bar

Temperature            333.15   K
Pressure               3.469          bar
Volume                 6.573E-02 m3 ( NPT )
Reaction enthalpy     -9.792E-01 kJ
Reaction entropy      -6.250E+00 J/K
Iterations             13        ( Limit =  100  )

                      INPUT AMOUNT EQUIL AMOUNT MOLE FRACT  ACTIVITY  ACTIVITY
PHASE 1:                   mol          mol              COEFFICI
H2O                      8.2713E+00  8.2540E+000  9.896E-01  1.00E+00  9.896E-01
H(+a)                    3.0000E-03  8.0274E-003  9.624E-04  1.00E+00  9.624E-04
OH(-a)                   1.0000E-03  2.6377E-013  3.162E-14  1.00E+00  3.162E-14
HSO3(-a)                 1.0000E-03  8.0274E-003  9.624E-04  1.00E+00  9.624E-04
SO3(-2a)                 5.0000E-04  5.3923E-009  6.465E-10  1.00E+00  6.465E-10
SO2(a)                   0.0000E+00  7.0361E-002  8.436E-03  1.00E+00  8.436E-03
O2(a)                    0.0000E+00  3.6096E-004  4.328E-05  1.00E+00  4.328E-05
Total :                8.2768E+00  8.3407E+000

PHASE 2 :                                     MOLE FRACT
H2O(g)                   0.0000E+00  1.1815E-002  5.658E-02  1.00E+00  5.658E-02
O2(g)                    1.3938E-01  1.3902E-001  6.658E-01  1.00E+00  6.658E-01
SO2(g)                   1.3487E-01  5.7977E-002  2.777E-01  1.00E+00  2.777E-01
Total :                2.7425E-01  2.0881E-001
```

```
O2(g)                      1.3938E-01  1.3902E-001  6.658E-01  1.00E+00  6.658E-01
SO2(g)                     1.3487E-01  5.7977E-002  2.777E-01  1.00E+00  2.777E-01
Total :                 2.7425E-01  2.0881E-001


******************************************************************************
Iteration  13  GMIN =       -945.935420210432

$60 deg, 0 to 5 bar

Temperature             333.15   K
Pressure                3.571          bar
Volume                  6.386E-02 m3  ( NPT )
Reaction enthalpy      -1.019E+00 kJ
Reaction entropy        -6.417E+00 J/K
Iterations              13         ( Limit =  100  )

                     INPUT AMOUNT EQUIL AMOUNT MOLE FRACT  ACTIVITY  ACTIVITY
PHASE 1:                     mol          mol              COEFFICI
H2O                        8.2713E+00  8.2543E+000  9.894E-01  1.00E+00  9.894E-01
H(+a)                      3.0000E-03  8.0924E-003  9.700E-04  1.00E+00  9.700E-04
OH(-a)                     1.0000E-03  2.6171E-013  3.137E-14  1.00E+00  3.137E-14
HSO3(-a)                   1.0000E-03  8.0924E-003  9.700E-04  1.00E+00  9.700E-04
SO3(-2a)                   5.0000E-04  5.3934E-009  6.465E-10  1.00E+00  6.465E-10
SO2(a)                     0.0000E+00  7.1502E-002  8.571E-03  1.00E+00  8.571E-03
O2(a)                      0.0000E+00  3.7457E-004  4.490E-05  1.00E+00  4.490E-05
```

```
Total :                 8.2768E+00  8.3424E+000

PHASE 2 :                                         MOLE FRACT
H2O(g)                     0.0000E+00  1.1385E-002  5.496E-02  1.00E+00  5.496E-02
O2(g)                      1.3938E-01  1.3901E-001  6.710E-01  1.00E+00  6.710E-01
SO2(g)                     1.3487E-01  5.6771E-002  2.740E-01  1.00E+00  2.740E-01
Total :                 2.7425E-01  2.0716E-001


******************************************************************************
Iteration  13  GMIN =       -945.929608196529

$60 deg, 0 to 5 bar

Temperature             333.15   K
Pressure                3.673          bar
Volume                  6.210E-02 m3  ( NPT )
Reaction enthalpy      -1.057E+00 kJ
Reaction entropy        -6.576E+00 J/K
Iterations              13         ( Limit =  100  )

                     INPUT AMOUNT EQUIL AMOUNT MOLE FRACT  ACTIVITY  ACTIVITY
PHASE 1:                     mol          mol              COEFFICI
H2O                        8.2713E+00  8.2547E+000  9.893E-01  1.00E+00  9.893E-01
H(+a)                      3.0000E-03  8.1547E-003  9.773E-04  1.00E+00  9.773E-04
OH(-a)                     1.0000E-03  2.5977E-013  3.113E-14  1.00E+00  3.113E-14
HSO3(-a)                   1.0000E-03  8.1547E-003  9.773E-04  1.00E+00  9.773E-04
SO3(-2a)                   5.0000E-04  5.3944E-009  6.465E-10  1.00E+00  6.465E-10
SO2(a)                     0.0000E+00  7.2603E-002  8.701E-03  1.00E+00  8.701E-03
O2(a)                      0.0000E+00  3.8827E-004  4.653E-05  1.00E+00  4.653E-05
Total :                 8.2768E+00  8.3440E+000

PHASE 2 :                                         MOLE FRACT
H2O(g)                     0.0000E+00  1.0983E-002  5.342E-02  1.00E+00  5.342E-02
O2(g)                      1.3938E-01  1.3899E-001  6.761E-01  1.00E+00  6.761E-01
SO2(g)                     1.3487E-01  5.5607E-002  2.705E-01  1.00E+00  2.705E-01
Total :                 2.7425E-01  2.0558E-001


******************************************************************************
Iteration  13  GMIN =       -945.923943725088

$60 deg, 0 to 5 bar
```



```
Iteration  13  GMIN =       -945.923943725088

$60 deg, 0 to 5 bar

Temperature             333.15   K
Pressure                3.776          bar
Volume                  6.042E-02 m3  ( NPT )
Reaction enthalpy      -1.093E+00 kJ
Reaction entropy        -6.731E+00 J/K
Iterations              13         ( Limit =  100  )

                     INPUT AMOUNT EQUIL AMOUNT MOLE FRACT  ACTIVITY  ACTIVITY
PHASE 1:                     mol          mol              COEFFICI
H2O                        8.2713E+00  8.2550E+000  9.892E-01  1.00E+00  9.892E-01
H(+a)                      3.0000E-03  8.2150E-003  9.844E-04  1.00E+00  9.844E-04
OH(-a)                     1.0000E-03  2.5793E-013  3.091E-14  1.00E+00  3.091E-14
HSO3(-a)                   1.0000E-03  8.2149E-003  9.844E-04  1.00E+00  9.844E-04
SO3(-2a)                   5.0000E-04  5.3954E-009  6.465E-10  1.00E+00  6.465E-10
SO2(a)                     0.0000E+00  7.3678E-002  8.828E-03  1.00E+00  8.828E-03
O2(a)                      0.0000E+00  4.0218E-004  4.819E-05  1.00E+00  4.819E-05
Total :                 8.2768E+00  8.3455E+000

PHASE 2 :                                         MOLE FRACT
H2O(g)                     0.0000E+00  1.0603E-002  5.196E-02  1.00E+00  5.196E-02
O2(g)                      1.3938E-01  1.3898E-001  6.811E-01  1.00E+00  6.811E-01
SO2(g)                     1.3487E-01  5.4472E-002  2.670E-01  1.00E+00  2.670E-01
Total :                 2.7425E-01  2.0405E-001


******************************************************************************
Iteration  13  GMIN =       -945.918524249999
```

```
$60 deg, 0 to 5 bar

Temperature             333.15   K
Pressure                3.878          bar
Volume                  5.884E-02 m3  ( NPT )
Reaction enthalpy      -1.127E+00 kJ
Reaction entropy        -6.877E+00 J/K
Iterations              13         ( Limit =  100  )

                     INPUT AMOUNT EQUIL AMOUNT MOLE FRACT  ACTIVITY  ACTIVITY
PHASE 1:                     mol          mol              COEFFICI
H2O                        8.2713E+00  8.2553E+000  9.890E-01  1.00E+00  9.890E-01
H(+a)                      3.0000E-03  8.2722E-003  9.910E-04  1.00E+00  9.910E-04
OH(-a)                     1.0000E-03  2.5619E-013  3.069E-14  1.00E+00  3.069E-14
HSO3(-a)                   1.0000E-03  8.2722E-003  9.910E-04  1.00E+00  9.910E-04
SO3(-2a)                   5.0000E-04  5.3963E-009  6.465E-10  1.00E+00  6.465E-10
SO2(a)                     0.0000E+00  7.4706E-002  8.950E-03  1.00E+00  8.950E-03
O2(a)                      0.0000E+00  4.1604E-004  4.984E-05  1.00E+00  4.984E-05
Total :                 8.2768E+00  8.3469E+000

PHASE 2 :                                         MOLE FRACT
H2O(g)                     0.0000E+00  1.0249E-002  5.059E-02  1.00E+00  5.059E-02
O2(g)                      1.3938E-01  1.3896E-001  6.859E-01  1.00E+00  6.859E-01
SO2(g)                     1.3487E-01  5.3387E-002  2.635E-01  1.00E+00  2.635E-01
Total :                 2.7425E-01  2.0260E-001


******************************************************************************
Iteration  13  GMIN =       -945.913282447337

$60 deg, 0 to 5 bar

Temperature             333.15   K
Pressure                3.98           bar
Volume                  5.734E-02 m3  ( NPT )
Reaction enthalpy      -1.160E+00 kJ
Reaction entropy        -7.018E+00 J/K
```



```
Pressure                3.98           bar
Volume                  5.734E-02 m3  ( NPT )
Reaction enthalpy      -1.160E+00 kJ
Reaction entropy        -7.018E+00 J/K
Iterations              13         ( Limit =  100  )

                     INPUT AMOUNT EQUIL AMOUNT MOLE FRACT  ACTIVITY  ACTIVITY
PHASE 1:                     mol          mol              COEFFICI
H2O                        8.2713E+00  8.2556E+000  9.889E-01  1.00E+00  9.889E-01
H(+a)                      3.0000E-03  8.3272E-003  9.975E-04  1.00E+00  9.975E-04
OH(-a)                     1.0000E-03  2.5455E-013  3.049E-14  1.00E+00  3.049E-14
HSO3(-a)                   1.0000E-03  8.3271E-003  9.975E-04  1.00E+00  9.975E-04
SO3(-2a)                   5.0000E-04  5.3972E-009  6.465E-10  1.00E+00  6.465E-10
SO2(a)                     0.0000E+00  7.5699E-002  9.068E-03  1.00E+00  9.068E-03
O2(a)                      0.0000E+00  4.2997E-004  5.150E-05  1.00E+00  5.150E-05
Total :                 8.2768E+00  8.3483E+000

PHASE 2 :                                         MOLE FRACT
H2O(g)                     0.0000E+00  9.9161E-003  4.928E-02  1.00E+00  4.928E-02
O2(g)                      1.3938E-01  1.3895E-001  6.906E-01  1.00E+00  6.906E-01
SO2(g)                     1.3487E-01  5.2339E-002  2.601E-01  1.00E+00  2.601E-01
Total :                 2.7425E-01  2.0121E-001


******************************************************************************
Iteration  13  GMIN =       -945.908207904683

$60 deg, 0 to 5 bar

Temperature             333.15   K
Pressure                4.082          bar
Volume                  5.592E-02 m3  ( NPT )
Reaction enthalpy      -1.191E+00 kJ
Reaction entropy        -7.153E+00 J/K
Iterations              13         ( Limit =  100  )

                     INPUT AMOUNT EQUIL AMOUNT MOLE FRACT  ACTIVITY  ACTIVITY
PHASE 1:                     mol          mol              COEFFICI
H2O                        8.2713E+00  8.2558E+000  9.888E-01  1.00E+00  9.888E-01
```

```
H(+a)                      3.0000E-03  8.3799E-003  1.004E-03  1.00E+00  1.004E-03
OH(-a)                     1.0000E-03  2.5300E-013  3.030E-14  1.00E+00  3.030E-14
HSO3(-a)                   1.0000E-03  8.3799E-003  1.004E-03  1.00E+00  1.004E-03
SO3(-2a)                   5.0000E-04  5.3981E-009  6.465E-10  1.00E+00  6.465E-10
SO2(a)                     0.0000E+00  7.6659E-002  9.181E-03  1.00E+00  9.181E-03
O2(a)                      0.0000E+00  4.4397E-004  5.317E-05  1.00E+00  5.317E-05
Total :                 8.2768E+00  8.3497E+000

PHASE 2 :                                         MOLE FRACT
H2O(g)                     0.0000E+00  9.6026E-003  4.805E-02  1.00E+00  4.805E-02
O2(g)                      1.3938E-01  1.3894E-001  6.952E-01  1.00E+00  6.952E-01
SO2(g)                     1.3487E-01  5.1326E-002  2.568E-01  1.00E+00  2.568E-01
Total :                 2.7425E-01  1.9986E-001


******************************************************************************
Iteration  13  GMIN =       -945.903291059502

$60 deg, 0 to 5 bar

Temperature             333.15   K
Pressure                4.184          bar
Volume                  5.456E-02 m3  ( NPT )
Reaction enthalpy      -1.221E+00 kJ
Reaction entropy        -7.282E+00 J/K
Iterations              13         ( Limit =  100  )

                     INPUT AMOUNT EQUIL AMOUNT MOLE FRACT  ACTIVITY  ACTIVITY
PHASE 1:                     mol          mol              COEFFICI
H2O                        8.2713E+00  8.2561E+000  9.886E-01  1.00E+00  9.886E-01
H(+a)                      3.0000E-03  8.4307E-003  1.010E-03  1.00E+00  1.010E-03
```



```
                     INPUT AMOUNT EQUIL AMOUNT MOLE FRACT  ACTIVITY  ACTIVITY
PHASE 1:                     mol          mol              COEFFICI
H2O                        8.2713E+00  8.2561E+000  9.886E-01  1.00E+00  9.886E-01
H(+a)                      3.0000E-03  8.4307E-003  1.010E-03  1.00E+00  1.010E-03
OH(-a)                     1.0000E-03  2.5152E-013  3.012E-14  1.00E+00  3.012E-14
HSO3(-a)                   1.0000E-03  8.4306E-003  1.010E-03  1.00E+00  1.010E-03
SO3(-2a)                   5.0000E-04  5.3989E-009  6.465E-10  1.00E+00  6.465E-10
SO2(a)                     0.0000E+00  7.7588E-002  9.291E-03  1.00E+00  9.291E-03
O2(a)                      0.0000E+00  4.5804E-004  5.485E-05  1.00E+00  5.485E-05
Total :                 8.2768E+00  8.3510E+000

PHASE 2 :                                         MOLE FRACT
H2O(g)                     0.0000E+00  9.3069E-003  4.687E-02  1.00E+00  4.687E-02
O2(g)                      1.3938E-01  1.3892E-001  6.996E-01  1.00E+00  6.996E-01
SO2(g)                     1.3487E-01  5.0347E-002  2.535E-01  1.00E+00  2.535E-01
Total :                 2.7425E-01  1.9858E-001


******************************************************************************
Iteration  13  GMIN =       -945.898523111164

$60 deg, 0 to 5 bar

Temperature             333.15   K
Pressure                4.286          bar
Volume                  5.327E-02 m3  ( NPT )
Reaction enthalpy      -1.250E+00 kJ
Reaction entropy        -7.407E+00 J/K
Iterations              13         ( Limit =  100  )

                     INPUT AMOUNT EQUIL AMOUNT MOLE FRACT  ACTIVITY  ACTIVITY
PHASE 1:                     mol          mol              COEFFICI
H2O                        8.2713E+00  8.2563E+000  9.885E-01  1.00E+00  9.885E-01
H(+a)                      3.0000E-03  8.4794E-003  1.015E-03  1.00E+00  1.015E-03
OH(-a)                     1.0000E-03  2.5012E-013  2.995E-14  1.00E+00  2.995E-14
HSO3(-a)                   1.0000E-03  8.4794E-003  1.015E-03  1.00E+00  1.015E-03
SO3(-2a)                   5.0000E-04  5.3998E-009  6.465E-10  1.00E+00  6.465E-10
SO2(a)                     0.0000E+00  7.8486E-002  9.397E-03  1.00E+00  9.397E-03
O2(a)                      0.0000E+00  4.7218E-004  5.653E-05  1.00E+00  5.653E-05
Total :                 8.2768E+00  8.3522E+000

PHASE 2 :                                         MOLE FRACT
H2O(g)                     0.0000E+00  9.0276E-003  4.575E-02  1.00E+00  4.575E-02
O2(g)                      1.3938E-01  1.3891E-001  7.039E-01  1.00E+00  7.039E-01
SO2(g)                     1.3487E-01  4.9400E-002  2.503E-01  1.00E+00  2.503E-01
```

```
Total :                 2.7425E-01  1.9733E-001


******************************************************************************
Iteration  13  GMIN =       -945.893895944641

$60 deg, 0 to 5 bar

Temperature             333.15   K
Pressure                4.388          bar
Volume                  5.204E-02 m3  ( NPT )
Reaction enthalpy      -1.277E+00 kJ
Reaction entropy        -7.527E+00 J/K
Iterations              13         ( Limit =  100  )

                     INPUT AMOUNT EQUIL AMOUNT MOLE FRACT  ACTIVITY  ACTIVITY
PHASE 1:                     mol          mol              COEFFICI
H2O                        8.2713E+00  8.2565E+000  9.884E-01  1.00E+00  9.884E-01
H(+a)                      3.0000E-03  8.5264E-003  1.021E-03  1.00E+00  1.021E-03
OH(-a)                     1.0000E-03  2.4879E-013  2.978E-14  1.00E+00  2.978E-14
HSO3(-a)                   1.0000E-03  8.5264E-003  1.021E-03  1.00E+00  1.021E-03
SO3(-2a)                   5.0000E-04  5.4005E-009  6.465E-10  1.00E+00  6.465E-10
SO2(a)                     0.0000E+00  7.9355E-002  9.500E-03  1.00E+00  9.500E-03
O2(a)                      0.0000E+00  4.8638E-004  5.823E-05  1.00E+00  5.823E-05
```

```
SO3(-2a)                5.0000E-04  5.4005E-009  6.465E-10  1.00E+00  6.465E-10
SO2(a)                  0.0000E+00  7.9355E-002  9.500E-03  1.00E+00  9.500E-03
O2(a)                   0.0000E+00  4.8638E-004  5.823E-05  1.00E+00  5.823E-05
Total :              8.2768E+00  8.3534E+000

PHASE 2 :                                MOLE FRACT
H2O(g)                  0.0000E+00  8.7634E-003  4.468E-02  1.00E+00  4.468E-02
O2(g)                   1.3938E-01  1.3889E-001  7.081E-01  1.00E+00  7.081E-01
SO2(g)                  1.3487E-01  4.8483E-002  2.472E-01  1.00E+00  2.472E-01
Total :              2.7425E-01  1.9614E-001


********************************************************************************
Iteration  13  GMIN =      -945.889402062346

§60 deg, 0 to 5 bar

Temperature             333.15   K
Pressure                4.49         bar
Volume                  5.086E-02 m3 ( NPT )
Reaction enthalpy     -1.304E+00 kJ
Reaction entropy       -7.642E+00 J/K
Iterations              13        ( Limit =  100  )

                     INPUT AMOUNT EQUIL AMOUNT MOLE FRACT  ACTIVITY  ACTIVITY
PHASE 1:                    mol         mol               COEFFICI
H2O                     8.2713E+00  8.2567E+000  9.883E-01  1.00E+00  9.883E-01
H(+a)                   3.0000E-03  8.5716E-003  1.026E-03  1.00E+00  1.026E-03
OH(-a)                  1.0000E-03  2.4751E-013  2.963E-14  1.00E+00  2.963E-14
HSO3(-a)                1.0000E-03  8.5716E-003  1.026E-03  1.00E+00  1.026E-03
SO3(-2a)                5.0000E-04  5.4013E-009  6.465E-10  1.00E+00  6.465E-10
SO2(a)                  0.0000E+00  8.0197E-002  9.599E-03  1.00E+00  9.599E-03
O2(a)                   0.0000E+00  5.0065E-004  5.992E-05  1.00E+00  5.992E-05
Total :              8.2768E+00  8.3546E+000

PHASE 2 :                                MOLE FRACT
H2O(g)                  0.0000E+00  8.5130E-003  4.366E-02  1.00E+00  4.366E-02
O2(g)                   1.3938E-01  1.3888E-001  7.122E-01  1.00E+00  7.122E-01
SO2(g)                  1.3487E-01  4.7597E-002  2.441E-01  1.00E+00  2.441E-01
Total :              2.7425E-01  1.9499E-001


********************************************************************************
Iteration  13  GMIN =      -945.885034524996

§60 deg, 0 to 5 bar

Temperature             333.15   K
Pressure                4.592        bar
Volume                  4.974E-02 m3 ( NPT )
Reaction enthalpy     -1.329E+00 kJ
```



```
Reaction entropy       -7.753E+00 J/K
Iterations              13        ( Limit =  100  )

                     INPUT AMOUNT EQUIL AMOUNT MOLE FRACT  ACTIVITY  ACTIVITY
PHASE 1:                    mol         mol               COEFFICI
H2O                     8.2713E+00  8.2569E+000  9.882E-01  1.00E+00  9.882E-01
H(+a)                   3.0000E-03  8.6151E-003  1.031E-03  1.00E+00  1.031E-03
OH(-a)                  1.0000E-03  2.4630E-013  2.948E-14  1.00E+00  2.948E-14
HSO3(-a)                1.0000E-03  8.6151E-003  1.031E-03  1.00E+00  1.031E-03
SO3(-2a)                5.0000E-04  5.4020E-009  6.465E-10  1.00E+00  6.465E-10
SO2(a)                  0.0000E+00  8.1011E-002  9.695E-03  1.00E+00  9.695E-03
O2(a)                   0.0000E+00  5.1497E-004  6.163E-05  1.00E+00  6.163E-05
Total :              8.2768E+00  8.3557E+000

PHASE 2 :                                MOLE FRACT
H2O(g)                  0.0000E+00  8.2757E-003  4.268E-02  1.00E+00  4.268E-02
O2(g)                   1.3938E-01  1.3887E-001  7.162E-01  1.00E+00  7.162E-01
SO2(g)                  1.3487E-01  4.6738E-002  2.411E-01  1.00E+00  2.411E-01
```



```
PHASE 2 :                                MOLE FRACT
H2O(g)                  0.0000E+00  8.2757E-003  4.268E-02  1.00E+00  4.268E-02
O2(g)                   1.3938E-01  1.3887E-001  7.162E-01  1.00E+00  7.162E-01
SO2(g)                  1.3487E-01  4.6738E-002  2.411E-01  1.00E+00  2.411E-01
Total :              2.7425E-01  1.9388E-001


********************************************************************************
Iteration  13  GMIN =      -945.880786898913

§60 deg, 0 to 5 bar

Temperature             333.15   K
Pressure                4.694        bar
Volume                  4.867E-02 m3 ( NPT )
Reaction enthalpy     -1.353E+00 kJ
Reaction entropy       -7.860E+00 J/K
Iterations              13        ( Limit =  100  )

                     INPUT AMOUNT EQUIL AMOUNT MOLE FRACT  ACTIVITY  ACTIVITY
PHASE 1:                    mol         mol               COEFFICI
H2O                     8.2713E+00  8.2571E+000  9.881E-01  1.00E+00  9.881E-01
H(+a)                   3.0000E-03  8.6571E-003  1.036E-03  1.00E+00  1.036E-03
OH(-a)                  1.0000E-03  2.4515E-013  2.934E-14  1.00E+00  2.934E-14
HSO3(-a)                1.0000E-03  8.6570E-003  1.036E-03  1.00E+00  1.036E-03
SO3(-2a)                5.0000E-04  5.4027E-009  6.465E-10  1.00E+00  6.465E-10
SO2(a)                  0.0000E+00  8.1801E-002  9.789E-03  1.00E+00  9.789E-03
O2(a)                   0.0000E+00  5.2934E-004  6.334E-05  1.00E+00  6.334E-05
Total :              8.2768E+00  8.3567E+000

PHASE 2 :                                MOLE FRACT
H2O(g)                  0.0000E+00  8.0503E-003  4.175E-02  1.00E+00  4.175E-02
O2(g)                   1.3938E-01  1.3885E-001  7.201E-01  1.00E+00  7.201E-01
SO2(g)                  1.3487E-01  4.5907E-002  2.381E-01  1.00E+00  2.381E-01
Total :              2.7425E-01  1.9281E-001


********************************************************************************
Iteration  13  GMIN =      -945.876653209255

§60 deg, 0 to 5 bar

Temperature             333.15   K
Pressure                4.796        bar
Volume                  4.764E-02 m3 ( NPT )
Reaction enthalpy     -1.376E+00 kJ
Reaction entropy       -7.963E+00 J/K
Iterations              13        ( Limit =  100  )

                     INPUT AMOUNT EQUIL AMOUNT MOLE FRACT  ACTIVITY  ACTIVITY
PHASE 1:                    mol         mol               COEFFICI
H2O                     8.2713E+00  8.2573E+000  9.880E-01  1.00E+00  9.880E-01
H(+a)                   3.0000E-03  8.6975E-003  1.041E-03  1.00E+00  1.041E-03
OH(-a)                  1.0000E-03  2.4404E-013  2.920E-14  1.00E+00  2.920E-14
HSO3(-a)                1.0000E-03  8.6975E-003  1.041E-03  1.00E+00  1.041E-03
SO3(-2a)                5.0000E-04  5.4033E-009  6.465E-10  1.00E+00  6.465E-10
SO2(a)                  0.0000E+00  8.2565E-002  9.879E-03  1.00E+00  9.879E-03
O2(a)                   0.0000E+00  5.4377E-004  6.506E-05  1.00E+00  6.506E-05
```



```
Total :              8.2768E+00  8.3578E+000

PHASE 2 :                                MOLE FRACT
H2O(g)                  0.0000E+00  7.8360E-003  4.086E-02  1.00E+00  4.086E-02
O2(g)                   1.3938E-01  1.3884E-001  7.240E-01  1.00E+00  7.240E-01
SO2(g)                  1.3487E-01  4.5102E-002  2.352E-01  1.00E+00  2.352E-01
Total :              2.7425E-01  1.9177E-001


********************************************************************************
Iteration  13  GMIN =      -945.872627898747
```



```
********************************************************************************
Iteration  13  GMIN =      -945.872627898747

§60 deg, 0 to 5 bar

Temperature             333.15   K
Pressure                4.898        bar
Volume                  4.665E-02 m3 ( NPT )
Reaction enthalpy     -1.399E+00 kJ
Reaction entropy       -8.063E+00 J/K
Iterations              13        ( Limit =  100  )

                     INPUT AMOUNT EQUIL AMOUNT MOLE FRACT  ACTIVITY  ACTIVITY
PHASE 1:                    mol         mol               COEFFICI
H2O                     8.2713E+00  8.2574E+000  9.879E-01  1.00E+00  9.879E-01
H(+a)                   3.0000E-03  8.7365E-003  1.045E-03  1.00E+00  1.045E-03
OH(-a)                  1.0000E-03  2.4298E-013  2.907E-14  1.00E+00  2.907E-14
HSO3(-a)                1.0000E-03  8.7365E-003  1.045E-03  1.00E+00  1.045E-03
SO3(-2a)                5.0000E-04  5.4040E-009  6.465E-10  1.00E+00  6.465E-10
SO2(a)                  0.0000E+00  8.3306E-002  9.966E-03  1.00E+00  9.966E-03
O2(a)                   0.0000E+00  5.5825E-004  6.679E-05  1.00E+00  6.679E-05
Total :              8.2768E+00  8.3588E+000

PHASE 2 :                                MOLE FRACT
H2O(g)                  0.0000E+00  7.6321E-003  4.001E-02  1.00E+00  4.001E-02
O2(g)                   1.3938E-01  1.3882E-001  7.277E-01  1.00E+00  7.277E-01
SO2(g)                  1.3487E-01  4.4322E-002  2.323E-01  1.00E+00  2.323E-01
Total :              2.7425E-01  1.9078E-001


********************************************************************************
Iteration  14  GMIN =      -945.868705790543

§60 deg, 0 to 5 bar

Temperature             333.15   K
Pressure                5            bar
Volume                  4.570E-02 m3 ( NPT )
Reaction enthalpy     -1.421E+00 kJ
Reaction entropy       -8.159E+00 J/K
Iterations              14        ( Limit =  100  )

                     INPUT AMOUNT EQUIL AMOUNT MOLE FRACT  ACTIVITY  ACTIVITY
PHASE 1:                    mol         mol               COEFFICI
H2O                     8.2713E+00  8.2576E+000  9.878E-01  1.00E+00  9.878E-01
H(+a)                   3.0000E-03  8.7742E-003  1.050E-03  1.00E+00  1.050E-03
OH(-a)                  1.0000E-03  2.4197E-013  2.895E-14  1.00E+00  2.895E-14
HSO3(-a)                1.0000E-03  8.7742E-003  1.050E-03  1.00E+00  1.050E-03
SO3(-2a)                5.0000E-04  5.4046E-009  6.465E-10  1.00E+00  6.465E-10
SO2(a)                  0.0000E+00  8.4025E-002  1.005E-02  1.00E+00  1.005E-02
O2(a)                   0.0000E+00  5.7278E-004  6.852E-05  1.00E+00  6.852E-05
Total :              8.2768E+00  8.3597E+000

PHASE 2 :                                MOLE FRACT
H2O(g)                  0.0000E+00  7.4379E-003  3.919E-02  1.00E+00  3.919E-02
O2(g)                   1.3938E-01  1.3881E-001  7.313E-01  1.00E+00  7.313E-01
SO2(g)                  1.3487E-01  4.3566E-002  2.295E-01  1.00E+00  2.295E-01
Total :              2.7425E-01  1.8981E-001
```

Appendix D.

Mathematica Calculations

```
(*-----------Begin Program to Calculate Equilibrium------------*)

TCel =25;
T=TCel + 273.15;
Barpressure =1.2;
Pressure = Barpressure * 0.987;
H2OIN =8.3;
SO2IN =0.3;
O2IN = 0.10;
H2SO4IN=0.01;
If[(T-273)≤50,do = (1.0-4.8*10^-6*(T-273)^2)];
If[(T-273)>50, do = (1.0064-(2.5*10^-4*(T-273))-(2.3*10^-6*(T-273)^2))];
alphaSO2 = -0.030;
elec = 4.8029*10^-10;
Dielec = 305.7*Exp[-Exp[-12.741+0.01875*T]-(T/219)];
k =1.38045*10^-16;
Mw = 0.01802;
Na = 6.0232*10^23;
PSH2O = (10^(7.96681-1668.21/(T-45.15)))/760;
R = 82.06;
rH = 3.8;
rHSO3 = 2.7;
rOH = 3.5;
rSO3 = 2.8;
zH = 1;
zHSO3 = -1;
zOH = -1;
zSO3 = -2;
Subst = {KSO2, KH2O, KHSO3};
kvalA = {-3768, -13445.9, 1333.4};
kvalB = {-20,-22.4773,0};
kvalC={0.0,0 , 0};
kvalD={122.53, 140.932, -21.274};
Kvalue = Exp[(kvalA/T)+(kvalB*Log[T]) + (kvalC*T)+kvalD];
KSO2 =Kvalue[[1]];
KH2O = Kvalue[[2]];
KHSO3 =Kvalue[[3]];
HenvalA =6211.22;
HenvalB = 60.239;
HenvalC = -0.102974;
HenvalD = -333.362;
HenrySO2 = Exp[(HenvalA/T)+(HenvalB*Log[T]) + (HenvalC*T) + HenvalD];
vstar2= 115.0;
vmolwater = 18.02*(1.001508+3.976412*10^-6*(T-273.15)^2);
If[(T-273)≤50,ρ = 1.0-4.8*10^-6*(T-273)^2];
If[(T-273)>50, ρ = 1.0064-(2.5*10^-4*(T-273))-(2.3*10^-6*(T-273)^2)];

Clear[C12subso, solution, solution1, solution2, K, partmolvol];
rhotil = ρ/18.012*46.4;

solution1 =Solve[Log[1 +18.02/((ρ)*K*R*T)]==(-0.42704*(rhotil-1)+2.089*(rhotil-1)^2-
0.42367*(rhotil-1)^3), K];

Flatten[solution1];
K = K/.solution1[[1]];

If[2≤rhotil≤2.785, series= -2.4467+ 2.12074*rhotil, "outside range"];

If[2.785≤rhotil≤3.2, series = 3.02214 - 1.87085*rhotil+0.71955*rhotil^2, "outside
range"];

For[i=2, i<3, ivalue = i;
  C12subso = (Subscript[vstar, ivalue]/46.4)^0.62*(-Exp[series]);
  vmol ivalue= K*R*T*(1-C12subso)
```

```
    i++];

partmolvolSO2 = vmol₂/1000;
partmolvolH2O = vmolwater/1000;
partmolvolH = -0.0047;
partmolvolHSO3 = 0.035;
partmolvolOH = 0.0005;
partmolvolSO3 = 0.0197;
Ionicstrength =0.5*(molalH + molalOH + molalHSO3 + 4*molalSO3);
A = (2*π*Na*do/1000)^(1/2) * (elec^2/(Dielec*k*T))^(3/2);
FAC=(-(A/3))*(√Ionicstrength /(1+1.2*√Ionicstrength )+2.0/1.2*Log[1+1.2*
√Ionicstrength ]);
Clear[Bi, Bypi, Bwateri];
Beta0 = {0.04, -0.06, 0.12};
Beta1 = {0.12, -0.54, 1.08};
ion= {1,2,3};
Bi[Beta0_, Beta1_, ion_] := (Beta0) + (Beta1)/(2*Ionicstrength)*(1-
(1+2*Sqrt[Ionicstrength])*Exp[-2*Sqrt[Ionicstrength]]);
Bypi [Beta0_, Beta1_, ion_] :=(Beta1)*(1-
(1+2*Sqrt[Ionicstrength]+2*Ionicstrength)*Exp[(-2*Sqrt[Ionicstrength])]);
Bwateri [Beta0_, Beta1_, ion_] := Beta0 +Beta1*Exp[-2*Sqrt[Ionicstrength]];
Bi = Bi[Beta0, Beta1, ion];
Bypi = Bypi[Beta0, Beta1, ion];
Bwateri = Bwateri[Beta0, Beta1, ion];
B1 = Bi[[1]];
Byp1 = Bypi[[1]];
Bwater1 = Bwateri[[1]];
B2 = Bi[[2]];
Byp2 = Bypi[[2]];
Bwater2 = Bwateri[[2]];
B3 = Bi[[3]];
Byp3 = Bypi[[3]];
Bwater3 = Bwateri[[3]];
Bsum = 2*molalH*((molalOH*Byp1)+(molalHSO3*Byp2)+(molalSO3*Byp3));
do;
Vm = (1/do)+molalSO2*partmolvolSO2;
Vi = (1/do)+(molalH*partmolvolH) +(molalOH*partmolvolOH)+ (molalHSO3*partmolvolHSO3)+
(molalSO3*partmolvolSO3);
vHc = (4/3)*π*Na*(rH^3)*(10^-27);
vOHc = (4/3)*π*Na*(rOH^3)*(10^-27) ;
vHSO3c =  (4/3)*π*Na*(rHSO3^3)*(10^-27);
vSO3c =  (4/3)*π*Na*(rSO3^3)*(10^-27);
Vc = (molalH*vHc) + (molalOH * vOHc) + (molalHSO3*vHSO3c)+(molalSO3*vSO3c);
Vf = Vi+(molalSO2*partmolvolSO2);
lambdaSO2 = -0.05+(0/T);
muSO2 = -(1/55.5)*(lambdaSO2+(1/166.5));
Ds = Dielec*(1+((alphaSO2*molalSO2)/Vm));
LH = ((elec^2)* (zH^2))/(2*rH*k*T*Dielec)*(10^8);

LHSO3 = ((elec^2)* (zHSO3^2))/(2*rHSO3*k*T*Dielec)*(10^8);

LOH = ((elec^2)* (zOH^2))/(2*rOH*k*T*Dielec)*(10^8);

LSO3 = ((elec^2)* (zSO3^2))/(2*rSO3*k*T*Dielec)*(10^8);
DIV = Dielec/Ds;
Vfc = Vf - Vc;
Vic = Vi - Vc;
SUML = (molalH*LH)+ (molalOH*LOH)+ (molalHSO3*LHSO3)+(molalSO3*LSO3);
BRAC = (DIV * molalSO2)*(-alphaSO2/Vm*(Vi+(0.5*Vc))/Vic-
(1.5*partmolvolSO2*Vc)/(Vic*Vfc));
activitycoeffH = Exp[FAC+2*((molalOH*B1)+(molalHSO3*B2)+(molalSO3*B3))-
(Bsum/(4*Ionicstrength²))+(BRAC*LH) + (1.5*SUML*((DIV*((Vf*vHc)-
(Vc*partmolvolH))/Vfc²)-(((Vi*vHc)-(Vc*partmolvolH))/Vic²)))];
activitycoeffOH = Exp[FAC + (2*B1*molalH)-(Bsum/(4*Ionicstrength²))+(BRAC*LOH) +
1.5*SUML*(DIV*((Vf*vOHc)-(Vc*partmolvolOH))/Vfc²-((Vi*vOHc)-(Vc*partmolvolOH))/Vic²)];
activitycoeffHSO3 = Exp[FAC + (2*B2*molalH)-(Bsum/(4*Ionicstrength²))+(BRAC*LHSO3) +
(1.5*SUML*((DIV*((Vf*vHSO3c)-(Vc*partmolvolHSO3))/Vfc²)-(((Vi*vHSO3c)-
(Vc*partmolvolHSO3))/Vic²)))];
activitycoeffSO3 = Exp[(4*FAC) + (2*B3*molalH)-(Bsum/Ionicstrength²)+(BRAC*LSO3) +
(1.5*SUML*((DIV*((Vf*vSO3c)-(Vc*partmolvolSO3))/Vfc²)-(((Vi*vSO3c)-
(Vc*partmolvolSO3))/Vic²)))];
```

```
activitycoeffSO2 = Exp[(2*lambdaSO2*molalSO2)+ (3*muSO2*molalSO2^2)+(SUML*DIV*(((-
1.5*partmolvolSO2*Vc)/Vfc^2)+(((Vf + (0.5*Vc))/Vfc)*(partmolvolSO2/Vm-
(DIV*(partmolvolSO2+alphaSO2))/Vm))))];
activityH2O = Exp[Mw*(((2*A)/3*Ionicstrength^1.5/(1 + 1.2*√Ionicstrength ))-
(2*molalH*(Bwater1*molalOH +Bwater2*molalHSO3+ Bwater3*molalSO3))-
(lambdaSO2*molalSO2^2)-(2*muSO2*molalSO2^3)-(molalH+molalOH+molalHSO3
+molalSO3+molalSO2)-(SUML*(((-
alphaSO2*molalSO2*DIV^2)/(do*Vm^2)*(Vf+(0.5*Vc))/Vfc)+((1.5*Vc*DIV)/(do*Vfc^2))-
((1.5*Vc)/(do*Vic^2)))))];


(α^o)1,1= 0;
(α^o)2,2 = 0;
(α^o)1,2 = 1.7;
(α^o)2,1 = 1.7;
c1=0.01;
c2 = 0.017;
αlp1 =3.1307;
αlp2 =  2.8730;
βeta1 =1161.7;
βeta2 =  1815.4;
γ1 =1.5589;
γ2 =  1.1043;
δ1 =0.593*10^-4;
δ2 =  2.721*10^-4;
(α^0)1=1.06;
(α^0)2=2.86;
(α^1)1=2.07;
(α^1)2=0.01;
(β^0)1=8.4;
(β^0)2=21.9;
(β^1)1=1153.3;
(β^1)2=1793.5;
R1 . atm = 0.082054;
Initguess = ((R1 . atm*T)/Pressure);
NVFUG = 2;
f1= 1;
PartpressureH2O =( (10^(7.96681-1668.21/(T-45.15)))/760);
PartpressureSO2 = Pressure - PartpressureH2O;
vapmolefracH2O = PartpressureH2O/Pressure;
vapmolefracSO2 = 1 -vapmolefracH2O;
y1 1= vapmolefracH2O;
y12 = vapmolefracSO2;
TOTY = y1 1+ y12;
y1 = y11/ TOTY;
y2 = y12/TOTY;
Tempa = T;
Pressa = Pressure;
Clear[V, ETA];
Do[b1 = Exp[2.30259*(-γi-δi*Tempa)];, {i, NVFUG}];
Do[
  Do[
    (β^0i,j)= 0.5*((β^0)i+(β^0)j);
    (β^1i,j)= Sqrt[(β^1)i*(β^1)j];
    If [i==j ,(βi,j)=βetai, (βi,j)= (β^0i,j)+ (β^1i,j)];
    (α^1i,j)= Sqrt[(α^1)i*(α^1)j];
    If [i==j ,(αi,j)=αlpi, (αi,j)= (α^o)i,j+ (α^1i,j)];
    ai,j= αi,j + (βi,j)/T;
    , {j,1, NVFUG}];
      , {i, 1,NVFUG}];
     NVFUG NVFUG
      ∑    ∑   yi * yj * ai,j
      i=1  j=1
aM =                  ;
     NVFUG
      ∑   yi * bi
      i=1
bM=          ;
      NVFUG
      ∑   yi * ci
      i=1
cM =         ;
ETA = bM/(4*V);

VLO = bM/(4*1.0000001);
```

```
VHI = Initguess * 100;
VIER = Solve[Pressure==(R1.atm*T)/V*((1+ETA+ETA^2-ETA^3)/(1-ETA)^3)-aM/(V(V+cM )), V];
Len = Length[VIER];
Do[Vsubs=V/.VIER[[subs]], {subs, 1, Len}];
V = Max[Table[Re[Vsubs], {subs, 1, Len}]];
z =( Pressure* V)/(R1.atm * T);
Do[fk= Exp[((4*ETA - 3*ETA^2)/(1-ETA)^2) +( bk/bM*((4*ETA - 2*ETA^2)/(1-ETA)^3))-(2/(R1.atm*T*V)*(
    Sum[yj * ak,j, {j=1, NVFUG}]
    ) *(Sum[(-1)^m/(m + 1) * (cM/V)^m, {m=1, 5}]
    +1))+((aM*ck)/(R1.atm*T*V^2)*(
    Sum[(-1)^m * (m + 1)/(m + 2) * (cM/V)^m, {m=1, 4}]
    +0.5))-Log[z]],
   {k,1, NVFUG}];

NVFUG = 1;
y1 1= 1;
y12 = 0;
TOTY = y1 1+ y12;
y1 = y11/ TOTY;
y2 = y12/TOTY;
Tempa = T;
Pressa = Pressure;
Clear[waterV, ETA];

Do[bi = Exp[2.30259*(-γi-δi*Tempa)];, {i, NVFUG}];
Do[
  Do[
    (β^0i,j)= 0.5*((β^0)i+(β^0)j);
    (β^1i,j)= Sqrt[(β^1)i*(β^1)j];
    If [i==j ,(βi,j)=βetai, (βi,j)= (β^0i,j)+ (β^1i,j)];
    (α^1i,j)= Sqrt[(α^1)i*(α^1)j];
    If [i==j ,(αi,j)=αlpi, (αi,j)= (α^o)i,j+ (α^1i,j)];
    ai,j= αi,j + (βi,j)/T;
    , {j,1, NVFUG}];
      , {i, 1,NVFUG}];
aM = Sum[Sum[yi * yj * ai,j, {j=1, NVFUG}], {i=1, NVFUG}];
bM= Sum[yi * bi, {i=1, NVFUG}];
cM = Sum[yi * ci, {i=1, NVFUG}];
Clear[waterV];
ETA = bM/(4*waterV);
BOX =( 1 + ETA + ETA^2+ETA^3)/(1-ETA)^3;
VVIER = Solve[Pressure == ((R1.atm*T)/waterV*BOX) - aM/(waterV*(waterV+cM)), waterV];

Len = Length[VVIER];
Do[waterVsubs=waterV/.VVIER[[subs]], {subs, 1, Len}];
waterV= Max[Table[Re[waterVsubs], {subs, 1, Len}]];
purez =( Pressure* waterV)/(R1.atm * T);
fpurewater= Exp[((4*ETA - 3*ETA^2)/(1-ETA)^2) +( b1/bM*((4*ETA - 2*ETA^2)/(1-ETA)^3))-(2/(R1.atm*T*waterV)*(
    Sum[yj * a1,j, {j=1, NVFUG}]
    ) *(Sum[(-1)^m/(m + 1) * (cM/waterV)^m, {m=1, 5}]
    +1))+((aM*c1)/(R1.atm*T*waterV)*(
    Sum[(-1)^m * (m + 1)/(m + 2) * (cM/waterV)^m, {m=1, 4}]
    +0.5))-Log[purez]];
fugcoeffpureH2O = f1purewater;
guesspartpressureH2O =( (10^(7.96681-1668.21/(T-45.15)))/760)*1;
Clear[vapmolefracSO2,vapmolefracH2O];
guessvapmolefracH2O = guesspartpressureH2O/Pressure;
guessvapmolefracSO2 = 1 - guessvapmolefracH2O;
guessmolesH2O = H2OIN;
guessmolalH = 0.9*10^-1;
guessmolalOH = KH2O/guessmolalH;
guessmolalSO2 = 0.05*(SO2IN);
guessmolalHSO3 =(KSO2*guessmolalSO2)/(guessmolalH);
guessmolalSO3 = (KHSO3*guessmolalHSO3)/(guessmolalH);
```

```
guessVaprate= 3;
S1=KH2O==(activitycoeffH * molalH *activitycoeffOH * molalOH)/(activityH2O);
S2 =KSO2 ==((activitycoeffH*molalH * activitycoeffHSO3 * molalHSO3)/(activitycoeffSO2
*molalSO2*activityH2O));
S3 =KHSO3== ((activitycoeffH*molalH * activitycoeffSO3 * molalSO3)/(activitycoeffHSO3
*molalHSO3));

(* Vapour liquid equilibria expressions labelled as book *)
S5 = vapmolefracH2O * f1 *Pressure ==activityH2O* PSH2O *
fugcoeffpureH2O*Exp[(partmolvolH2O *1000*(Pressure- PSH2O))/(R*T)];
S6 =  vapmolefracSO2 * f2 * Pressure == molalSO2*activitycoeffSO2*HenrySO2*
Exp[(partmolvolSO2 *1000*(Pressure- PSH2O))/(R*T)];

(*-------------------------------------------------------------------------------
----*)

(* other system equations*)

(* vapour phase balance *)
S8 = vapmolefracSO2 + vapmolefracH2O == 1;

(* sulphur balance *)
S9 = (molesH2O/55.51*(molalSO2 + molalHSO3 + molalSO3)) + (vapmolefracSO2*Vaprate) ==
SO2IN ;

(* hydrogen balance *)
S10 = (2*molesH2O) + (molesH2O/55.51*(molalH + molalOH + molalHSO3)) +
(2*vapmolefracH2O*Vaprate)==2*H2OIN ;

(* electroneutrality *)
S11 = molalH == (molalOH + molalHSO3 + (2*molalSO3));

Unknowns= FindRoot[
   {S1, S2, S3, S5,S6,S8, S9,S10,S11},
    {{molesH2O, guessmolesH2O,10}, {molalH, guessmolalH,1}, {molalOH,
guessmolalOH,1}, {molalSO2, guessmolalSO2,10}, {molalHSO3, guessmolalHSO3,1},
{molalSO3, guessmolalSO3,1}, {vapmolefracH2O, guessvapmolefracH2O,1},
{vapmolefracSO2, guessvapmolefracSO2,1}, {Vaprate,
guessVaprate,5}},Method→"Secant"];

molesH2O = molesH2O/.Unknowns;
molalH = molalH/.Unknowns;
molalOH = molalOH/.Unknowns;
molalSO2 = molalSO2/.Unknowns;
molalHSO3 = molalHSO3/.Unknowns;
molalSO3 = molalSO3/.Unknowns;
vapmolefracH2O = vapmolefracH2O/.Unknowns;
vapmolefracSO2 = vapmolefracSO2/.Unknowns;
Vaprate= Vaprate/.Unknowns;
molalHSO4=molalHSO3;
molalSO4=molalSO3;
vapmolefracO2=1-vapmolefracH2O-vapmolefracSO2+0.01;
molalSO2aq=molalSO3+molalHSO3-.1;
molalSO3aq=molalSO3*0.001;
molalH2SO4aq=molalHSO4+molalSO4+.02;



(*-----------Do Not Clear Variables------------*)
(*
(* Clear the values for Vapour Mole Fractions *)
Clear[vapmolefracO2, vapmolefracSO3, vapmolefracSO2, vapmolefracH2SO4,
vapmolefracH2O];
(* Clear the values for Ion Mole values *)
Clear[molalH, molalOH, molalHSO3, molalHSO4, molalSO3, molalSO4];
(* Clear the values for Liquid Mole values *)
Clear[molesSO2, molesH2O, molesO2, molesSO3, molesH2SO4, molalSO3aq, molalSO2aq,
molalH2SO4aq];
(* Clear the values for K Values *)
Clear[KH2O, KH2SO4, KHSO4, KH2SO4G, KSO3, KSO2,KHSO3];
(* Clear the values for Partial Molar Volumes*)
Clear[partmolvolH2SO4, partmolvolH2O, partmolvolO2, partmolvolSO3,  partmolvolSO2];
(* Clear the values for Partial Pressures*)
Clear[vapmolefracH2SO4, vapmolefracH2O, vapmolefracO2,  vapmolefracSO3,
vapmolefracSO2]
(* Clear the values for the other necessary variables*)
```

```
Clear[ρ,Subst,Vaprate, IonicStrength,Totpress, TotalMolalH2SO4, TotalMolalSO2,
TotalMolalSO3];*)

Pressure = Barpressure * 0.987;
T=TCel + 273.15;
guesspartpressureH2O =Pressure*.1;
guesspartpressureSO2 =Pressure*.5*SO2IN;
guesspartpressureO2 = Pressure - (guesspartpressureH2O +
guesspartpressureSO2+guesspartpressureH2SO4 );
guesspartpressureH2SO4 =Pressure*.01*H2SO4IN;

(*---------------------Define Constants-----------------------------------------*)

If[(T-273)≤50,do = (1.0-4.8*10^-6*(T-273)^2)];
If[(T-273)>50, do = (1.0064-(2.5*10^-4*(T-273))-(2.3*10^-6*(T-273)^2))];(*Density of
Water*)
alphaSO2 = -0.030;
alphaSO3 = -0.030;(*added*)
alphaH2SO4 = -0.030;(*added*)
elec = 4.8029*10^-10;
Dielec = 305.7*Exp[-Exp[-12.741+0.01875*T]-(T/219)];
k =1.38045*10^-16;(*Boltzmann Constant*)
Mw = 0.01802;(*MW of Water*)
Na = 6.0232*10^23;(*Avogadros Number*)
PSH2O = (10^(7.96681-1668.21/(T-45.15)))/760;(*Vapour Pressure of Water*)
R = 82.06;(*Gas Constant, need units*)

(*Ionic Radius - Check Numbers of sulfate and bisulfate*)
rH = 3.8;
rHSO3 = 2.7;
rOH = 3.5;
rSO3 = 2.8;
rHSO4 = 2.7;
rSO4 = 2.8;

(*Electric Charge*)
zH = 1;
zHSO3 = -1;
zOH = -1;
zSO3 = -2;
zHSO4 = -1;
zSO4 = -2;
(*-------------------------------------------------------------*)
(*-------------------------------------------------------------*)

(* Calculation of equilibrium constants for liquid phase reactions
The order is the following:
1=SO2 dissociation
2=Water hydrolysis
3=Bisulphite formation
4=Sulphuric Acid Strong dissociation
5=Bisulfate formation
6=Sulfuric acid formation
*)
(* Substituted K values for values within property databanks *)
(*
Subst = {KSO2, KH2O, KHSO3, KH2SO4, KHSO4, KSO3, KH2SO4G};
kvalA = {-3768, -13445.9, 1333.4,1333.4,1333.4,1333.4,1333.4};
kvalB = {-20,-22.4773,0,0,0,0,0};
kvalC={0.0,0 , 0,0,0,0,0};
kvalD={122.53, 140.932, -21.274, -21.274, -21.274, -21.274, -21.274};
Kvalue = Exp[(kvalA/T)+(kvalB*Log[T]) + (kvalC*T)+kvalD];

(*Print["Equilibrium constants for liquid phase reactions"]*)

KSO2 =Kvalue[[1]];
KH2O = Kvalue[[2]];
KHSO3 =Kvalue[[3]];
KH2SO4 =Kvalue[[4]];
KHSO4 =Kvalue[[5]];
KSO3 =Kvalue[[6]];
KH2SO4G =Kvalue[[7]];

*)
(*These values are fitted from the HSC rate bank - Reaction Equations - Correct if
needed*)
KSO2 =N[3*10^(-6)*TCel*TCel-0.0006*TCel+0.0292];
```

```
KH2O =N[9*10^(-17)*TCel*TCel-5*10^(-15)*TCel+9*10^(-14)];
KHSO3 =N[3*10^(-12)*TCel*TCel-1*10^(-9)*TCel+9*10^(-8)];
KH2SO4 =N[3*10^(12)*Exp[-0.089*TCel]];
KHSO4 =N[2*10^(-6)*TCel^2-0.0004*TCel+0.0183];
KSO3 =N[9*10^(-15)*Exp[0.1245*TCel]];(*Formation of acid under trioxide dissolution*)
KH2SO4G =N[3*10^(-11)*Exp[0.111*TCel]];

(*-----------------------------------------------------------------*)
(*Calculation of ionic quantities for activity coefficient calculation*)
(*
litwater=H2OIN*Mw/do;
Print["Liters of water: ", litwater];
contribH1=Sqrt[KH2O];
molalO2=Sqrt[KH2O];
molalHSO3=

*)



(*-----------------------------------------------------------------*)
(*Calculation of Henry's constant for Subscript[SO, 2]*)

HenvalA =6211.22;
HenvalB = 60.239;
HenvalC = -0.102974;
HenvalD = -333.362;

HenrySO2 = Exp[(HenvalA/T)+(HenvalB*Log[T]) + (HenvalC*T) + HenvalD];
(*Print["Calculated Henry's Constant = ", HenrySO2];*)

(*-------------------------------------------------------------------------*)
(*Calculation of Henry's constant for Subscript[SO, 3] - INCORRECT VALUES*)

HenvalA =6211.22;
HenvalB = 60.239;
HenvalC = -0.102974;
HenvalD = -333.362;

HenrySO3 = Exp[(HenvalA/T)+(HenvalB*Log[T]) + (HenvalC*T) + HenvalD];

(*-------------------------------------------------------------------------*)
(*Calculation of Henry's constant for Subscript[H, 2] Subscript[SO, 4] - INCORRECT
VALUES*)

HenvalA =6211.22;
HenvalB = 60.239;
HenvalC = -0.102974;
HenvalD = -333.362;

HenryH2SO4 = Exp[(HenvalA/T)+(HenvalB*Log[T]) + (HenvalC*T) + HenvalD];


(*-------------------------------------------------------------------------*)

(* Calculation of Henry's Constant for O2 *)

KHdash = Exp[1/(8.3144*T) ((0.046*T^2)+(203.357*T*Log[T/298])-((299.378+0.092*T)*(T-
298))-20.591*10^3)];
HenryO2 = 1/KHdash;
(*
Print["Calculated Henry's Constant = ", HenryH2SO4];
Print["Calculated Henry's Constant Subscript[O, 2] = ", HenryO2];
Print["Calculated Henry's Constant = ", HenrySO3];

*)
(* ------------------------------------------------------------------------ *)

(*Brelvi & O'Connell Correlation for Partial Molar volume*)

(* vsubso = partial molar volume at infinite dilution, cm^3/g mole (Overscript[v,
_]^o);
R = gas constant, 82.06  atm cm^3/g mole K (R);
T = Temperature, Kelvins;
C12subso = reduced volume integral of the molecular direct correlation function
Subscript[c, ij] at infinite dilution (Subscript[C, 12]^o);
```

```
K2subso = isothermal compressibility at infinite dilution, atm^-1 (Subscript[K,
2]^o);
vistar = characteristic volume of i, cm^3/g mole.  For nonpolar species the critical
volume, Subscript[v, c], may be used; experimental compressibility data may be used
to determaine v^* for polar compounds. (Subscript[v, i]^*);
rho = pure solvent density, g mole/cm^3 (ρ);
rhotil = reduced density = Subscript[ρv, 2]^* (Overscript[ρ, ~]); *)
(* the numbers 1 2 and 3 are the opposite way round to the book *)

(* 1 - water           *)
(* 2 - sulphur dioxide *)
(* 3 - oxygen *)
(* 4 - sulphur trioxide *)
(* 5 - sulfuric acid *)

(*vstar and molecular weight Linear Solution - see Vstar Calculation*)
(*END vstar and molecular weight Linear Solution*)

(* vstar values from Zemaitis *)
vstar1= 46.4;
vstar2= 115.0;
vstar3 = 74.4;
vstar4= 132;
vstar5= 154;

(* the molar volume of water is calculated using this equation *)
vmolwater = 18.02*(1.001508+3.976412*10^-6*(T-273.15)^2);

(*Calculation of density of water using equation from Handbook*)
If[(T-273)≤50,ρ = 1.0-4.8*10^-6*(T-273)^2];
If[(T-273)>50, ρ = 1.0064-(2.5*10^-4*(T-273))-(2.3*10^-6*(T-273)^2)];

Clear[C12subso, solution, solution1, solution2, K, partmolvol];
rhotil = ρ/18.012*46.4;

solution1 =Solve[Log[1 +18.02/((ρ)*K*R*T)]==(-0.42704*(rhotil-1)+2.089*(rhotil-1)^2-
0.42367*(rhotil-1)^3), K];

Flatten[solution1];
K = K/.solution1[[1]];

If[2≤rhotil≤2.785, series= -2.4467+ 2.12074*rhotil, "outside range"];

If[2.785≤rhotil≤3.2, series = 3.02214 - 1.87085*rhotil+0.71955*rhotil^2, "outside
range"];

For[i=2, i<6, ivalue = i;
 C12subso = (Subscript[vstar, ivalue]/46.4)^0.62*(-Exp[series]);
 vmol ivalue= K*R*T*(1-C12subso);
 i++]

partmolvolSO2aq = vmol2/1000;
partmolvolSO2 = vmol2/1000;
partmolvolH2O = vmolwater/1000;
partmolvolO2 = vmol3/1000;
partmolvolSO3aq = vmol4/1000;
partmolvolH2SO4 = vmol5/1000;

(*Print["Calculated partial molar volumes"]
Print["Partial molar volume of SO2 = ", partmolvolSO2, " dm3/mol"]
Print["Partial molar volume of H2O = ", partmolvolH2O, " dm3/mol"]
Print["Partial molar volume of O2 = ", partmolvolO2, "dm3/mol"]
Print[]
Print["in zemaitis the henry's law equation says these should be in dm3 per mole but
then in the calculations they give cm3 per mole and analysis of the exponential term
would indicate that cm3 mol is the appropriate unit, need to calculate in dm3 for the
activity coefficient equations though"]
Print[]*)

(* rest of partial molar volumes from table in appendix 9.1 Zemaitis - Check Partial
Molar Volumes*)
partmolvolH = -0.0047;
partmolvolHSO3 = 0.035;
partmolvolOH = 0.0005;
partmolvolSO3 = 0.0197;
partmolvolHSO4 = 0.035*1.2;
```

```
partmolvolSO4 = 0.035*1.2;
(* partial molar volume of oxygen in water from Bignell J Phys Chem 1984, 88, 5409 -
5412 *)

partmolvolO2bignell = (31.73 - 0.0919*TCel + 0.00267*(TCel^2))/1000;
(*
Print["Partial molar volume of O2 from bignell = ", partmolvolO2bignell, " m^3 mol^-
1"];
*)

(* Bignells paper had an incorrect unit the value given by Brelvi and O'Connell is in
the right unit *)
(* partial molar volume is the contribution that a component makes to the total
volume of a sample partial molar volume of a substance A in a mixture is the change
in volume on the addition of 1 mol A to a large excess of the mixture *)
(* Zhou and Battino gave the partial molar volume of oxygen as 32 cm3 mol-1 *)
(*-------------------------------------------------------------*)

(* Calculation of fugacity coefficients for each species using Nakamura equation of
state *)
(*<<Miscellaneous`RealOnly`*)
(* Define constants;  1 = water, 2 = sulphur dioxide 3 = oxygen , 4 = sulfur
trioxide, 5 = sulphuric acid
THESE ARE ALL FAKE*)

(α^o)1,1= 0;
(α^o)1,2 = 1.7;
(α^o)1,3 = 2.19;
(α^o)1,4 = 2.19;
(α^o)1,5 = 2.19;

(α^o)2,1 = 1.7;
(α^o)2,2 = 1;
(α^o)2,3 = 2;
(α^o)2,4 = 1;
(α^o)2,5 =1;

(α^o)3,1 = 2.19;
(α^o)3,2 = 2;
(α^o)3,3 = 2;
(α^o)3,4 = 2;
(α^o)3,5 = 2;

(α^o)4,1 = 2;
(α^o)4,2 = 2;
(α^o)4,3 = 2;
(α^o)4,4 = 4;
(α^o)4,5 = 4;

(α^o)5,1 = 3;
(α^o)5,2 = 3;
(α^o)5,3 = 3;
(α^o)5,4 = 4;
(α^o)5,5 = 5;

c1=0.01;
c2 = 0.017;
c3 = 0;
c4 = .017;
c5 = 0;

αlp1 =3.1307;
αlp2 =  2.8730;
αlp3 =  1.5324;
αlp4 =  1.5324;
αlp5 =  1.5324;

βeta1 =1161.7;
βeta2 =  1815.4;
βeta3 =  8.56;
βeta4 =  8.56;
βeta5 =  8.56;

γ1 =1.5589;
```

```
γ2 =  1.1043;
γ3 =  1.2458;
γ4 =1.5589;
γ5 =1.5589;

δ1 =0.593*10^-4;
δ2 =  2.721*10^-4;
δ3 = 1.199*10^-4;
δ4 = 1.199*10^-4;
δ5 = 1.199*10^-4;

(* nonpolar and polar contributions *)

(α^0)1=1.06;
(α^0)2=2.86;
(α^0)3=1.5324;
(α^0)4=1.5324;
(α^0)5=1.5324;

(α^1)1=2.07;
(α^1)2=0.01;
(α^1)3=0.0;
(α^1)4=0.0;
(α^1)5=0.0;

(β^0)1=8.4;
(β^0)2=21.9;
(β^0)3=8.56;
(β^0)4=8.56;
(β^0)5=8.56;

(β^1)1=1153.3;
(β^1)2=1793.5;
(β^1)3=0;
(β^1)4=0;
(β^1)5=0;

(* ---------------- Calculation of fugacity coefficients ---------------------- *)

R1 . atm = 0.082054;
Initguess = ((R1 . atm*T)/Pressure);
NVFUG = 5;
(* 1 = water, 2 = sulphur dioxide, 3 = oxygen , 4= SO3, 5=H2SO4*)

guessvapmolefracH2O = guesspartpressureH2O/Pressure;
guessvapmolefracSO2 = guesspartpressureSO2/Pressure;
guessvapmolefracO2 = guesspartpressureO2/Pressure;
guessvapmolefracSO3 = guesspartpressureSO2/Pressure*.075;
guessvapmolefracH2SO4 = guesspartpressureH2SO4/Pressure;

y11= guessvapmolefracH2O;
y12 = guessvapmolefracSO2;
y13 = guessvapmolefracO2;
y14 = guessvapmolefracSO3;
y15 = guessvapmolefracH2SO4;

TOTY = y1 1+ y12 + y13+y14+y15;

y1 = y11/ TOTY;
y2 = y12/TOTY;
y3=y13/TOTY;
y4=y14/TOTY;
y5=y15/TOTY;

Tempa = T;
Pressa = Pressure;
Clear[V, ETA];
Do[bi = Exp[2.30259*(-γi-δi*Tempa)];, {i, NVFUG}];

Do[
  Do[
    (β^0i,j)= 0.5*((β^0)i+(β^0)j);
    (β^1i,j)= Sqrt[(β^1)i*(β^1)j];
    If [i==j ,(βi,j)=βetai, (βi,j)= (β^0i,j)+ (β^1i,j)];
```

```
    (α^1i,j)= Sqrt[(α^1)i*(α^1)j];
    If [i==j ,(αi,j)=αlpi, (αi,j)= (α^o)i,j+ (α^1i,j)];
    ai,j= αi,j + (βi,j)/T;
    , {j,1, NVFUG}];
      , {i, 1,NVFUG}];
```

$$a_M = \frac{\sum_{i=1}^{NVFUG}\sum_{j=1}^{NVFUG} y_i * y_j * a_{i,j}}{}\ ;$$

$$b_M = \frac{\sum_{i=1}^{NVFUG} y_i * b_i}{}\ ;$$

$$c_M = \frac{\sum_{i=1}^{NVFUG} y_i * c_i}{}\ ;$$

```
ETA = bM/(4*V);


VLO = bM/(4*1.0000001);
VHI = Initguess * 100;

(*
Print["Initial Guess for Molar Volume from ideal gas law = ", Initguess];
Print["Molar volume boundary"];
Print["Possible highest value = ", VHI];
Print["Possible lowest value = ", VLO];
Print[];
*)

VIER = Solve[Pressure==(R1 . atm*T)/V*((1+ETA+ETA^2-ETA^3)/(1-ETA)^3)-aM/(V(V+cM )), V];

Len = Length[VIER];
Do[Vsubs=V/.VIER[[subs]], {subs, 5, Len}];
Vsol = Table[Vsubs, {subs, 5, Len}];
Vsol;
V  = Max[Vsol];
z =( Pressure* V)/(R1 . atm * T);

Do[fk= Exp[((4*ETA - 3*ETA^2)/(1-ETA)^2) +( bk/bM*((4*ETA - 2*ETA^2)/(1-ETA)^3))-(2/(R1 .
```

$$\text{atm}*T*V)*\left(\sum_{j=1}^{NVFUG} y_j * a_{k,j}\right) * \left(\sum_{m=1}^{5} \frac{(-1)^m}{m+1} * \left(\frac{c_M}{V}\right)^m\right.$$

```
+1))+((aM*ck)/(R1 . atm*T*V^2)*(
```

$$\left.\sum_{m=1}^{4} \frac{(-1)^m * (m+1)}{(m+2)} * \left(\frac{c_M}{V}\right)^m\right.$$

```
+0.5))-Log[z]],
   {k,1, NVFUG}];
(*
Print["molar volume = ", V, " l/mole"]
Print ["fugacity coefficient of water = ",Subscript[f, 1]];
Print["Fugacity coefficient of sulphur dioxide = ", Subscript[f, 2]];
Print["Fugacity coefficient of oxygen = ", Subscript[f, 3]];
Print["Fugacity coefficient of SO3 = ", Subscript[f, 4]];
Print["Fugacity coefficient of H2SO4 = ", Subscript[f, 5]];
*)

(* ----------------------------------------*)
(* ----------------------------------------*)
(* calculation of pure water fugacity using Nakamura equation of state *)
(* 1 = water, 2 = nothing *)
NVFUG = 1;

y1 1= 1;
y12 = 0;
TOTY = y1 1+ y12;
y1 = y11/ TOTY;
y2 = y12/TOTY;

Tempa = T;
Pressa = Pressure;

Clear[waterV, ETA];

Do[bi = Exp[2.30259*(-γi-δi*Tempa)];
```

```
  (*Print[SubscriptBox["b",i]//DisplayForm, " = ",Subscript[b, i] ];*), {i, NVFUG}];

Do[
  Do[
    (β^0i,j)= 0.5*((β^0)i+(β^0)j);
    (β^1i,j)= Sqrt[(β^1)i*(β^1)j];
    If [i==j ,(βi,j)=βetai, (βi,j)= (β^0i,j)+ (β^1i,j)];
    (α^1i,j)= Sqrt[(α^1)i*(α^1)j];
    If [i==j ,(αi,j)=αlpi, (αi,j)= (α^o)i,j+ (α^1i,j)];
    ai,j= αi,j + (βi,j)/T;
    , {j,1, NVFUG}];
      , {i, 1,NVFUG}];
```

$$a_M = \frac{\sum_{i=1}^{NVFUG}\sum_{j=1}^{NVFUG} y_i * y_j * a_{i,j}}{}\ ;$$

$$b_M = \frac{\sum_{i=1}^{NVFUG} y_i * b_i}{}\ ;$$

$$c_M = \frac{\sum_{i=1}^{NVFUG} y_i * c_i}{}\ ;$$

```
Clear[waterV]
ETA = bM/(4*waterV);
BOX =( 1 + ETA + ETA^2+ETA^3)/(1-ETA)^3;
VVIER = Solve[Pressure == ((R1 . atm*T)/waterV*BOX) - aM/(waterV*(waterV+cM)), waterV];

Len = Length[VVIER];
Do[waterVsubs=waterV/.VVIER[[subs]], {subs, 5, Len}];
Vsol = Table[waterVsubs, {subs,5, Len}];
waterV  = Max[Vsol];

(* Calculation of compressibility factor*)

purez =( Pressure* waterV)/(R1 . atm * T);
```

$$f_{purewater} = \text{Exp}[((4*ETA - 3*ETA^2)/(1-ETA)^2) + (b_1/b_M*((4*ETA - 2*ETA^2)/(1-ETA)^3))-(2/(R_{1\ .\ atm}*T*waterV)*(\sum_{j=1}^{NVFUG} y_j * a_{1,j}) *(\sum_{m=1}^{5} \frac{(-1)^m}{m+1} * \left(\frac{c_M}{waterV}\right)^m +1))+((a_M*c_1)/(R_{1\ .\ atm}*T*waterV)*(\sum_{m=1}^{4} \frac{(-1)^m * (m+1)}{(m+2)} * \left(\frac{c_M}{waterV}\right)^m +0.5))-\text{Log}[purez]];$$

```
fugcoeffpureH2O = f1purewater;
(*Print["fugacity coefficient for pure water = ", fugcoeffpureH2O]*)
(* ---------------------------------------------------------------------- *)
(* Calculation of activity coefficient of oxygen in sulphur dioxide electrolyte
solution from UEA paper Clegg and Brimblecombe
Modify with sulphuric Acid and Sulfur Trioxide*)

λO2,H= -0.2379 + 81.450/T;

λO2,OH= 0.93318 - 430.552/T+49860.8/T^2;

λO2,HSO3= (15.571/T)/2;

λO2,SO3= 15.571/T;

ζO2,H,OH=0;
ζO2,H,HSO3=0;
ζO2,H,SO3=0;

activitycoeffO2 = Exp[(2*molalH*λO2,H) +2*((molalOH*λO2,OH) +(molalHSO3 *
λO2,HSO3)+(molalSO3 *λO2,SO3))+((molalH*molalOH*ζO2,H,OH)+
(molalH*molalHSO3*ζO2,H,HSO3)+(molalH*molalSO3 * ζO2,H,SO3))];
(* ionic strength *)
IonicStrength =0.5*(molalH + molalOH + molalHSO3 + 4*molalSO3+4*molalSO4+molalHSO4);
(*
Print["Ionic strength = ", IonicStrength];
*)
```

```
(*-------------------------------------------------------------------*)

(*-------------------------------------------------------------------*)
(* The Debye-Huckel constant, A, is calculated as follows *)
A = (2 * π * Na * do / 1000)^(1/2) * (elec^2 / (Dielec * k * T))^(3/2) ;
(*
Print["Debye-Huckel constant A = ", A];
*)
(* Debye-Huckel term *)

FAC=(-(A/3))*(√IonicStrength /(1+1.2*√IonicStrength )+2.0/1.2*Log[1+1.2*
√IonicStrength ]);
(*
Print["Debye-Huckel term FAC = ", FAC];
*)
(*-------------------------------------------------------------------*)
(*-------------------------------------------------------------------*)
(*ion-ion interactions using standard Pitzer terms*)

Clear[Bi, Bypi, Bwateri];

(* species specific coefficients (water-sulphur dioxide system) values in order,
H+OH-, H+HSO3-, H+SO3- , H+HSO4-, H+SO4--
INCORRECT DATA - MODIFY!*)

Beta0 = {0.04, 0.06, 0.12, .02, .02};
Beta1 = {0.12, 0.54, 1.08, .02, .02};
ion= {1,2,3, 4, 5};

Bi[Beta0_, Beta1_, ion_] := (Beta0) + (Beta1)/(2*IonicStrength)*(1-
(1+2*Sqrt[IonicStrength])*Exp[-2*Sqrt[IonicStrength]]);

Bypi [Beta0_, Beta1_, ion_] :=(Beta1)*(1-
(1+2*Sqrt[IonicStrength]+2*IonicStrength)*Exp[(-2*Sqrt[IonicStrength])]);

Bwateri [Beta0_, Beta1_, ion_] := Beta0 +Beta1*Exp[-2*Sqrt[IonicStrength]];

Bi = Bi[Beta0, Beta1, ion];
Bypi = Bypi[Beta0, Beta1, ion];
Bwateri = Bwateri[Beta0, Beta1, ion];

B1 = Bi[[1]];
Byp1 = Bypi[[1]];
Bwater1 = Bwateri[[1]];

B2 = Bi[[2]];
Byp2 = Bypi[[2]];
Bwater2 = Bwateri[[2]];

B3 = Bi[[3]];
Byp3 = Bypi[[3]];
Bwater3 = Bwateri[[3]];

B4 = Bi[[4]];
Byp4 = Bypi[[4]];
Bwater4 = Bwateri[[4]];

B5 = Bi[[5]];
Byp5 = Bypi[[5]];
Bwater5 = Bwateri[[5]];

Bsum =
2*molalH*((molalOH*Byp1)+(molalHSO3*Byp2)+(molalSO3*Byp3)+(molalHSO4*Byp4)+(molalSO4*
Byp5));

(*-------------------------------------------------------------------------*)
(*ion molecule interaction coefficients from dielectric effects*)
do;
(*
Print["Density of water = ", do, " kg/dm^3"]
*)
```

```
(* a. volume of neutral solution excluding ions, dm^3/kg of Subscript[H, 2]O  / NOTE
THAT THERE IS NO H2SO4!*)
Vm = (1/do)+molalSO2aq*partmolvolSO2+molalSO3aq*partmolvolSO3aq;

(* b. volume of ionic solution excluding neutral solutes, dm^3/kg Subscript[H, 2]O *)
Vi = (1/do)+(molalH*partmolvolH) +(molalOH*partmolvolOH)+ (molalHSO3*partmolvolHSO3)+
(molalSO3*partmolvolSO3)+(molalSO4*partmolvolSO4)+(molalHSO4*partmolvolHSO4);

(* c. volume of ionic cavities for ion i, dm/mole *)
vHc = (4/3)*π*Na*(rH^3)*(10^-27);
vOHc = (4/3)*π*Na*(rOH^3)*(10^-27) ;
vHSO3c =  (4/3)*π*Na*(rHSO3^3)*(10^-27);
vSO3c =  (4/3)*π*Na*(rSO3^3)*(10^-27);
vHSO4c =  (4/3)*π*Na*(rHSO4^3)*(10^-27);
vSO4c =  (4/3)*π*Na*(rSO4^3)*(10^-27);

(* d. volume of all ionic cavities, dm^3/kg Subscript[H, 2]O *)
Vc = (molalH*vHc) + (molalOH * vOHc) +
(molalHSO3*vHSO3c)+(molalSO3*vSO3c)+(molalSO4*vSO4c)+(molalHSO4*vHSO4c);

(* e. volume of real solution dm^3/kg Subscript[H, 2]O *)
Vf = Vi+(molalSO2aq*partmolvolSO2)+(molalSO3aq*partmolvolSO3aq);
(*-------------------------------------------------------------------------------
*)
(* molecule molecule interactions + CORRECT FOR SO3-SO3 and O2-O2?*)
(*lambdaSO2 = 0.0275+(0/T)*)
lambdaSO2 = -0.05+(0/T);
muSO2 = -(1/55.5)*(lambdaSO2+(1/166.5));

(*SAME LAMBDA WITH SO2*)
lambdaSO3 = -0.05+(0/T);
muSO3 = -(1/55.5)*(lambdaSO3+(1/166.5));
muH2SO4=muSO3*3;
(* What is this haha get rid of this!*)
(*--------------Dielectric constant of soln without ions-------------------------*)
Ds = Dielec*(1+(((alphaSO2*molalSO2aq)+(alphaSO3*molalSO3))/Vm));
(* ------------------------------------------------------------------ *)
vapmolefracH2SO4=vapmolefracSO2*.1;
vapmolefracSO3=vapmolefracSO2*01;

(*-------------------------------------------------------------------------------*)
(*dimensionless constant of dielectric contribution of ion i in activity
coefficient*)

LH = ((elec^2)* (zH^2))/(2*rH*k*T*Dielec)*(10^8);

LHSO3 = ((elec^2)* (zHSO3^2))/(2*rHSO3*k*T*Dielec)*(10^8);

LOH = ((elec^2)* (zOH^2))/(2*rOH*k*T*Dielec)*(10^8);

LSO3 = ((elec^2)* (zSO3^2))/(2*rSO3*k*T*Dielec)*(10^8);

LHSO4 = ((elec^2)* (zHSO4^2))/(2*rHSO4*k*T*Dielec)*(10^8);

LSO4 = ((elec^2)* (zSO4^2))/(2*rSO4*k*T*Dielec)*(10^8);

(*-------------------------------------------------------------------------------*)
(*Definition of terms often used to simplify the activity coefficient equations*)

DIV = Dielec/Ds;
Vfc = Vf - Vc;
Vic = Vi - Vc;
SUML = (molalH*LH)+ (molalOH*LOH)+ (molalHSO3*LHSO3)+(molalSO3*LSO3);
BRAC = (DIV * molalSO2aq)*(-alphaSO2/Vm*(Vi+(0.5*Vc))/Vic-
(1.5*partmolvolSO2*Vc)/(Vic*Vfc));

(*-----------------------------------OXYGEN-------------------------------------*)
Calcppoxygen = vapmolefracO2 * Barpressure;
PartialO2bar = Calcppoxygen;
PartialO2atm = PartialO2bar * 0.987;
T =TCel + 273.15;
conc = PartialO2atm*Exp[1/(8.3144*T) ((0.046*T^2)+(203.357*T*Log[T/298])-
((299.378+0.092*T)*(T-298))-20.591*10^3)];

(*-------------------------------------------------------------------------------*)
(*ERASE AFTER THIS : DEBUGGING AREA*)
```

```
activitycoeffH = Exp[FAC+2*((molalOH*B1)+(molalHSO3*B2)+(molalSO3*B3))-
(Bsum/(4*IonicStrength^2))+(BRAC*LH) + (1.5*SUML*((DIV*((Vf*vHc)-
(Vc*partmolvolH))/Vfc^2)-(((Vi*vHc)-(Vc*partmolvolH))/Vic^2)))];

(*-------------------------------------------------------------------------------
*)
(* OH- hydroxide ion activity coefficient *)
activitycoeffOH = Exp[FAC + (2*B1*molalH)-(Bsum/(4*IonicStrength^2))+(BRAC*LOH) +
1.5*SUML*(DIV*((Vf*vOHc)-(Vc*partmolvolOH))/Vfc^2-((Vi*vOHc)-(Vc*partmolvolOH))/Vic^2)];

(*-------------------------------------------------------------------------------
*)
(* HSO4- bisulphate ion activity coefficient - CORRECT?*)
activitycoeffHSO4= Exp[FAC + (2*B2*molalH)-(Bsum/(4*IonicStrength^2))+(BRAC*LHSO4) +
(1.5*SUML*((DIV*((Vf*vHSO4c)-(Vc*partmolvolHSO4))/Vfc^2)-(((Vi*vHSO4c)-
(Vc*partmolvolHSO4))/Vic^2)))];
(*-------------------------------------------------------------------------------
*)
(* HSO3- bisulphite ion activity coefficient *)
activitycoeffHSO3 = Exp[FAC + (2*B2*molalH)-(Bsum/(4*IonicStrength^2))+(BRAC*LHSO3) +
(1.5*SUML*((DIV*((Vf*vHSO3c)-(Vc*partmolvolHSO3))/Vfc^2)-(((Vi*vHSO3c)-
(Vc*partmolvolHSO3))/Vic^2)))];

(*-------------------------------------------------------------------------------
*)
(* SO3-- sulphite ion activity coefficient *)
activitycoeffSO3 = Exp[(4*FAC) + (2*B3*molalH)-(Bsum/IonicStrength^2)+(BRAC*LSO3) +
(1.5*SUML*((DIV*((Vf*vSO3c)-(Vc*partmolvolSO3))/Vfc^2)-(((Vi*vSO3c)-
(Vc*partmolvolSO3))/Vic^2)))];

(*-------------------------------------------------------------------------------
*)
(* SO4-- Sulphate Ion activity coefficient *)
activitycoeffSO4 = Exp[(4*FAC) + (2*B3*molalH)-(Bsum/IonicStrength^2)+(BRAC*LSO4) +
(1.5*SUML*((DIV*((Vf*vSO4c)-(Vc*partmolvolSO4))/Vfc^2)-(((Vi*vSO4c)-
(Vc*partmolvolSO4))/Vic^2)))];
(*-------------------------------------------------------------------------------
*)
(*SO2 Sulphur dioxide activity coefficient*)
activitycoeffSO2 = Exp[(2*lambdaSO2*molalSO2aq)+ (3*muSO2*molalSO2aq^2)+(SUML*DIV*(((-
1.5*partmolvolSO2aq*Vc)/Vfc^2)+(((Vf + (0.5*Vc))/Vfc)*(partmolvolSO2aq/Vm-
(DIV*(partmolvolSO2aq+alphaSO2))/Vm))))];
(*-------------------------------------------------------------------------------
*)
(*SO3 Sulphur trioxide activity coefficient*)
activitycoeffSO3aq = Exp[(2*lambdaSO3*molalSO3aq)+
(3*muSO3*molalSO3aq^2)+(SUML*DIV*(((-1.5*partmolvolSO3aq*Vc)/Vfc^2)+(((Vf +
(0.5*Vc))/Vfc)*(partmolvolSO3aq/Vm-(DIV*(partmolvolSO3aq+alphaSO3))/Vm))))];
(*-------------------------------------------------------------------------------
*)
(*H2SO4 Sulfuric Acid activity coefficient*)
activitycoeffH2SO4 = Exp[ (3*muH2SO4*molalH2SO4aq^2)+(SUML*DIV*(((-
1.5*partmolvolH2SO4*Vc)/Vfc^2)+(((Vf + (0.5*Vc))/Vfc)*(partmolvolH2SO4/Vm-
(DIV*(partmolvolH2SO4+alphaH2SO4))/Vm))))];
(*-------------------------------------------------------------------------------
*)
(* Water activity *)
activityH2O = Exp[Mw*(((2*A)/3*IonicStrength^1.5/(1 + 1.2*Sqrt[IonicStrength]))-
      (2*molalH*(Bwater1*molalOH +Bwater2*molalHSO3+
Bwater3*molalSO3+Bwater4*molalHSO4+Bwater5*molalSO4))
      -(lambdaSO2*molalSO2aq^2)-(lambdaSO3*molalSO3^2)
      -(2*muSO2*molalSO2aq^3)-(2*muSO3*molalSO3^3)
      -(molalH+molalOH+molalHSO3 +molalSO3+molalSO2aq)-(SUML*(((-
alphaSO2*molalSO2aq*DIV^2)/(do*Vm^2)*(Vf+(0.5*Vc))/Vfc)+((1.5*Vc*DIV)/(do*Vfc^2))-
((1.5*Vc)/(do*Vic^2)))))];


(*-------------------------------------------------------------------------*)



(* Liquid phase reaction equations labelled as book *)
S1=KH2O==(activitycoeffH * molalH *activitycoeffOH * molalOH)/(activityH2O);
S2 =KSO2 ==((activitycoeffH*molalH * activitycoeffHSO3 * molalHSO3)/(activitycoeffSO2
*molalSO2aq*activityH2O));
```

```
S3 =KHSO3== ((activitycoeffH*molalH * activitycoeffSO3 * molalSO3)/(activitycoeffHSO3
*molalHSO3));
S4 =KHSO4== ((activitycoeffH*molalH * activitycoeffSO4 * molalSO4)/(activitycoeffHSO4
*molalHSO4));
S5= KH2SO4 == ((activitycoeffH*molalH * activitycoeffHSO4 *
molalHSO4)/(activitycoeffH2SO4 *molalH2SO4aq*activityH2O));
S6= KSO3 == ((activitycoeffH2SO4 * molalH2SO4aq)/(activitycoeffSO3aq
*molalSO3aq*activityH2O));
(* Gas phase reaction equation *)
S7 = KH2SO4G
==(fugcoeffpureH2O*vapmolefracH2O*f4*vapmolefracSO3)/(f5*vapmolefracH2SO4);
(* Vapour liquid equilibria expressions labelled as book *)
S8 = vapmolefracH2O * f1 *Pressure ==activityH2O* PSH2O *
fugcoeffpureH2O*Exp[(partmolvolH2O *1000*(Pressure- PSH2O))/(R*T)];
S9=  vapmolefracSO2 * f2 * Pressure == molalSO2aq*activitycoeffSO2*HenrySO2*
Exp[(partmolvolSO2 *1000*(Pressure- PSH2O))/(R*T)];
S10= vapmolefracO2 * f3 * Pressure == molalO2 * activitycoeffO2 * HenryO2 *
Exp[(partmolvolO2*1000* (Pressure - PSH2O))/(R*T)];
S11= vapmolefracSO3 * f4 * Pressure == molalSO3aq * activitycoeffSO3aq * HenrySO3 *
Exp[(partmolvolSO3*1000* (Pressure - PSH2O))/(R*T)];
S12= vapmolefracH2SO4 * f5 * Pressure == molalH2SO4aq * activitycoeffH2SO4 *
HenryH2SO4 * Exp[(partmolvolH2SO4*1000* (Pressure - PSH2O))/(R*T)];

(*-------------------------------------------------------------------------------------
----*)
(*-------------------------------------------------------------------------------------
----*)
(* other system equations*)
(* vapour phase balance *)
S13 = vapmolefracSO2 + vapmolefracH2O +
vapmolefracO2+vapmolefracSO3+vapmolefracH2SO4== 1;
(* sulphur balance *)
S14 = (molesH2O/55.51*(molalSO2aq + molalHSO3 +
molalSO3+molalSO4+molalHSO4+molalSO3aq+molalH2SO4aq)) + (vapmolefracSO2*Vaprate)
+(vapmolefracH2SO4*Vaprate)== SO2IN+H2SO4IN ;
(* hydrogen balance *)
S15 = (2*molesH2O) + (molesH2O/55.51*(molalH + molalOH + molalHSO3+molalHSO4)) +
(2*vapmolefracH2O*Vaprate)+(2*vapmolefracH2SO4*Vaprate)==2*H2OIN +2H2SO4IN;
(* oxygen balance *)
S16 =molesH2O +(molesH2O/55.51*(2*molalO2+2*molalSO2aq + 3*molalHSO3 +
3*molalSO3+molalOH+4*molalSO4+4*molalHSO4+3*molalSO3aq+4molalH2SO4aq))+(2*vapmolefrac
O2 * Vaprate)+(2*vapmolefracSO2*Vaprate)+(3*vapmolefracSO3*Vaprate)+
(4*vapmolefracH2SO4*Vaprate)+(vapmolefracH2O*Vaprate)== 2*O2IN + 2*SO2IN +
H2OIN+4*H2SO4IN;
(* electroneutrality *)
S17 = molalH == (molalOH + molalHSO3 + molalHSO4 + (2*molalSO3)+(2*molalSO4));
$RecursionLimit=1000;
(*-------------------------------------------------------------------------*)
(* set initial guess for the liquid compositions *)
(*guessmolesH2O = H2OIN;*)
guessmolalO2 =O2IN/H2OIN/0.01801*.01;
guessmolalH =0.19462654819466652`;
guessmolalOH = _1.1249617342965978`*^-10;
guessmolalSO2aq = 1;
guessmolalSO3aq =_ 1.412569707920273`*^-7;
guessmolalHSO3 =_0.19462626556822873`;
guessmolalSO3 = 0.0000000000005/H2OIN/0.018;
guessmolalSO3aq =0.00000000006/H2OIN/0.018;
guessmolalHSO4 =0.098/H2OIN/0.018;
guessmolalH2SO4aq =0.007/H2SO4IN/0.018;
guessmolalSO4 = 0.003/H2OIN/0.018;
guessmolalO2=guessmolalSO2aq;
(* initial guess for vapour rate AND vapmolefracs *)
guessvapmolefracSO2 = .3;
guessvapmolefracO2 = .65;
guessvapmolefracSO3 =.001;
guessvapmolefracH2SO4 = .001;
guessVaprate=3.5;
guessvapmolefracH2O = .02;
(*-----------------------------------------------------------*)
(*NSolve[{S1,S2,S3,S4,S5,S6,S7,S8,S9,S10,S11,S12,S13,S14,S15,S16,S17},{molesH2O,molal
H, molalOH,
molalSO2aq,molalSO3aq,molalHSO3,molalHSO4,molalH2SO4aq,molalSO4,molalSO3,vapmolefracH
2O,vapmolefracSO2,vapmolefracSO3,vapmolefracH2SO4,Vaprate,molalO2,vapmolefracO2}]*)
(*
Module[{s=0,e=0},{
```

```
*)
minimalroots=1.6589141546643201`*^-36;
FindRoot[
  {S1, S2, S3,S4,  S5,S6,S7, S8, S9,S10,S11, S12, S13,S14, S15, S16, S17},
(*Equations*)
  {
   {molesH2O,H2OIN,10},
   {molalH,guessmolalH,.01},
   {molalOH,guessmolalOH,.0001},
   {molalSO2aq,guessmolalSO2aq,5},
   {molalSO3aq, guessmolalSO3aq,10},
   {molalHSO3,guessmolalHSO3,10},
    {molalHSO4,guessmolalHSO4,10},
   {molalH2SO4aq,guessmolalH2SO4aq,10},
    {molalSO4,guessmolalSO4,100},
    {molalSO3,guessmolalSO3,100},
    {vapmolefracH2O, .01,100},
    {vapmolefracSO2, .1,100},
    {vapmolefracSO3, .001,100},
   {vapmolefracH2SO4, .005,100},
    {Vaprate, 1,100},
    {molalO2, 0.0005,100},
    {vapmolefracO2, 0.5,100}
   }  , MaxIterations→5000, Method→"Secant", AccuracyGoal→20,PrecisionGoal→20
  ];


(*--------------------------------------------------------------------*)
PSO2 = -131.2450+1.66627*T-0.00705849*T^2+0.00001001305*T^3; (*Second Phase SO2*)
VessVol =((Vaprate* R * T)/Pressure)/1000;
VessVol2 = Vaprate * V;
kgwater = molesH2O*0.018015;
volumeofliquid  = Vf * kgwater;
Vesselvolume = VessVol2 + volumeofliquid;
Calcppoxygen = vapmolefracO2 * Barpressure;
CalcppSO2 = vapmolefracSO2 * Barpressure;
CalcppH2O = vapmolefracH2O * Barpressure;
TotalMolalSO2 = molalSO2 + molalHSO3 + molalSO3;
moleslitreH = molalH/Vf;
moleslitreSO3 = molalSO3 /Vf;
moleslitreHSO3 = molalHSO3 /Vf;
moleslitreSO2 = molalSO2 /Vf;
moleslitreOH = molalOH /Vf;
molesH = molalH*kgwater;
molesOH = molalOH*kgwater;
molesSO2 = molalSO2*kgwater;
molesSO3 = molalSO3*kgwater;
molesHSO3 = molalHSO3*kgwater;
molesSO4 = molalSO4*kgwater;
molesHSO4 = molalHSO4*kgwater;
molesO2 = molalO2*kgwater;
totalmolesSO2 = molesSO2 + molesSO3+ molesHSO3;
pHact = -Log[10,(moleslitreH*activitycoeffH)];
pH = -Log[10, moleslitreH];
PartialO2bar = Calcppoxygen;
PartialO2atm = PartialO2bar * 0.987-PartialO2bar*H2SO4IN;
T =TCel + 273.15;
conc = PartialO2atm*Exp[1/(8.3144*T) ((0.046*T^2)+(203.357*T*Log[T/298])-
((299.378+0.092*T)*(T-298))-20.591*10^3)];

(*End of Calculations*)
```

Appendix E.

Macros in Visual Basic

```
Example to generate a continuous buffered sample clocked digital pulse train
from a Counter Output Channel.

Public Class MainForm
    Inherits System.Windows.Forms.Form

    Private idleState As COPulseIdleState
    Private WithEvents dutyCycleMaxTextBox As System.Windows.Forms.TextBox
    Private WithEvents channelParameterGroupBox As
System.Windows.Forms.GroupBox
    Private WithEvents counterComboBox As System.Windows.Forms.ComboBox
    Private WithEvents idleStateGroupBox As System.Windows.Forms.GroupBox
    Private WithEvents highRadioButton As System.Windows.Forms.RadioButton
    Private WithEvents lowRadioButton As System.Windows.Forms.RadioButton
    Private WithEvents physicalChannelLabel As System.Windows.Forms.Label
    Friend WithEvents clockSourceLabel As System.Windows.Forms.Label
    Private WithEvents dutyCycleMaxLabel As System.Windows.Forms.Label
    Private WithEvents dutyCycleMinTextBox As System.Windows.Forms.TextBox
    Private WithEvents frequencyTextBox As System.Windows.Forms.TextBox
    Private WithEvents frequencyLabel As System.Windows.Forms.Label
    Private WithEvents pwmParametersGroupBox As
System.Windows.Forms.GroupBox
    Private WithEvents dutyCycleMinLabel As System.Windows.Forms.Label
    Private WithEvents timingParametersGroupBox As
System.Windows.Forms.GroupBox
    Friend WithEvents clockSourceTextBox As System.Windows.Forms.TextBox
    Friend WithEvents rateLabel As System.Windows.Forms.Label
    Friend WithEvents samplesLabel As System.Windows.Forms.Label
    Friend WithEvents samplesPerChannelNumeric As
System.Windows.Forms.NumericUpDown
    Friend WithEvents rateNumeric As System.Windows.Forms.NumericUpDown
    Private WithEvents stopButton As System.Windows.Forms.Button
    Private WithEvents startButton As System.Windows.Forms.Button
    Private myTask As Task

#Region " Windows Form Designer generated code "

    Public Sub New()
        MyBase.New()
        Application.EnableVisualStyles()

        'This call is required by the Windows Form Designer.
        InitializeComponent()

        'Add any initialization after the InitializeComponent() call
        idleState = COPulseIdleState.Low


counterComboBox.Items.AddRange(DaqSystem.Local.GetPhysicalChannels(PhysicalC
hannelTypes.CO, PhysicalChannelAccess.External))
        If (counterComboBox.Items.Count > 0) Then
```

```
            counterComboBox.SelectedIndex = 0
        End If

    End Sub

    'Form overrides dispose to clean up the component list.
    Protected Overloads Overrides Sub Dispose(ByVal disposing As Boolean)
        If disposing Then
            If Not (components Is Nothing) Then
                components.Dispose()
            End If
        End If
        MyBase.Dispose(disposing)
    End Sub

    'Required by the Windows Form Designer
    Private components As System.ComponentModel.IContainer

    'NOTE: The following procedure is required by the Windows Form Designer
    'It can be modified using the Windows Form Designer.
    'Do not modify it using the code editor.
    <System.Diagnostics.DebuggerStepThrough()> Private Sub
InitializeComponent()
        Dim resources As System.ComponentModel.ComponentResourceManager =
New System.ComponentModel.ComponentResourceManager(GetType(MainForm))
        Me.dutyCycleMaxTextBox = New System.Windows.Forms.TextBox
        Me.channelParameterGroupBox = New System.Windows.Forms.GroupBox
        Me.counterComboBox = New System.Windows.Forms.ComboBox
        Me.idleStateGroupBox = New System.Windows.Forms.GroupBox
        Me.highRadioButton = New System.Windows.Forms.RadioButton
        Me.lowRadioButton = New System.Windows.Forms.RadioButton
        Me.physicalChannelLabel = New System.Windows.Forms.Label
        Me.clockSourceLabel = New System.Windows.Forms.Label
        Me.dutyCycleMaxLabel = New System.Windows.Forms.Label
        Me.dutyCycleMinTextBox = New System.Windows.Forms.TextBox
        Me.frequencyTextBox = New System.Windows.Forms.TextBox
        Me.frequencyLabel = New System.Windows.Forms.Label
        Me.pwmParametersGroupBox = New System.Windows.Forms.GroupBox
        Me.dutyCycleMinLabel = New System.Windows.Forms.Label
        Me.timingParametersGroupBox = New System.Windows.Forms.GroupBox
        Me.clockSourceTextBox = New System.Windows.Forms.TextBox
        Me.rateLabel = New System.Windows.Forms.Label
        Me.samplesLabel = New System.Windows.Forms.Label
        Me.samplesPerChannelNumeric = New System.Windows.Forms.NumericUpDown
        Me.rateNumeric = New System.Windows.Forms.NumericUpDown
        Me.stopButton = New System.Windows.Forms.Button
        Me.startButton = New System.Windows.Forms.Button
        Me.channelParameterGroupBox.SuspendLayout()
        Me.idleStateGroupBox.SuspendLayout()
        Me.pwmParametersGroupBox.SuspendLayout()
        Me.timingParametersGroupBox.SuspendLayout()
        CType(Me.samplesPerChannelNumeric,
System.ComponentModel.ISupportInitialize).BeginInit()
        CType(Me.rateNumeric,
System.ComponentModel.ISupportInitialize).BeginInit()
        Me.SuspendLayout()
        '
        'dutyCycleMaxTextBox
        '
        Me.dutyCycleMaxTextBox.Location = New System.Drawing.Point(112, 82)
        Me.dutyCycleMaxTextBox.Name = "dutyCycleMaxTextBox"
```

```
        Me.dutyCycleMaxTextBox.Size = New System.Drawing.Size(132, 20)
        Me.dutyCycleMaxTextBox.TabIndex = 11
        Me.dutyCycleMaxTextBox.Text = "0.8"
        '
        'channelParameterGroupBox
        '
        Me.channelParameterGroupBox.Controls.Add(Me.counterComboBox)
        Me.channelParameterGroupBox.Controls.Add(Me.idleStateGroupBox)
        Me.channelParameterGroupBox.Controls.Add(Me.physicalChannelLabel)
        Me.channelParameterGroupBox.FlatStyle =
System.Windows.Forms.FlatStyle.System
        Me.channelParameterGroupBox.Location = New System.Drawing.Point(10,
9)
        Me.channelParameterGroupBox.Name = "channelParameterGroupBox"
        Me.channelParameterGroupBox.Size = New System.Drawing.Size(250, 117)
        Me.channelParameterGroupBox.TabIndex = 7
        Me.channelParameterGroupBox.TabStop = False
        Me.channelParameterGroupBox.Text = "Channel Parameters:"
        '
        'counterComboBox
        '
        Me.counterComboBox.Location = New System.Drawing.Point(112, 16)
        Me.counterComboBox.Name = "counterComboBox"
        Me.counterComboBox.Size = New System.Drawing.Size(132, 21)
        Me.counterComboBox.TabIndex = 1
        Me.counterComboBox.Text = "Dev1/ctr0"
        '
        'idleStateGroupBox
        '
        Me.idleStateGroupBox.Controls.Add(Me.highRadioButton)
        Me.idleStateGroupBox.Controls.Add(Me.lowRadioButton)
        Me.idleStateGroupBox.FlatStyle =
System.Windows.Forms.FlatStyle.System
        Me.idleStateGroupBox.Location = New System.Drawing.Point(6, 43)
        Me.idleStateGroupBox.Name = "idleStateGroupBox"
        Me.idleStateGroupBox.Size = New System.Drawing.Size(238, 64)
        Me.idleStateGroupBox.TabIndex = 6
        Me.idleStateGroupBox.TabStop = False
        Me.idleStateGroupBox.Text = "Idle State:"
        '
        'highRadioButton
        '
        Me.highRadioButton.FlatStyle = System.Windows.Forms.FlatStyle.System
        Me.highRadioButton.Location = New System.Drawing.Point(123, 24)
        Me.highRadioButton.Name = "highRadioButton"
        Me.highRadioButton.Size = New System.Drawing.Size(64, 24)
        Me.highRadioButton.TabIndex = 1
        Me.highRadioButton.Text = "High"
        '
        'lowRadioButton
        '
        Me.lowRadioButton.Checked = True
        Me.lowRadioButton.FlatStyle = System.Windows.Forms.FlatStyle.System
        Me.lowRadioButton.Location = New System.Drawing.Point(51, 24)
        Me.lowRadioButton.Name = "lowRadioButton"
        Me.lowRadioButton.Size = New System.Drawing.Size(64, 24)
        Me.lowRadioButton.TabIndex = 0
        Me.lowRadioButton.TabStop = True
        Me.lowRadioButton.Text = "Low"
        '
        'physicalChannelLabel
```

```
        '
        Me.physicalChannelLabel.FlatStyle =
System.Windows.Forms.FlatStyle.System
        Me.physicalChannelLabel.Location = New System.Drawing.Point(8, 23)
        Me.physicalChannelLabel.Name = "physicalChannelLabel"
        Me.physicalChannelLabel.Size = New System.Drawing.Size(72, 16)
        Me.physicalChannelLabel.TabIndex = 0
        Me.physicalChannelLabel.Text = "Counter(s):"
        '
        'clockSourceLabel
        '
        Me.clockSourceLabel.FlatStyle =
System.Windows.Forms.FlatStyle.System
        Me.clockSourceLabel.Location = New System.Drawing.Point(8, 21)
        Me.clockSourceLabel.Name = "clockSourceLabel"
        Me.clockSourceLabel.Size = New System.Drawing.Size(80, 16)
        Me.clockSourceLabel.TabIndex = 6
        Me.clockSourceLabel.Text = "Clock Source:"
        '
        'dutyCycleMaxLabel
        '
        Me.dutyCycleMaxLabel.FlatStyle =
System.Windows.Forms.FlatStyle.System
        Me.dutyCycleMaxLabel.Location = New System.Drawing.Point(6, 86)
        Me.dutyCycleMaxLabel.Name = "dutyCycleMaxLabel"
        Me.dutyCycleMaxLabel.Size = New System.Drawing.Size(104, 16)
        Me.dutyCycleMaxLabel.TabIndex = 10
        Me.dutyCycleMaxLabel.Text = "Duty Cycle Max:"
        '
        'dutyCycleMinTextBox
        '
        Me.dutyCycleMinTextBox.Location = New System.Drawing.Point(112, 51)
        Me.dutyCycleMinTextBox.Name = "dutyCycleMinTextBox"
        Me.dutyCycleMinTextBox.Size = New System.Drawing.Size(132, 20)
        Me.dutyCycleMinTextBox.TabIndex = 9
        Me.dutyCycleMinTextBox.Text = "0.5"
        '
        'frequencyTextBox
        '
        Me.frequencyTextBox.Location = New System.Drawing.Point(112, 19)
        Me.frequencyTextBox.Name = "frequencyTextBox"
        Me.frequencyTextBox.Size = New System.Drawing.Size(132, 20)
        Me.frequencyTextBox.TabIndex = 7
        Me.frequencyTextBox.Text = "1000.0"
        '
        'frequencyLabel
        '
        Me.frequencyLabel.FlatStyle = System.Windows.Forms.FlatStyle.System
        Me.frequencyLabel.Location = New System.Drawing.Point(8, 24)
        Me.frequencyLabel.Name = "frequencyLabel"
        Me.frequencyLabel.Size = New System.Drawing.Size(120, 16)
        Me.frequencyLabel.TabIndex = 6
        Me.frequencyLabel.Text = "Frequency (Hz):"
        '
        'pwmParametersGroupBox
        '
        Me.pwmParametersGroupBox.Controls.Add(Me.dutyCycleMaxTextBox)
        Me.pwmParametersGroupBox.Controls.Add(Me.dutyCycleMaxLabel)
        Me.pwmParametersGroupBox.Controls.Add(Me.dutyCycleMinTextBox)
        Me.pwmParametersGroupBox.Controls.Add(Me.dutyCycleMinLabel)
        Me.pwmParametersGroupBox.Controls.Add(Me.frequencyTextBox)
```

```
        Me.pwmParametersGroupBox.Controls.Add(Me.frequencyLabel)
        Me.pwmParametersGroupBox.Location = New System.Drawing.Point(10,
252)
        Me.pwmParametersGroupBox.Name = "pwmParametersGroupBox"
        Me.pwmParametersGroupBox.Size = New System.Drawing.Size(250, 110)
        Me.pwmParametersGroupBox.TabIndex = 9
        Me.pwmParametersGroupBox.TabStop = False
        Me.pwmParametersGroupBox.Text = "Pulse-width Modulation Parameters:"
        '
        'dutyCycleMinLabel
        '
        Me.dutyCycleMinLabel.FlatStyle =
System.Windows.Forms.FlatStyle.System
        Me.dutyCycleMinLabel.Location = New System.Drawing.Point(8, 55)
        Me.dutyCycleMinLabel.Name = "dutyCycleMinLabel"
        Me.dutyCycleMinLabel.Size = New System.Drawing.Size(104, 16)
        Me.dutyCycleMinLabel.TabIndex = 8
        Me.dutyCycleMinLabel.Text = "Duty Cycle Min:"
        '
        'timingParametersGroupBox
        '
        Me.timingParametersGroupBox.Controls.Add(Me.clockSourceLabel)
        Me.timingParametersGroupBox.Controls.Add(Me.clockSourceTextBox)
        Me.timingParametersGroupBox.Controls.Add(Me.rateLabel)
        Me.timingParametersGroupBox.Controls.Add(Me.samplesLabel)

Me.timingParametersGroupBox.Controls.Add(Me.samplesPerChannelNumeric)
        Me.timingParametersGroupBox.Controls.Add(Me.rateNumeric)
        Me.timingParametersGroupBox.Location = New System.Drawing.Point(10,
132)
        Me.timingParametersGroupBox.Name = "timingParametersGroupBox"
        Me.timingParametersGroupBox.Size = New System.Drawing.Size(250, 114)
        Me.timingParametersGroupBox.TabIndex = 8
        Me.timingParametersGroupBox.TabStop = False
        Me.timingParametersGroupBox.Text = "Timing Parameters:"
        '
        'clockSourceTextBox
        '
        Me.clockSourceTextBox.Location = New System.Drawing.Point(112, 19)
        Me.clockSourceTextBox.Name = "clockSourceTextBox"
        Me.clockSourceTextBox.Size = New System.Drawing.Size(132, 20)
        Me.clockSourceTextBox.TabIndex = 7
        Me.clockSourceTextBox.Text = "/Dev1/PFI7"
        '
        'rateLabel
        '
        Me.rateLabel.FlatStyle = System.Windows.Forms.FlatStyle.System
        Me.rateLabel.Location = New System.Drawing.Point(8, 85)
        Me.rateLabel.Name = "rateLabel"
        Me.rateLabel.Size = New System.Drawing.Size(64, 16)
        Me.rateLabel.TabIndex = 10
        Me.rateLabel.Text = "Rate (Hz):"
        '
        'samplesLabel
        '
        Me.samplesLabel.FlatStyle = System.Windows.Forms.FlatStyle.System
        Me.samplesLabel.Location = New System.Drawing.Point(8, 53)
        Me.samplesLabel.Name = "samplesLabel"
        Me.samplesLabel.Size = New System.Drawing.Size(104, 16)
        Me.samplesLabel.TabIndex = 8
        Me.samplesLabel.Text = "Samples / Channel:"
```

```
        '
        'samplesPerChannelNumeric
        '
        Me.samplesPerChannelNumeric.Location = New System.Drawing.Point(112,
51)
        Me.samplesPerChannelNumeric.Maximum = New Decimal(New Integer()
{1000000, 0, 0, 0})
        Me.samplesPerChannelNumeric.Name = "samplesPerChannelNumeric"
        Me.samplesPerChannelNumeric.Size = New System.Drawing.Size(132, 20)
        Me.samplesPerChannelNumeric.TabIndex = 9
        Me.samplesPerChannelNumeric.Value = New Decimal(New Integer() {1000,
0, 0, 0})
        '
        'rateNumeric
        '
        Me.rateNumeric.DecimalPlaces = 2
        Me.rateNumeric.Location = New System.Drawing.Point(112, 83)
        Me.rateNumeric.Maximum = New Decimal(New Integer() {1000000, 0, 0,
0})
        Me.rateNumeric.Name = "rateNumeric"
        Me.rateNumeric.Size = New System.Drawing.Size(132, 20)
        Me.rateNumeric.TabIndex = 11
        Me.rateNumeric.Value = New Decimal(New Integer() {100, 0, 0, 0})
        '
        'stopButton
        '
        Me.stopButton.Enabled = False
        Me.stopButton.FlatStyle = System.Windows.Forms.FlatStyle.System
        Me.stopButton.Location = New System.Drawing.Point(266, 56)
        Me.stopButton.Name = "stopButton"
        Me.stopButton.Size = New System.Drawing.Size(96, 32)
        Me.stopButton.TabIndex = 6
        Me.stopButton.Text = "Stop"
        '
        'startButton
        '
        Me.startButton.FlatStyle = System.Windows.Forms.FlatStyle.System
        Me.startButton.Location = New System.Drawing.Point(266, 18)
        Me.startButton.Name = "startButton"
        Me.startButton.Size = New System.Drawing.Size(96, 32)
        Me.startButton.TabIndex = 5
        Me.startButton.Text = "Start"
        '
        'MainForm
        '
        Me.AutoScaleBaseSize = New System.Drawing.Size(5, 13)
        Me.ClientSize = New System.Drawing.Size(372, 370)
        Me.Controls.Add(Me.channelParameterGroupBox)
        Me.Controls.Add(Me.pwmParametersGroupBox)
        Me.Controls.Add(Me.timingParametersGroupBox)
        Me.Controls.Add(Me.stopButton)
        Me.Controls.Add(Me.startButton)
        Me.FormBorderStyle =
System.Windows.Forms.FormBorderStyle.FixedDialog
        Me.Icon = CType(resources.GetObject("$this.Icon"),
System.Drawing.Icon)
        Me.MaximizeBox = False
        Me.Name = "MainForm"
        Me.StartPosition =
System.Windows.Forms.FormStartPosition.CenterScreen
        Me.Text = "Digital Pulse Train - Continuous - Buffered"
```

```
        Me.channelParameterGroupBox.ResumeLayout(False)
        Me.idleStateGroupBox.ResumeLayout(False)
        Me.pwmParametersGroupBox.ResumeLayout(False)
        Me.pwmParametersGroupBox.PerformLayout()
        Me.timingParametersGroupBox.ResumeLayout(False)
        Me.timingParametersGroupBox.PerformLayout()
        CType(Me.samplesPerChannelNumeric,
System.ComponentModel.ISupportInitialize).EndInit()
        CType(Me.rateNumeric,
System.ComponentModel.ISupportInitialize).EndInit()
        Me.ResumeLayout(False)

    End Sub

#End Region



    Private Sub startButton_Click(ByVal sender As System.Object, ByVal e As
System.EventArgs) Handles startButton.Click
        Dim samplesPerChannel As Integer =
Convert.ToInt32(samplesPerChannelNumeric.Value)
        Dim rate As Double = Convert.ToDouble(rateNumeric.Value)
        Dim frequency As Double = Convert.ToDouble(frequencyTextBox.Text)
        Dim dutyCycleMin As Double =
Convert.ToDouble(dutyCycleMinTextBox.Text)
        Dim dutyCycleMax As Double =
Convert.ToDouble(dutyCycleMaxTextBox.Text)
        Dim dutyStep As Double = (dutyCycleMax - dutyCycleMin) /
samplesPerChannel

        Try
            Dim data(samplesPerChannel - 1) As CODataFrequency
            For I As Integer = 0 To data.Length - 1
                data(I) = New CODataFrequency(frequency, dutyCycleMin +
dutyStep * I)
            Next

            myTask = New Task()


myTask.COChannels.CreatePulseChannelFrequency(counterComboBox.Text, _
                "ContinuousPulseTrain", COPulseFrequencyUnits.Hertz,
idleState, 0.0, _
                frequency, _
                dutyCycleMin)

            myTask.Timing.ConfigureSampleClock(clockSourceTextBox.Text,
rate, _
                SampleClockActiveEdge.Rising,
SampleQuantityMode.ContinuousSamples)

            Dim writer As CounterSingleChannelWriter = New
CounterSingleChannelWriter(myTask.Stream)
            writer.WriteMultiSample(False, data)

            AddHandler myTask.Done, AddressOf OnTaskDone
            myTask.Start()

            startButton.Enabled = False
            stopButton.Enabled = True
```

```
        Catch ex As DaqException
            MessageBox.Show(ex.Message)
            myTask.Dispose()
            startButton.Enabled = True
            stopButton.Enabled = False
        End Try

    End Sub

    Private Sub stopButton_Click(ByVal sender As System.Object, ByVal e As
System.EventArgs) Handles stopButton.Click
        myTask.Stop()
        myTask.Dispose()
        startButton.Enabled = True
        stopButton.Enabled = False
    End Sub

    Private Sub lowRadioButton_CheckedChanged(ByVal sender As Object, ByVal
e As System.EventArgs) Handles lowRadioButton.CheckedChanged
        idleState = COPulseIdleState.Low
    End Sub

    Private Sub highRadioButton_CheckedChanged(ByVal sender As Object, ByVal
e As System.EventArgs) Handles highRadioButton.CheckedChanged
        idleState = COPulseIdleState.High
    End Sub

    Private Sub OnTaskDone(ByVal sender As Object, ByVal e As
TaskDoneEventArgs)
        Try
            stopButton.Enabled = False
            startButton.Enabled = True
            e.CheckForException()
            myTask.Stop()
            myTask.Dispose()
            myTask = Nothing
        Catch ex As Exception
            MessageBox.Show(ex.Message)
            myTask.Stop()
            myTask.Dispose()
            myTask = Nothing
        End Try
    End Sub
End Class
```

Appendix F.

Publications

In progress

April 2013 to date: Ternary model with preliminary ternary and quaternary data using Mathematica. M.Romero, R.Elder, R.W.K.Allen. Date to publish approximately: September 2013.

Conference Proceeding

Low temperature SO_2-O_2-H_2O VLE in the sulphur family of thermochemical cycles

M.Romero, R. Allen, R. Elder

01/2011; In proceeding of: International Conference on Hydrogen Production 2011, At Thessaloniki, Greece

ABSTRACT

Thermochemical cycles have great potential for massive scale, carbon-neutral hydrogen production. Of particular interest are the Sulphur Iodine (SI) and the Hybrid Sulphur (HyS) cycles, both having a common step consisting on the high temperature thermal decomposition of H2SO4. The energy requirements are large and there is no known thermodynamic data for this particular system. In order for a design-based approach to be taken for the low temperature separation, accurate vapour-liquid equilibrium data is needed for the decomposition products: SO2-H2O-O2. This work experimentally investigates both the binary SO2-H2O and ternary SO2-O2-H2O system at pressures up to 15 bar and temperatures up to 80° C. Results are compared to a theoretical model based on weak electrolyte thermodynamics. Good correlation between the model and experimental results is seen at low pressures for the binary solution and across the pressure range for the ternary solution. The divergence at high pressures in the binary comparison is thought to be due to the formation of two liquid phases, and the underestimation of the dissolved SO2 salting-out effect. Online spectroscopic measurements are being developed to measure this phenomenon.

Conference Proceeding

Low Temperature Separations in the Sulphuric Acid Decomposition Stage of the Sulphur Iodine and Hybrid Sulphur Thermochemical Water Splitting Cycles

M. Romero R.H. Elder A. Shaw N. Elbakhbakhi G.H. Priestman R.W.K. Allen Detlef Stolten (Hrsg.) Thomas Grube (Hrsg.)

01/2010; In proceeding of: 18th World Hydrogen Energy Conference 2010 - WHEC 2010, At Essen, Germany

ABSTRACT

The Sulphur Iodine and Hybrid Sulphur thermochemical cycles are promising routes for large scale production of hydrogen from water. The thermal decomposition of aqueous sulphuric acid to form SO2, O2 and H2O is common to both cycles and involves high temperatures and difficult separations. The energy requirement is large due to the excess of water present. This work investigates the separations involved with a view to improving efficiency.

Conference Proceeding

Simultaneous Solubilities of Oxygen and Sulphur Dioxide in Water: Thermodynamic Data for the Sulphur Family of Thermochemical Cycles

M. Romero, R. Elder, A. Shaw, R. Allen

01/2010; In proceeding of: 2010 AIChE Annual Meeting, At Salt Lake City, US

ABSTRACT

The Sulphur family of thermochemical cycles shows great promise for the massive scale production of hydrogen from water. The decomposition of sulphuric acid is a common stage in the cycles and poses design problems due to the corrosive nature of the solution, the high temperatures involved and the difficult separations required. The work considered here focuses on the oxygen separation stage of the process where, in order for a science based design approach to be taken, thermodynamic data are required for multicomponent phase equilibrium relationships between water, sulphur dioxide and oxygen; H2O-SO2-O2. A bespoke vapour-liquid-equilibrium still is used to measure the simultaneous solubilities of the ternary solution. The results are presented, along with a comparison to a model based on weak electrolyte thermodynamics. The model can be used for flash calculations, necessary for the design of the separation equipment.

Journal Article

Measurements of the solubility of sulphur dioxide in water for the sulphur family of thermochemical cycles

Moises A. Romero, Andrew C. Shaw, Rachael H. Elder, Bruce C.R. Ewan, Ray W.K. Allen

International Journal of Hydrogen Energy (impact factor: 4.05). 01/2010; 38:4749.

ABSTRACT

In recent years, the Hybrid Sulphur (HyS) and Sulphur Iodine (SI) cycles have emerged as promising routes for the massive scale thermochemical production of Hydrogen from water. Common to these two cycles is a high temperature stage involving the decomposition of sulphuric acid to sulphur dioxide, water and oxygen. The work considered here focuses on the oxygen separation stage of the process where, in order for a science based design approach to be taken, thermodynamic data are required for multicomponent phase equilibrium relationships between the decomposition products; H2O–SO2–O2. A method of making flash calculations, useful in the separation equipment design, has been proposed and coded into Mathematica®. Further, a vapour–liquid equilibrium still has been designed and built to make measurements of the multicomponent solubility of sulphur dioxide and oxygen in water. The experiments presented here concentrate on the binary SO2–H2O system, covering a wider range of pressures than that found in the literature. Solubility, expressed in molality, was obtained at 25 and 40 °C and pressures ranging from 0.2 to 3.6 atm. Good agreement is seen between the experimental data and the model at lower pressures, however improvements are needed at higher pressure. Preliminary data for the ternary system at 40 °C is presented, showing good agreement with the multicomponent model. Future work will focus on the three component system.

Appendix G.
Technical Drawings

Mark IV Laboratory Setup

The following diagram represents the laboratory setup used for the Mark IV experiments that were performed during this project

A Reactor Thermocouple	F Fume cupboard
B Waterbath Thermocouple	G NI DAQ Interface
C Bath Controller	H LabVIEW PC
D Mark IV Reactor	I Sulphur Dioxide and Oxygen
E Heating Media	J FTIR Spectrometer

Chemical & Biological Engineering
University of Sheffield

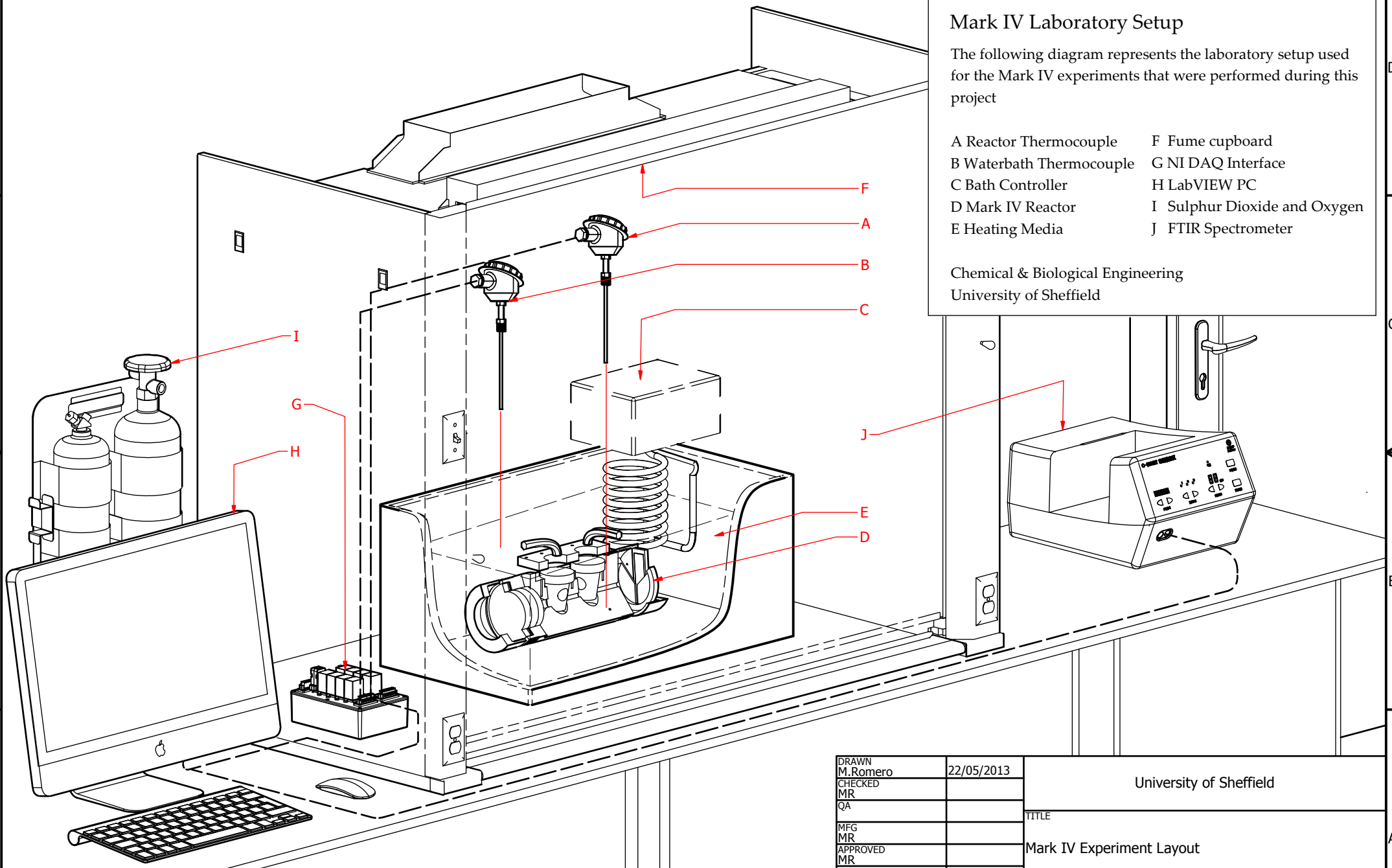

DRAWN M.Romero	22/05/2013	University of Sheffield	
CHECKED MR			
QA		TITLE Mark IV Experiment Layout	
MFG MR			
APPROVED MR			
		SIZE A3	DWG NO Final Reactor Thesis 2013 REV 1
		SCALE	SHEET 1 OF 1

Mark IV VLE Reactor

A - GAS LID
B - OUTER PTFE GASKET
C - SIGHT GLASS
D - INNER PTFE GASKET
E - REACTOR BODY
F - BSP THREAD
G - VALVE HOLDER
H - PLUG HOLES
I - GAS VALVE
J - LIQUID VALVE
K - SLOTTED PTFE GASKET
L - THERMOCOUPLE INSERT
M - ATR GERMANIUM PRISM
N - PTFE GERMANIUM SEAT
O - 45° FIBER OPTIC INSERTS
P - LIQUID LID
Q - GAS CHAMBER
R - VALVE SEAT
S - MULTIPHASE AREA
T - ALIGNMENT PIN

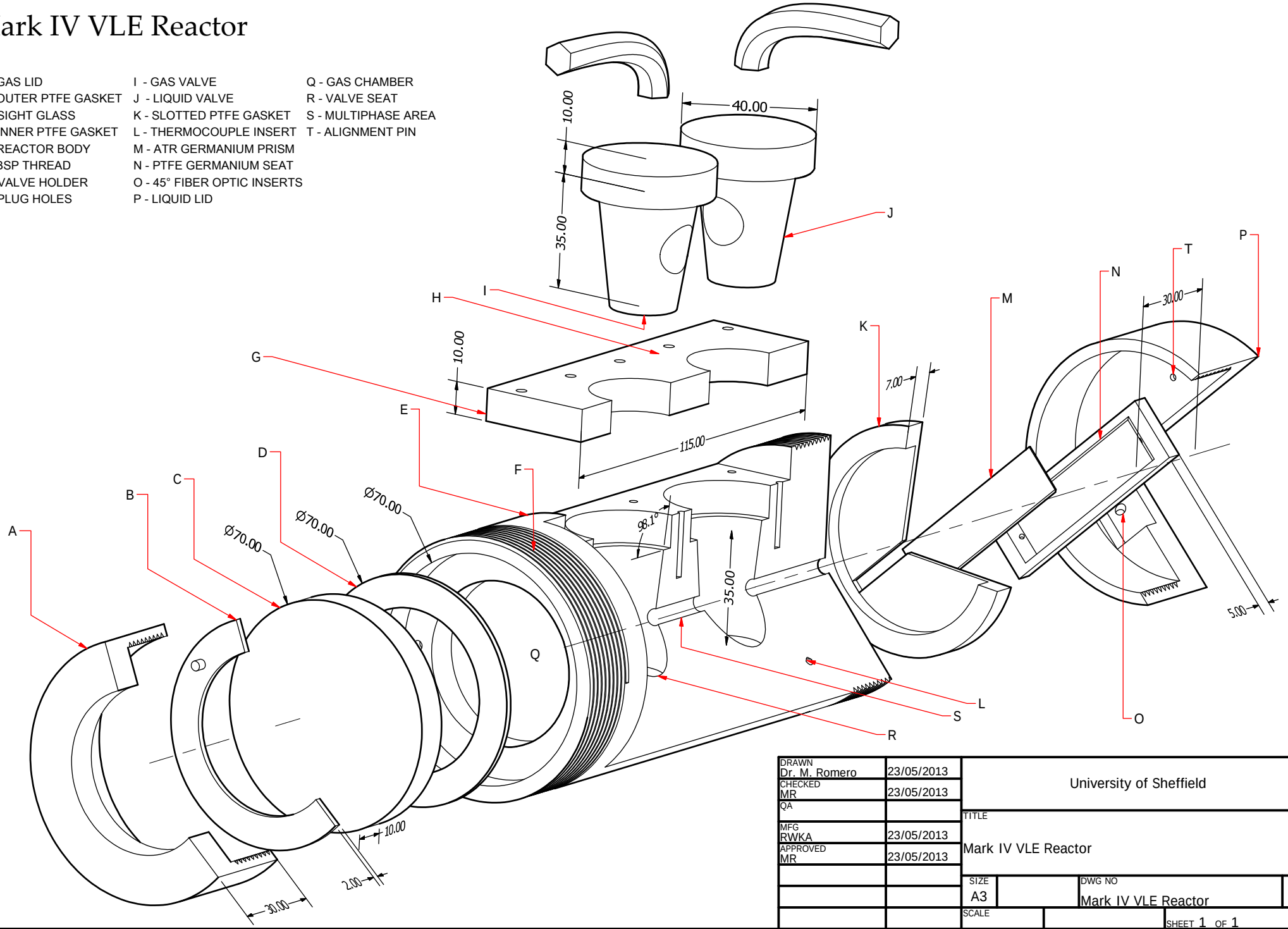

DRAWN Dr. M. Romero	23/05/2013	University of Sheffield	
CHECKED MR	23/05/2013		
QA		TITLE Mark IV VLE Reactor	
MFG RWKA	23/05/2013		
APPROVED MR	23/05/2013		
		SIZE A3	DWG NO Mark IV VLE Reactor
		SCALE	REV 1
			SHEET 1 OF 1

Consolidated Reference List

ABAOUD, H. & STEEB, H. 1998. The German-Saudi HYSOLAR program. International Journal of Hydrogen Energy, 23, 445-449.

BASS, M., DECUSATIS, C., ENOCH, J., LAKSHMINARAYANAN, V., LI, G., MACDONALD, C., MAHAJAN, V. & VAN STRYLAND, E. 2009. Handbook of Optics, Third Edition Volume I: Geometrical and Physical Optics, Polarized Light, Components and Instruments(set), McGraw-Hill Companies,Incorporated.

BATTINO, R. & CLEVER, H. L. 1966. The Solubility of Gases in Liquids. Chemical Reviews, 66, 395-463.

CARROLL, J. J. 1991. What is Henry's Law? Chemical Engineering Progress, 87, 48-52.

CLARK, S. R. 2007. Elements of Fractional Distillation, Read Books.

CLARK, S. R. 2007. Elements of Fractional Distillation, Read Books.

CRYSTRAN. 2012. Optical Properties of Materials [Online]. Available: http://www.crystran.co.uk/materials-data.htm.

DAUBERT, T. E. 1985. Chemical engineering thermodynamics, McGraw-Hill.

DREWNOWSKI, A. & SPECTER, S. 2004. Poverty and obesity: the role of energy density and energy costs. The American Journal of Clinical Nutrition, 79, 6-16.

DROLET, B., GRETZ, J., KLUYSKENS, D., SANDMANN, F. & WURSTER, R. 1996. The euro-québec hydro-hydrogen pilot project [EQHHPP]: demonstration phase. International Journal of Hydrogen Energy, 21, 305-316.

DUDLEY, B. 2012. BP statistical review of world energy.

DUNN, S. 2002. Hydrogen futures: toward a sustainable energy system. International Journal of Hydrogen Energy, 27, 235-264.

EHA. 2012. EHA March Newsletter [Online]. Available: http://www.h2euro.org/category/publications/newsletters/newsletters-2012/eha-newsletter-march-2012.

ELDER, R. & ALLEN, R. 2009. Nuclear heat for hydrogen production: Coupling a very high/high temperature reactor to a hydrogen production plant. Progress in Nuclear Energy, 51, 500-525.

ELDER, R. H., SHAW, A., ROMERO, M., ELBAKHBAKHI, N., PRIESTMAN, G. H. & ALLEN, R. W. K. 2010. Low Temperature Separations in the Sulphuric Acid Decomposition Stage of the Sulphur Iodine and Hybrid Sulphur Thermochemical Water Splitting Cycles. In: DETLEF STOLTEN, T. G. E. F. J. G. (ed.) WHEC 2010. Essen, Germany: Forschungszentrum Jülich GmbH, Zentralbibliothek, Verlag.

GAUGLITZ, G. & VO-DINH, T. 2006. Handbook of Spectroscopy, Wiley.

GOLTSOV, V. A. & VEZIROGLU, T. N. 2001. From hydrogen economy to hydrogen civilization. International Journal of Hydrogen Energy, 26, 909-915.

GUBBINS, K. & WALKER, R. 1965. The Solubility and Diffusivity of Oxygen in Electrolytic Solutions. Journal of the Electrochemical Society, 112, 469.

HARVEY, K. B., MCCOURT, F. R. & SHURVELL, H. F. 1964. INFRARED ABSORPTION OF THE SO2 CLATHRATE-HYDRATE MOTION OF THE SO2 MOLECULE. Canadian Journal of Chemistry, 42, 960-963.

HAYDUK, W., ASATANI, H. & LU, B. C. Y. 1988. Solubility of sulfur dioxide in aqueous sulfuric acid solutions. Journal of Chemical and Engineering Data, 33, 506-9.

HIJIKATA, T. 2002. Research and development of international clean energy network using hydrogen energy (WE-NET). International Journal of Hydrogen Energy, 27, 115-129.

HIPPLER, M. & HAYNES, A. 2010. RE: Raman Spectroscopy Laboratory, Introduction. Type to M.ROMERO.

HIRSCH, R., BEZDEK, R. & WENDLING, R. Peaking of world oil production. Proceedings of the IV International Workshop on Oil and Gas Depletion, 2005. 19-20.

HUDSON, J. C. 1925. The solubility of sulphur dioxide in water and in aqueous solutions of potassium chloride and sodium sulphate. Journal of the Chemical Society, 127, 1332-1347.

J.JOOSTEN, P. G., A. KYDES, J.D.MAPLES 2008. The Impact of Increased Use of Hydrogen on Petroleum Consumption and Carbon Dioxide Emissions. 1 ed. Washington, D.C. U.S. 20585: Energy Information Administration, U.S.DOE.

JEONG, Y. H., K. HOHNHOLT, M. S. KAZIMI AND B. YILDIZ. 2005. Optimization of the hybrid sulfur cycle for hydrogen generation. Nuclear Energy and Sustainability Program (NES) Technical Report: MIT-NES-TR-004. Massachusetts, NE: Center for Advanced Nuclear Energy Systems, MIT.

JORGENSON, D. W. 1984. The Role of Energy in Productivity Growth. The American Economic Review, 74, 26-30.

KHAMIS, I. 2011. An overview of the IAEA HEEP software and international programmes on hydrogen production using nuclear energy. International Journal of Hydrogen Energy, 36, 4125-4129.

KRICHEVSKY, I. R. & KASARNOVSKY, J. S. 1935. Thermodynamical Calculations of Solubilities of Nitrogen and Hydrogen in Water at High Pressures. Journal of the American Chemical Society, 57, 2168-2171.

LEIVA, M. A. & VIVANCO, V. 1986. Vapour-liquid equilibria of aqueous solutions containing volatile weak electrolytes by using the free energy minimization method. Fluid Phase Equilibria, 27, 483-490.

LEIVA, M. A. & VIVANCO, V. 1986. Vapour-liquid equilibria of aqueous solutions containing volatile weak electrolytes by using the free energy minimization method. Fluid Phase Equilibria, 27, 483-490.

LIN, C.-T. & DAUBERT, T. E. 1978. Prediction of the Fugacity Coefficients of Nonpolar Hydrocarbon Systems from Equations of State. Industrial & Engineering Chemistry Process Design and Development, 17, 544-549.

MAASS, C. E. & MAASS, O. 1928. Sulfur Dioxide and its aqueous solutions. I. Analytical Methods, Vapor Density and Vapor Pressure of Sulfur Dioxide. Vapor Pressure and Concentrations of the Solutions. . Journal of the American Chemical Society, 50, 1352-1368.

MALANOWSKI, S. & ANDERKO, A. 1992. Modelling phase equilibria: thermodynamic background and practical tools, Wiley.

MARTIN, L. R. & GOOD, T. W. 1991. Catalyzed oxidation of sulfur dioxide in solution: The iron-manganese synergism. Atmospheric Environment. Part A. General Topics, 25, 2395-2399.

MAURER, G. 1980. On the solubility of volatile weak electrolytes in aqueous solutions. Thermodynamics of aqueous systems with industrial applications; ACS Symposium Series, 133, 139-172.

MITSUGI, C., HARUMI, A. & KENZO, F. 1998. WE-NET: Japanese hydrogen program. International Journal of Hydrogen Energy, 23, 159-165.

MOHAMMADI, A. H. & RICHON, D. 2010. Equilibrium Data of Sulfur Dioxide and Methyl Mercaptan Clathrate Hydrates. Journal of Chemical & Engineering Data, 56, 1666-1668.

MOMIRLAN, M. & VEZIROGLU, T. N. 2002. Current status of hydrogen energy. Renewable and Sustainable Energy Reviews, 6, 141-179.

MORIARTY, P. & HONNERY, D. 2009. Hydrogen's role in an uncertain energy future. International Journal of Hydrogen Energy, 34, 31-39.

NAKAMURA, R., BREEDVELD, G. J. F. & PRAUSNITZ, J. M. 1976. Thermodynamic properties of gas mixtures containing common polar and nonpolar components. Industrial & Engineering Chemistry Process Design and Development, 15, 557-64.

OTHMER, D. F., SILVIS, S. J. & SPIEL, A. 1952. Composition of Vapors from Boiling Binary Solutions: Pressure Equilibrium Still for Studying Water–Acetic Acid System. Industrial & Engineering Chemistry, 44, 1864-1872.

OUTOKUMPU 2002. Software: HSC chemistry version 5.0. Chemical Engineering Progress, 98, 28.

PASTOWSKI, A. & GRUBE, T. 2010. Scope and perspectives of industrial hydrogen production and infrastructure for fuel cell vehicles in North Rhine-Westphalia. Energy Policy, 38, 5382-5387.

PRAUSNITZ, J. M. 1969. Molecular Thermodynamics of Fluid-Phase Equilibria (Prentice-Hall International Series in the Physical and Chemical Engineering Sciences).

PRAUSNITZ, J. M., LICHTENTHALER, R. N. & DE AZEVEDO, E. G. 1986a. Molecular thermodynamics of fluid-phase equilibria, Prentice-Hall.

PRAUSNITZ, J. M., LICHTENTHALER, R. N. & DE AZEVEDO, E. G. 1986b. Molecular thermodynamics of fluid-phase equilibria. Prentice-Hall.

QUADRANT. 2011. Fluorosint® 207 Product Data Sheet [Online]. Available: http://www.quadrantplastics.com/fileadmin/quadrant/documents/QEPP/EU/Product_Data_Sheets_PDF/AEP/Fluorosint_207_E_PDS_2011.pdf.

RABE, A. E. & HARRIS, J. F. 1963. Vapor Liquid Equilibrium Data for the Binary System Sulfur Dioxide and Water. Journal of Chemical & Engineering Data, 8, 333-336.

REID, R. C., PRAUSNITZ, J. M. & POLING, B. E. 1987. The properties of gases and liquids, McGraw-Hill.

ROMERO, M. Low temperature SO2-O2-H2O VLE in the sulphur family of thermochemical cycles. In: ALLEN, R. W. K., ed. International Conference on Hydrogen Production, 2011 Thessaloniki, Greece. Hellas Research Centre, Greece.

RUMPF, B., WEYRICH, F. & MAURER, G. 1993. Simultaneous solubility of ammonia and sulfur dioxide in water at temperatures from 313.15 K to 373.15 K and pressures up to 2.2 MPa. Fluid Phase Equilibria, 83, 253-260.

SHAW, A. C. 2008a. The simultaneous solubility of sulphur dioxide and oxygen in water for the hybrid sulphur thermochemical cycle. Ph.D. Doctoral Thesis, University of Sheffield.

SHAW, A. C. 2008b. The simultaneous solubility of sulphur dioxide and oxygen in water for the hybrid sulphur thermochemical cycle. PhD Thesis, University of Sheffield.

SHAW, A., ROMERO, MOISES, ELDER, R. H., EWAN, B. C. R. & ALLEN, R. W. K. 2011. Measurements of the solubility of sulphur dioxide in water for the sulphur family of thermochemical cycles. International Journal of Hydrogen Energy, 36, 4749-4756.

SHERWOOD, T. K. 1925. Solubilities of Sulfur Dioxide and Ammonia in Water. Industrial & Engineering Chemistry, 17, 745-747.

SMITH, J. M. & VAN NESS, H. C. 1996. Introduction to chemical engineering thermodynamics, McGraw-Hill.

STOLTEN, D. 2010. Hydrogen and Fuel Cells: Fundamentals, Technologies and Applications, John Wiley & Sons.

STUART, B. H. 2004. Infrared Spectroscopy: Fundamentals and Applications, John Wiley & Sons.

TAYLOR, M. 2006. Improvement of the Sulphur-Iodine cycle through the addition of ionic liquids. M.Phil, University of Sheffield.

THOMSEN, K., RASMUSSEN, P. & GANI, R. 1996. Correlation and prediction of thermal properties and phase behaviour for a class of aqueous electrolyte systems. Chemical Engineering Science, 51, 3675-3683.

TOWLER, G. & SINNOTT, R. K. 2007. Chemical Engineering Design: Principles, Practice and Economics of Plant and Process Design, Elsevier Science.

VAN BERKUM, J. G. & DIEPEN, G. A. M. 1979. Phase equilibria in SO2 + H2O: the sulfur dioxide gas hydrate, two liquid phases, and the gas phase in the temperature range 273 to 400 K and at pressures up to 400 MPa. The Journal of Chemical Thermodynamics, 11, 317-334.

VEZIROĞLU, T. N. & TAKAHASHI, P. K. Hydrogen energy progress VIII : proceedings of the 8th World Hydrogen Energy Conference, Honolulu and Waikoloa, Hawaii, U.S.A., 22-27 July 1990. In: VEZIROĞLU, T. N. & TAKAHASHI, P. K., eds., 1990 New York :. Pergamon Press.

WARN, J. R. W. & PETERS, A. P. H. 1996. Concise Chemical Thermodynamics, 2nd Edition, N. Thornes.

WESTON, K. C. 1992. Energy Conversion, West Publishing Company.

ZEMAITIS, J. F., CLARK, D. M., RAFAL, M. & SCRIVINER, N. C. 1986. Handbook of Aqueous Electrolyte Thermodynamics, New York, AIChE